

2000

Synthesis of mechanisms for function, path, and motion generation using invariant characterization, storage and search methods

George Randall Wandling Sr.
Iowa State University

Follow this and additional works at: <https://lib.dr.iastate.edu/rtd>

 Part of the [Mechanical Engineering Commons](#)

Recommended Citation

Wandling, George Randall Sr., "Synthesis of mechanisms for function, path, and motion generation using invariant characterization, storage and search methods " (2000). *Retrospective Theses and Dissertations*. 12383.
<https://lib.dr.iastate.edu/rtd/12383>

This Dissertation is brought to you for free and open access by the Iowa State University Capstones, Theses and Dissertations at Iowa State University Digital Repository. It has been accepted for inclusion in Retrospective Theses and Dissertations by an authorized administrator of Iowa State University Digital Repository. For more information, please contact digirep@iastate.edu.

INFORMATION TO USERS

This manuscript has been reproduced from the microfilm master. UMI films the text directly from the original or copy submitted. Thus, some thesis and dissertation copies are in typewriter face, while others may be from any type of computer printer.

The quality of this reproduction is dependent upon the quality of the copy submitted. Broken or indistinct print, colored or poor quality illustrations and photographs, print bleedthrough, substandard margins, and improper alignment can adversely affect reproduction.

In the unlikely event that the author did not send UMI a complete manuscript and there are missing pages, these will be noted. Also, if unauthorized copyright material had to be removed, a note will indicate the deletion.

Oversize materials (e.g., maps, drawings, charts) are reproduced by sectioning the original, beginning at the upper left-hand corner and continuing from left to right in equal sections with small overlaps.

Photographs included in the original manuscript have been reproduced xerographically in this copy. Higher quality 6" x 9" black and white photographic prints are available for any photographs or illustrations appearing in this copy for an additional charge. Contact UMI directly to order.

Bell & Howell Information and Learning
300 North Zeeb Road, Ann Arbor, MI 48106-1346 USA
800-521-0600

UMI[®]

Synthesis of mechanisms for function, path, and motion generation
using invariant characterization, storage and search methods

by

George Randall Wandling, Sr.

A dissertation submitted to the graduate faculty
in partial fulfillment of the requirements for the degree of

DOCTOR OF PHILOSOPHY

Major: Mechanical Engineering

Major Professors: Donald R. Flugrad, Jr. and Abir Qamhiyah

Iowa State University

Ames, Iowa

2000

Copyright © George Randall Wandling, 2000. All rights reserved.

UMI Number: 9990510

Copyright 2000 by
Wandling, George Randall, Sr.

All rights reserved.

UMI[®]

UMI Microform 9990510

Copyright 2001 by Bell & Howell Information and Learning Company.
All rights reserved. This microform edition is protected against
unauthorized copying under Title 17, United States Code.

Bell & Howell Information and Learning Company
300 North Zeeb Road
P.O. Box 1346
Ann Arbor, MI 48106-1346

Graduate College
Iowa State University

This is to certify that the Doctoral dissertation of

George Randall Wandling, Sr.

has met the dissertation requirements of Iowa State University

Signature was redacted for privacy.

Co-major Professor

Signature was redacted for privacy.

Co-major Professor

Signature was redacted for privacy.

For the Major Program

Signature was redacted for privacy.

For the Graduate College

TABLE OF CONTENTS

LIST OF TABLES	vii
LIST OF FIGURES	xlv
ACKNOWLEDGEMENTS	xxxii
CHAPTER 1. INTRODUCTION	1
Research Goals	9
Dissertation Organization	10
CHAPTER 2. THE FOUR-BAR MECHANISM	12
CHAPTER 3. LITERATURE REVIEW	22
Synthesis Techniques	22
Synthesis Limitations	53
CHAPTER 4. SOLUTION REPRESENTATION	54
Spatial Representation	54
Fourier Transforms	58
One-Dimensional Fourier Transforms	78
Two-Dimensional Fourier Transforms	89
Moments	94
CHAPTER 5. SOLUTION COMPARISON AND MATCHING METHODS	99
Spatial Similarity and Difference Measures	107
Solution Matching Using Fourier Descriptors	109
Solution Matching Using Moments	115
CHAPTER 6. FUNCTION GENERATION	118

Normalized Cross Correlation	128
Sum of Absolute Differences	131
Sum of Squared Differences	134
Correlation using Fourier Descriptors	136
Phase-Only Filter	139
Symmetric Phase-Only Matched Filter	141
Amplitude Difference of Fourier Descriptors	143
Amplitude and Phase Difference of Fourier Descriptors	145
Partial Curves	147
Partial Curves - Sum of Absolute Differences	149
Partial Curves - Amplitude and Phase Difference of Fourier Descriptors	152
Summary	154
CHAPTER 7. PATH GENERATION	158
Sum of Absolute Differences	167
Sum of Squared Differences	170
One-Dimensional Correlation using Fourier Descriptors	173
One-Dimensional Phase-Only Filter	175
One-Dimensional Symmetric Phase-Only Matched Filter	176
Amplitude Difference of Fourier Descriptors	180
Amplitude and Phase Difference of Fourier Descriptors	182
Correlation with Two-Dimensional Fourier Transform	184
Phase-Only Filter with Two-Dimensional Fourier Transform	186
Symmetric Phase-Only Matched Filter with Two-Dimensional Fourier Transform	188
Moment Normalized Cross Correlation	190
Moment Sum of Percentage Difference	192
Partial Curves	195

Partial Curves - Sum of Absolute Differences	197
Partial Curves - Amplitude and Phase Difference of Fourier Descriptors	200
Partial Curves - Symmetric Phase-Only Matched Filter with Two-Dimensional Fourier Transforms	202
Summary	204
CHAPTER 8. MOTION GENERATION	208
Sum of Absolute Differences	213
Amplitude and Phase Difference of Fourier Descriptors	214
Symmetric Phase-Only Matched Filter	220
Partial Curves	223
Partial Curves - Sum of Absolute Differences	226
Partial Curves - Amplitude and Phase Difference of Fourier Descriptors	228
Partial Curves - Symmetric Phase-Only Matched Filter	231
Summary	233
CHAPTER 9. DESCRIPTION OF A DESIRED SOLUTION	237
Parametric Cubic Curve	238
Cubic Spline Function	241
Sum of Absolute Differences - Path Generation	244
Fourier Descriptor Amplitude and Phase Difference Measure - Path Generation	247
Sum of Absolute Differences - Partial Path Generation	249
Fourier Descriptor Amplitude and Phase Difference Measure - Partial Path Generation	251
Sum of Absolute Differences - Motion Generation	254
Amplitude and Phase Difference Using Fourier Descriptors - Motion Generation	257
Sum of Absolute Differences - Partial Curve Motion Generation	260

Amplitude and Phase Difference Using Fourier Descriptors - Partial Curve Motion Generation	262
B-Splines	265
Sum of Absolute Differences - Path Generation	270
Fourier Descriptor Amplitude and Phase Difference Measure - Path Generation	272
Sum of Absolute Differences - Partial Path Generation	274
Fourier Descriptor Amplitude and Phase Difference Measure - Partial Path Generation	276
Sum of Absolute Differences - Motion Generation	280
Amplitude and Phase Difference Using Fourier Descriptors - Motion Generation	282
Sum of Absolute Differences - Partial Curve Motion Generation	285
Amplitude and Phase Difference Using Fourier Descriptors - Partial Curve Motion Generation	288
Summary	291
CHAPTER 10. DATABASE GENERATION	295
CHAPTER 11. CONCLUSIONS	313
Recommendations for Future Work	318
APPENDIX A. FOURIER AMPLITUDE & PHASE DIFFERENCE: WEIGHTING SELECTION AND VARIOUS PATH TYPES	319
APPENDIX B. MOTION GENERATION WEIGHTING FACTORS	327
APPENDIX C. SOLUTION GENERATION: MECHANISMS AND PATHS	349
REFERENCES	371

LIST OF TABLES

Table 3.1:	Summary of design considerations for motion generation	38
Table 3.2:	Summary of design considerations for path generation	40
Table 4.1:	Function generation - data string of input/output	55
Table 4.2:	Path generation - data string of input/output	56
Table 4.3:	Motion generation - data string of input/output	57
Table 4.4:	Fourier coefficients of $f(x)$ and $g(x)$, $g(x) = 2*f(x)$	68
Table 4.5:	Fourier coefficients of $f(x)$ and $g(x)$, $g(x) = f(x) + 2$	70
Table 4.6:	Fourier coefficients of $f(x)$ and $g(x)$, $g(x) = f(x + 32)$	72
Table 4.7:	Fourier coefficients of trace point path	81
Table 4.8:	Fourier coefficients of trace point path with centroid translated to global axis	82
Table 4.9:	Fourier coefficients of trace point path spatially transformed to global axis, rotated, and scaled	83
Table 4.10:	Fourier coefficients of trace point path, starting point for tracing curve shifted by 180 degrees	85
Table 4.11:	Top 8 Fourier descriptors of trace point path	87
Table 4.12:	Top 16 Fourier descriptors of trace point path	90
Table 4.13:	Error in Trace Point Path Reconstruction	90
Table 4.14:	Invariant moments of selected trace point paths	98
Table 6.1:	Summary of database four-bar mechanisms	123

Table 6.2:	Summary of database four-bar mechanisms	124
Table 6.3:	Summary of database four-bar mechanisms	125
Table 6.4:	Summary of database four-bar mechanisms	126
Table 6.5:	Summary of database search using cross-correlation	131
Table 6.6:	Summary of database search using absolute difference	134
Table 6.7:	Summary of database search using squared difference	136
Table 6.8:	Summary of database search using frequency correlation	138
Table 6.9:	Summary of database search using phase-only filter	140
Table 6.10:	Summary of database search using symmetric phase-only matched filtering	142
Table 6.11:	Summary of database search using amplitude difference of Fourier descriptors	144
Table 6.12:	Summary of database search using amplitude and phase difference of Fourier descriptors	146
Table 6.13:	Summary of database search using absolute difference	151
Table 6.14:	Summary of database search using amplitude and phase difference of Fourier descriptors	153
Table 6.15:	Performance of various methods to measure the similarity of a desired solution to 145 filed solutions - full drive crank rotation	156
Table 6.16:	Performance of various methods to measure the similarity of a desired solution to 145 filed solutions - partial drive crank rotation	156
Table 6.17:	Performance of various methods to generate 145 solutions and to search and identify similar solutions	157
Table 7.1:	Top 16 Fourier descriptors of example trace point path	162
Table 7.2:	Summary of grid configuration of database four-bar mechanisms	164

Table 7.3:	Summary of database search of trace point paths using absolute differences	168
Table 7.4:	Summary of database search of trace point paths using squared differences	171
Table 7.5:	Summary of database search of trace point paths using correlation of Fourier descriptors	175
Table 7.6:	Summary of database search of trace point paths using phase-only filter	176
Table 7.7:	Summary of database search of trace point paths using symmetric phase-only matched filter	178
Table 7.8:	Summary of database search using amplitude difference of Fourier descriptors	181
Table 7.9:	Summary of database search using amplitude and phase difference of Fourier descriptors	183
Table 7.10:	Summary of database search of trace point paths using correlation of Fourier descriptors	185
Table 7.11:	Summary of database search of trace point paths using phase-only filter	186
Table 7.12:	Summary of database search of trace point paths using symmetric phase-only matched filter	188
Table 7.13:	Summary of database search of trace point paths using invariant moments and normalized cross correlation	191
Table 7.14:	Summary of database search of trace point paths using invariant moments and sum of percentage difference	194
Table 7.15:	Summary of database search of trace point paths using absolute difference	199
Table 7.16:	Summary of database search of partial trace point paths using amplitude and phase difference	201
Table 7.17:	Summary of database search of partial trace point paths using symmetric phase only matched filter	203

Table 7.18:	Performance of various methods to measure the similarity of a desired solution to 145 filed solutions - full drive crank rotation	205
Table 7.19:	Performance of various methods to measure the similarity of a desired solution to 145 filed solutions - partial drive crank rotation	206
Table 7.20:	Performance of various methods to generate 145 solutions and to search and identify similar solutions	209
Table 8.1:	Summary of database search using absolute difference	216
Table 8.2:	Summary of database search using amplitude and phase difference of Fourier descriptors	219
Table 8.3:	Summary of database search using symmetric phase only matched filtering	222
Table 8.4:	Summary of database search of trace point paths using absolute difference	228
Table 8.5:	Summary of database search of partial trace point paths using amplitude and phase difference	230
Table 8.6:	Summary of database search of partial trace point paths using symmetric phase only matched filter	233
Table 8.7:	Performance of various methods to measure the similarity of a desired solution to 145 filed solutions - full drive crank rotation	235
Table 8.8:	Performance of various methods to measure the similarity of a desired solution to 145 filed solutions - partial drive crank rotation	235
Table 8.9:	Performance of various methods to generate 145 solutions and to search and identify similar solutions	236
Table 9.1:	Summary of database search of trace point paths using absolute difference - Cubic Spline	245
Table 9.2:	Summary of database search of trace point paths using amplitude and phase difference measure of Fourier descriptors - Cubic Spline	248

Table 9.3:	Summary of database search of partial trace point paths using absolute difference - Cubic Spline	249
Table 9.4:	Summary of database search of partial trace point paths using amplitude and phase difference measure of Fourier descriptors - Cubic Spline	252
Table 9.5:	Summary of database search of trace point motion using absolute difference - Cubic Spline	256
Table 9.6:	Summary of database search of trace point motion using amplitude and phase difference measure of Fourier descriptors - Cubic Spline	259
Table 9.7:	Summary of database search of partial trace point motion using absolute difference - Cubic Spline	262
Table 9.8:	Summary of database search of partial trace point motion using amplitude and phase difference measure of Fourier descriptors - Cubic Spline	265
Table 9.9:	Summary of database search of trace point paths using absolute difference - B-Spline	271
Table 9.10:	Summary of database search of trace point paths using amplitude and phase difference measure of Fourier descriptors - B-Spline	274
Table 9.11:	Summary of database search of partial trace point paths using absolute difference - B-Spline	275
Table 9.12:	Summary of database search of partial trace point paths using amplitude and phase difference measure of Fourier descriptors - B-Spline	278
Table 9.13:	Summary of database search of trace point motion using absolute difference - B-Spline	282
Table 9.14:	Summary of database search of trace point motion using amplitude and phase difference measure of Fourier descriptors - B-Spline	285
Table 9.15:	Summary of database search of partial trace point motion using absolute difference - B Spline	287

Table 9.16:	Summary of database search of partial trace point motion using amplitude and phase difference measure of Fourier descriptors - B-Spline	290
Table 9.17:	Performance of cubic splines and B-splines for path generation using 16 data points from database curve number 3 - full crank rotation	293
Table 9.18:	Performance of cubic splines and B-splines for path generation using 16 data points from database curve number 3 - partial crank rotation	293
Table 9.19:	Performance of cubic splines and B-splines for motion generation using 16 data points from database curve number 3 - full crank rotation	294
Table 9.20:	Performance of cubic splines and B-splines for motion generation using 16 data points from database curve number 3 - partial crank rotation	294
Table 10.1:	Summary of database search of 500 candidate trace point paths using amplitude and phase difference	299
Table 10.2:	Summary of database search of 550 candidate trace point paths using amplitude and phase difference	301
Table 10.3:	Summary of database search of 600 candidate trace point paths using amplitude and phase difference	303
Table 10.4:	Summary of candidate trace point paths generated through the random search and refinement process	304
Table 10.5:	Summary of database search of 500 candidate partial trace point paths using amplitude and phase difference	307
Table 10.6:	Summary of database search of 550 candidate partial trace point paths using amplitude and phase difference	309
Table 10.7:	Summary of database search of 600 candidate partial trace point paths using amplitude and phase difference	311

Table 10.8:	Summary of candidate partial curves generated through the random search and refinement process	312
Table A.1:	Fourier amplitude and phase difference ranking. Solutions matching absolute difference ranking Desired Solution = #3	320
Table A.2:	Database Solution Ranking Weighting applied to Fourier amplitude and phase difference: $n = 0.3$	321
Table B.1:	Absolute difference measure, path and angle difference contributions. $p = 1.0, q = 0.0$	330
Table B.2:	Absolute difference measure, path and angle difference contributions. $p = 0.5, q = 0.5$	332
Table B.3:	Absolute difference measure, path and angle difference contributions. $p = 0.0, q = 1.0$	334
Table B.4:	Absolute difference measure, path and angle difference contributions. $p = 0.7, q = 0.3$	336
Table B.5:	Amplitude and phase difference measure, path and angle difference contributions. $p = 1.0, q = 0.0$	340
Table B.6:	Amplitude and phase difference measure, path and angle difference contributions. $p = 0.5, q = 0.5$	342
Table B.7:	Amplitude and phase difference measure, path and angle difference contributions. $p = 0.0, q = 1.0$	344
Table B.8:	Amplitude and phase difference measure, path and angle difference contributions. $p = 0.6, q = 0.4$	346
Table C.1:	Summary of candidate trace point paths generated through the random search and refinement process - closed curves	349
Table C.2:	Summary of candidate trace point paths generated through the random search and refinement process - partial curves	360

LIST OF FIGURES

Figure 1.1:	Four-bar mechanism	2
Figure 1.2:	Function generation	4
Figure 1.3:	Path generation	5
Figure 1.4:	Motion generation	6
Figure 1.5:	Four-bar mechanism variables	6
Figure 2.1:	Crank-rocker four-bar mechanism	13
Figure 2.2:	Double-crank four-bar mechanism	14
Figure 2.3:	Double-rocker four-bar mechanism	15
Figure 2.4:	Parallel-crank four-bar mechanism	16
Figure 2.5:	Four-bar mechanism transmission angle	17
Figure 2.6:	Four-bar mechanism minimum transmission angle	18
Figure 2.7:	Closures of a four-bar mechanism	19
Figure 2.8:	Cognates of a four-bar mechanism	20
Figure 3.1:	Example page from "Analysis of the Four-Bar Linkage"	24
Figure 3.2:	Example of a grid configuration fixed to connecting rod	26
Figure 3.3:	Graphical synthesis - two position motion generation	29
Figure 3.4:	Graphical synthesis - three position motion generation	29
Figure 3.5:	Graphical synthesis - three position path generation	30
Figure 3.6:	Dyads forming a closed loop	34
Figure 3.7:	Dyads used between two positions	37
Figure 3.8:	Function generation - dyads at three positions	39

Figure 3.9:	Desired curve path and a candidate curve solution	43
Figure 3.10:	Angle function of a plane, closed curve	44
Figure 4.1:	Function generation - graph of input/output	55
Figure 4.2:	Plot of $f(x)$ and $g(x)$, $g(x) = 2*f(x)$	67
Figure 4.3:	Plot of the Fourier spectrum $ F(u) $	69
Figure 4.4:	Plot of $f(x)$ and $g(x)$, $g(x) = f(x) + 2$	69
Figure 4.5:	Plot of $f(x)$ and $g(x)$, $g(x) = f(x + \gamma)$, $\gamma = 32$	71
Figure 4.6:	Graph of trace point path for four-bar mechanism	74
Figure 4.7:	Graph of matrix of trace point path	75
Figure 4.8:	Two-dimensional gray scale representation of the Fourier transform of trace point path	75
Figure 4.9:	Spatially transformed trace point path	76
Figure 4.10:	Graph of matrix of spatially transformed trace point path	77
Figure 4.11:	Gray scale representation of the Fourier transform of spatially transformed trace point path	77
Figure 4.12:	Plot of Fourier spectrum of trace point path	80
Figure 4.13:	Plot of Fourier spectrum of trace point path with centroid spatially transformed to global axis	81
Figure 4.14:	Plot of Fourier spectrum of trace point path spatially transformed to the origin of global axis, rotated, and scaled	83
Figure 4.15:	Spatially transformed trace point path described 128 points	86
Figure 4.16:	Trace point path reconstructed using 8 Fourier descriptors	88
Figure 4.17:	Trace Point path reconstructed using 16 Fourier descriptors	89

Figure 4.18: Top 16 Fourier descriptors for trace point path	92
Figure 4.19: Inverse Fourier transform of top 16 Fourier descriptors	92
Figure 4.20: Top 128 Fourier descriptors for trace point path	93
Figure 4.21: Inverse Fourier transform of top 128 Fourier descriptors	93
Figure 4.22: Spatially transformed trace point path	97
Figure 4.23: Trace point path rotated 90°	97
Figure 4.24: Trace point path rotated 180°	98
Figure 5.1: Trace point path and spatially transformed path	101
Figure 5.2: Centroid of trace point path - Xcen, Ycen	102
Figure 5.3: Maximum radius of trace point path - Rmax	104
Figure 5.4: Angle θ of trace point path	105
Figure 5.5: Spatially transformed trace point path	106
Figure 6.1: Follower crank angle as a function of drive crank angle	119
Figure 6.2: Drive crank angle and follower crank angle	119
Figure 6.3: Follower crank angle normalized for average value	121
Figure 6.4: Follower crank angle normalized for average value and for phase shift	122
Figure 6.5: Fourier transform of normalized follower crank angle	122
Figure 6.6: Plot of normalized follower crank angle of desired curve	128
Figure 6.7: Graph of cross-correlation of desired function with 145 database functions	130
Figure 6.8: Graph of top 5 cross-correlation functions	130

Figure 6.9:	Graph of absolute difference of desired function with 145 database functions	132
Figure 6.10:	Graph of top 5 absolute difference functions	133
Figure 6.11:	Graph of squared difference of desired function with 145 database functions	135
Figure 6.12:	Graph of correlation using Fourier descriptors	137
Figure 6.13:	Graph of top 5 functions using frequency correlation	138
Figure 6.14:	Graph of phase-only filter using Fourier descriptors	139
Figure 6.15:	Graph of top 5 functions using phase-only filter	140
Figure 6.16:	Graph of symmetric phase-only matched filtering	141
Figure 6.17:	Graph of top 5 functions using symmetric phase-only matched filtering	142
Figure 6.18:	Graph of amplitude difference of Fourier descriptors	143
Figure 6.19:	Graph of top 5 functions using amplitude difference of Fourier descriptors	144
Figure 6.20:	Graph of amplitude and phase difference of Fourier descriptors	145
Figure 6.21:	Graph of top 5 functions using amplitude and phase difference of Fourier descriptors	146
Figure 6.22:	Follower crank angle as a function of drive crank angle from 0 to 90 degrees	147
Figure 6.23:	Follower crank angle normalized for average value	148
Figure 6.24:	Graph of absolute difference of partial curve with 145 database functions	150
Figure 6.25:	Graph of top 5 functions using absolute difference	151
Figure 6.26:	Graph of amplitude and phase difference of Fourier descriptors	152

Figure 6.27:	Graph of top 5 functions using amplitude and phase difference of Fourier descriptors	153
Figure 7.1:	Example four-bar mechanism trace point path	159
Figure 7.2:	Normalized trace point path	161
Figure 7.3:	Plot of normalized desired trace point path	166
Figure 7.4:	Graph of absolute difference of desired trace point path with 145 database trace point paths	169
Figure 7.5:	Graph of the top 5 database trace point paths identified by absolute difference	169
Figure 7.6:	Graph of squared difference of desired trace point path with 145 database trace point paths	172
Figure 7.7:	Graph of the top 5 database trace point paths identified by squared difference	172
Figure 7.8:	Graph of the correlation using Fourier descriptors of the desired trace point path with 145 database trace point paths	174
Figure 7.9:	Graph of the top 5 database trace point paths identified using correlation of Fourier descriptors	174
Figure 7.10:	Graph of the correlation using phase-only filter	177
Figure 7.11:	Graph of the top 5 database trace point paths identified by using a phase-only filter	177
Figure 7.12:	Graph of the correlation using symmetric phase-only matched filter	179
Figure 7.13:	Graph of the top 5 database trace point paths identified using a symmetric phase-only matched filter	179
Figure 7.14:	Graph of amplitude difference of Fourier descriptors	180
Figure 7.15:	Graph of top 5 database trace point paths using amplitude difference of Fourier descriptors	181
Figure 7.16:	Graph of amplitude and phase difference of Fourier descriptors	182

Figure 7.17:	Graph of top 5 trace point paths using amplitude and phase difference of Fourier descriptors	183
Figure 7.18:	Graph of the correlation using Fourier descriptors of the desired trace point path with 145 database trace point paths	184
Figure 7.19:	Graph of the top 5 database trace point paths identified using correlation of Fourier descriptors	185
Figure 7.20:	Graph of correlation using phase-only filter	187
Figure 7.21:	Graph of top 5 database trace point paths identified by using a phase-only filter	187
Figure 7.22:	Graph of the correlation using symmetric phase-only matched filter	189
Figure 7.23:	Graph of the top 5 database trace point paths identified using a symmetric phase-only matched filter	189
Figure 7.24:	Graph of the correlation using invariant moments and normalized cross correlation	191
Figure 7.25:	Graph of the top 5 database trace point paths identified using invariant moments and normalized cross correlation	192
Figure 7.26:	Graph of the correlation using invariant moments and sum of percentage difference	193
Figure 7.27:	Graph of the top 5 database trace point paths identified using invariant moments and sum of percentage difference	194
Figure 7.28:	Trace point path resulting from the drive crank angle moving from 0 to 90 degrees	195
Figure 7.29:	Trace point path normalized for position, rotation, and scale	197
Figure 7.30:	Graph of absolute difference of partial curve path with 145 database trace point paths	198
Figure 7.31:	Graph of the top 5 database partial trace point paths identified by absolute difference	199
Figure 7.32:	Graph of amplitude and phase difference of Fourier descriptors	200

Figure 7.33:	Graph of top 5 partial trace point paths identified using amplitude and phase difference	201
Figure 7.34:	Graph of correlation using symmetric phase only matched filter	202
Figure 7.35:	Graph of top 5 partial trace point paths identified using symmetric phase only matched filter	203
Figure 8.1:	Two-dimensional plot of the trace point path	209
Figure 8.2:	Normalized plot of the trace point relative angle	210
Figure 8.3:	Three-dimensional plot of the trace point path and connecting rod angle for the defined example crank-rocker	210
Figure 8.4:	Two-Dimensional Fourier transform of trace point path	211
Figure 8.5:	Two-Dimensional Fourier transform of trace point path and connecting rod angle	211
Figure 8.6:	Normalized plot of desired motion	212
Figure 8.7:	Graph of absolute difference of desired motion with 145 filed trace point motion	215
Figure 8.8:	Graph of the top 5 filed trace point paths identified by absolute difference measure (motion generation)	215
Figure 8.9:	Graph of the top 5 filed connecting rod angle identified by absolute difference (motion generation)	216
Figure 8.10:	Graph of amplitude and phase difference of desired motion with 145 database candidate solutions	218
Figure 8.11:	Graph of the top 5 filed trace point paths identified by amplitude and phase difference (motion generation)	218
Figure 8.12:	Graph of the top 5 filed connecting rod angle identified by amplitude and phase difference of Fourier descriptors (motion generation)	219

Figure 8.13:	Graph of symmetric phase only filter correlation of desired motion with 145 database candidate solutions	221
Figure 8.14:	Graph of the top 5 filed trace point paths identified by symmetric phase only filter (motion generation)	221
Figure 8.15:	Graph of the top 5 filed connecting rod angle identified by symmetric phase only filter (motion generation)	222
Figure 8.16:	Three-dimensional plot of the trace point motion	224
Figure 8.17:	Normalized trace point path	225
Figure 8.18:	Graph of absolute difference of partial curve motion with 145 database candidate solutions	226
Figure 8.19:	Graph of the top 5 database trace point paths identified by absolute difference	227
Figure 8.20:	Graph of the top 5 database connecting rod angle identified by absolute difference (motion generation)	227
Figure 8.21:	Graph of amplitude and phase difference of partial curve motion with 145 database candidate solutions	229
Figure 8.22:	Graph of top 5 partial trace point paths identified using amplitude and phase difference of Fourier descriptors	229
Figure 8.23:	Graph of the top 5 database connecting rod angle identified using amplitude and phase difference measure	230
Figure 8.24:	Graph of Fourier two-dimensional symmetric phase only matched filter correlation of partial curve motion with 145 database candidate solutions	231
Figure 8.25:	Graph of the top 5 database partial trace point paths identified using symmetric phase only matched filter	232
Figure 8.26:	Graph of the top 5 database connecting rod angle identified by symmetric phase only filter (motion generation)	232
Figure 9.1:	Trace point path generated by cubic spline	243

Figure 9.2:	Trace point path generated by four-bar mechanism	244
Figure 9.3:	Graph of absolute difference of desired trace point path with 145 database trace point paths - cubic spline	246
Figure 9.4:	Graph of the top 5 database trace point paths identified by absolute difference measure - cubic spline	246
Figure 9.5:	Graph of Fourier descriptor amplitude and phase difference measure of desired trace point path with 145 database trace point paths - cubic spline	247
Figure 9.6:	Graph of the top 5 database trace point paths identified by amplitude and phase difference of Fourier descriptors - cubic spline	248
Figure 9.7:	Graph of absolute difference of desired partial trace point path with 145 database trace point paths - cubic spline	250
Figure 9.8:	Graph of the top 5 database partial trace point paths identified by absolute difference measure - cubic spline	250
Figure 9.9:	Graph of Fourier descriptor amplitude and phase difference measure of desired partial trace point path with 145 database trace point paths - cubic spline	251
Figure 9.10:	Graph of the top 5 database partial trace point paths identified by amplitude and phase difference of Fourier descriptors - cubic spline	252
Figure 9.11:	Normalized path and angle generated by cubic spline	253
Figure 9.12:	Normalized path and angle generated by four-bar mechanism	254
Figure 9.13:	Graph of absolute difference of desired motion with 145 database candidate solutions - cubic spline	255
Figure 9.14:	Graph of the top 5 database trace point paths identified by absolute difference measure (motion generation) - cubic spline	255

Figure 9.15:	Graph of the top 5 database connecting rod angles identified by absolute difference measure (motion generation) - cubic spline	256
Figure 9.16:	Graph of Fourier descriptor amplitude and phase difference measure of desired motion with 145 database candidate solutions - cubic spline	258
Figure 9.17:	Graph of the top 5 database trace point paths identified by amplitude and phase difference of Fourier descriptors (motion generation) - cubic spline	258
Figure 9.18:	Graph of the top 5 database connecting rod angles identified by amplitude and phase difference of Fourier descriptors (motion generation) - cubic spline	259
Figure 9.19:	Graph of absolute difference of desired partial trace point motion with 145 database trace point paths - cubic spline	260
Figure 9.20:	Graph of the top 5 database partial trace point paths identified by absolute difference measure (motion generation) - cubic spline	261
Figure 9.21:	Graph of the top 5 database partial connecting rod angles identified by absolute difference measure (motion generation) - cubic spline	261
Figure 9.22:	Graph of Fourier descriptor amplitude and phase difference measure of desired motion with 145 database candidate solutions - cubic spline	263
Figure 9.23:	Graph of the top 5 database partial trace point paths identified by amplitude and phase difference of Fourier descriptors (motion generation) - cubic spline	264
Figure 9.24:	Graph of the top 5 database partial connecting rod angles identified by amplitude and phase difference of Fourier descriptors (motion generation) - cubic spline	264
Figure 9.25:	Trace point path generated by B-spline	269
Figure 9.26:	Trace point path generated by four-bar mechanism	270

Figure 9.27:	Graph of absolute difference of desired trace point path with 145 database trace point paths - B-spline	271
Figure 9.28:	Graph of the top 5 database trace point paths identified by absolute difference measure - B-spline	272
Figure 9.29:	Graph of Fourier descriptor amplitude and phase difference measure of desired trace point path with 145 database trace point paths - B-spline	273
Figure 9.30:	Graph of the top 5 database trace point paths identified by amplitude and phase difference of Fourier descriptors - B-spline	273
Figure 9.31:	Graph of absolute difference of desired partial trace point path with 145 database trace point paths - B-spline	275
Figure 9.32:	Graph of the top 5 database partial trace point paths identified by absolute difference measure - B-spline	276
Figure 9.33:	Graph of Fourier descriptor amplitude and phase difference measure of desired partial trace point path with 145 database trace point paths - B-spline	277
Figure 9.34:	Graph of the top 5 database partial trace point paths identified by amplitude and phase difference of Fourier descriptors - B-spline	277
Figure 9.35:	Normalized trace point motion generated by B-spline	279
Figure 9.36:	Normalized trace point motion generated by four-bar mechanism	279
Figure 9.37:	Graph of absolute difference of desired trace point motion with 145 database candidate curves - B-spline	280
Figure 9.38:	Graph of the top 5 database trace point paths identified by absolute difference measure (motion generation) - B-spline	281
Figure 9.39:	Graph of the top 5 database connecting rod angles identified by absolute difference measure (motion generation) - B-spline	281

Figure 9.40:	Graph of Fourier descriptor amplitude and phase difference measure of desired motion with 145 database candidate solutions - B-spline	283
Figure 9.41:	Graph of the top 5 database trace point paths identified by amplitude and phase difference of Fourier descriptors (motion generation) - B-spline	284
Figure 9.42:	Graph of the top 5 database connecting rod angles identified by amplitude and phase difference of Fourier descriptors (motion generation) - B-spline	284
Figure 9.43:	Graph of absolute difference of desired motion with 145 database candidate solutions - B-spline	286
Figure 9.44:	Graph of the top 5 database partial trace point paths identified by absolute difference measure (motion generation) - B-spline	286
Figure 9.45:	Graph of the top 5 database partial connecting rod angles identified by absolute difference measure (motion generation) - B-spline	287
Figure 9.46:	Graph of Fourier descriptor amplitude and phase difference measure of desired motion with 145 database candidate solutions - B-spline	289
Figure 9.47:	Graph of the top 5 database partial trace point paths identified by amplitude and phase difference of Fourier descriptors (motion generation) - B-spline	289
Figure 9.48:	Graph of the top 5 database connecting rod angles identified by amplitude and phase difference of Fourier descriptors (motion generation) - B-spline	290
Figure 10.1:	Graph of amplitude and phase difference of Fourier descriptors of desired trace point path and 500 candidate paths	298
Figure 10.2:	Graph of amplitude and phase difference of Fourier descriptors of desired trace point path and 550 candidate paths	300

Figure 10.3: Graph of amplitude and phase difference of Fourier descriptors of desired trace point path and 600 candidate paths	302
Figure 10.4: Graph of synthesized trace point path using amplitude and phase difference measure of Fourier descriptors	303
Figure 10.5: Graph of amplitude and phase difference of Fourier descriptors of desired trace point path and 500 candidate paths	306
Figure 10.6: Graph of amplitude and phase difference of Fourier descriptors of desired trace point path and 550 candidate paths	308
Figure 10.7: Graph of amplitude and phase difference of Fourier descriptors of desired trace point path and 600 candidate paths	310
Figure 10.8: Graph of synthesized trace point path using amplitude and phase difference measure of Fourier descriptors	311
Figure A.1: Database Trace Point Path #14	322
Figure A.2: Database Trace Point Path #28	322
Figure A.3: Database Trace Point Path #42	323
Figure A.4: Database Trace Point Path #56	323
Figure A.5: Database Trace Point Path #70	324
Figure A.6: Database Trace Point Path #84	324
Figure A.7: Database Trace Point Path #98	325
Figure A.8: Database Trace Point Path #112	325
Figure A.9: Database Trace Point Path #126	326
Figure A.10: Database Trace Point Path #140	327
Figure B.1: Graph of absolute difference of desired motion with 145 candidate solutions, $p=1.0$, $q=0.0$	330
Figure B.2: Graph of the top 5 trace point paths identified by absolute difference (motion generation), $p=1.0$, $q=0.0$	331

Figure B.3: Graph of the top 5 connecting rod angles identified by absolute difference (motion generation), $p=1.0$, $q=0.0$	331
Figure B.4: Graph of absolute difference of desired motion with 145 candidate solutions, $p=0.5$, $q=0.5$	332
Figure B.5: Graph of the top 5 trace point paths identified by absolute difference (motion generation), $p=0.5$, $q=0.5$	333
Figure B.6: Graph of the top 5 connecting rod angles identified by absolute difference (motion generation), $p=0.5$, $q=0.5$	333
Figure B.7: Graph of absolute difference of desired motion with 145 candidate solutions, $p=0.0$, $q=1.0$	334
Figure B.8: Graph of the top 5 trace point paths identified by absolute difference (motion generation), $p=0.0$, $q=1.0$	335
Figure B.9: Graph of the top 5 connecting rod angles identified by absolute difference (motion generation), $p=0.0$, $q=1.0$	335
Figure B.10: Graph of absolute difference of desired motion with 145 candidate solutions, $p=0.7$, $q=0.3$	336
Figure B.11: Graph of the top 5 trace point paths identified by absolute difference (motion generation), $p=0.7$, $q=0.3$	337
Figure B.12: Graph of the top 5 connecting rod angles identified by absolute difference (motion generation), $p=0.7$, $q=0.3$	337
Figure B.13: Graph of amplitude and phase difference of desired motion with 145 candidate solutions, $p=1.0$, $q=0.0$	341
Figure B.14: Graph of the top 5 trace point paths identified by amplitude and phase difference (motion generation), $p=1.0$, $q=0.0$	341
Figure B.15: Graph of the top 5 connecting rod angles identified by amplitude and phase difference (motion generation), $p=1.0$, $q=0.0$	342
Figure B.16: Graph of amplitude and phase difference of desired motion with 145 candidate solutions, $p=0.5$, $q=0.5$	343

Figure B.17: Graph of the top 5 trace point paths identified by amplitude and phase difference (motion generation), $p=0.5$, $q=0.5$	343
Figure B.18: Graph of the top 5 connecting rod angles identified by amplitude and phase difference (motion generation), $p=0.5$, $q=0.5$	344
Figure B.19: Graph of amplitude and phase difference of desired motion with 145 candidate solutions, $p=0.0$, $q=1.0$	345
Figure B.20: Graph of the top 5 trace point paths identified by amplitude and phase difference (motion generation), $p=0.0$, $q=1.0$	345
Figure B.21: Graph of the top 5 connecting rod angles identified by amplitude and phase difference (motion generation), $p=0.0$, $q=1.0$	346
Figure B.22: Graph of amplitude and phase difference of desired motion with 145 candidate solutions, $p=0.6$, $q=0.4$	347
Figure B.23: Graph of the top 5 trace point paths identified by amplitude and phase difference (motion generation), $p=0.6$, $q=0.4$	347
Figure B.24: Graph of the top 5 connecting rod angles identified by amplitude and phase difference (motion generation), $p=1.0$, $q=0.0$	348
Figure C.1: Synthesized trace point path #1 and desired path	350
Figure C.2: Synthesized four-bar mechanism #1	350
Figure C.3: Synthesized trace point path #2 and desired path	351
Figure C.4: Synthesized four-bar mechanism #2	351
Figure C.5: Synthesized trace point path #3 and Desired path	352
Figure C.6: Synthesized four-bar mechanism #3	352
Figure C.7: Synthesized trace point path #4 and desired path	353
Figure C.8: Synthesized four-bar mechanism #4	353

Figure C.9: Synthesized trace point path #5 and desired path	354
Figure C.10: Synthesized four-bar mechanism #5	354
Figure C.11: Synthesized trace point path #6 and desired path	355
Figure C.12: Synthesized four-bar mechanism #6	355
Figure C.13: Synthesized trace point path #7 and desired path	356
Figure C.14: Synthesized four-bar mechanism #7	356
Figure C.15: Synthesized trace point path #8 and desired path	357
Figure C.16: Synthesized four-bar mechanism #8	357
Figure C.17: Synthesized trace point path #9 and desired path	358
Figure C.18: Synthesized four-bar mechanism #9	358
Figure C.19: Synthesized trace point path #10 and desired path	359
Figure C.20: Synthesized four-bar mechanism #10	359
Figure C.21: Synthesized partial path #11 and desired path	361
Figure C.22: Synthesized four-bar mechanism #11	361
Figure C.23: Synthesized partial path #12 and desired path	362
Figure C.24: Synthesized four-bar mechanism #12	362
Figure C.25: Synthesized partial path #13 and desired path	363
Figure C.26: Synthesized four-bar mechanism #13	363
Figure C.27: Synthesized partial path #14 and desired path	364
Figure C.28: Synthesized four-bar mechanism #14	364
Figure C.29: Synthesized partial path #15 and Desired path	365
Figure C.30: Synthesized four-bar mechanism #15	365
Figure C.31: Synthesized partial path #16 and desired path	366
Figure C.32: Synthesized four-bar mechanism #16	366

Figure C.33: Synthesized partial path #17 and desired path	367
Figure C.34: Synthesized four-bar mechanism #17	367
Figure C.35: Synthesized partial path #18 and desired path	368
Figure C.36: Synthesized four-bar mechanism #18	368
Figure C.37: Synthesized partial path #19 and desired path	369
Figure C.38: Synthesized four-bar mechanism #19	369
Figure C.39: Synthesized partial path #20 and Desired path	370
Figure C.40: Synthesized four-bar mechanism #20	370

ACKNOWLEDGEMENTS

I dedicated this work to my wife, Mary, and my children, Chip, Daniel, Elizabeth and Alyse. Thank you for your love and support.

I express my sincere thanks to Dr. Donald Flugrad, Jr. And Dr. Abir Qamhiyah for being my major professors and advisors.

Many thanks to Professor Greg Luecke, Professor Kenneth McConnell and Professor Loren Zachary for serving on the committee and taking their valuable time to read and comment on my dissertation.

CHAPTER 1. INTRODUCTION

A mechanism is a mechanical device that has a purpose of transferring motion and/or a force from a source to an output. A linkage consists of links or bars (generally considered rigid) which are connected by joints to form open or closed loops. A four-bar linkage is the simplest closed loop linkage and has three moving links, one fixed link and four pin joints (Figure 1.1). Planar rigid-body motion consists of rotation about an axis perpendicular to the plane of motion and translation where all points in a body move along identical straight paths. All points embedded in a body remain parallel to their original orientation.

Approaches for the synthesis of four-bar planar mechanisms address the transformation of input motion to an output (e.g. a desired function, path and/or motion) through the use of pivots, links and pin joints. Current synthesis techniques cover a broad range from documented displacement paths and velocities [Hrones & Nelson, 1951], graphical methods [Sandor, 1962][Lindholm, 1969] [Hain, 1967], analytical techniques using precision points [Sandor and Erdman, 1991] [Freudenstein, 1955], analytical techniques using initial estimates of the type and configuration of a mechanism

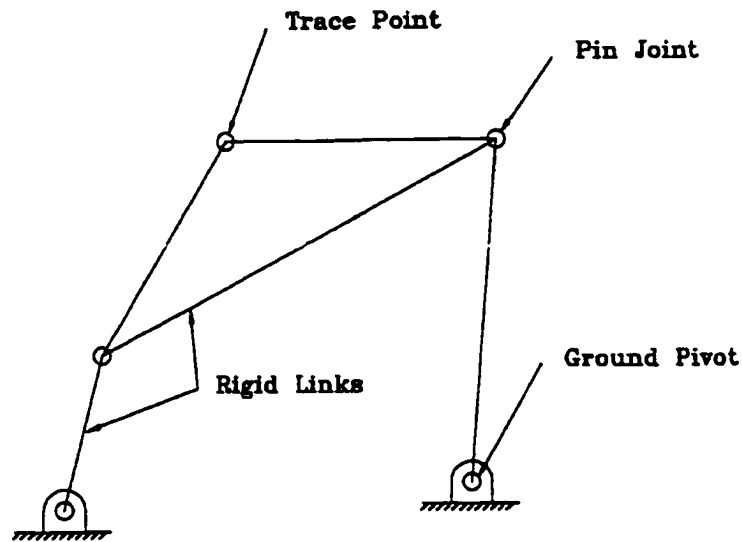


Figure 1.1: Four-bar mechanism

[Subbian,1990], and techniques using Fourier descriptors and global search methods [Kota and Ullah, 1997].

This work deals with the "synthesis" of four-bar linkage mechanisms that have planar rigid-body motion. Hrones and Nelson [1951] characterized the four-bar linkage as "one of the simplest mechanisms and indeed may be regarded as a basic mechanism." The kinematic "synthesis" design problem is focused on the study of the relative motion of the linkage and does not take into account the other two major sub-branches of solid mechanics: statics (the study of forces and moments separate from motion) and kinetics (the study of action of forces). Kinematic "analysis" of a particular mechanism is based on an evaluation of a defined mechanism's

geometry while kinematic "synthesis" is the process of designing a mechanism to accomplish a desired task. Sandor and Erdman [1991] describe kinematic "analysis" as determining the performance of a given mechanism and kinematic "synthesis" as dealing with the systematic design of a mechanism for a given performance. With "Type Synthesis" the first part of the process is to determine the "type" of mechanism to address the required performance [Titus, Erdman and Riley, 1989]. The type of a mechanism may be a cam and follower, a gear train, or a linkage. Determining the type of a mechanism involves defining the number of links and the degrees of freedom. The second part of the synthesis process is related to dimensional synthesis of the mechanism. Based upon the defined type of a linkage (four-bar linkage, slider-crank, cam with roller follower), dimensional synthesis defines the dimensions and the starting point of the mechanism. Specifically this determines the link lengths, pivot distances, angles, gear ratios, cam dimensions, etc.

The design or synthesis of mechanisms has typically been focused on solving three different functional tasks or requirements:

- 1) Function Generation: where the functional requirement is the relative motion between links, which are generally connected to ground pivots (Figure 1.2), or where a specific input position will result in a specific output position;

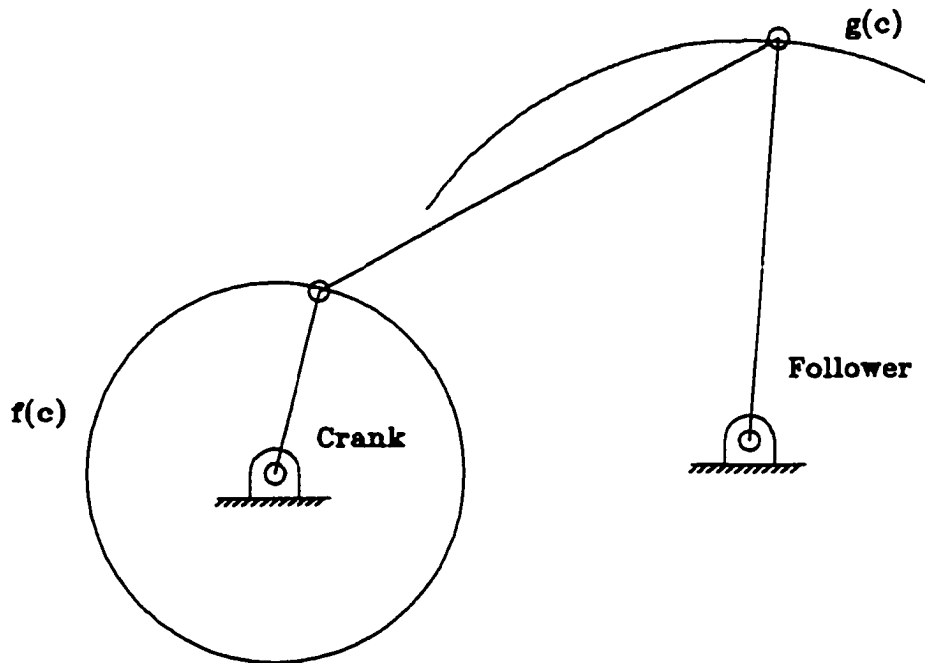


Figure 1.2: Function generation

2) Path Generation: where the functional requirement is the output path of a trace point, which is typically on a coupler link (Figure 1.3);

3) Motion Generation: where the functional requirement is the entire motion, path and angle, of a trace point on a coupler link (Figure 1.4).

The motion or path of a trace point on a coupling link can be expressed as a function of the dimensions of the mechanism and the angle of the input link (Figure 1.5).

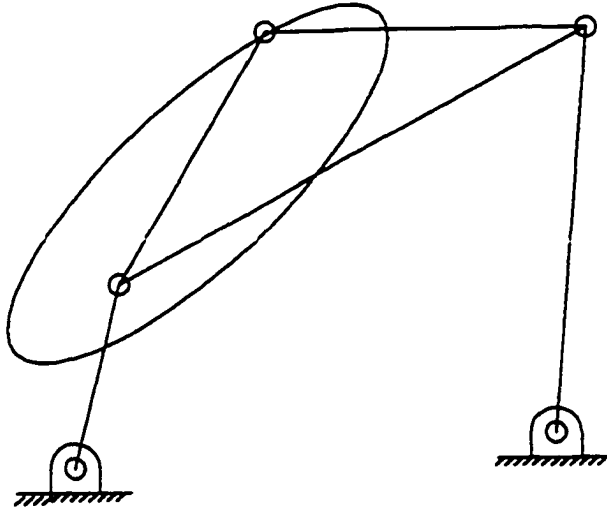


Figure 1.3: Path generation

$$\text{Path} = F(r, \text{DCA}) \quad [1.1]$$

Where:

$$r = (X_0, Y_0, DC, CR, FC, GP, TP, GPA, TPA)$$

DCA = Drive Crank Angle

Where:

X_0 = X Position of Drive Crank Pivot

Y_0 = Y Position of Drive Crank Pivot

DC = Drive Crank Length

CR = Connecting Rod Length

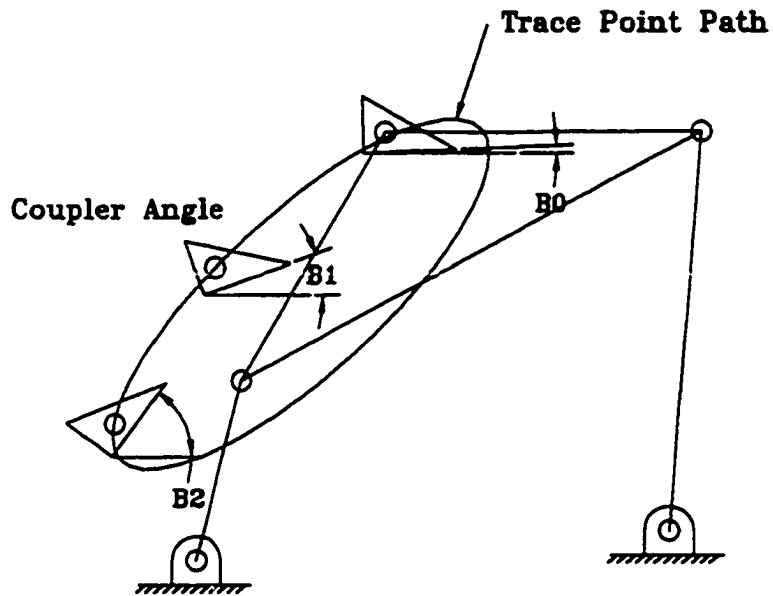


Figure 1.4: Motion generation

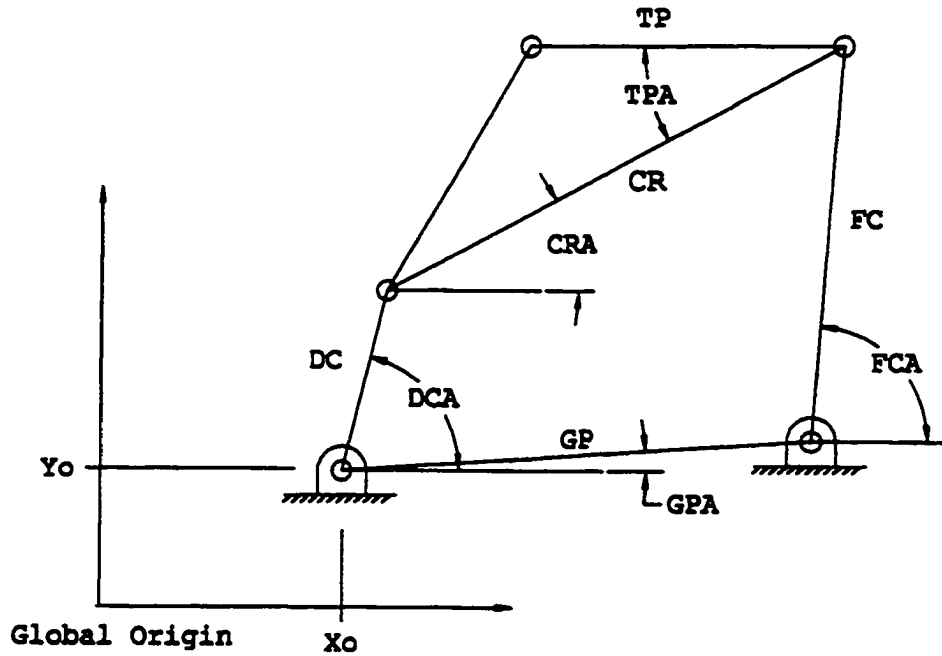


Figure 1.5: Four-bar mechanism variables

FC = Follower Crank Length

GP = Ground Pivot Length

TP = Trace Point Length

GPA = Ground Pivot Angle

TPA = Trace Point Angle

The following angles may easily be derived during the analysis and description of the position and motion of the four-bar mechanism. The angles will over constrain the mechanism if defined with the previously listed variables.

CRA = Connecting Rod Angle

FCA = Follower Crank Angle

The connecting rod angle is always used in conjunction with the body path to fully describe motion generation. The follower crank angle is always used to fully describe the output for function generation.

For planar motion there are three independent variables (or three degrees of freedom) associated with each link in a plane: these can be taken as the X position of the center of gravity, the Y position of the center of gravity, and the angle of the link. A pin, or revolute joint, is located at the end of each link. A pin joint is a lower pair connector where each pin removes two degrees of freedom of relative motion between successive links. The degrees of freedom of a mechanism is the number of independent inputs

required to determine the position of all the links of the mechanism with respect to ground. The degrees of freedom of a four bar linkage with four pin joints can be found by applying Kutzbach Criterion:

$$\text{DOF} = 3(n-1) - 2*f_1 - f_2 \quad [1.2]$$

Where:

DOF = Degrees of Freedom of the mechanism;

n = Number of links,

f1 = Sum of the number of pin joints plus the number of slider joints or pure rolling joints,

f2 = Number of roll-slide joints

Therefore, the degrees of freedom of a four-bar planar mechanism is:

$$\text{DOF} = 3(3-1) - 2*4 - 0 = 1 \quad [1.3]$$

The importance of having one degree of freedom is that by defining the motion of one of the links, which is typically a link attached to ground (i.e. the drive crank) driven by a device (e.g. motor, solenoid, hydraulic cylinder, etc.), the motion of the entire mechanism is defined.

When synthesizing mechanisms, the output function, path, or motion is of interest based upon a specified input. A mechanism is then sought to produce the desired motion with optimization focused

on various aspects of the mechanism (drive angle, ground or mounting locations, drive configuration and type, etc.).

Research Goals

This work presents an approach for the synthesis of four-bar planar mechanisms for function, path, and motion generation based upon the use of invariant descriptors and local database generation and search methods.

Transformation and descriptor methods are used to characterize the output of four-bar planar mechanisms (function, path or motion) and to store the invariant characteristic information in a database. Spatial transforms, one-dimensional Fourier transforms, two-dimensional Fourier transforms, and invariant moments are used to generate invariant characteristic descriptors. The resulting characteristic information for each curve is invariant regardless of the rotation, translation, or scaling of the curves. A description of each method and the relative performance of file development and search methods are developed. Over 8,000 function, path, and motion solutions are generated for global search solutions for each transform and descriptor method. The function, path, and motion solutions are based on the solutions developed by Hrones and Nelson [1951] and on the implementation of a random search of a local design space. Solution comparison and matching techniques are discussed and implemented, which evaluate the deviation of a candidate curve to curves stored in a database.

A methodology is developed to allow the designer to investigate a local design space by generating a database of candidate solutions based on the random development of four-bar mechanisms. The designer may then define a desired solution and search the generated candidate solution files. This technique supports the evaluation of a local solution space, and generation, characterization, and identification of candidate mechanisms that may be practical to implement. After the identification of candidate mechanisms, local optimization techniques may be used with candidate mechanisms.

Dissertation Organization

An overview of four-bar mechanisms, the different types of four-bar mechanisms, and common design considerations are contained in Chapter 2.

The third chapter of the dissertation presents a literature review. The review is focused on synthesis techniques of four-bar mechanisms for function, path, and motion generation.

Details regarding the characterization of solutions for function, path, and motion generation for four-bar mechanisms is contained in Chapter 4.

Details regarding solution comparison and matching methods of a desired solution with solutions stored in a database are contained in Chapter 5.

Details regarding the implementation and performance of the synthesis of four-bar mechanisms for function generation using invariant characterizations, storage, and search methods are contained in Chapter 6.

Details regarding the implementation and performance of the synthesis of four-bar mechanisms for path generation using invariant characterizations, storage, and search methods are contained in Chapter 7.

Details regarding the implementation and performance of the synthesis of four-bar mechanisms for motion generation using invariant characterizations, storage, and search methods are contained in Chapter 8.

Chapter 9 contains details regarding the generation of desired solutions by a designer through the use of parametric cubic splines and B-splines.

Chapter 10 contains a methodology for the development of a database of candidate solutions for a local design space based on the random generation and refinement of system variables for four-bar mechanisms.

Chapter 11 contains the conclusions and recommendations for future work.

CHAPTER 2. THE FOUR-BAR MECHANISM

The four-bar mechanism is a connection of four rigid "link" members that are pin-connected to each other. In many applications one of the links is stationary. This link typically is assumed to be fixed to the ground and each end of that link is called a "ground pivot". A second link attached to one of the ground pivots is typically the drive crank. The drive crank establishes an interface for the four-bar linkage to an external power source. The power source may be a linear actuator, such as a hydraulic cylinder, a linear solenoid, or possibly a rotary actuator such as an electric motor, hydraulic motor, stepping motor, etc. Each link in the four-bar mechanism is a solid body and usually considered a rigid body.

Various classes of four-bar mechanism may be defined based on the input crank motion and the follower crank response: crank and rocker mechanism, drag link mechanism and a double rocker mechanism.

A crank-rocker mechanism is one where the drive crank can make a complete revolution while the follower crank can only oscillate through a limited range (Figure 2.1). The forward and return stroke of the end of the follower crank does not necessarily correspond to equal angular rotations of the drive crank. The criteria for this class of operation is:

- 1) The drive crank must be the shortest length,
- 2) $GPD < CR + FC - DC$ [2.1]
- 3) $GPD > |CR - FC| + DC$ [2.2]

Where:

GPD = Ground Pivot Distance

CR = Connecting Rod Length

FC = Follower Crank Length

DC = Drive Crank Length

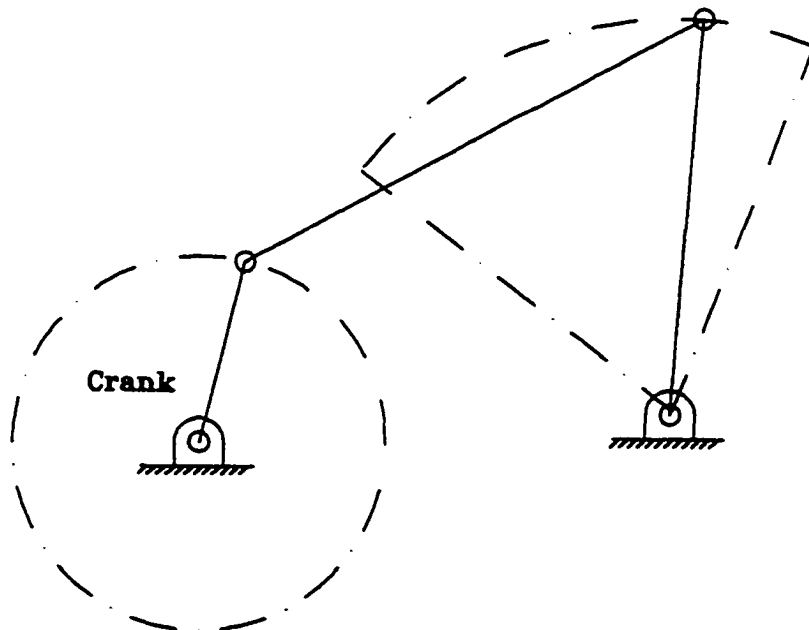


Figure 2.1: Crank-rocker four-bar mechanism

A double-crank or drag-link mechanism is where both cranks are capable of rotating through a complete 360 degrees of angular rotation (Figure 2.2). A uniform rotation of the drive crank typically produces a non-uniform rotation of the follower crank. The criteria for this class of operation is:

- 1) The ground pivot distance must be the shortest link
- 2) $GPD < CR + FC - DC$ [2.3]
- 3) $GPR > |CR - FC| + DR$ [2.4]

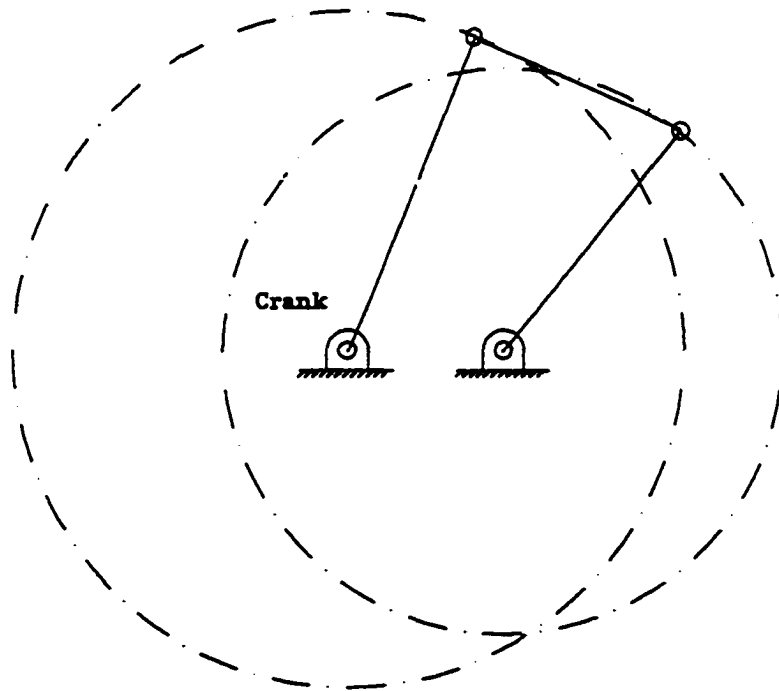


Figure 2.2: Double-crank four-bar mechanism

A double-rocker mechanism is where both cranks can oscillate, but neither can rotate through a complete revolution (Figure 2.3).

The criteria for this class of operation is:

1) The connecting rod is the shortest link

2) $GPD > CR + FC - DC$ [2.5]

3) $GPR < |CR - FC| + DR$ [2.6]

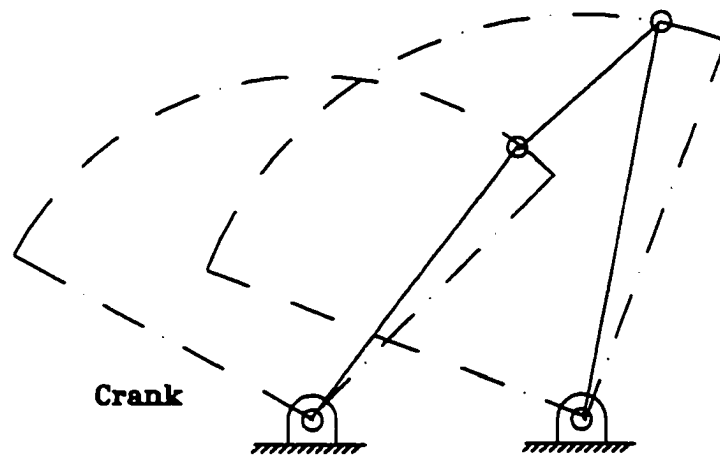


Figure 2.3: Double-rocker four-bar mechanism

All three type of mechanisms can be obtained as inversions of the same linkage (change the link considered to contain the ground pivots) as long as the sum of the lengths of the shortest and longest link is less than the other two (Grashof's rule).

Crank-rocker: shortest link is the drive crank

Drag-link: Shortest link contains the ground pivots

Double-Rocker: shortest link is the connecting rod.

In the event that Grashof's rule is not satisfied, no matter the configuration of links, only a double-rocker mechanism with oscillating couplers is attained.

Mechanisms that approach the limits of Grashof's rule generally do not operate well in practice. One example of a four-bar mechanism that demonstrates this is the parallel-crank (Figure 2.4).

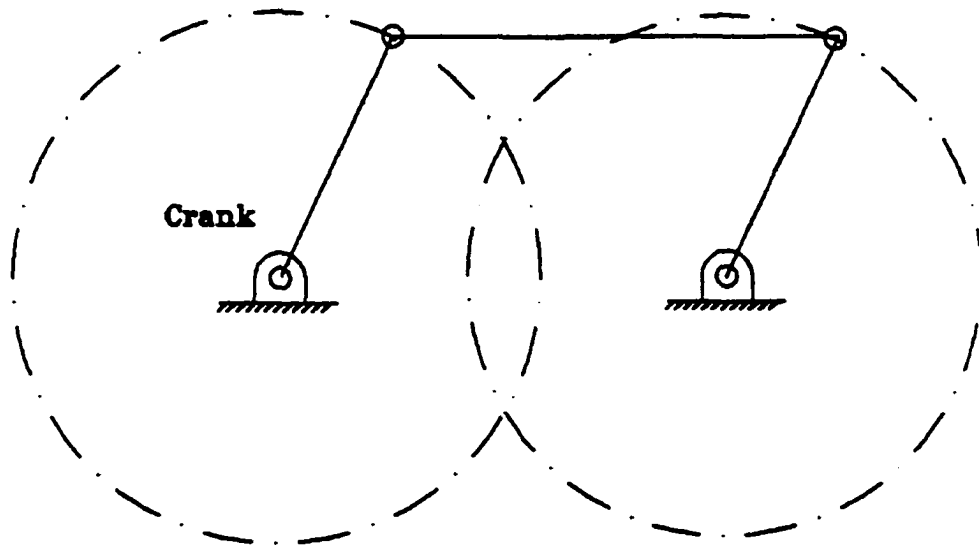


Figure 2.4: Parallel-crank four-bar mechanism

With this mechanism the drive crank and follower crank are the same length and the connecting rod and the ground pivots are the same length. The drive crank and the follower crank will always have the same angular velocity. There are two positions in the cycle when the system is not constrained: when the follower link, the drive crank and the connecting rod are co-linear. At these two positions, called dead points or dead center, the follower could begin to rotate in a direction opposite to that of the drive crank. Inertia, springs, or gravity usually prevent the reversal at the dead point.

One measure to evaluate the acceptability of a four-bar mechanism is with respect to the transmission angle. The transmission angle is the angle between the connecting rod and the output link (Figure 2.5).

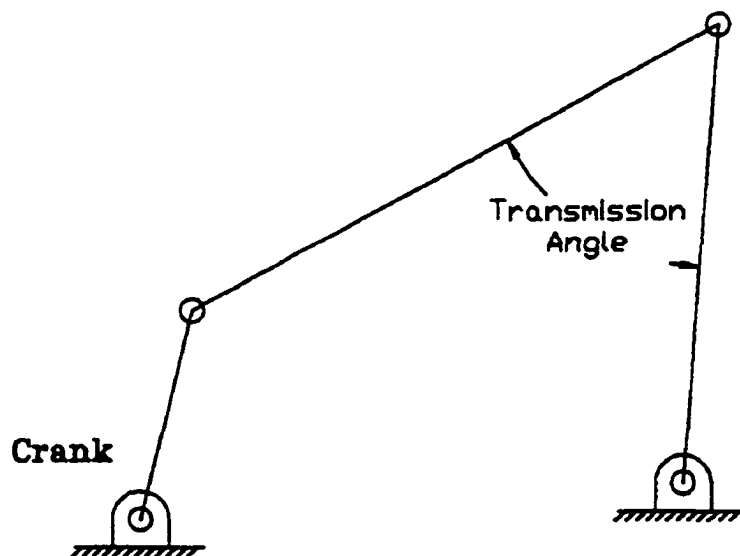


Figure 2.5: Four-bar mechanism transmission angle

H. Alt [1932] first suggested the use of the transmission angle as a quality index for the transmission of motion. Alt recommended a minimum of 40° (maximum 140°) for low-speed and 50° (maximum 130°) for high-speed applications. For crank-rocker four-bar mechanisms, the minimum and maximum angles occur when the drive crank is in line with the ground pivot link (Figure 2.6). For the transmission of forces, an optimum angle would be a transmission angle of 90° , while a transmission angle of 0° would be incapable of transmitting a drive force.

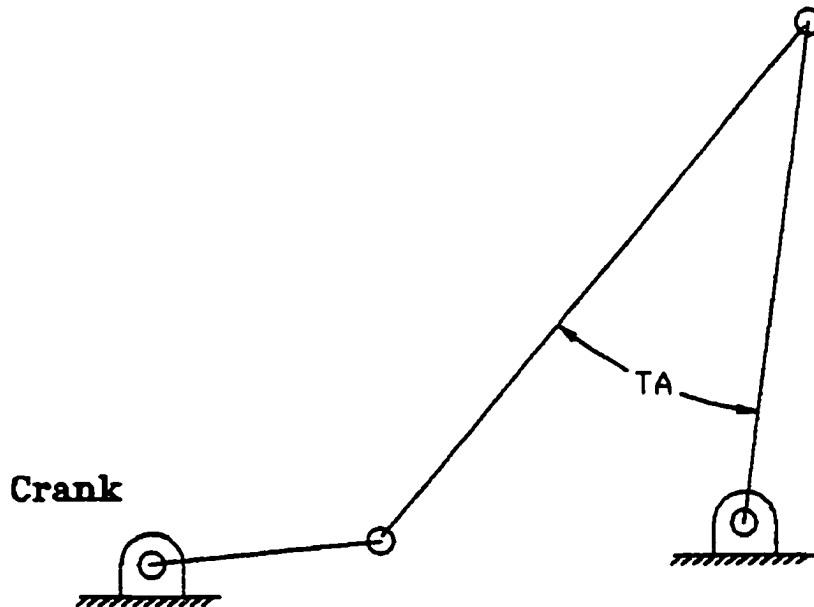


Figure 2.6: Four-bar mechanism minimum transmission angle

For a specific four-bar mechanism, the linkage can be assembled in two configurations (Figure 2.7). The choice between the two configurations is made when the mechanism is closed, and thus the configurations are called "closures".

The choice between the two mechanisms is made based on the alignment of the connecting rod and the follower crank. Grashof's rule applies to each four-bar mechanism.

Cognate mechanisms are two or more mechanisms that give the same motion of a point or link. The cognate for a trace point of a four-bar mechanism is asserted to exist in the Roberts-Chebyshev

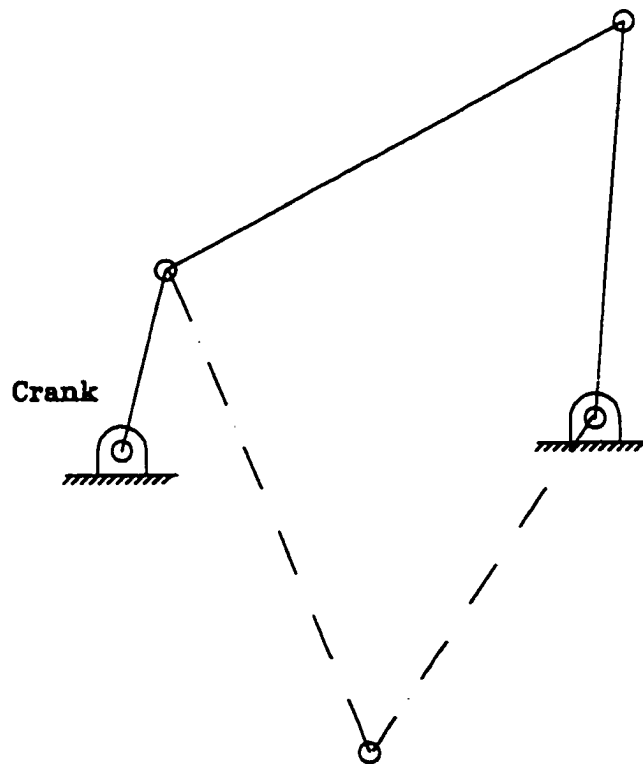


Figure 2.7: Closures of a four-bar mechanism

theorem. A cognate may be found by following the following procedure for a four-bar linkage with a trace point (Figure 2.8):

- Construct parallelograms $A-B-TP-A_1$ and $D-C-TP-D_2$
- Construct triangles A_1-P-C_1 and D_2-P-C_2
- Construct parallelogram $TP-C_1-C_3-C_2$

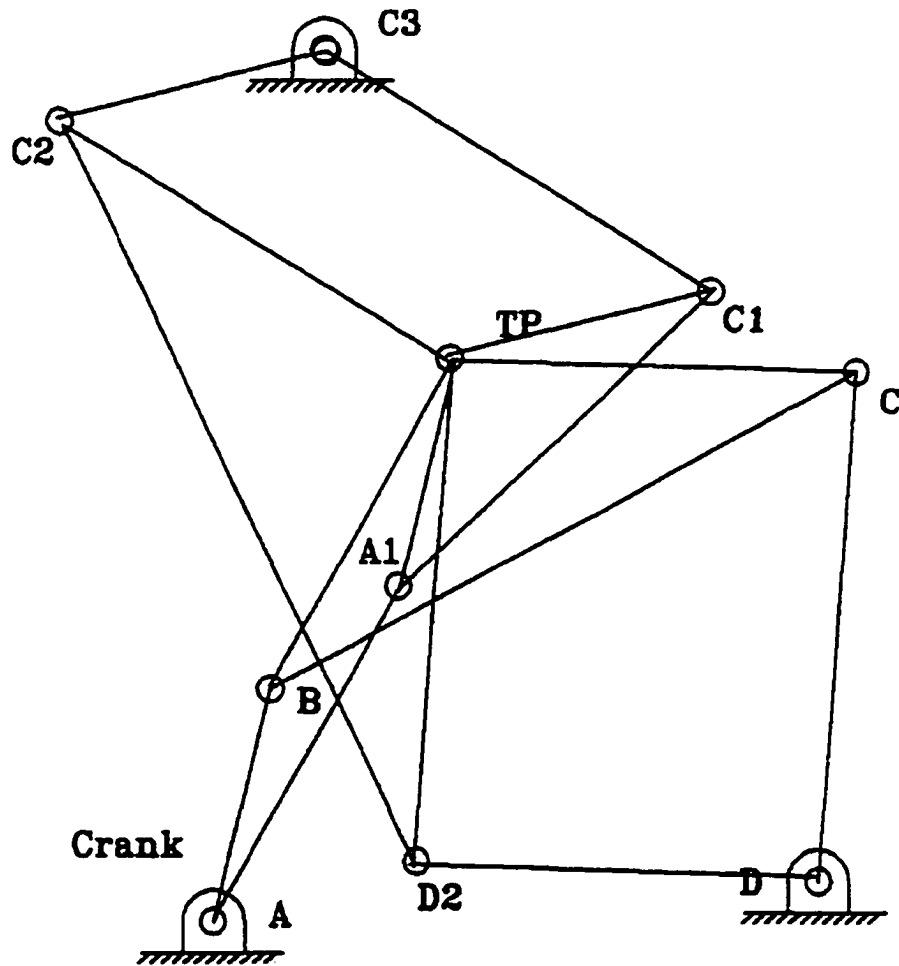


Figure 2.8: Cognates of a four-bar mechanism

The cognate of the original four-bar linkage are $A-A_1-C_1-C_3$ and $B-B_2-C_2-C_3$. In each case TP is the trace point. If A-B is the drive crank in the four-bar linkage, the right hand cognate will generate the same timing on the trace point if C_3C_2 is used as the drive crank and driven at the same speed. The other cognate will produce the same trace point path but will not have similar timing.

CHAPTER 3. LITERATURE REVIEW

The literature review accomplished in this dissertation is focused on an understanding of the established techniques for the synthesis of four-bar mechanisms. The synthesis techniques may address function, path, and motion generation or may be specific to one of the three types of solutions. The techniques include graphed solutions, graphical synthesis, analytical synthesis, and numerical synthesis. A focus of the literature review is also to identify prior work in the area related to four-bar mechanism solution characterization, search, and storage techniques.

Synthesis Techniques

Graphed Displacement Paths

John A. Hrones and George L. Nelson authored "Analysis of the Four-Bar Linkage - Its Application to the Synthesis of Mechanisms" in 1951. The information published represented an "exhaustive survey of the displacement and velocity characteristics of a four-bar linkage in the range of operation where the driving crank makes

a complete revolution while the follower crank oscillates" (ie. crank rocker four-bar mechanism). The focus of the publication was to make available, in a readily usable form, information that would allow the designer to "rapidly synthesize" a linkage to do a specific task. The publication documented over 7,000 displacement paths and velocities at 72 equal intervals of drive crank angles along each solution path. The authors stated that the publication represented about 500,000 solutions and bracketed the complete displacement and velocity performance of the four-bar linkage where the driving crank makes a complete revolution while the follower crank oscillates (crank rocker mechanism). In addition, the authors stated by rapidly looking through the pages the designer can "in a few minutes" determine the basic dimensions of the four-bar linkage that meet a set of requirements, provided that the requirements can be satisfied by the linkage. The publication contained 730 pages of graphed solutions. Each page contained eight to ten curve solutions with a graphical representation of the four-bar mechanism.

Figure 3.1 is a similar graphed solution where the length of the drive crank is 1.0 unit (a default value), the length of the connecting rod is 1.5 units, the length of the follower crank is 1.5 units, and the length between the ground pivots is 1.5 units.

Hrones and Nelson [1951] established a grid relative to the connecting rod to establish a set of "Trace Points", which were used to generate candidate solution curves. The grid was assumed to be

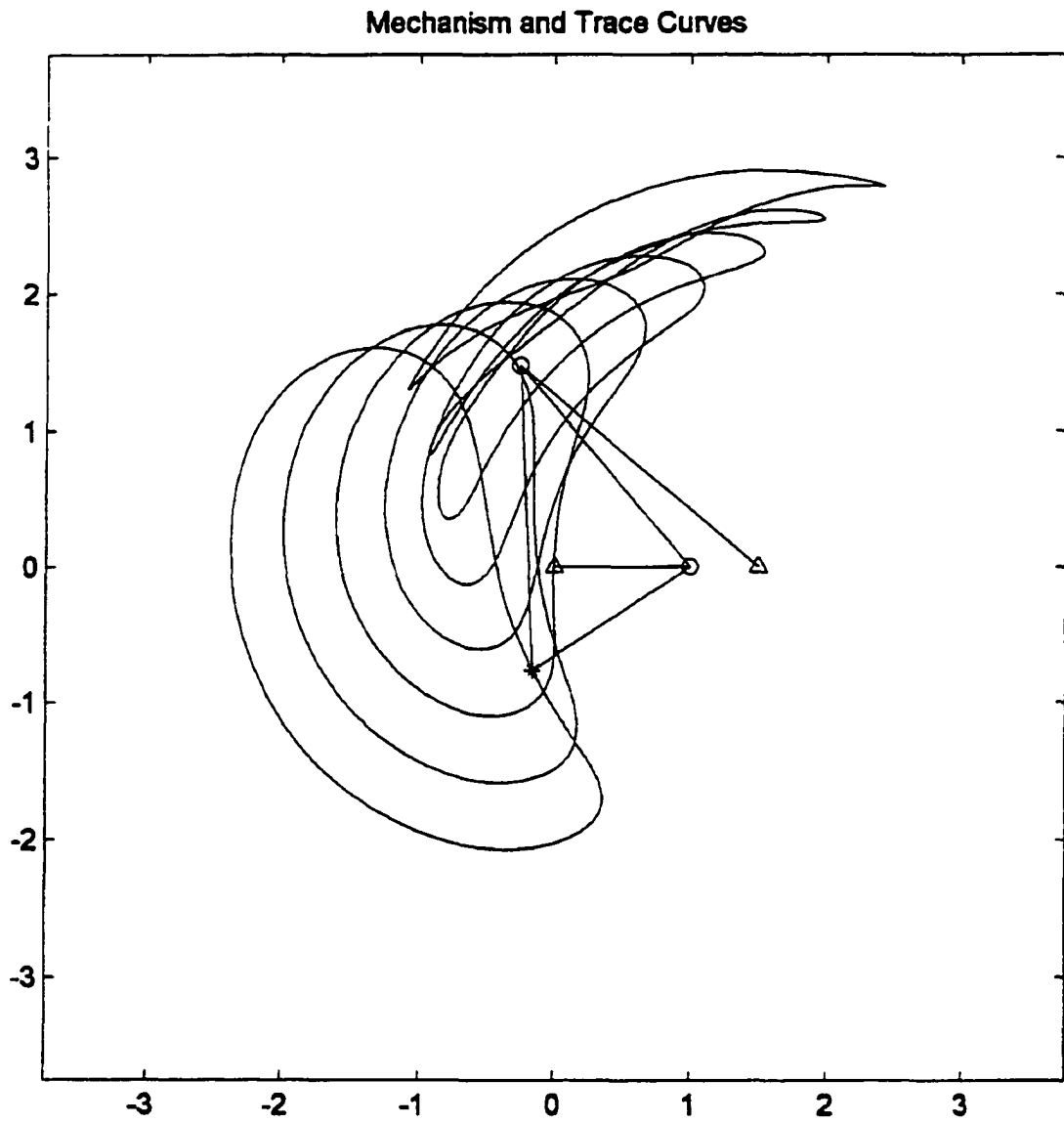


Figure 3.1: Example page from "Analysis of the Four Bar Linkage"

fixed relative to the connecting rod as the four-bar crank rotated through a complete revolution. Complete rotation of the drive crank produced a closed curve for each trace point within the grid. Figure 3.2 is an example of the grid and contains a line of eight trace points parallel to the connecting rod. The line was then replicated in five rows. Each row of trace curves was used to generate one page in the publication. Therefore, by establishing the length of the drive crank (default of 1.0 unit), the connecting rod, the follower crank and the distance between the ground pivots generated five pages in the publication. For the example mechanism in Figure 3.1, there would be a total of 38 candidate solution curves generated. A candidate solution curve was not generated at the end of the drive crank and at the end of the follower crank. The curve generated at the end of the drive crank would be a circle, and an arc would be generated at the end of the follower crank. Each trace curve consisted of 72 dashes that corresponded to a displacement of the point for a 5-degree angular displacement of the drive crank. The authors describe that the trace point acceleration could then be "rapidly" obtained by subtracting vectorially one dash length from an adjacent one and dividing by the square of the time required for the drive crank to rotate through 5 degrees.

Since the charts were generated with the drive crank at a unit length, changing all the links with a specific ratio would not alter the motion characteristic of the mechanism but would only generate a scale change. In cases where linkages shown in the chart bracket

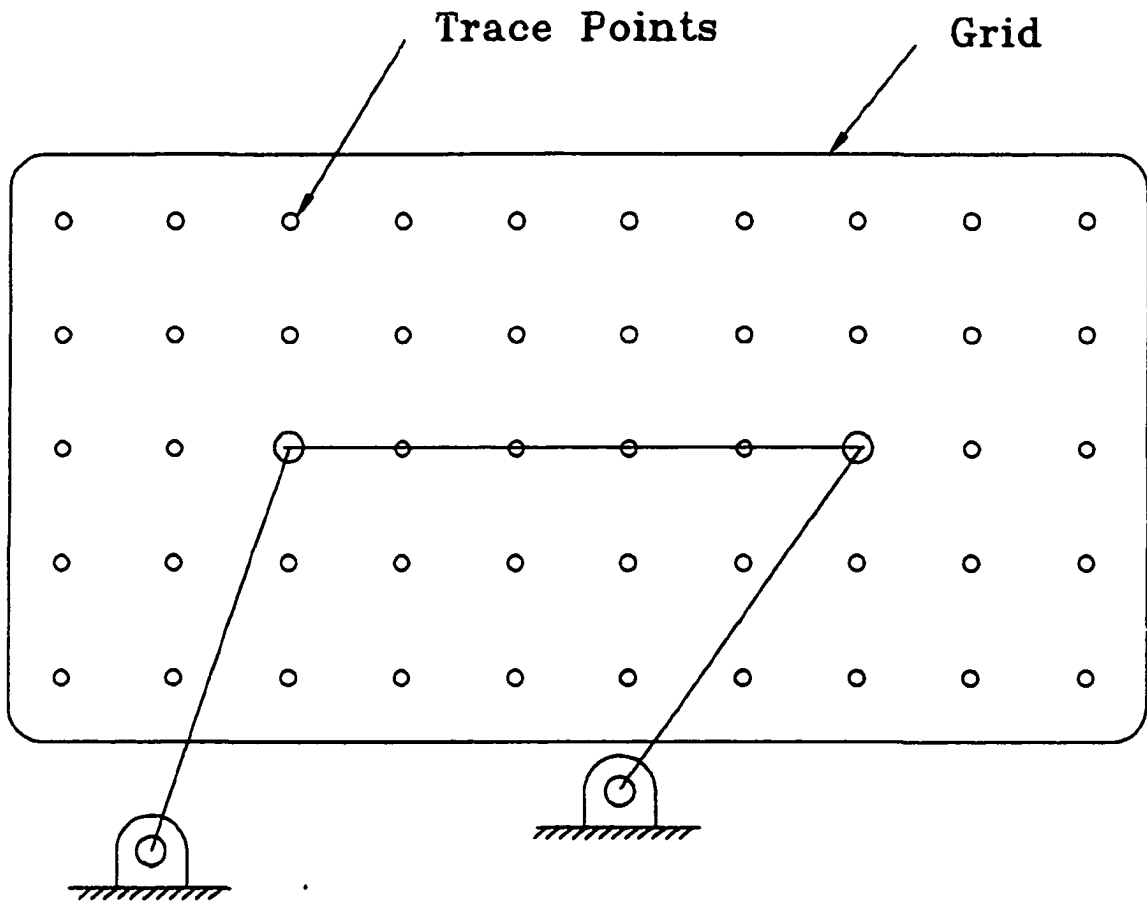


Figure 3.2: Example of a grid configuration fixed to connecting rod

the desired curve characteristics, the authors suggested that models whose ratios lie intermediate between the bracketing linkages could be built from cardboard or sheet aluminum and their behavior studied.

Graphical Synthesis

Graphical synthesis may be used to synthesize a four-bar linkage to move a body through two specified positions at specified angles (motion generation). Two points are established in the translated body. A line segment is constructed which connects each point at the two specified positions. The rotocenter of the body is then found graphically by establishing the normal bisectors of the two line segments and identifying where the normal bisectors cross (Figure 3.3). Two fixed pivots may be established anywhere along the two normal bisectors to define a four-bar linkage which will move a body through the two positions at the prescribed angles. Thus, an infinite number of four-bar mechanisms may be defined which produce a solution. If a pivot is capable of being established at the rotocenter of the body, a rigid body that pivots at the rotocenter may be used as a solution.

Graphical synthesis may be used to synthesize a four-bar linkage to move a body through three specified positions at specified angles (motion generation). With three positions, the two ground pivot points are defined by the intersection of the normal

bisectors generated between defined positions 1 and 2 and defined positions 3 and 4 (Figure 3.4). If one assumes that the pivot points in the moving body are capable of being placed at any location in the body, there exists an infinite number of ground pivot locations that may be established.

Graphical synthesis may be used to synthesize a path generation four-bar linkage for three prescribed positions (Path Generation). The pivot points A_0 and B_0 are free choices left to the designer to select (Figure 3.5). In addition, the length of the drive crank and the distance from the end of the drive crank to the trace point is arbitrary and defined by the designer. The ground pivots are selected and a circle generated about the drive crank pivot at the desired length of the ground pivot. An arc is scribed from the first prescribed point to intersect with the scribed drive crank circle. The intersection is one end of the connecting rod that attaches to the drive crank (A_1). This distance P_1-A_1 is then scribed from P_2 and P_3 to the drive crank circle (define A_2 and A_3). The drive crank length is then scribed about point A_1 and angles $P_2-A_1-A_0$ and $P_3-A_1-A_0$ marked about A_1 ; A_0' and A_0'' are thus defined on the circle scribed about A_1 . An arc is scribed about P_1 with the length of P_2-B_0 and an arc is scribed from A_0' with the length of A_0-B_0 ; the intersection is labeled B_0' . An arc is scribed about P_1 with the length of P_3-B_0 and an arc is scribed from A_0'' with the length of A_0-B_0 ; the intersection is labeled B_0'' . The intersection

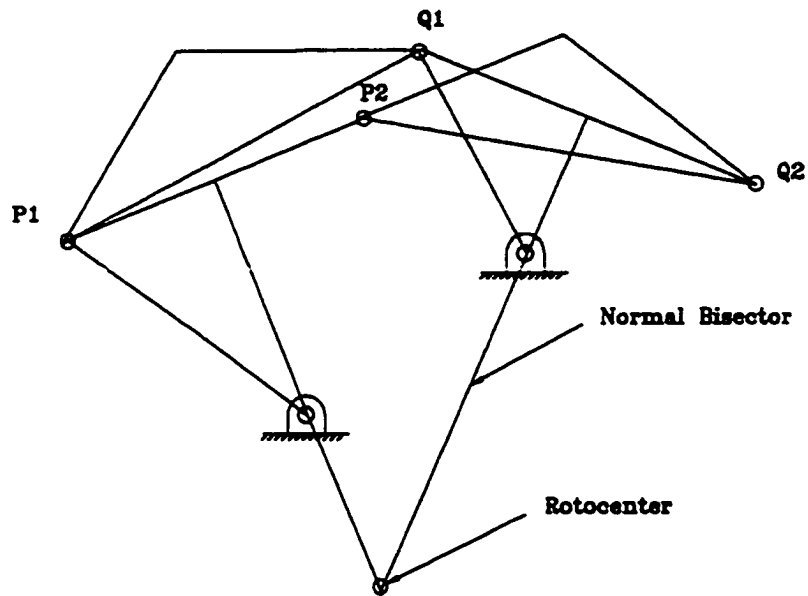


Figure 3.3: Graphical synthesis - two position motion generation

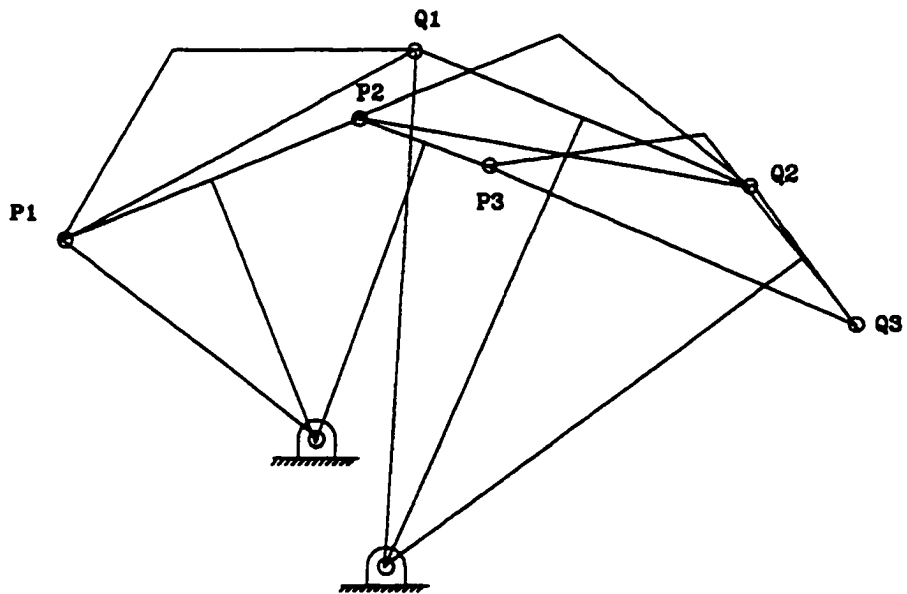


Figure 3.4: Graphical synthesis - three position motion generation

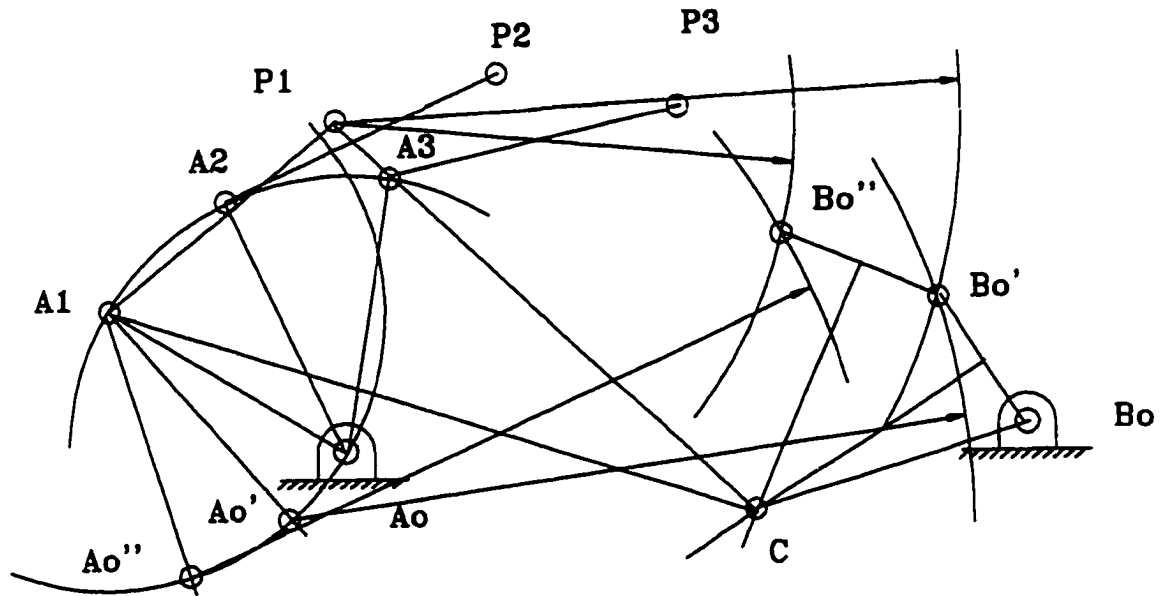


Figure 3.5: Graphical synthesis - three position path generation

of the perpendicular bisection of B_0-B_0' and B_0' and B_0'' is one end of the connecting rod.

We have discussed "motion" generation for a body through two prescribed positions and three prescribed positions and "path" generation for a body through three prescribed points. J. Hirschhorn [1962] in "Kinematics and Dynamics of Plane Mechanisms" reviews graphical methods for the synthesis of four-bar mechanisms in depth. Graphical methods discussed are "motion" generation for a

body through four distinct points, "function" generation for a body with up to five precision positions, and "path" generation for a body with up to six point positions. A graphical "overlay" method is also discussed, which is a trial-and-error procedure for function generation that yields a generated output based upon a tolerance band throughout the range of the mechanism; precision points are not used. Sandor and Erdman [1991] detail a graphical procedure for addressing "path" generation with prescribed timing for three prescribed positions.

With regards to "function" generation using a four-bar linkage, the use of precision points defines the position of the mechanism over a range of the function. Of interest is the "structural error", which is the difference between the function generated by the mechanisms and the desired function. Chebyshev [1961] ascertained that the best linkage approximation to a function occurs when the absolute value of the maximum structural error between precision points and at the ends of the range is equalized [Erdman & Sandor, 1991]. "Chebyshev spacing of precision points" is an analytical method used to identify the spacing of the precision points to minimize the structural error. The identified precision points are then used in a graphical synthesis process for generating the four-bar linkage.

Graphical methods become more complex to implement as the number of precision points increase. The process is also time

consuming when iteration is required to explore different design variables.

Analytical Synthesis

One class of analytical synthesis relies on complex-number modeling of the planar linkages as vector pairs called Dyads. Loop closure equations are derived by summing the vectors around the mechanism and by defining displacement vectors to prescribed positions the mechanism must pass through. As with the graphical method, one drawback in the generation of a solution is based upon a set number of specified points that are part of the desired coupler path. Depending on the number of prescribed positions, a series of equations is generated that must be simultaneously satisfied to reach a solution. As the number of prescribed positions increases, the designer is allowed fewer choices with regards to attributes of the four-bar linkage (e.g. mounting location, link angles, link length, etc). Closed form solutions can effectively be addressed for up to four precision points and solutions may be obtained for five precision points. For six up to nine precision points, non-linear equations must be solved. Numerical methods, such as Newton-Raphson, are used for the more complex mechanisms that do not have closed form solutions. Numerical methods used for precision point synthesis of mechanisms have two key limitations:

- 1) Convergence requires a relatively close estimate of a mechanism for the solutions,
- 2) Numerical methods converge to a single solution that depends on the initial estimate and does not generate all the possible designs that satisfy the constraint equations.

An analytical model of a four-bar mechanism provides the capability to apply mathematical techniques for synthesis of mechanisms. Sandor and Erdman [1991] apply complex-numbers as a tool for modeling linkage members of the four-bar mechanism. Each link in the mechanism is defined by a relative position vector Z_k and is expressed as a complex number. The first position of a link may be written:

$$Z_k = Z_k * e^{i\theta_1} = Z_k (\cos\theta_1 + i * \sin\theta_1) \quad [3.1]$$

Where:

$$i = (-1)^{0.5}$$

k = kth bar of the mechanism

$Z_k = |Z_k|$ = Length of link between pin joints

θ_1 = Angle measured to the axis of Z_k from a fixed oriented rectangular coordinate system

The four-bar mechanism may be viewed analytically as a combination of vector pairs, or dyads, which when added together form a closed

loop (Figure 3.6). Adding each of the link vectors together forms a loop closure equation:

$$Z_{DC} + Z_{CR} - Z_{FC} - Z_{GP} = 0 \quad [3.2]$$

or

$$Z_{DC} * e^{i\theta_{DC}} + Z_{CR} * e^{i\theta_{CR}} - Z_{FC} * e^{i\theta_{FC}} - Z_{GP} * e^{i\theta_{GP}} = 0 \quad [3.3]$$

or

$$Z_{DC} * \cos\theta_{DC} + Z_{CR} * \cos\theta_{CR} - Z_{FC} * \cos\theta_{FC} - Z_{GP} * \cos\theta_{GP} = 0 \quad [3.4]$$

$$Z_{DC} * \sin\theta_{DC} + Z_{CR} * \sin\theta_{CR} - Z_{FC} * \sin\theta_{FC} - Z_{GP} * \sin\theta_{GP} = 0 \quad [3.5]$$

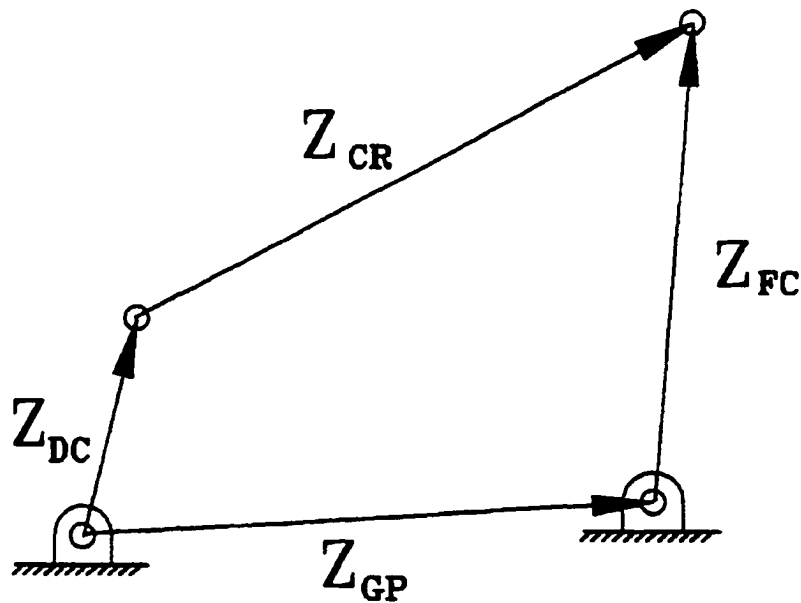


Figure 3.6: Dyads forming a closed loop

Where:

Z_{DC} = Drive crank vector

Z_{CR} = Connecting rod vector

Z_{FC} = Follower crank vector

Z_{GP} = Ground pivot vector

The known variables are Z_{DC} , Z_{CR} , Z_{FC} , Z_{GP} , θ_{GP} and θ_{DC} . The unknown variables are θ_{CR} and θ_{FC} . Since there are two equations created by the closed loop equation (real and imaginary parts must equal zero) the unknown variables may be expressed as the following:

$$\theta_{CR} = \Psi \pm \arccos [(Z_{FC}^2 - L^2 - Z_{CR}^2) / 2 * L * Z_{CR}] \quad [3.6]$$

$$\theta_{FC} = \arctan [(L * \sin \Psi + Z_{CR} * \sin \theta_{CR}) / L * \cos \Psi + Z_{CR} * \cos \theta_{CR}] \quad [3.7]$$

Where:

$$\Psi = \arctan [(Z_{DC} * \sin \theta_{DC}) / (Z_{DC} * \cos \theta_{DC} - Z_{GP})]$$

$$L = (Z_{DC}^2 - 2 * Z_{GP} * Z_{DC} * \cos \theta_{DC} + Z_{GP}^2)^{0.5}$$

With these variables expressed as a function of known variables, an equation may be developed to identify the position of the trace point on a coupler link (Figure 1.5):

$$R = Z_{DC} + Z_{CR} + Z_{TP} \quad [3.8]$$

$$R_x = Z_{DC} * \cos \theta_{DC} + Z_{CR} * \cos \theta_{CR} + Z_{TP} * \cos (180 - \theta_{TP}) \quad [3.9]$$

$$R_y = Z_{DC} \sin \theta_{DC} + Z_{CF} \sin \theta_{CF} + Z_{TF} \sin(180 - \theta_{TF}) \quad [3.10]$$

Where:

R_x = Horizontal position of trace point

R_y = Vertical position of trace point

The position of any point on the coupler link may be expressed as a function of known variables. These equations may be differentiated to obtain an expression for the velocity and acceleration of a coupler link point.

For motion generation, these equations may be used to generate a four-bar mechanism [Erdman & Sandor, 1991]. When there are two positions that are specified, the position and the angle of a body is known. There are two scalar equations that may be solved (Figure 3.7):

$$Z_{DC} + Z_{TF} + \delta_1 - Z_{DC} e^{i\beta_1} - Z_{TF} e^{i\alpha_1} = 0 \quad [3.11]$$

or

$$Z_{DC} (e^{i\beta_1} - 1) + Z_{TF} (e^{i\alpha_1} - 1) = \delta_1 \quad [3.12]$$

Where:

δ_1 = Vector from position 1 to position 2

β_1 = Angle the drive crank rotates from position 1 to position 2

α_1 = Angle the connecting rod rotates from position 1 to position 2

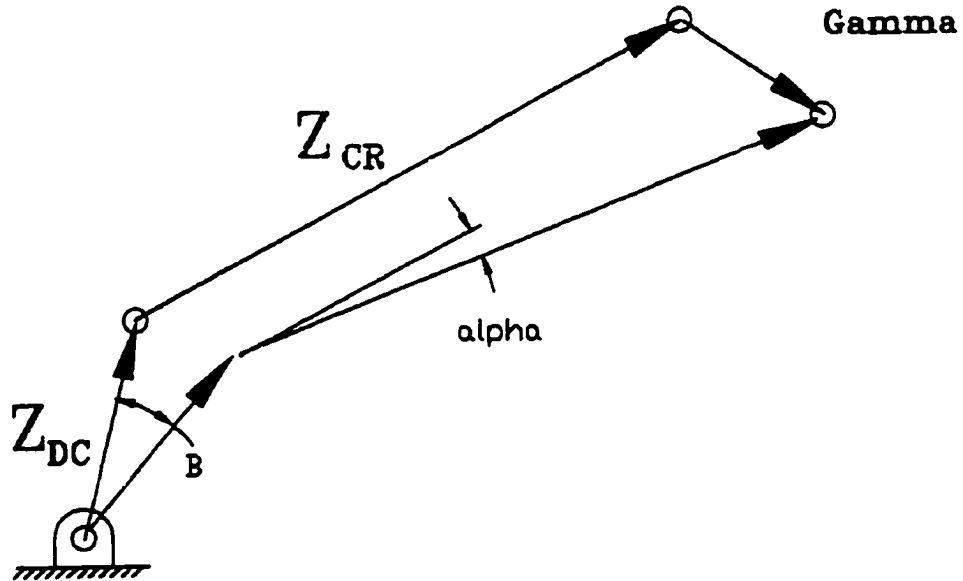


Figure 3.7: Dyads used between two positions

Since the position and the angle of the body are specified for two positions, δ_1 and α_1 are known. There are five scalar unknowns: β_1 , Z_{DC} , and Z_{TP} . Therefore, there are three of the scalar unknowns that the designer may specify.

For 3 position motion generation there are four scalar equations and six scalar unknowns: β_1 , β_2 , Z_{DC} , and Z_{TP} . Therefore, there are two of the scalar unknowns that the designer may specify. Table 3.1 shows a summary of positions, equations, and unknowns for motion generation.

Table 3.1: Summary of design considerations for motion generation

Number of Positions	Number of Scalar Eqns	Number of Scalar Unknowns	Number of Free Choices
2	2	5	3
3	4	6	2
4	6	7	1
5	8	8	0

The maximum number of prescribed positions for motion generation of a four-bar mechanism, without over constraining the system, is five. The maximum number of prescribed positions for a linear solution for motion generation of a four-bar mechanism is three.

For function generation for three prescribed positions, the following loop closure equation is developed for each position (Figure 3.8):

$$\text{Position 1: } \mathbf{z}_{DC} + \mathbf{z}_{CR} + \mathbf{z}_{FC} - \mathbf{z}_{GF} = 0 \quad [3.13]$$

$$\text{Position 2: } \mathbf{z}_{DC}' + \mathbf{z}_{CR}' + \mathbf{z}_{FC}' - \mathbf{z}_{GF} = 0 \quad [3.14]$$

$$\text{Position 3: } \mathbf{z}_{DC}'' + \mathbf{z}_{CR}'' + \mathbf{z}_{FC}'' - \mathbf{z}_{GF} = 0 \quad [3.15]$$

For function generation for three precision points, the angles which the drive crank and follower crank rotate are specified. Setting

the length between the ground pivots equal to one unit and aligned with the real axis, the following set of equations is generated:

$$\text{Position 1:} \quad z_{DC} + z_{CR} + z_{FC} = 1 \quad [3.16]$$

$$\text{Position 2:} \quad z_{DC}' + z_{CR}' + z_{FC}' = 1 \quad [3.17]$$

$$\text{Position 3:} \quad z_{DC}'' + z_{CR}'' + z_{FC}'' = 1 \quad [3.18]$$

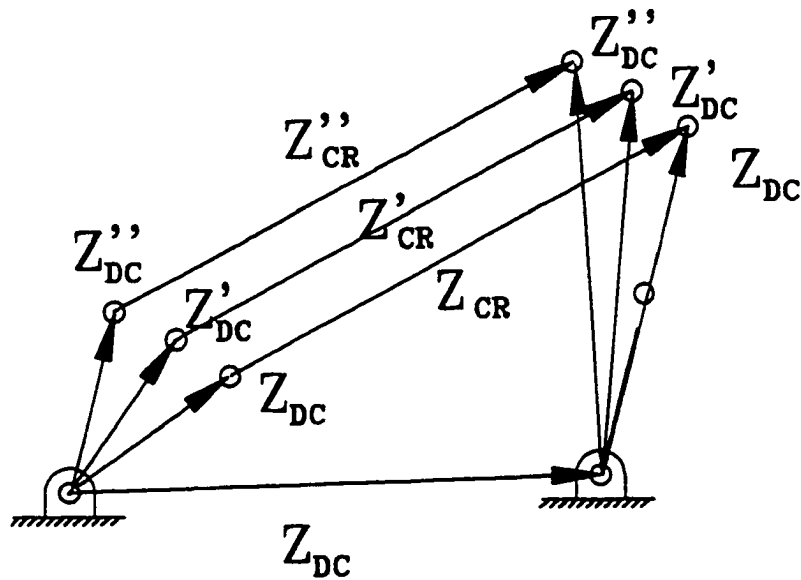


Figure 3.8: Function generation - dyads at three positions

There are eight unknowns: z_{DC} , z_{CR} , z_{FC} , γ_1 , and γ_2 . The angle that the connecting rod travels between each precision point is γ_1 , and γ_2 . There are six equations and the designer is allowed to specify two of the unknowns. Specifying γ_1 , and γ_2 and applying Cramer's

rule supports a solution to the following set of equations for Z_{DC} , Z_{CR} , and Z_{FC} :

$$Z_{DC} + Z_{CR} + Z_{FC} - 1 = 0 \quad [3.19]$$

$$Z_{DC} * e^{i\phi} + Z_{CR} * e^{i\gamma} + Z_{FC} * e^{i\psi} - 1 = 0 \quad [3.20]$$

$$Z_{DC} * e^{2\phi} + Z_{CR} * e^{2\gamma} + Z_{FC} * e^{2\psi} - 1 = 0 \quad [3.21]$$

For path generation, the angle of the body is not specified and therefore there are fewer constraints placed on the analytical solution when compared to motion generation. Table 3.2 shows a summary of positions, equations and unknowns for path generation.

Table 3.2: Summary of design considerations for path generation

Number of Positions	Number of Scalar Eqns	Number of Scalar Unknowns	Number of Free Choices
2	4	11	7
3	8	14	6
4	12	17	5
5	16	20	4
6	20	23	3
7	24	26	2
8	28	29	1
9	32	32	0

Freudenstein [1955] developed an analytical method for designing a four-bar linkage to address function generation. Freudenstein's equation relates the crank angles and the lengths of the links for a four-bar linkage. It may be written:

$$R1*\cos(\pi-DCA) - R2*\cos(\pi-FCA) + R3 = \cos(FCA-DCA) \quad [3.22]$$

Where:

$$R1 = GP/FC$$

$$R2 = GP/DC$$

$$R3 = (GP^2 + DC^2 + FC^2 - CR^2) / 2*DC*FC$$

Freudenstein's equation may be used to design a four-bar mechanism that will generate a given function accurately at a set number of precision points and approximate the function between the precision points. The amount that the function differs from the desired function between the precision points is dependent on the number of precision points, the distance between the points, and the make-up of the desired functions. Up to five precision points may be addressed with this method.

Kinematic synthesis may be addressed through several methods. Graphed displacement paths, graphical and analytical methods reviewed so far have been "classical" methods that have addressed the various types of four-bar mechanisms: function generation, path generation and motion generation.

Graphed displacement paths provide the designer with a visual understanding of a mechanism. Tools used for geometric or graphical synthesis methods provide the designer with a quick, straightforward method of design but have the drawback of only utilizing specified points on the entire required path. Analytical methods of synthesis are suitable for computer evaluation and optimization and have the advantages of repeatability, accuracy and computing power. Analytical synthesis offer techniques to optimize the design of a mechanism with respect to design constraints on ground and moving pivots, transmission angle, line-length ratios, and mechanical advantage. Analytic methods also have the capability to take velocity and acceleration equations into consideration.

Four-Bar Path Generation by Optimal Synthesis Method

Optimal synthesis methods are specialized techniques used for synthesizing mechanisms for path generation, and most techniques require an initial estimate of a mechanism design. The mechanism which generates a curve needs to be close to the desired required functional description of the path. From the initial guess, a curve is generated and the difference from the required curve is expressed as a function of the dimensions of the mechanism. Changing the mechanism's dimensions may have an effect of minimizing the function. The solution produces a mechanism design that generates a design curve with a minimum error to the required curve. Optimal synthesis techniques do not address curves that are identical in

shape but have different orientation, translation and rotation, and scaling (Figure 3.9) to a world axis. As with numerical techniques, convergence to a single solution depends on the initial estimate.

Kota and Ullah [1997] defined an alternative procedure that compares purely the shape of two plane, closed curves while taking into account location, size, and orientation differences between the specified and the design curve. Fourier descriptors were introduced in the early 1960's as a set of numbers that embody the shape of a function and were utilized by Kota and Ullah [1997] to evaluate curve shape deviations between a desired curve path and candidate curves. In defining Fourier Descriptors, a tangent to the curve is defined with respect to the positive x-axis (Figure 3.10).

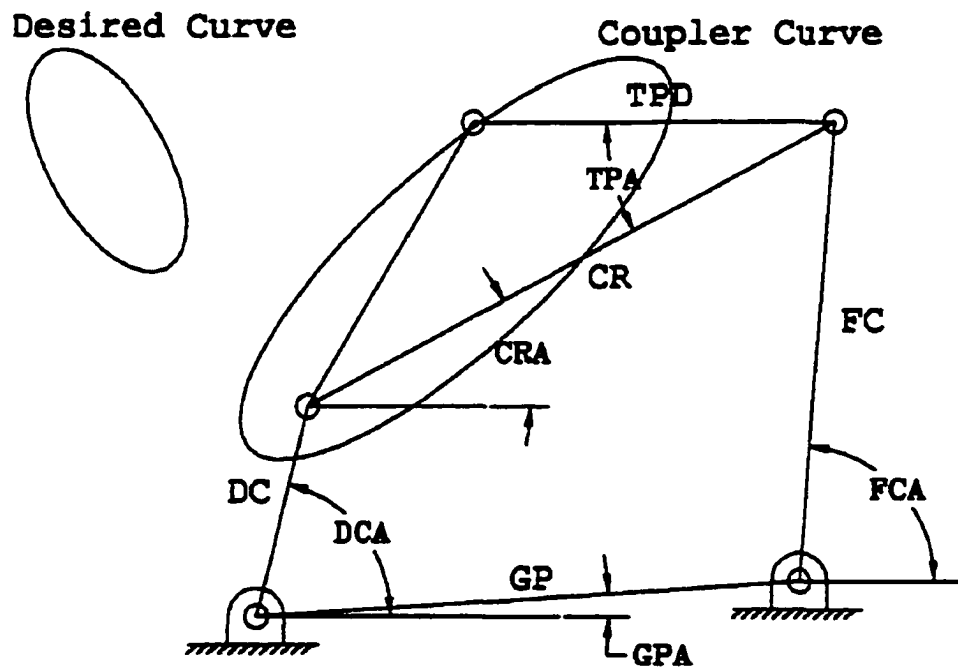


Figure 3.9: Desired curve path and a candidate curve solution

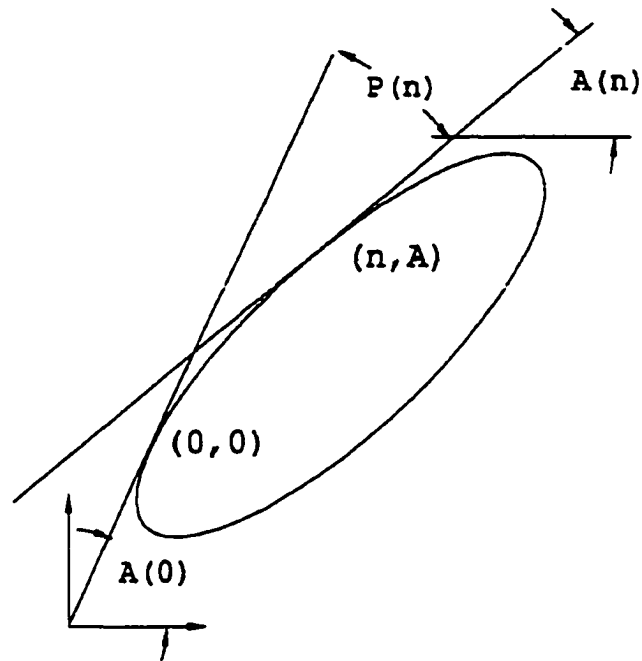


Figure 3.10: Angle function of a plane, closed curve

When the angle is expressed as a function of the arc length, it can be used to represent the shape of the curve. The effect of orientation is removed by defining the cumulative angular function as the net angular bend between the starting point and point n :

$$P(n) = A(n) - A(0) \quad [3.23]$$

A variable change is then introduced to make the function independent of the total length of the curve L :

$$\tau = 2\pi n/L \quad [3.24]$$

Since the curve is simple, clockwise oriented and closed, it will have a net angular bend of -2π . A linearly increasing angle is added to the cumulative angular function to obtain the cumulative angular deviant function that describes pure shape and is invariant under translation, rotations, and changes to the perimeter of the curve.

$$P^*(t) = P(Lt/2\pi) + t \quad t \in \{0, 2\pi\} \quad [3.25]$$

As the curve is traced continuously, the cumulative angular deviant function repeats with a period of 2π and can therefore be expanded in a Fourier series. The cumulative angular deviant function, and therefore the Fourier descriptors, are invariant under rotation, translation, or scaling of the curve. Parker [1984] defines invariance as the property of a physical quantity of physical law of being unchanged by certain transformations or operations, such as reflection or spatial coordinates, time reversal, charge conjugation, rotations, or scale.

The harmonic amplitudes in the Fourier descriptors are independent of the particular starting point used on the curve and the sense of the curve (clockwise or counterclockwise). To extract the shape information contained in phase angles while filtering out the effect of starting point, the following function is defined:

$$F_{k_j} = j^* \alpha_k - k^* \alpha_j \quad [3.26]$$

Where:

$$j^* = j/\text{gcd}(j, k)$$

$$k^* = k/\text{gcd}(j, k)$$

gcd = denotes the greatest common divisor.

Zahn and Roskies [1972] showed that F_{k_j} are independent of the starting point on the curve.

Given two plane, closed curves C and C' with Fourier descriptors (A, α) and (A', α') respectively, an amplitude deviation, Ampdev, and an angle deviation, Angdev, were defined. Finally a Fourier Deviation function was defined as a combination of the amplitude and angle deviation:

$$F_{dev} = m \cdot \text{Ampdev} + n \cdot \text{Angdev} \quad [3.27]$$

Where 'm' and 'n' are weighting parameters whose value can be changed to emphasize one or the other of the two component deviations. The authors validated the use of Fourier descriptors by considering a coupler curve C_d of a four-bar mechanism and varying the coupler angle from 0 to 2π in 20 steps. A comparison between the desired curve C_d and the twenty generated candidates or coupler curves was made by evaluating F_{dev} , Ampdev, and Angdev. In

calculating the deviations, the first 20 harmonics from the Fourier series were included. Examination of the plotted results showed that the Fourier deviation decreased as the shape of the candidate coupler curves became closer to the desired curve C_d and increased when the shape became progressively unlike curve C_d .

Optimal synthesis procedures usually employ local optimization algorithms, which converge to the local minimum nearest to the starting mechanism design. Therefore, the results of using such synthesis procedures are dependent on the initial starting design and the chance that the starting design is close to an optimum solution. There are two key features that are central to the approach proposed by Kota and Ullah [1997]:

- 1) a curve shape is optimized separately from the size, orientation and location of the curve, and
- 2) an effective objective function based on Fourier descriptors is used to evaluate curve shape deviation.

Four-Bar Path Generation Synthesis by a Continuation Method

Continuation methods form a family of mathematical procedures used to solve systems of equations that are nonlinear. The implementation of the system starts with a system of equations for which the solutions are known and then proceeds along a path towards the solutions of the original system. Subbian [1990], Wampler, Morgan and Sommese [1988], Freudenstien and Roth [1963], Flugrad and

Subbian [1991] have investigated continuation methods. Flugrad and Subbian demonstrated an approach for the synthesis of four-bar path generating mechanisms utilizing the continuation method. The procedure was outlined for a system of two equations with two unknowns by considering two polynomial equations:

$$F1(z1, z2) = 0 \quad [3.28]$$

$$F2(z1, z2) = 0 \quad [3.29]$$

A simple system of two equations in two unknowns is considered to implement the method:

$$G1 = C11*z1^{d1} - C12 = 0 \quad [3.30]$$

$$G2 = C21*z2^{d2} - C22 = 0 \quad [3.31]$$

The terms C11, C12, C21, and C22 are randomly chosen complex constants, and d1 and d2 are the degree of functions F1 and F2 respectively. The process relies on homotopy functions that are utilized when combining the two systems of equations (F1, F2, G1 and G2):

$$H1(z1, z2, t) = t*F1 + (1-t)*G1 = 0 \quad [3.32]$$

$$H2(z1, z2, t) = t*F2 + (1-t)*G2 = 0 \quad [3.33]$$

The homotopy parameter is "t". When t = 0, the homotopy functions reduce to the simple set of equations. When t = 1, they

represent the original system. By increasing t from zero to one, and by solving the intermediate sub-problems along the way, the solutions for the original system are found. There are various ways to move a " t " value from 0 to 1. In the approach presented, basic differential equations are formed and ordinary differential equations involving the variables with respect to " t " are determined. The differential equations are integrated numerically to determine the solution for the given system of equations. The solution is refined using Newton's method. The procedure is repeated using all the combinations of solutions for the simple assumed equations as starting points.

Vector pairs (dyads) represent a four-bar mechanism in finitely separated positions. The equations are transformed into polynomial form by treating $\cos(\theta_j)$ and $\sin(\theta_j)$ as two independent variables, $C\theta_j$ and $S\theta_j$. Constraint equations are introduced to establish the relationship between sine and cosine. This process is also carried out for the angles defining the coupler curve and the non-drive ground pivot link. Development of the equations support the elimination of $C\theta_j$, $S\theta_j$, and the other angle variables. In the final analysis, a five-position path generation synthesis problem yields four equations with four complex " Z " variables involved. Therefore, a maximum number of precision points that may be solved for is nine.

The system of equations for five positions will produce a maximum of 256 complex solutions, real solutions and/or solutions at

infinity. As the system has 256 combinations of solutions, there are 256 paths and they proceed to all of the solutions of the original system with multiple paths converging toward repeated solutions. If the original system has solutions at infinity, paths will diverge toward those solutions. Among the total number of solutions, real solutions are the only useful candidates. The solutions at infinity and complex solutions are not useful.

The continuation method was demonstrated by Flugrad and Subbian [1991] to systematically solve a five-position path generation problem. A four-bar mechanism was designed to pass through five precision points by applying the continuation method. A total of 256 real, complex and solutions at infinity were obtained from 256 starting points. Of the solutions, only 25 were real and eight of the 25 resulted in mechanisms that would be usable to solve the path generation problem. The application of the continuation method finds solutions to path generation where prescribed precision points are used. The method does not require a initial solution which is close to the final mechanism.

Development of an Algorithm for Mechanism Synthesis

Rentz [1994] generated an algorithm for implementation on a Personal Computer that allows the engineer to sketch a mechanism on the screen with a mouse and the computer program uses the mechanism as the starting point for the design algorithm. Rentz [1994] uses the homotopy parameter to transform an original sketched mechanism

to a synthesized mechanism. The transformation is accomplished by solving the position analysis problem of the original mechanism and using those values as a starting point for a solution path to a desired mechanism.

The development of the algorithms was based on the use of the Newton-Raphson method of solving systems of nonlinear equations and applying ideas from continuation theory. The implementation of the Newton-Raphson method is associated with two underlying principles. The method is similar to minimizing a system of functions, but does not guarantee a global minimum; failure to find a global minimum may result in undesired roots. The second principle is that the functions must be continuous and differentiable. Both principles can lead to problems if large systems of equations are used. Continuation theoretically assures convergence without an initial estimate of the solution. However, the implementation of continuation to a complicated system is difficult, and following all possible solution paths can be time consuming.

Rentz's [1994] work was concerned with the application of the homotopy parameter to track a *single* solution path from an original concept mechanism to a mechanism satisfying the constraints of the problem. The algorithm generated used Newton-Raphson to solve a system of equations using the solution at a previous "t" as the initial guess of the solution at the current "t". The homotopy parameter was applied to alleviate the problems associated with the initial guesses and the Newton-Raphson method.

The application of the algorithm was applied to three-position function generation, three position path generation, and five position path generation problems. With three-position function generation, the algorithm was able to find an acceptable design for approximately 95% of the cases attempted. The path generation problems resulted in systems of equations larger than the system used for function generation and limited the performance of the algorithm. For the three-position path generation problem, the algorithm was able to find acceptable solutions for 50-60% of the attempts made. For five-position path generation problem, the algorithm was only able to find one acceptable solution for one specific combination of equations and test mechanism. For all other combinations attempted, the algorithm either found an unacceptable solution or would not converge to a solution. The difficulties encountered with the three and five position path generation problems indicated the limited applications possible with the algorithm.

Rentz's algorithm addressed synthesis of function and path generation mechanisms and was limited to the definition of precision points and an initial estimate of a mechanism design.

Synthesis Limitations

The techniques currently used for the synthesis of mechanisms to address function generation, path generation, and motion

generation are generally limited due to one or more of the following:

- A synthesis process that requires the definition of the type of mechanism as a first step may not identify valid candidate solutions from the design process.
- Individual Precision Points on the trace point path are required to be specified by the designer. The location of specific precision points may be critical to the function of the mechanism while other precision points may have less significance.
- The number of precision points is limited based upon the synthesis technique used. A maximum of nine precision points may be defined on the output path; selecting a lower number of precision points provides more choices to the designer for selection of the mechanisms attributes such as pivot points, link lengths, and angles.
- An initial guess of a mechanism that is "close" to a desired solution may be required so numerical techniques may find a local solution.
- Kota and Ullah [1997] have addressed the synthesis of path generation mechanisms that generate closed path curves using Fourier descriptors. Synthesis for partial path curves, function generation and motion generation have not been addressed.

CHAPTER 4. SOLUTION REPRESENTATION

Solutions for a four-bar mechanism have typically been represented in a documented form. Hrones and Nelson [1951] documented the paths of over 7,000 curves for a crank-rocker four-bar mechanism. A desired solution is compared with documented candidate solutions, and the designer makes a visual comparison between desired and candidate solutions. Size, shape, and orientation must be addressed by the designer during the process of comparison. This process addresses path generation for a four-bar mechanism but does not address function or motion generation.

Spatial Representation

For a function generation four-bar mechanism, the output of the follower crank may be represented as a function of the input crank angle in several forms. One representation form would be to record the input and output angles as strings of data stored in a vector. Each position of the follower crank is recorded with each input crank angle (Table 4.1). Another form would be to record the data as a graph where the output angle of the follower crank is a

function of the input crank drive crank angle (Figure 4.1). To record the angular position of the drive crank and follower crank for each degree of rotation there would be 720 numbers stored or plotted.

Table 4.1: Function generation - data string of input/output

Drive Crank Angle, degrees	0.00	1.00	2.00	3.00	4.00	5.00	6.00	7.00	8.00
Follower Crank Angle, degrees	35.5	35.4	35.4	35.3	35.2	35.0	34.8	34.6	34.3

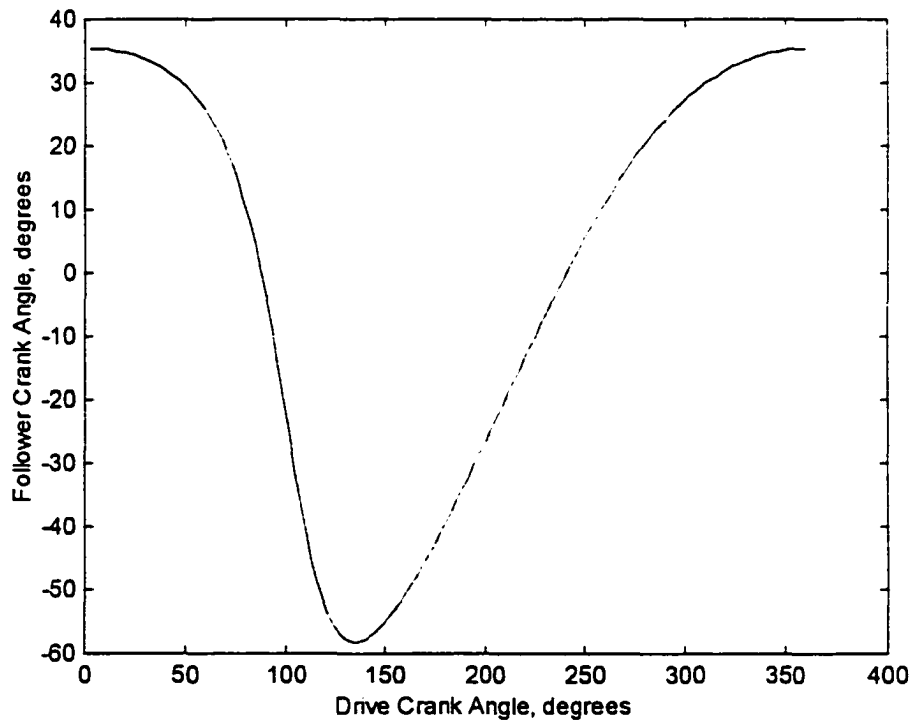


Figure 4.1: Function generation - graph of input/output

For a path generation four-bar mechanism, the output of a trace point affixed to the connecting rod may be represented as a function of the input crank angle. One representation form would be to record the input angle and the output trace point position as strings of data stored in a vector. Each position of the trace point is recorded with each input crank angle (Table 4.2). To record the angular position of the drive crank and the spatial position of the follower crank for each degree of rotation there would be 1080 numbers stored. Another representation form would be to record the path of the trace point (Figure 3.1). In this simple two dimension plot of the trace point path, the information regarding the crank angle is not visible. In addition, the size, orientation, and position of the four-bar mechanism will affect the size, orientation, and position of the output path.

Table 4.2: Path generation - data string of input/output

Drive Crank Angle, degrees	0.000	1.000	2.000	3.000	4.000	5.000	6.000	7.000	8.000
Trace Point Horizontal Position	1.000	0.999	0.999	0.999	0.998	0.997	0.996	0.994	0.992
Trace Point Vertical Position	0.000	0.008	0.015	0.022	0.030	0.038	0.045	0.053	0.061

For a motion generation four-bar mechanism, the output of a trace point affixed to the connecting rod and the connecting rod angular displacement is of interest. Once again, a representation form would be to record the input angle, the output angle, and the trace point position as strings of data stored in a vector. Each position of the trace point, the angle of the connecting rod, and the input crank angle is recorded (Table 4.3). To record this information for each degree of rotation of the drive crank would require 1460 numbers. Another representation form would be to record the path of the trace point in one graph and the angle of the connecting rod in a second graph. Another representation form would be to record the path of the trace point in one graph and the angle of the connecting rod in the 3rd dimension, or z axis, of the trace point plot. Once again, the size, orientation, and position of the four-bar mechanism will affect the size, orientation, and position of the output path.

Table 4.3: Motion generation - data string of input/output

Drive Crank Angle, degrees	0.000	1.000	2.000	3.000	4.000	5.000	6.000	7.000	8.000
Trace Point Horizontal Position	1.000	0.999	0.999	0.999	0.998	0.996	0.996	0.994	0.992
Trace Point Vertical Position	0.000	0.008	0.015	0.022	0.030	0.038	0.046	0.053	0.061
Trace Point Angle, degrees	35.47	35.44	35.38	35.28	35.16	34.99	34.79	34.55	34.27

There are common characteristics for the input and output of function, path, and motion generation four-bar mechanisms. The input and output angles and paths repeat themselves as the input drive is taken through a complete cycle. For a crank-rocker and a double-crank, the output trace points form closed curves and the motion of the connecting rod and follower crank are repeated as the drive crank is taken through each complete cycle. For a double-rocker mechanism, the input drive crank and output follower crank are discontinuous at the limits of the drive crank angular motion. With these characteristics in mind, representation methods must address the description, and encoding techniques should be able to address one, two, or three dimensions.

Fourier Transforms

One, two, and three-dimensional Fourier transforms may be used for encoding, restoration, and descriptive information related to a four-bar mechanism. The one dimensional Fourier transform of a function $f(x)$ is denoted by $F(f(x))$ and is defined by [Gonzalez, 1977]:

$$\mathfrak{J}(f(x)) = F(u) = \int f(x) \exp(-j*2\pi*u*x) dx \quad [4.1]$$

Where:

$$j = \sqrt{-1}$$

x = real variable

u = Frequency variable

$F(u)$ = Fourier transform of $f(x)$

The function $f(x)$ is considered to be in the spatial domain and $F(u)$ to be in the frequency domain. If $F(u)$ is known, then $f(x)$ may be obtained by using the inverse Fourier transform:

$$\mathcal{F}^{-1}(F(u)) = f(x) = \int F(u) \exp(j*2\pi*u*x) du \quad [4.2]$$

If $f(x)$ is a real function, then the Fourier transform of $f(x)$ is generally complex:

$$F(u) = R(u) + j*I(u) \quad [4.3]$$

Where:

$R(u)$ = Real component of the Fourier transform

$I(u)$ = Imaginary component of the Fourier transform

The Fourier spectrum of $f(x)$ is the magnitude of $F(u)$ which is equal to:

$$|F(u)| = [(R(u))^2 + (I(u))^2]^{0.5} \quad [4.4]$$

The phase angle of the Fourier spectrum is:

$$\phi(u) = \text{atan} [I(u)/R(u)] \quad [4.5]$$

Applying Euler's formula to the exponential term results in:

$$\exp[(+/-)j2\pi ux] = \cos(2\pi ux) \pm j\sin(2\pi ux) \quad [4.6]$$

If discrete terms are considered, $F(u)$ is composed of an infinite sum of sine and cosine terms and the value of u determines the frequency of the sine-cosine pair.

If a continuous function $f(x)$ has N samples taken at Δx apart the function may be expressed where x assumes the discrete values $0, 1, 2, \dots, N-1$ and

$$f(x) = f(x_0 + x\Delta x) \quad [4.7]$$

The sequence $\{f(0), f(1), f(2), \dots, f(N-1)\}$ is used to represent any N uniformly spaced samples from the continuous function. Therefore, when considering a discrete signal or curve, the discrete Fourier transform that would apply to a sampled function:

$$F(u) = \frac{1}{N} \sum_{x=0}^{N-1} f(x) \exp[-j2\pi ux/N] \quad [4.8]$$

Where:

N = Number of data points sampled

$u = 0, 1, 2, \dots, N-1$ Samples of continuous transform at values $0, \Delta u, 2\Delta u, \dots, (N-1) \Delta u$.

The inverse of the discrete Fourier transform is:

$$f(x) = \frac{1}{N} \sum_{u=0}^{N-1} F(u) \exp[j2\pi ux/N] \quad [4.9]$$

The samples of $F(u)$ start at the origin of the frequency axis. The variables Δu and Δx are related by the following equation:

$$\Delta u = 1/(N \Delta x) \quad [4.10]$$

The Fourier transform may be extended to a two dimensional function $f(x, y)$

$$\mathfrak{F}(f(x, y)) = F(u, v) = \int f(x, y) \exp(-j*2\pi*(u*x+v*y)) dx \quad [4.11]$$

Where:

v = Frequency variable

and,

$$\mathfrak{F}^{-1}(F(u, v)) = f(x, y) = \int F(u, v) \exp(j*2\pi*(u*x+v*y)) du \quad [4.12]$$

In a similar fashion to the one-dimensional Fourier transform, the Fourier spectrum and phase is given by the following equations:

$$|F(u, v)| = [(R(u, v))^2 + (I(u, v))^2]^{0.5} \quad [4.13]$$

$$\phi(u, v) = \text{atan} [I(u, v)/R(u, v)] \quad [4.14]$$

The discrete Fourier transform pair for two-dimensions is:

$$F(u, v) = 1/(N*M) \sum_{x=0}^{N-1} \sum_{y=0}^{M-1} f(x, y) \exp\{-j2\pi[(ux/N)+(vy/M)]\} \quad [4.15]$$

Where:

N = Number of data points sampled in x direction

M = Number of data points sampled in y direction

and the inverse of the two dimensional discrete Fourier transform is:

$$f(x, y) = 1/(N*M) \sum_{u=0}^{N-1} \sum_{v=0}^{M-1} F(u, v) \exp\{j2\pi[(ux/N)+(vy/M)]\} \quad [4.16]$$

Where:

$$\Delta u = 1/N*\Delta x$$

$$\Delta v = 1/M*\Delta y$$

When images are sampled in a square array, M=N and:

$$F(u, v) = 1/N \sum_{x=0}^{N-1} \sum_{y=0}^{N-1} f(x, y) \exp\{-j2\pi[(ux+vy)/N]\} \quad [4.17]$$

The inverse of the two-dimensional discrete Fourier transform is:

$$f(x,y) = 1/N \sum_{u=0}^{N-1} \sum_{v=0}^{N-1} F(u,v) \exp[j2\pi(ux+vy)/N] \quad [4.18]$$

The discrete Fourier transform may be expressed in the separable forms:

$$F(u,v) = 1/N \sum_{x=0}^{N-1} \exp(-j2\pi ux/N) \sum_{y=0}^{N-1} f(x,y) \exp(-j2\pi vy/N) \quad [4.19]$$

and the inverse of the two-dimensional discrete Fourier transform is:

$$f(x,y) = 1/N \sum_{u=0}^{N-1} \exp(j2\pi ux/N) \sum_{v=0}^{N-1} F(u,v) \exp(j2\pi vy/N) \quad [4.20]$$

The advantage of separability is the $F(u,v)$ or $f(x,y)$ may be evaluated on a square image matrix by first taking the one-dimensional Fourier transform along each row of $f(x,y)$, multiplying the result by N and then taking the transform along each column. The same results will be obtained by first taking the transform along the columns of $f(x,y)$ and then along the rows of the results.

The discrete Fourier transform and its inverse are periodic with the period N :

$$F(u) = F(u + N) \quad [4.21]$$

and

$$F(u, v) = F(u + N, v) = F(u, v + N) = F(u + N, v + N) \quad [4.22]$$

As a result, only the N values of each variable in any one period are required to obtain $f(x)$ or $f(x, y)$ from $F(u)$ or $F(u, v)$. In a similar fashion only the N values of each variable in any one period are required to obtain $F(u)$ or $F(u, v)$ from $f(x)$ or $f(x, y)$. The Fourier transform may thus be applied to one period of a function to obtain the Fourier coefficients.

If $f(x, y)$ is rotated by an angle θ , then $F(u, v)$ is rotated by the same angle. Considering the polar coordinates:

$$x = r \cos \alpha \quad y = r \sin \alpha \quad u = \omega \cos \phi \quad v = \omega \sin \phi \quad [4.23]$$

then $f(x, y)$ becomes $f(r, \alpha)$ and $F(u, v)$ becomes $F(\omega, \phi)$. Substitution of these relationships in the Fourier transform shows that if $f(x, y)$ is rotated by an angle α , then $F(u, v)$ is rotated by the same angle.

The Fourier transform and its inverse are distributed over addition:

$$\mathfrak{J}[f_1(x, y) + f_2(x, y)] = \mathfrak{J}[f_1(x, y)] + \mathfrak{J}[f_2(x, y)] \quad [4.24]$$

And in general, are not distributed over multiplication:

$$\mathfrak{J}[f_1(x, y) * f_2(x, y)] \neq \mathfrak{J}[f_1(x, y)] * \mathfrak{J}[f_2(x, y)] \quad [4.25]$$

For scalar multiplication and scaling where a and b are scalar quantities:

$$a \cdot f(x, y) \Leftrightarrow a \cdot F(u, v) \quad [4.26]$$

and

$$f(ax, by) \Leftrightarrow (1/|ab|) \cdot F(u/a, v/b) \quad [4.27]$$

Here, \Leftrightarrow indicates the relationship between a function and its Fourier transform.

The translation properties of the Fourier transform pair are:

$$f(x-x_0, y-y_0) \Leftrightarrow F(u, v) \exp[-j2\pi(ux_0 + vy_0)/N] \quad [4.28]$$

and

$$f(x, y) \exp[j2\pi(u_0x + v_0y)/N] \Leftrightarrow F(u-u_0, v-v_0) \quad [4.29]$$

Understanding the magnitude, phase, translation, scaling, and rotation properties of the Fourier transform pairs permits an understanding regarding how Fourier coefficients are affected by the size, location, and rotation of a curve path. Assume that $f(x)$ and $g(x)$ are the same function with $g(x)$ being at a different scale and average value:

$$g(x) = \sigma f(x) + c \quad [4.30]$$

Where:

σ = a scale factor

c = a change in average value

The Fourier transforms of $f(x)$ and $g(x)$ are related by:

$$G(u) = \sigma/N \sum_{x=0}^{N-1} \{f(x) \{(\cos[2\pi u(x)] - j\sin[2\pi u(x)])\} + c\} \quad [4.31]$$

$$F(u) = 1/N \sum_{x=0}^{N-1} f(x) [(\cos(2\pi ux) - j\sin(2\pi ux))] \quad [4.32]$$

Since $f(x)$ is assumed to be periodic over the sampled range, and the function is simply shifted within the sampled range, the magnitude of the Fourier transform coefficients are the same and the value of the coefficients are simply changed:

$$G(u) = \sigma |F(u) + c| \quad [4.33]$$

or:

$$\mathfrak{J}[g(x)] = \sigma^* |\mathfrak{J}[f(x)] + c| \quad [4.34]$$

The following simple examples using a sine wave will demonstrate the properties of scaling, translation, and a phase shift.

Assume that $f(x) = \sin(2\pi x)$ and $g(x) = 2*f(x)$ as x varies between 0 and 1. The independent variable x will be incremented so

that discrete values of $f(x)$ and $g(x)$ are generated in 128 equal increments, therefore, $\Delta x = 1/128$.

Figure 4.2 plots the dependent functions $f(x)$ and $g(x)$ against the independent variable x . The Fourier transform of $f(x)$ and $g(x)$ are then generated. Figure 4.3 plots the Fourier Spectrum $|F(u)|$ (magnitude of the Fourier coefficients). Based on the definition of the Fourier Transform, the effect of multiplying $f(x)$ by a scalar should have the same effect on the magnitude of the Fourier coefficients. For this example, the Fourier Spectrum of $g(x)$ should be twice as large as the Fourier Spectrum of $f(x)$. There should be no effect on the phase of the Fourier coefficients.

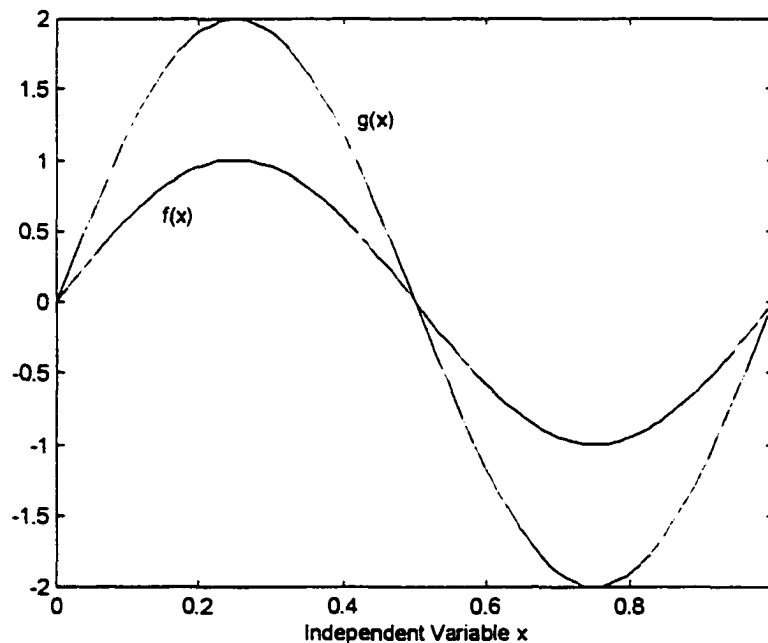


Figure 4.2: Plot of $f(x)$ and $g(x)$, $g(x) = 2*f(x)$

Table 4.4 lists the magnitude and phase of the first three and last two Fourier coefficients for both $f(x)$ and $g(x)$. All of the other Fourier coefficients have a magnitude of zero. Assume that $f(x) = \sin(2\pi x)$ and $g(x) = f(x) + 2$. Figure 4.4 plots the dependent functions $f(x)$ and $g(x)$ against the independent variable x .

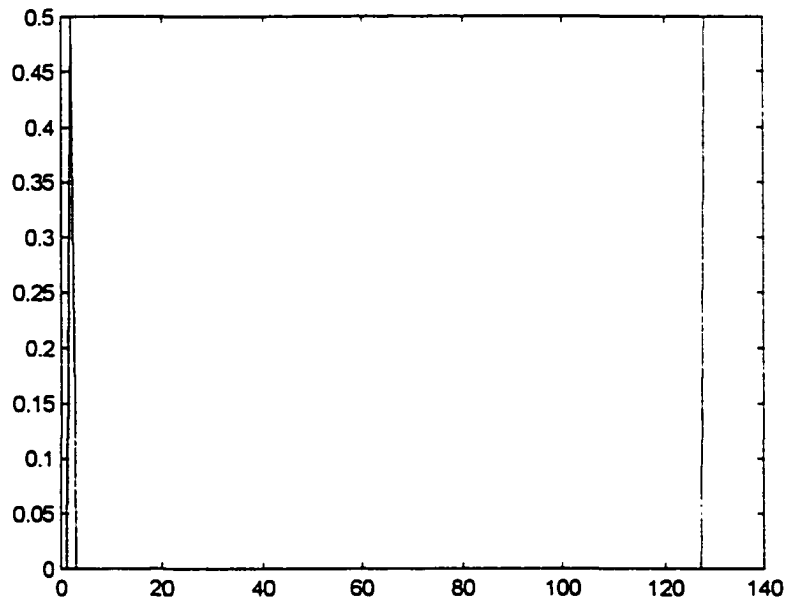


Figure 4.3: Plot of the Fourier spectrum $|F(u)|$

Table 4.4: Fourier coefficients of $f(x)$ and $g(x)$, $g(x) = 2*f(x)$

Fourier Coefficient Number	F(u)		G(u)	
	Magnitude	Phase	Magnitude	Phase
0	0.000	0.000	0.000	0.000
1	0.500	-1.571	1.000	-1.571
2	0.000	0.000	0.000	0.000
-				
126	0.000	0.000	0.000	0.000
127	0.500	1.571	1.000	1.571

The effect of adding a scalar to $f(x)$ affects only the magnitude of the first Fourier coefficient. The average value of $f(x)$ will change from 0 to 2 over the period being sampled. For this example, the Fourier Spectrum of $g(x)$ will be affected by the value of the scalar added to $f(x)$. The first Fourier Transform reflects the average value of the function over the period which is $2 \cdot N$, where N = number of discrete samples of $f(x)$. There should be no effect on the phase of the Fourier coefficients. Table 4.5 lists the magnitude and phase of the first three and last two Fourier coefficients for both $f(x)$ and $g(x)$.

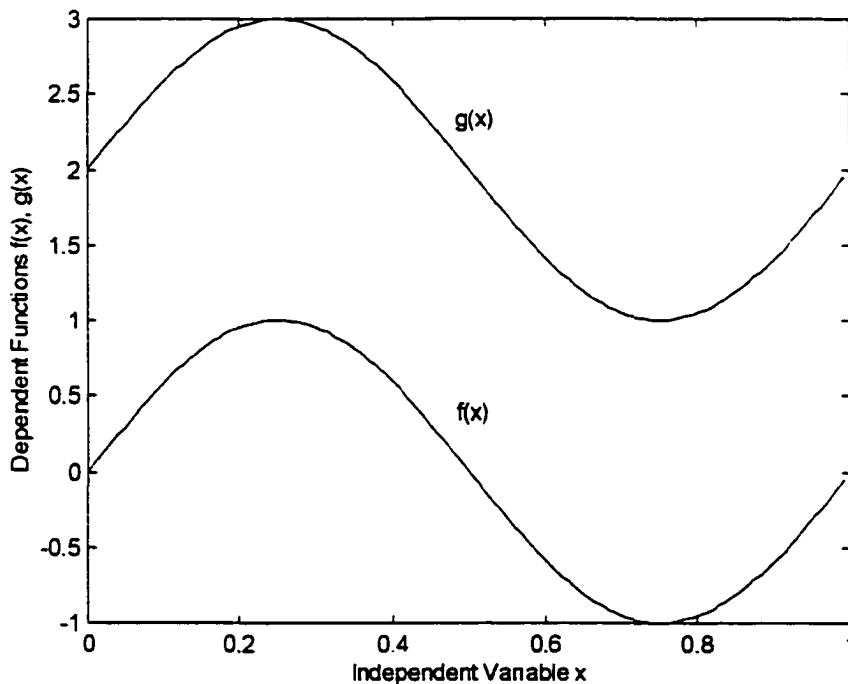


Figure 4.4: Plot of $f(x)$ and $g(x)$, $g(x) = f(x) + 2$

Table 4.5: Fourier coefficients of $f(x)$ and $g(x)$, $g(x) = f(x) + 2$

Fourier Coefficient Number	F(u)		G(u)	
	Magnitude	Phase	Magnitude	Phase
0	0.000	0.000	2.000	0.000
1	0.500	-1.571	0.500	-1.571
2	0.000	0.000	0.000	0.000
-				
126	0.000	0.000	0.000	0.000
127	0.500	1.571	0.500	1.571

Assume that $f(x) = \sin(2\pi x)$ and $g(x) = f(x + 32)$. Figure 4.5 plots the dependent functions $f(x)$ and $g(x)$ against the independent variable x . The effect of a phase shift on $f(x)$ does not have an effect on the magnitude of the Fourier coefficients. For this example, the Fourier Spectrum of $g(x)$ will be affected by phase shift applied to $f(x)$. The effect on the phase shift is given by $\exp[(+i2\pi u \gamma)/N]$. Therefore, the phase shift will be different for each Fourier coefficient. For the second Fourier coefficient:

$$\exp(i*2\pi*u*\gamma/N) \quad [4.35]$$

$$\exp(i*2\pi*1*0.25) = 0 + i*1 \quad [4.36]$$

$$\text{Phase Shift} = \text{atan}(1.0/0.0) = 1.571 \quad [4.37]$$

Where:

$$u = 1$$

$$N = 128$$

$$\gamma = 32$$

For the last Fourier coefficient:

$$\exp(i*2\pi*127*32/128) = 0.0 - i*1.000 \quad [4.38]$$

$$\text{Phase Shift} = \text{atan}(-1/0) = -1.571 \quad [4.39]$$

Where:

$$u = 128$$

$$N = 127$$

$$\gamma = 32$$

Table 4.6 lists the magnitude and phase of the first three and last two Fourier coefficients for both $f(x)$ and $g(x)$.

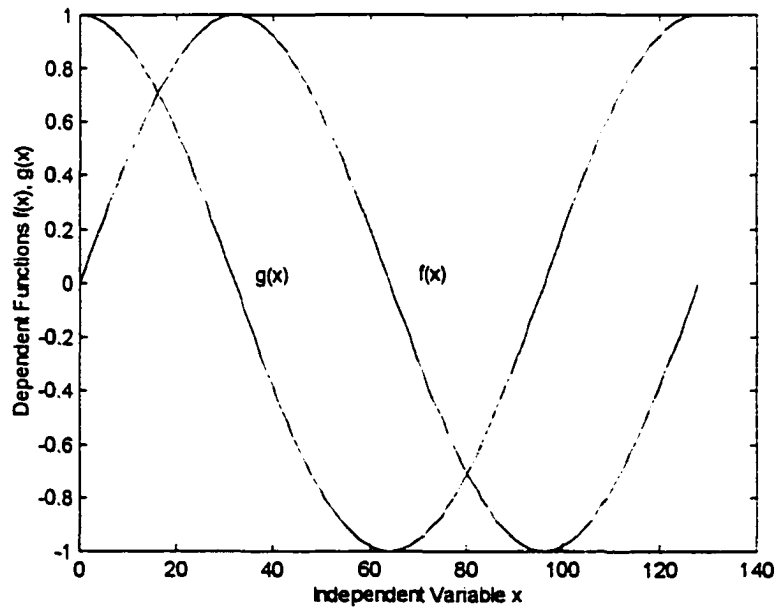


Figure 4.5: Plot of $f(x)$ and $g(x)$, $g(x) = f(x + \gamma)$, $\gamma = 32$

Table 4.6: Fourier coefficients of $f(x)$ and $g(x)$, $g(x) = f(x + 32)$

Fourier Coefficient Number	F(u)		G(u)	
	Magnitude	Phase	Magnitude	Phase
0	0.000	0.000	0.000	0.000
1	0.500	-1.571	0.500	0.000
2	0.000	0.000	0.000	0.000
-				
126	0.000	0.000	0.000	0.000
127	0.500	1.571	0.500	0.000

From these examples several steps may be defined to identify similar functions that differ only in size, average value, or phase. These steps may be considered "normalizing" the Fourier coefficients. To obtain a standard size the Fourier coefficient, $F(1)$ must have a standard magnitude (i.e. 1). To obtain a standard position, the Fourier coefficient $F(0)$ must be set to a standard value (i.e. 0). To obtain a standard phase, the maximum value of the dependent function, $f(x)$, may be shifted to coincide with the origin of the independent variable x .

Assume that $f(x,y)$ and $g(x,y)$ are the same curve path with $g(x,y)$ being at a different rotation, scale and translation:

$$g(x,y) = f[\sigma(x\cos\theta + y\sin\theta) - x_0, \sigma(-x\sin\theta + y\cos\theta) - y_0] \quad [4.40]$$

Where:

σ = a scale factor

θ = a rotation angle

x_c, y_c = a translation length

The Fourier transforms of $g(x,y)$ and $f(x,y)$ are related by:

$$G(u,v) = \exp[-j2\pi(ux_c+vy_c)/N] * \sigma^{-2} * F[(u\cos\theta + v\sin\theta)/\sigma, (u\cos\theta + v\sin\theta)/\sigma] \quad [4.41]$$

As with the one-dimensional Fourier transform, a simple example for the two-dimensional Fourier transform using the trace point path of a four-bar mechanism will demonstrate the properties of scaling, translation, and a rotation of the path.

Assume that a crank-rocker four-bar mechanism with the following construction generates a trace point path.

Drive Crank Length = 1.0 units
 Connecting Rod Length = 1.5 units
 Follower Crank Length = 1.5 units
 Ground Pivot Length = 1.5 units
 Trace Point Distance = 1.5 units
 Ground Pivot Angle = 0 radians
 Trace Point Angle = 1 radian
 Number of Crank Positions = 128

A graph of the trace point path for the four-bar mechanism is contained in Figure 4.6. A matrix grid 128 by 128 units is placed over the curve to digitize the figure. The center of the matrix is placed at the centroid of the trace point curve, and the matrix is scaled such that the largest radius from the centroid is 64 units. Figure 4.7 shows the two dimensional matrix of the trace point curve. A two-dimensional discrete Fourier transform is then taken of the image. Figure 4.8 shows a two dimensional gray scale representation the Fourier transform of the trace path curve.

The trace point path is taken through a spatial transform to move the centroid of the curve to the global origin, to rotate the curve so the largest radius coincides with the x axis, and to scale the trace point path so the largest radius has a value of 1. Figure

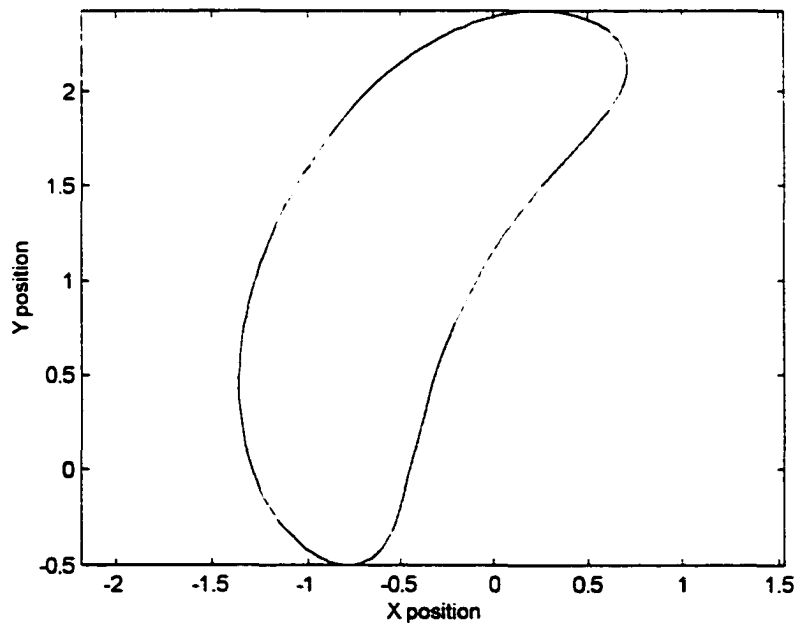


Figure 4.6: Graph of trace point path for four-bar mechanism

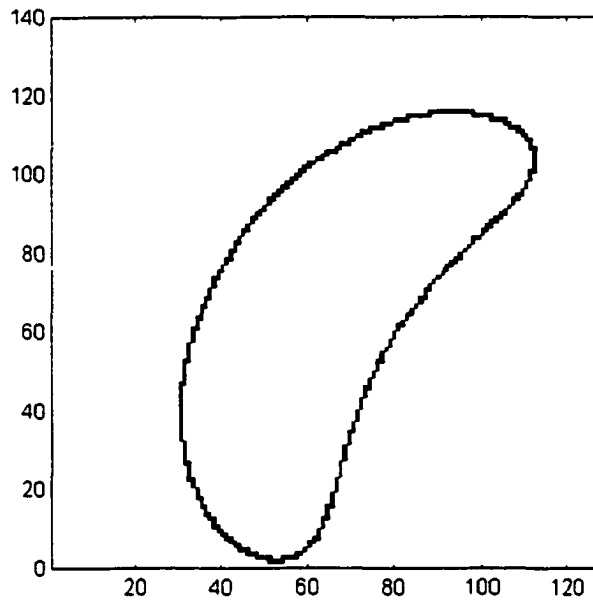


Figure 4.7: Graph of matrix of trace point path

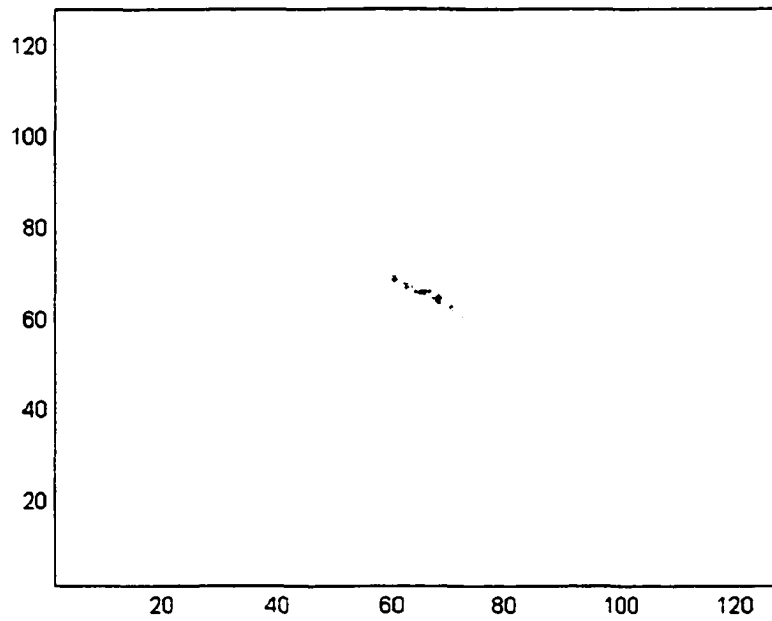


Figure 4.8: Two dimensional gray scale representation of the Fourier transform of trace point path

4.9 shows the spatially transformed trace point path. A grid matrix 128 by 128 units is placed over the curve to digitize the figure. The center of the matrix is placed at the centroid of the trace point curve, and the matrix is scaled such that the largest radius from the centroid is 64 units. Figure 4.10 shows the two dimensional matrix of the trace point curve. A two-dimensional discrete Fourier transform is then taken of the image. Figure 4.11 shows the gray scale Fourier transform of the trace path curve.

One may see that rotating the trace point path through a angle will have the same rotational effect on the Fourier Transform of the path of the image. The process of placing a matrix over the image

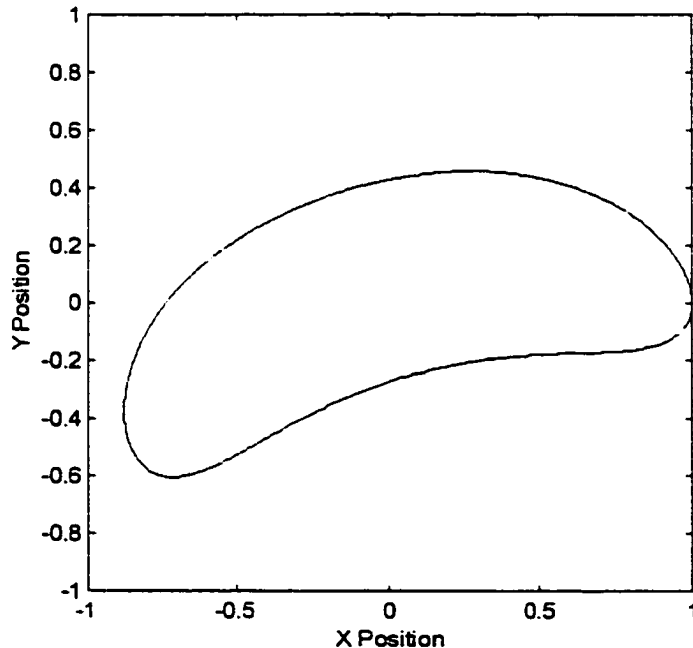


Figure 4.9: Spatially transformed trace point path

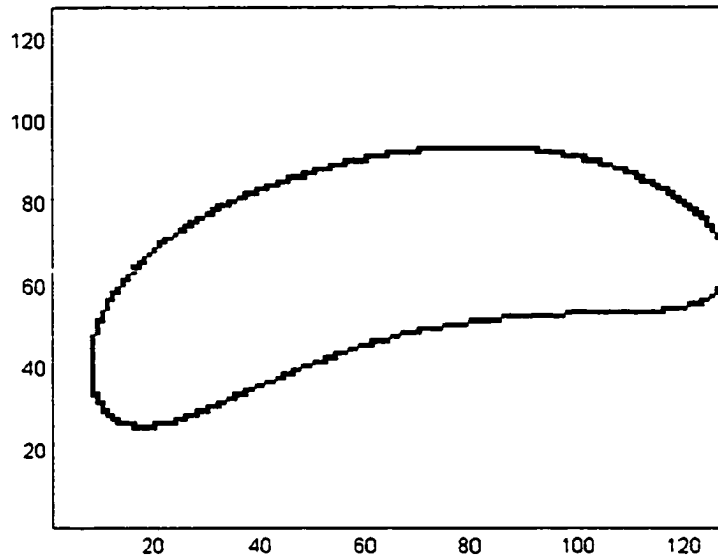


Figure 4.10: Graph of matrix of spatially transformed trace point

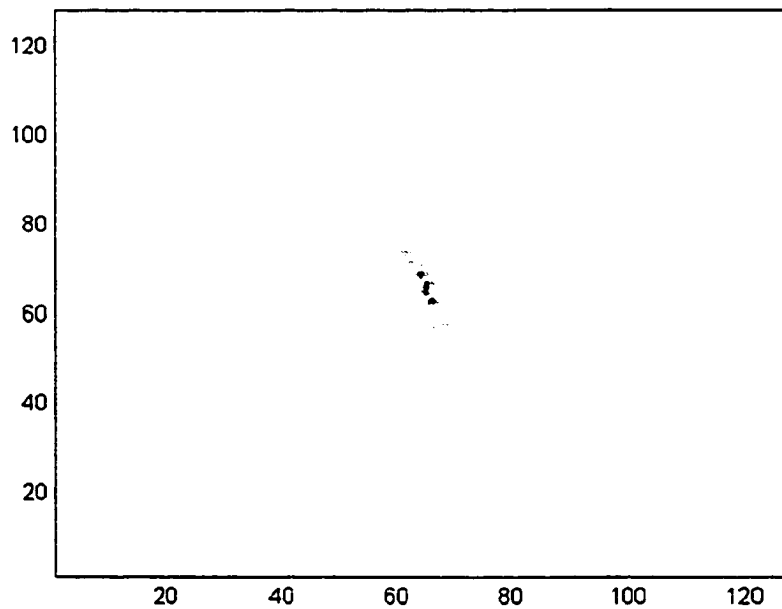


Figure 4.11: Gray scale representation of the Fourier transform of spatially transformed trace point path

of the trace point path such that the size of the matrix is related to the largest curve radius to the path centroid renders the Fourier Transform invariant to size. Placing the largest curve radius on the x-axis renders the Fourier Transform invariant to rotation.

One-Dimensional Fourier Transform

For a characterization of a function, $f(x)$, the application of a one-dimensional Fourier Transform has been applied. For a two dimensional curve path, $f(x,y)$, the application of a two-dimensional Fourier Transform has been applied. A technique described by Gonzalez [1977] describes the application of one-dimensional Fourier Transform to a curve path, $f(x,y)$, for the matching of different region shapes.

The points on the curve path may be viewed as a region in a complex plane with the x-axis being the real axis and the y-axis being the imaginary axis. Each discrete point on the curve path becomes a complex number $x + iy$. Beginning with one point on the curve path and following the path to the next connected discrete point will generate a series of complex numbers. The one-dimensional discrete Fourier transform of this series will generate a set of Fourier coefficients for the contour.

The scale or size of the path may be changed by simply multiplying each point on the curve by a single constant, σ , in both the x and y direction. This scales the path to a larger or smaller

size and results in a scalar multiplication to the Fourier transform.

$$\sigma f(x) = \sigma x + \sigma iy = \sigma F(u) \quad [4.42]$$

To rotate the path in the spatial domain simply requires multiplying each coordinate by $\exp(i\theta)$. This will rotate the path by the angle θ since $\exp(i\theta) = \cos\theta + i\sin\theta$. In a similar respect to scaling, the Fourier Transform may be multiplied by $\exp(i\theta)$.

$$\exp(i\theta) f(x) = \exp(i\theta) x + \exp(i\theta) iy = \exp(i\theta) F(u) \quad [4.43]$$

Changing the starting point of the curve path in the spatial domain has no effect on the results of the Fourier transform. Changing the angular rotation of the curve does have an effect on the Fourier transform. This is similar to a phase shift in the one-dimensional Fourier Transform.

Figure 4.6 graphs the trace point path for a defined four-bar mechanism. Applying the complex number technique described by Gonzalez [1977] the one-dimensional Fourier Transform of the path may be taken. Figure 4.12 is a plot of the Fourier spectrum of the trace point path using 128 discrete points to represent the curve. Note that the Fourier coefficient $F(0)$ is not zero since the curve is not centered on the global axis. Table 4.7 lists the magnitude and phase of the first five and last four Fourier coefficients.

If the trace curve path is spatially transformed to place the centroid of the path on the global axis, the Fourier coefficient $F(0)$ will be reduced to zero. Figure 4.13 is a plot of the Fourier spectrum of the trace point path with the centroid moved to the origin of the global axis. Note that the Fourier coefficient $F(0)$ has been reduced to zero. Table 4.8 lists the magnitude and phase of the first five and last four Fourier coefficients.

The trace point path is then scaled so the maximum radius from the path centroid to the curve is 1. The trace point path is then

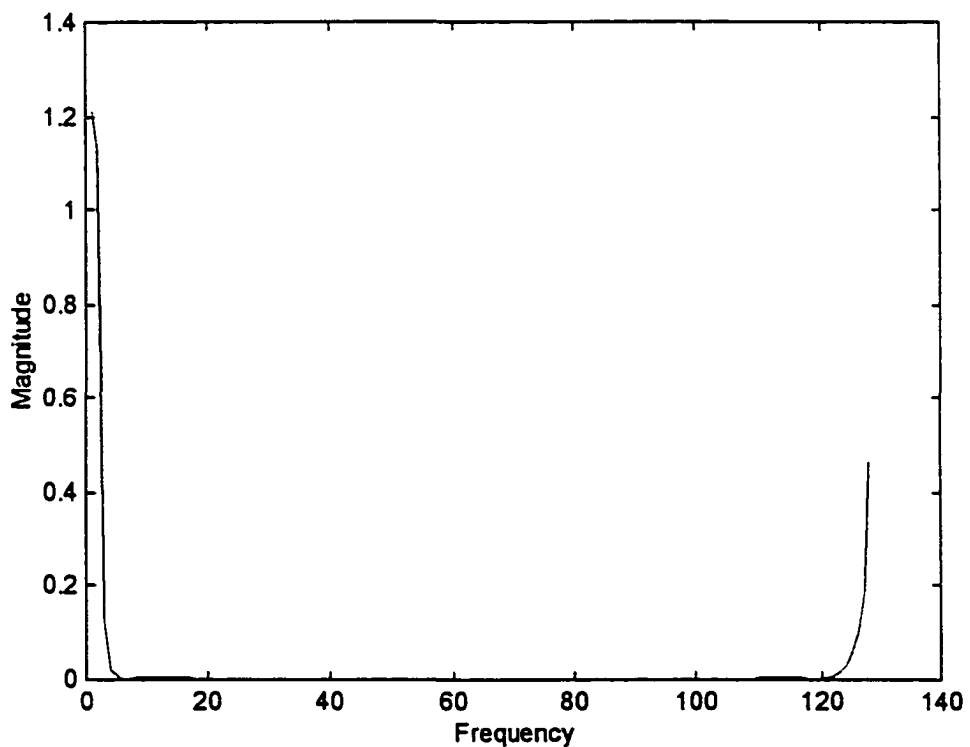


Figure 4.12: Plot of Fourier spectrum of trace point path

Table 4.7: Fourier coefficients of trace point path

Fourier Coefficient Number	F(u)	
	Magnitude	Phase
0	1.2103	2.0050
1	1.1305	-0.4376
2	0.1276	-0.4536
3	0.0221	-0.4330
4	0.0079	-0.4161
5	0.0009	-0.4701
-		
123	0.0307	2.5170
124	0.0554	2.5422
125	0.1020	2.5671
126	0.1885	2.5919
127	0.4650	2.6167

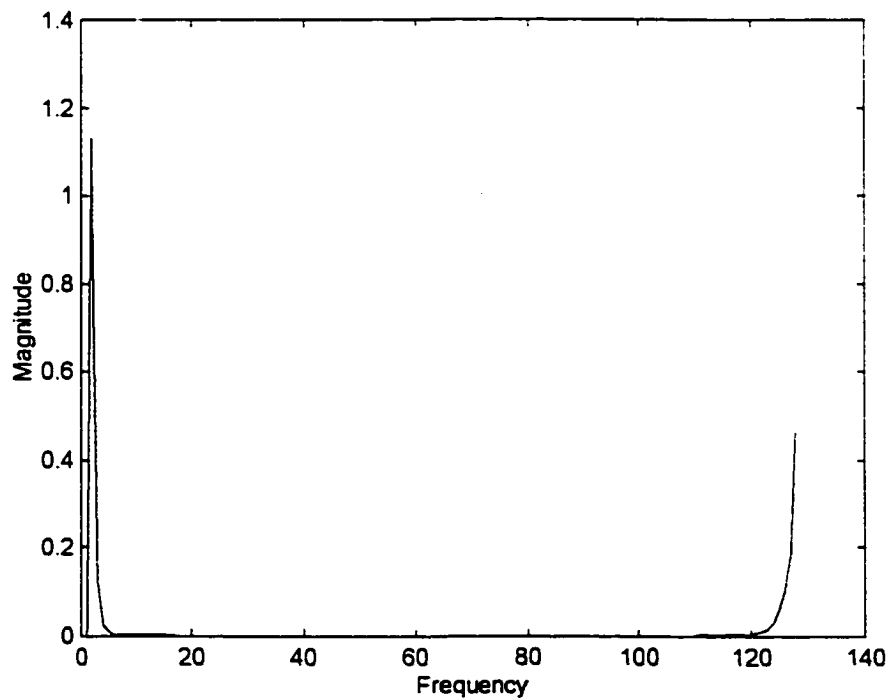


Figure 4.13: Plot of Fourier spectrum of trace point path with centroid spatially translated to global axis.

Table 4.8: Fourier coefficients of trace point path with centroid translated to global axis

Fourier Coefficient Number	F(u)	
	Magnitude	Phase
0	0.0000	0.0000
1	1.1309	1.1305
2	0.1280	0.1276
3	0.0228	0.0221
4	0.0090	0.0079
5	0.0031	0.0009
-		
123	0.0313	1.9391
124	0.0559	2.1002
125	0.1023	2.2455
126	0.1886	2.3808
127	0.4650	2.5125

rotated so the maximum radius is aligned with the x-axis. The starting point for the generation of the curve is then processed logically to start at the point on the curve aligned with the x-axis. Figure 4.14 is a plot of the Fourier spectrum of the trace point path that has been translated, rotated, and scaled. Table 4.9 lists the magnitude and phase of the first five and last four Fourier coefficients.

When using this technique to compare curve paths, a normalization process is required to ensure the curve paths have a standard size, orientation, and location of the trace point curve centroid.

To normalize the Fourier coefficients two different processes may be taken. One process would be to normalize the Fourier

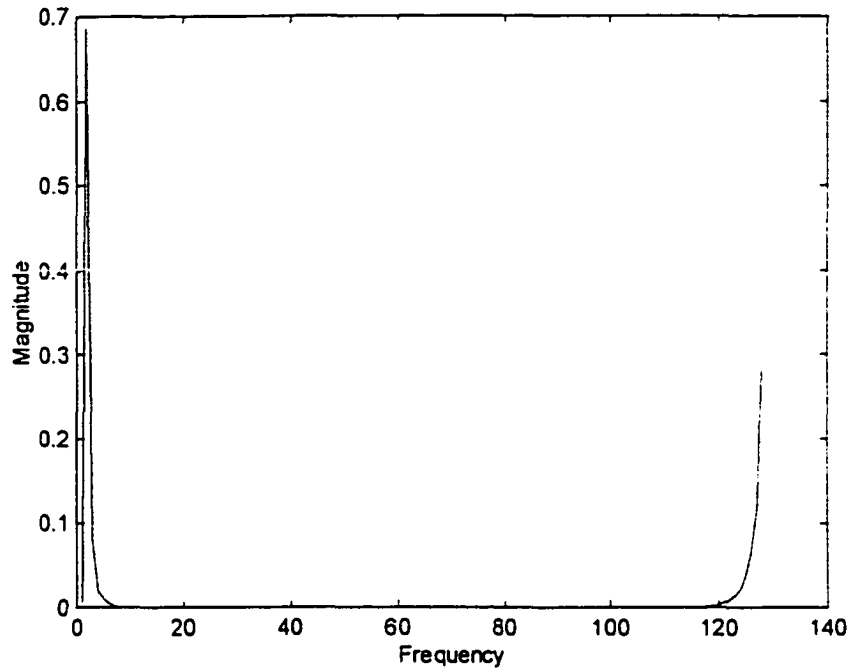


Figure 4.14: Plot of Fourier spectrum of trace point path spatially transformed to the origin of global axis, rotated and scaled.

Table 4.9: Fourier coefficients of trace point path spatially transformed to global axis, rotated and scaled.

Fourier Coefficient Number	F(u)	
	Magnitude	Phase
0	0.0000	0.0000
1	0.6868	-0.2553
2	0.0818	0.7728
3	0.0193	1.9032
4	0.0103	2.8674
5	0.0049	-2.5518
-		
123	0.0217	2.9548
124	0.0367	-2.2828
125	0.0649	-1.2496
126	0.1169	-0.2256
127	0.2832	0.8022

coefficients so they are invariant to translation, scale, and rotation. A standard size may be obtained by requiring the first Fourier Coefficient to have a unity magnitude. When the curve path is closed and traced in the counterclockwise direction, the first Fourier Coefficient, $F(1)$, will be the largest [Gonzalez, 1977]. The orientation of the trace point curve will have an effect only on the phase of the Fourier Transform coefficients. Therefore, the establishment of a standard orientation is essential for phase comparisons. The translation of the curve, (x_0, y_0) , will have an effect only on the initial Fourier Transform coefficient $F(0)$. The point at which the trace point curve is generated will not affect the Fourier coefficients. Table 4.9 lists selected Fourier coefficients for trace point path when the centroid is placed on the global axis. The curve is scaled so the maximum radius is equal to 1. The curve is also rotated so the maximum radius lies on the x-axis, and the starting point for tracing the curve is at the maximum radius on the x-axis. Table 4.10 lists the same Fourier coefficients for the trace point path but with the starting point for tracing the curve shifted by 180 degrees; there is no effect.

The majority of the Fourier coefficients have a magnitude close to zero. This attribute of the Fourier transform highlights one of the key advantages of using this linear transform. A

Table 4.10: Fourier coefficients of trace point path, starting point for tracing curve shifted by 180 degrees

Fourier Coefficient Number	F(u)	
	Magnitude	Phase
0	0.0000	0.0000
1	0.6868	-0.2553
2	0.0818	0.7728
3	0.0193	1.9032
4	0.0103	2.8674
5	0.0049	-2.5518
-		
123	0.0217	2.9548
124	0.0367	-2.2828
125	0.0649	-1.2496
126	0.1169	-0.2256
127	0.2832	0.8022

small number of Fourier coefficients, or Fourier Descriptors, may be used to not only characterize a curve but may be used to reconstruct the curve path. Rather than using 128 points to describe the trace point path a smaller number of Fourier descriptors may be used. Figure 4.15 is a plot of the spatially transformed trace point path of the crank-rocker four-bar mechanism specified on page 72 and is plotted using 128 points.

The magnitude of the Fourier Coefficients for this trace point path was plotted in Figure 4.14. The Fourier coefficients with the largest magnitude may be selected for use in the characterization and reconstruction of the trace point path. If the inverse Fourier Transform is evaluated with all of the 128 Fourier coefficients, each of the 128 points of the original trace point path will be generated. A select number of Fourier coefficients may be

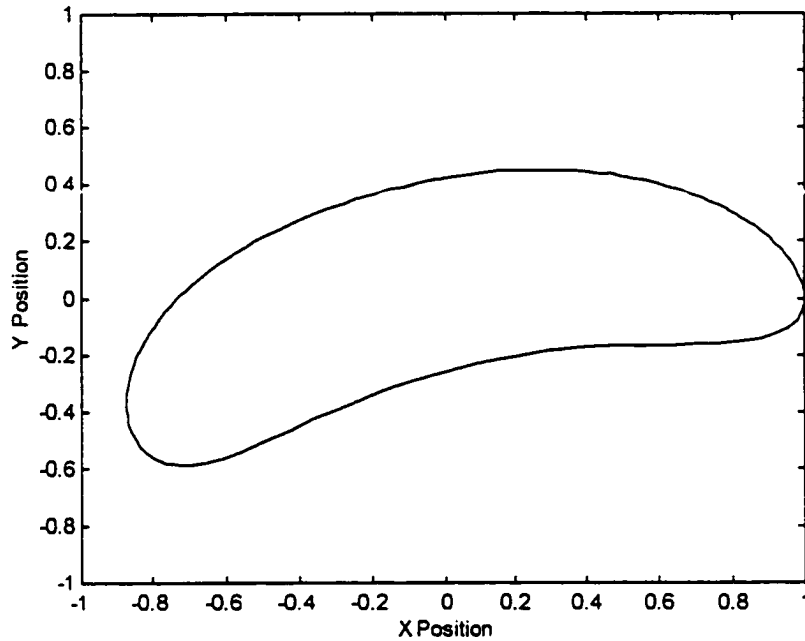


Figure 4.15: Spatially transformed trace point path described by 128 points

stored for the characterization and reconstruction of the trace point curve path. These Fourier coefficients will be called Fourier Descriptors. The value of each of the Fourier Descriptors and the number of the descriptor (0 through 127) must be retained for use in characterization and reconstruction processes.

As an example, 8 Fourier coefficients with the largest magnitude may be selected. Table 4.11 lists the value and position of the 8 Fourier coefficients for the defined trace point path. The eight Fourier descriptors are used in the evaluation of the inverse Fourier transform and zeros are used as the other 120 Fourier

Table 4.11: Top 8 Fourier descriptors of trace point path

Fourier Coefficient Number	F(u)	
	Magnitude	Phase
1	0.6812	-1.2592
2	0.0806	-1.3196
3	0.0167	-1.3697
123	0.0215	1.8032
124	0.0364	1.8123
125	0.0642	1.8184
126	0.1156	1.8255
127	0.2817	1.8249

coefficients. Figure 4.16 plots the trace point path when reconstructed from the top eight Fourier descriptors.

The error in reconstructing the trace point path may be calculated by evaluating the sum of the total error in each of the trace points.

$$\text{Error} = \sum [(|OTP| - |RTP|)^2]^{0.5} \quad [4.44]$$

Where:

OTP = Original trace point

RTP = Reconstructed trace point

The error in reconstructing the trace point path using 8 Fourier descriptors is 1.9876 units for the 128 points.

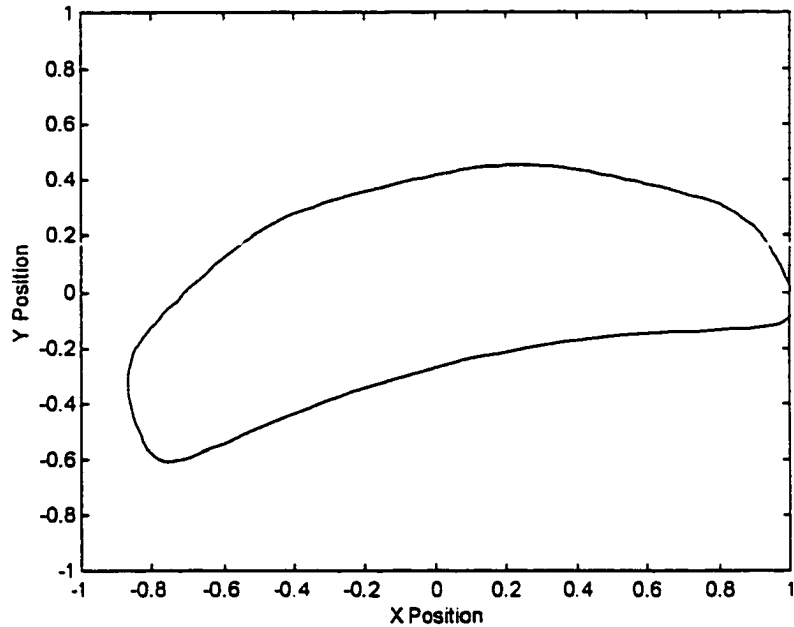


Figure 4.16: Trace point path reconstructed using 8 Fourier descriptors

The 16 Fourier coefficients with the largest magnitudes are then retained. Table 4.12 lists the value and position of the 16 Fourier coefficients for the defined trace point path. The 16 Fourier descriptors are used in the evaluation of the inverse Fourier transform and zeros are used as the other 120 Fourier coefficients. Figure 4.17 plots the trace point path when reconstructed from the top 16 Fourier descriptors. The difference between the original trace point path and the reconstructed trace point path cannot be seen with the eye. The error in reconstructing the trace point path using 16 Fourier descriptors is 0.1904 units for the 128 points.

The error in reconstructing the trace point path based on various numbers of Fourier descriptors is summarized in Table 4.13.

A requirement for comparison of various trace point paths or functions based upon Fourier Descriptors is that the number of discrete points sampled in each path or functions must be the same. In the previous examples 128 points were sampled.

Two-Dimensional Fourier Transforms

The previous examples show the advantages of using a one-dimensional Fourier transform to reduce the amount of information that is required to characterize and reconstruct a two dimensional trace point path. A similar process may be conducted to understand the possible advantages of using a two-dimensional Fourier transform to characterize and reconstruct the trace point path.

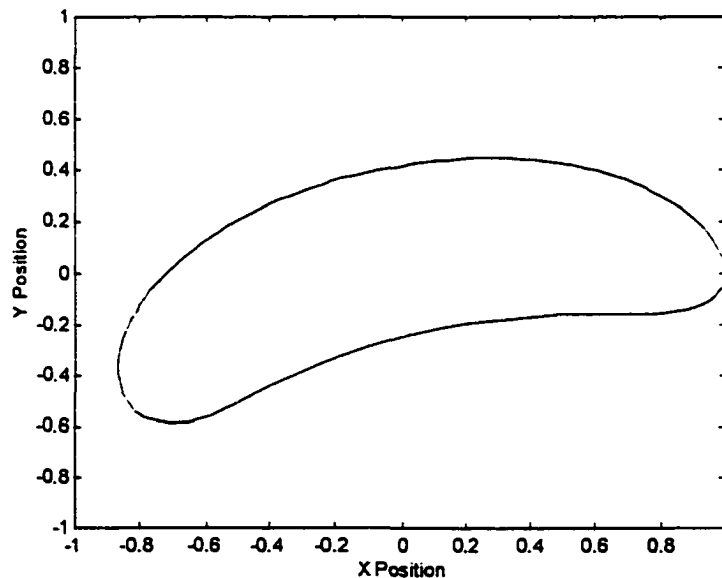


Figure 4.17: Trace point path reconstructed using 16 Fourier descriptors

Table 4.12: Top 16 Fourier descriptors of trace point path

Fourier Coefficient Number	F(u)	
	Magnitude	Phase
1	0.6812	-1.2592
2	0.0806	-1.3196
3	0.0167	-1.3697
4	0.0076	-1.3932
5	0.0030	-1.4938
6	0.0014	-1.6655
118	0.0016	1.6808
119	0.0028	1.7256
120	0.0047	1.7555
121	0.0078	1.7764
122	0.0129	1.7918
123	0.0215	1.8032
124	0.0364	1.8123
125	0.0642	1.8184
126	0.1156	1.8255
127	0.2817	1.8249

Table 4.13: Error in Trace Point Path Reconstruction

Number of Fourier Descriptors	Error in Trace Point Path
8	1.9876
12	0.5471
14	0.3082
16	0.1904
20	0.1060
24	0.0951
28	0.0853
32	0.0795
64	0.0568
128	0.0000

A matrix grid has been used to digitize and generate a two dimensional image for the trace point path (Figure 4.10). The number of cells in the image is 128x128 or 16,384 cells. Each cell in the image contains either a zero or a one. A gray scale is used for the image with values of "zero" generating a white cell and a "one" generating a black cell. As seen in Figure 4.11, the two-dimensional Fourier transform of an image generates a two dimensional matrix of Fourier Coefficients. As with the one-dimensional Fourier transform, the largest Fourier coefficients may be identified for use in the characterization and reconstruction of the trace point path curve.

The top 16 Fourier Descriptors used to in the one-dimensional Fourier transform of the trace point path constitutes 12.5% of the total Fourier coefficients. The top 12.5% Fourier Descriptors for the two-dimensional Fourier transform would be 2048 Fourier Descriptors. Figure 4.18 shows a matrix plot of the top 16 Fourier Descriptors for the spatially transformed trace point path (Figure 4.10). The Inverse Fourier Transform of the top 16 Fourier Descriptors is plotted in Figure 4.19. The top 128 Fourier Descriptors for the spatially transformed trace point path is plotted in Figure 4.20. The Inverse Fourier Transform of the top 128 Fourier Descriptors is plotted in Figure 4.21.

The figures highlight the major issue with using a two dimensional Fourier transform on an image of the trace point path. The majority of the image is white space while a small number of

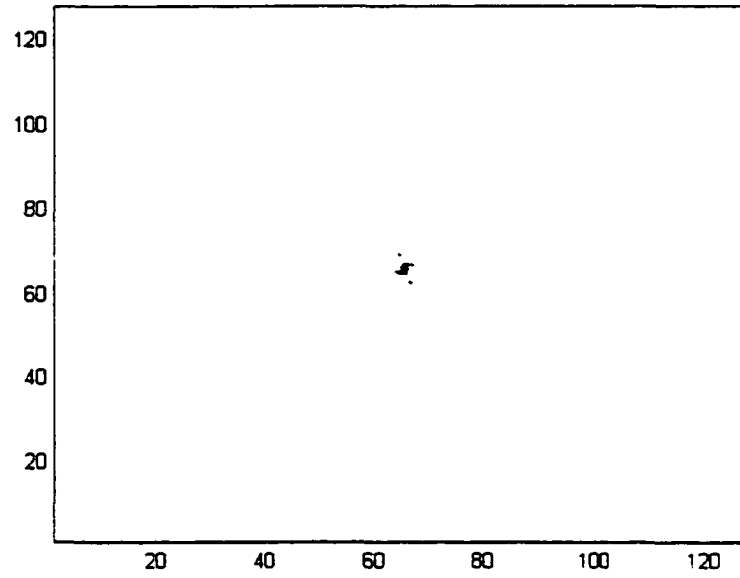


Figure 4.18: Top 16 Fourier descriptors for trace point path

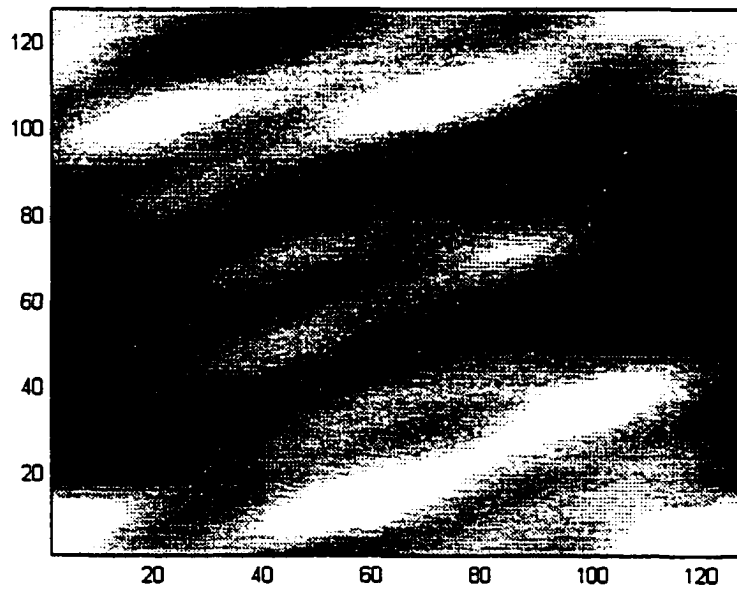


Figure 4.19: Inverse Fourier transform of top 16 Fourier descriptors

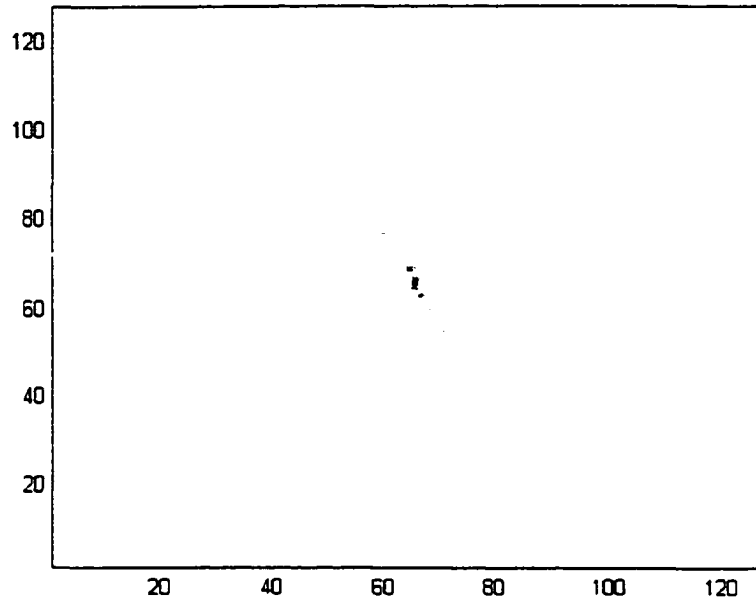


Figure 4.20: Top 128 Fourier descriptors for trace point path

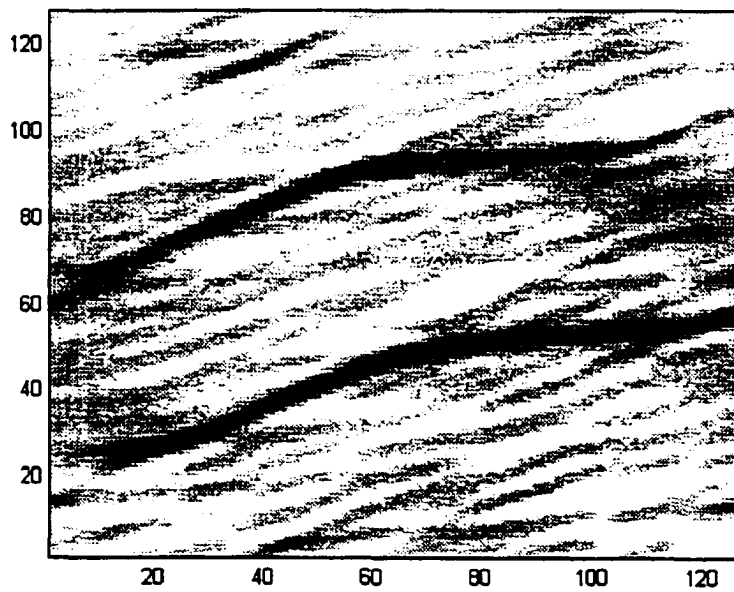


Figure 4.21: Inverse Fourier transform of top 128 Fourier descriptors

image cells are used to define the trace point path. The top 128 Fourier Descriptors does not perform an adequate job in reconstructing the trace point path and requires a substantially large amount of computing power to process when compared to the one-dimensional Fourier Transform.

Moments

There are other techniques for generating descriptors that are invariant to translation, rotation and size. An approach using moments is often used to generate invariant moments for pattern recognition. Moment invariants were first introduced by Hu [1961] and were further addressed by Reiss [1991]. A uniqueness theorem states that if $f(x,y)$ is piecewise continuous and has non-zero values only in a finite part of the x - y plane, then moments of all orders exist, and the moment sequence (m_{pq}) is uniquely determined by $f(x,y)$, and, conversely, (m_{pq}) uniquely determines $f(x,y)$. This means that the following summation may be viewed as a one to one mapping of the continuous, finite area image $f(x,y)$ onto the infinite discrete moment matrix \mathbf{M} with entries m_{pq} [Reiss]. The regular moment of an image $f(x,y)$ may be expressed as:

$$m_{pq} = \sum_x \sum_y x^p y^q f(x,y) \quad [4.45]$$

The central moments are defined as:

$$\mu_{pq} = \sum_x \sum_y (x - \bar{x})^p (y - \bar{y})^q f(x, y) \quad [4.46]$$

Where:

$$p, q = 0, 1, 2, \dots$$

$$\bar{x} = m_{10}/m_{00}$$

$$\bar{y} = m_{01}/m_{00}$$

The central moments are equivalent to the regular moments of an image that has been shifted so that the image centroid (\bar{x}, \bar{y}) is at the origin. Therefore, the central moments are invariant to image translations.

The central moments of order 3 are:

$$\mu_{10} = m_{10} - m_{10} * m_{00} / m_{10} = 0 = \mu_{01} \quad [4.47]$$

$$\mu_{11} = m_{11} - m_{10} * m_{01} / m_{00} \quad [4.48]$$

$$\mu_{20} = m_{20} - m_{10} * m_{10} / m_{10} \quad [4.49]$$

$$\mu_{02} = m_{02} - m_{01} * m_{01} / m_{10} \quad [4.50]$$

$$\mu_{30} = m_{30} - 3 * \bar{x} * m_{20} + 2 * m_{10} * \bar{x}^2 \quad [4.51]$$

$$\mu_{12} = m_{12} - 2 * \bar{y} * m_{11} - \bar{x} * m_{02} + 2 * m_{10} * \bar{y}^2 \quad [4.52]$$

$$\mu_{21} = m_{210} - 2 * \bar{x} * m_{11} - \bar{y} * m_{20} + 2 * m_{01} * \bar{y}^2 \quad [4.53]$$

$$\mu_{03} = m_{03} - 3 * \bar{y} * m_{02} + 2 * m_{01} * \bar{y}^2 \quad [4.54]$$

The normalized central moments are defined as:

$$\eta_{pq} = \mu_{pq} / \mu_{00}^p \quad [4.55]$$

Where:

$$\gamma = (p + q)/2$$

$$p, q = 2, 3, \dots$$

From the second and third moments a set of seven invariant moments, φ_n , may be derived [Hu and Bell].

$$\varphi_1 = \eta_{20} + \eta_{02} \quad [4.56]$$

$$\varphi_2 = (\eta_{20} - \eta_{02})^2 + 4\eta_{11}^2 \quad [4.57]$$

$$\varphi_3 = (\eta_{30} - 3\eta_{12})^2 + (3\eta_{21} + \eta_{03})^2 \quad [4.58]$$

$$\varphi_4 = (\eta_{30} + \eta_{12})^2 + (\eta_{21} + \eta_{03})^2 \quad [4.59]$$

$$\begin{aligned} \varphi_5 = & (\eta_{30} - 3\eta_{12})(\eta_{30} + \eta_{12}) [(\eta_{30} + \eta_{12})^2 - 3(\eta_{21} + \eta_{03})^2] \\ & + (3\eta_{21} - \eta_{03})(\eta_{21} + \eta_{03}) [3(\eta_{30} + \eta_{12})^2 - (\eta_{21} + \eta_{03})^2] \quad [4.60] \end{aligned}$$

$$\begin{aligned} \varphi_6 = & (\eta_{20} - \eta_{02}) [(\eta_{30} + \eta_{12})^2 - (\eta_{21} + \eta_{03})^2] \\ & + 4\eta_{11}(\eta_{30} + \eta_{12})(\eta_{21} + \eta_{03}) \quad [4.61] \end{aligned}$$

$$\begin{aligned} \varphi_7 = & (3\eta_{12} - \eta_{30})(\eta_{30} + \eta_{12}) [(\eta_{30} + \eta_{12})^2 - 3(\eta_{21} + \eta_{03})^2] \\ & + (3\eta_{21} - \eta_{03})(\eta_{21} + \eta_{03}) [3(\eta_{30} + \eta_{12})^2 - (\eta_{21} + \eta_{03})^2] \quad [4.62] \end{aligned}$$

This set of seven invariant moments is invariant to translation, rotation, and scale change [Hu, 1962].

Figure 4.22 is a graph of the spatially transformed trace point path. Figure 4.23 is a graph of the spatially transformed trace point path rotated 90°, and Figure 4.24 is a graph of the spatially transformed trace point path rotated 180°. Table 4.24 is a summary of the seven invariant moments of the three trace point paths and demonstrates invariance with rotation.

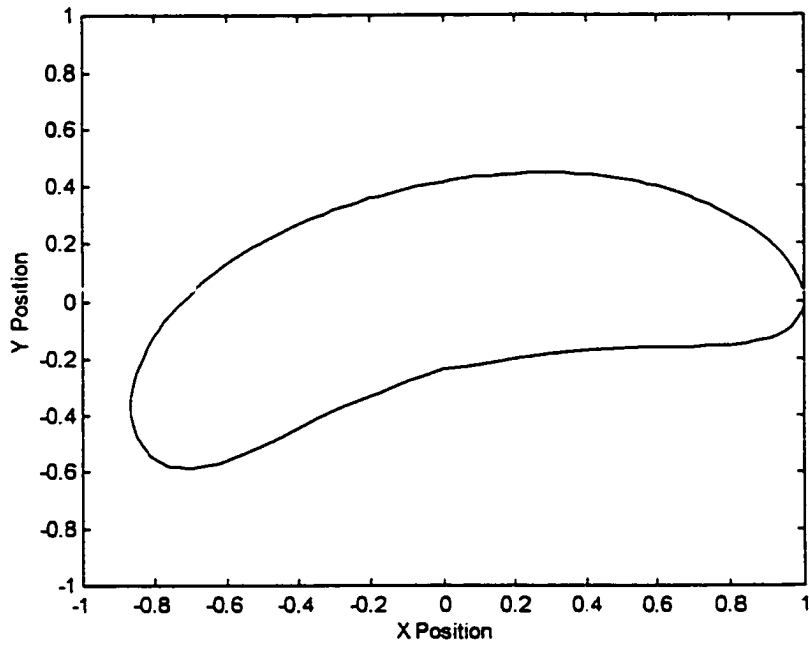


Figure 4.22: Spatially transformed trace point path

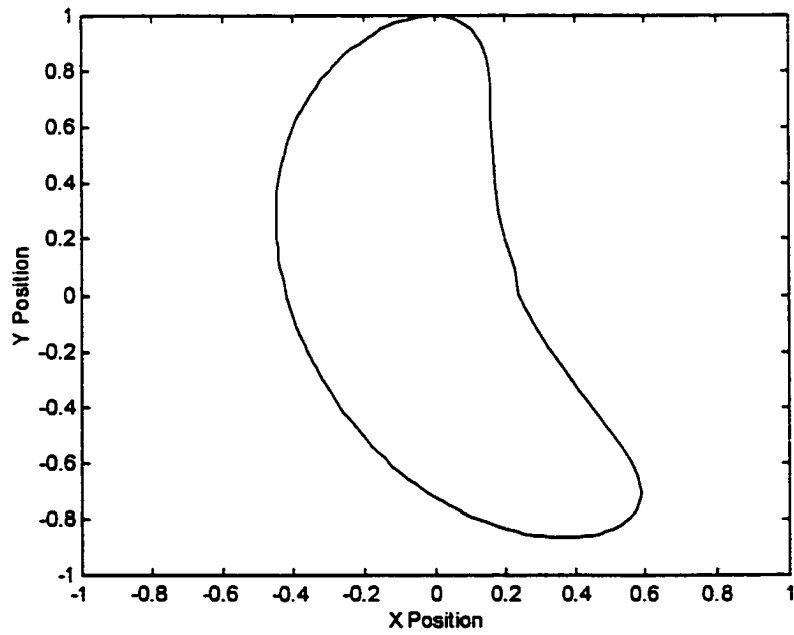


Figure 4.23: Trace point path rotated 90°

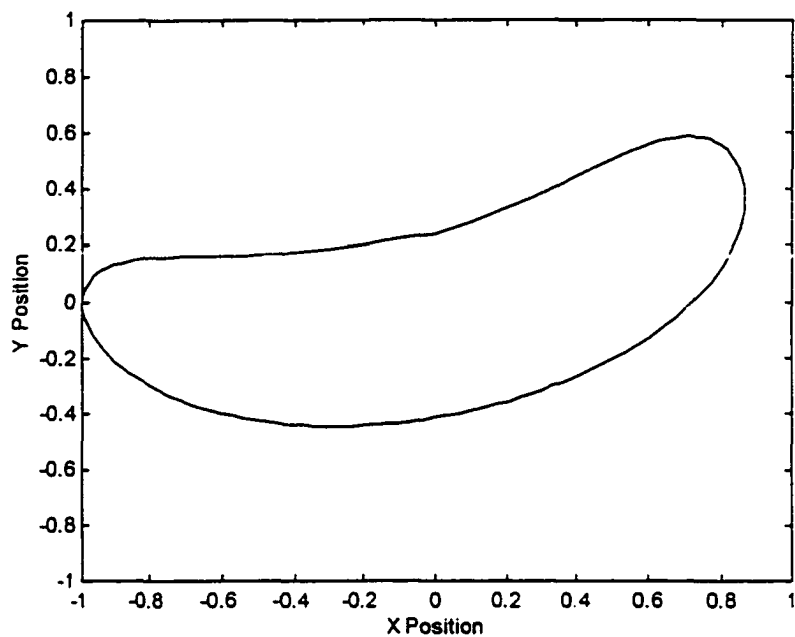


Figure 4.24: Trace point path rotated 180°

Table 4.14: Invariant moments of selected trace point paths

Invariant (log)	Original Trace Point Path	Rotated 90°	Rotated 180°
φ_1	3.3066	3.3066	3.3035
φ_2	6.2175	6.2175	6.2071
φ_3	5.8921	6.3776	5.8506
φ_4	5.1788	5.1788	5.1759
φ_5	10.8637	10.8637	10.8050
φ_6	8.2372	8.2372	8.2071
φ_7	10.8629	10.8629	10.8881

CHAPTER 5. SOLUTION COMPARISON AND MATCHING METHODS

This chapter addresses the matching of the desired output of a four-bar mechanism (function, path or motion generation) with each candidate solution stored in a database. The technique used for matching a desired output with a candidate solution will need to identify the best candidate solution based on a measure of similarity. The technique should also identify candidate solutions that are close to the desired solution even though there may not be an exact match. In evaluating a match, the desired output is compared to each candidate solution in a database. A measure of similarity, or difference, is generated between the desired output and each candidate solution. The candidate solutions in the database with the best measure of similarity are identified as possible solutions, or all measures that meet a defined threshold are identified as a possible solution. These matching technique may be carried out in the spatial domain or a transform domain and may be based on the similarity or difference between the objects.

Matching a desired solution with candidate solutions is used in two dimensional image processing applications such as optical character recognition, locating changes in an image, identifying

objects in a photograph, estimating object motion, and so on. Many matching applications must deal with noise that may be in the two dimensional image. With character recognition, noise may be dirt on a typed page or a smudged character. With many matching applications, different intensities of the image gray scale, or color, must be considered. An object may also have skew distortion, which is due to the projection angle between the camera and the object. A camera that is not normal to a square object will generate a picture of a rectangle. Image intensity must be considered if one is trying to identify objects in an x-ray or a in photographs that are taken during the day and at night. Noise, skew, and image intensity must be addressed in addition to object orientation and scale of the object. Matching, as it relates to matching a function or a path stored in a database, does not have issues with background noise, skew, or image intensities.

For any matching technique, a common basis must be developed to support the characterization of a solution in the spatial domain, or a transform domain, that is invariant under translation, scaling, and rotation. Figure 5.1 shows two different trace point paths. The larger trace point path is generated by the four-bar mechanism defined in Chapter 4. The smaller closed curve is the larger path that has been spatially transformed to a normalized position, size and rotation. From a design perspective, all four-bar mechanisms capable of producing the solution are of interest. A mechanism that is merely scaled to a different size, rotated to a different angle,

or located at a different physical location may be a viable candidate. Therefore, attaining a basis where the characterized output (function, path or motion) of a four-bar mechanism which is invariant to size, rotation, and translation is of interest.

There are many different methods that have been developed for matching [Hussain, 1991] [Chen, Defrise and Deconick, 1994] [Dudani, 1977] [Gonzalez, 1977] [Hall, Wong, Chen Sadjadi and Frie, 1976] [Wong and Hall, 1978]. For a two-dimensional object, shape properties such as perimeter length, area, eccentricity, number of corners, number of holes, texture, and minimum bounding angle may be used to label objects in an image. For two functions, $f(x)$ and $g(x)$, there are many methods of determining a match between them. We will review several of these methods in this chapter, but first an overview of spatial transforms to address translation, rotation, and scale of a trace point path.

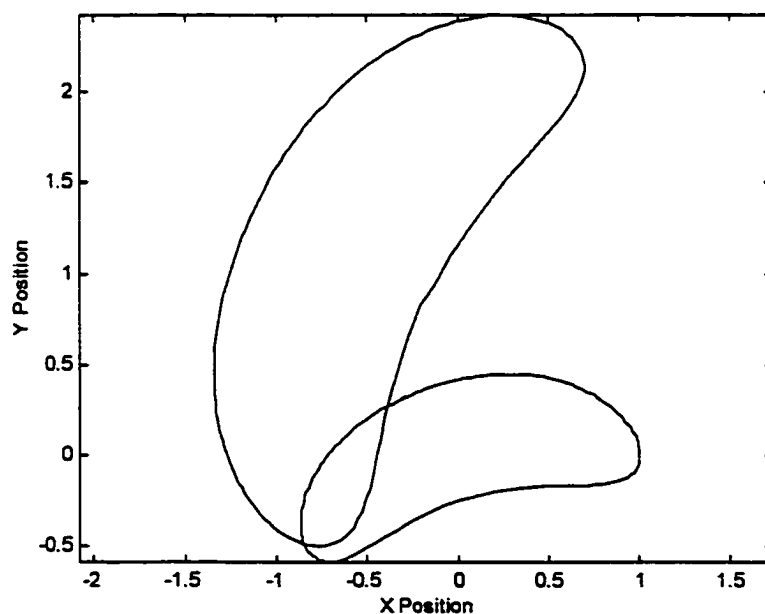


Figure 5.1: Trace point path and spatially transformed path

We have reviewed several different methods of attaining invariant characteristics of the output. One is through spatial transforms. For a trace point path the centroid of the path is found by the following (Figure 5.2 plots the path and centroid):

$$X_{cen} = \sum_{i=1}^N P_{i_x}/N \quad [5.1]$$

$$Y_{cen} = \sum_{i=1}^N P_{i_y}/N \quad [5.2]$$

Where:

X_{cen} = Horizontal position of the path centroid

Y_{cen} = Vertical position of the path centroid

P_{x_i} = X position of a discrete point

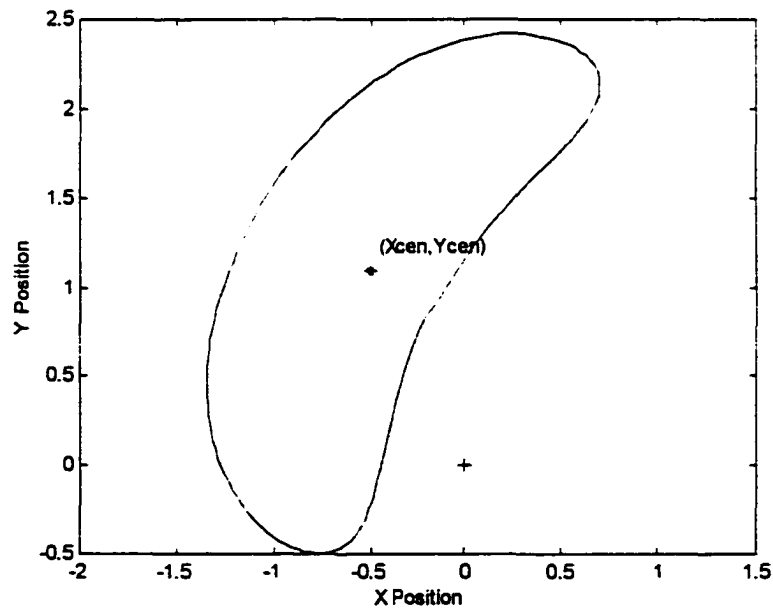


Figure 5.2: Centroid of trace point path - X_{cen} , Y_{cen}

P_{y_i} = Y position of a discrete point

N = Number of total points defining the path

The trace point path is then translated to the origin of the world axis by the following transformation (Figure 5.3 plots the translated path):

$$P_{i_x'} = P_{i_x} - X_{cen} \quad [5.3]$$

$$P_{i_y'} = P_{i_y} - Y_{cen} \quad [5.4]$$

Where:

$P_{i_x'}$ = Translated X position of a discrete point

$P_{i_y'}$ = Translated Y position of a discrete point

For the translated trace point path, the largest radius between the centroid and the path is found by the following (Figure 5.3 plots the path and the largest radius):

$$R_{max} = \text{Maximum} [(P_{i_x'} - X_{cen})^2 + (P_{i_y'} - Y_{cen})^2]^{0.5} \quad [5.5]$$

Where:

R_{max} = Maximum radius

The trace point path is then scaled by the following transformation (Figure 5.4 plots the scaled path):

$$Pi_x'' = Pi_x' / Rmax \quad [5.6]$$

$$Pi_y'' = Pi_y' / Rmax \quad [5.7]$$

Where:

Pi_x'' = Scaled X position of a discrete point

Pi_y'' = Scaled Y position of a discrete point

For the translated and scaled trace point path, the angle between the largest radius and the positive x-axis is found by the following (Figure 5.4 plots the path and the angle θ):

$$\theta = \text{atan}(Pi_y'_{Rmax} / Pi_x'_{Rmax}) \quad [5.8]$$

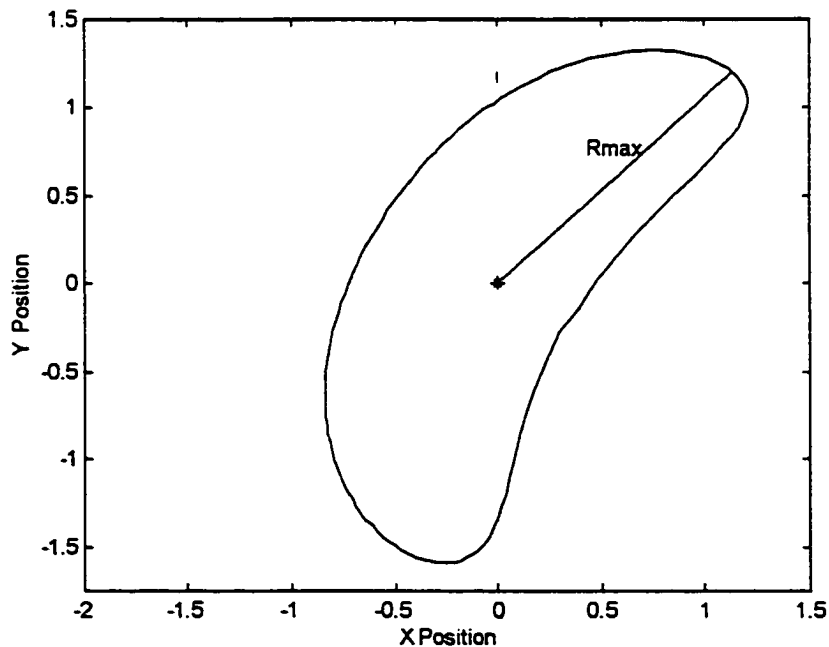


Figure 5.3: Maximum radius of trace point path - Rmax

Where:

$P_{i_x'}'_{R_{max}}$ = X position of a discrete point where R_{max} occurs

$P_{i_y'}'_{R_{max}}$ = Y position of a discrete point where R_{max} occurs

The trace point path is then rotated using the following transformation (Figure 5.5 plots the rotated path):

$$P_{i_x'''} = P_{i_x''} \cos\theta + P_{i_y''} \sin\theta \quad [5.9]$$

$$P_{i_y'''} = P_{i_x''} \sin\theta - P_{i_y''} \cos\theta \quad [5.10]$$

Where:

$P_{i_x'''} =$ Rotated X position of a discrete point

$P_{i_y'''} =$ Rotated Y position of a discrete point

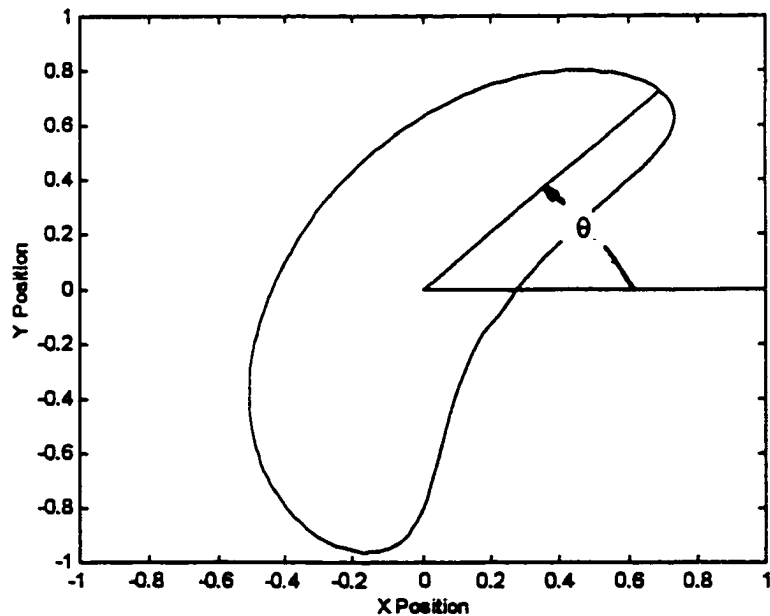


Figure 5.4: Angle θ of trace point path

Figure 5.5 plots the translated, scaled, and rotated trace point path.

The first consideration when matching two discrete functions, or, for example, when matching two trace point paths, is that the number of discrete sampled points must be the same. The number of points that a designer may use to originally define the curve need not be the same. But, when evaluating the similarity of difference between two different solutions, whether in the spatial domain or in the Fourier frequency domain, the number of points used in evaluating the desired solution and candidate solutions must be the same.

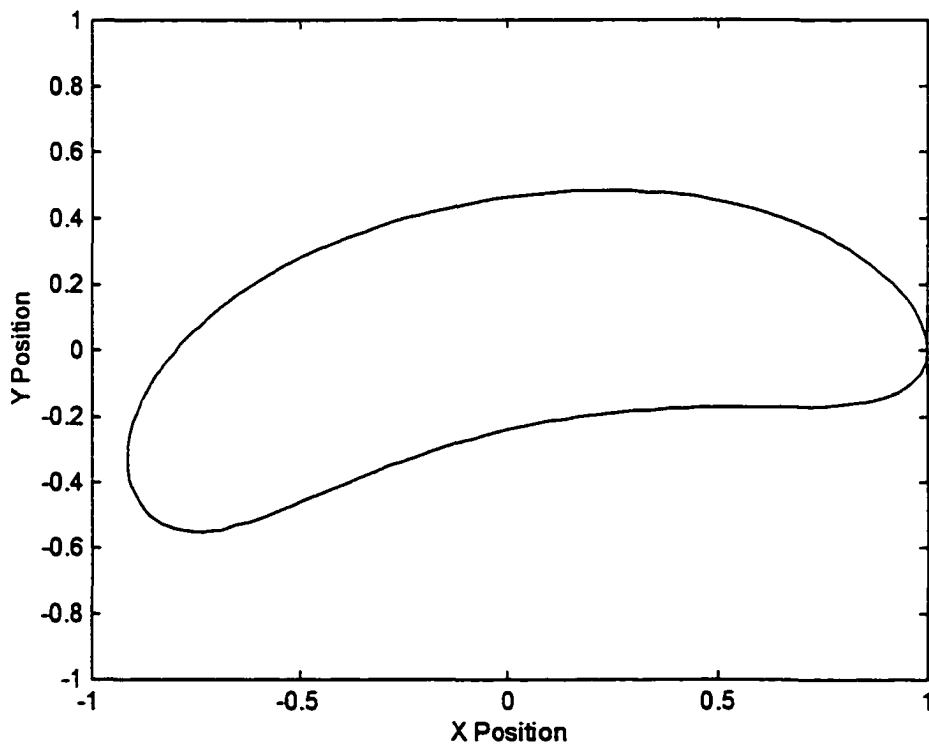


Figure 5.5: Spatially transformed trace point path

If two identical curves are being compared in the spatial domain, there must be the capability to make a comparison between each curve point by point, and there must be some common basis on each curve with regards as where to start the comparison. In the spatial domain, rotating the trace point path so the largest radius lies on the x-axis provides a common point at which to start the comparison.

The second consideration when matching two objects in the spatial or frequency domain is that the objects being compared must be invariant to translation, rotation, and scaling. Comparing the two curves in Figure 5.1 would not generate a good correlation, or match, even though the path shapes are identical. A good correlation would be attained if the trace point paths were normalized for translation, rotation and scale.

Spatial Similarity and Difference Measures

The matching of two functions is of interest to identify a match for a function generation four-bar mechanism, an image match is of interest for a path generation four-bar mechanism, and an image and a function match is of interest for a motion generation four-bar mechanism. The determination of a match between a desired function or curve, $f(x)$, and a curve stored in a database, $g(x)$, may be handled by several different methods.

Before discussing methods to measure the similarity or difference between objects, a basis must be established for making a

comparison between two objects. Matching methods evaluated in the spatial domain will compare points between the two functions. To perform this type of evaluation, a curve stored in a database must have an x and y value for each point on the trace point curve. The designer determines the total number of points that defines the path or a curve. Two points may define a straight-line path, while a complex trace point path of a four-bar mechanism may need hundreds of points to specify a required motion. In any case, a common basis must be established to correlate a desired object with a set of objects stored in a database.

Several methods for measuring the similarity or differences between two functions $f(x)$ and $g(x)$ are described by Hussain [1991].

- Normalized cross-correlation (similarity measure)

$$C(x) = P(x)/Q(x) \quad [5.11]$$

Where:

$$P(x) = \sum f(x) * g(x)$$

$$Q(x) = (\sum f(x)^2 * g(x)^2)^{0.5}$$

- Sum of absolute differences (difference measure)

$$A(x) = \sum |f(x) - g(x)| \quad [5.12]$$

- Sum of squared differences (difference measure)

$$S(x) = \sum [f(x) - g(x)]^2 \quad [5.13]$$

Solution Matching Using Fourier Descriptors

The first consideration to be addressed for pattern matching in the frequency domain is with regards to how many discrete samples are required to ensure there is an understanding of what is lost in using the Fourier transform. The Whittaker-Shannon sampling theorem is described in Bracewell [1978]. The premise of the sampling theorem is that any continuous function that is limited in how rapidly it can vary can be completely characterized by its samples as long as the samples are spaced a specific interval apart. The maximum permissible spacing between the samples of a curve or a path is inversely proportional to the bandlimit of the curve or path. The bandlimit is a measure of the variability of the curve or path. The minimum sampling rate, or the maximum sampling spacing, is called the Nyquist rate. If the sampling rate is significantly above or below the Nyquist rate it is oversampled or undersampled. Undersampling may lead to variations and detail that is lost completely or may generate a phenomenon known as aliasing. For sampling data at least eight data samples must be taken between amplitude peaks to obtain meaningful information regarding the waveform from a Fourier transform. Oversampling leads to excessive data computations and data storage.

For two continuous functions $f(x)$ and $g(x)$, the correlation of the two functions is defined by:

$$f(x) \circ g(x) = \int f^*(\alpha)g(x+\alpha) d\alpha \quad [5.14]$$

Where:

' = indicates the complex conjugate

α = a dummy variable of integration

The complex conjugate is one of a pair of complex numbers with identical real parts and with imaginary parts differing only in sign. The discrete representation of the correlation of the two continuous functions is defined by:

$$f(x) \circ g(x) = \sum_{m=0}^{M-1} f^*(m)g(x+m) \quad [5.15]$$

Where:

$x = 0, 1, 2, \dots, M-1$

M = Number of discrete points in a sampled array

The correlation theorem for the two functions is:

$$f(x) \circ g(x) \Leftrightarrow F^*(u)G(u) \quad [5.16]$$

and

$$f^*(x)g(x) \Leftrightarrow F^*(u)G(u) \quad [5.17]$$

The correlation of the two functions in the spatial domain corresponds to multiplication in the frequency domain. The spatial correlation of $f(x) \circ g(x)$ corresponds to multiplication in the frequency domain. Therefore, the correlation of the two functions, $f(x)$ and $g(x)$ in the spatial domain is a simple point by point multiplication of a $G(u)$ with the complex conjugate $F^*(u)$ followed by an evaluation of the inverse Fourier transform of the results.

When addressing the similarity, or matching, between two functions, one approach is to compute the correlation between an unknown function and a known function. The closest match is found by selecting the functions that yield the correlation function with the largest value. The evaluation of $f(x) \circ g(x)$ is easily evaluated in the frequency domain and the inverse Fourier transform taken to evaluate the largest amplitude of each comparison.

$$f(x) \circ g(x) = \mathcal{F}^{-1}[F^*(u) * G(u)] \quad [5.18]$$

One limitation to evaluating the correlation values between a function and a database of functions as defined here is that the output is dependent on the amplitudes of $f(x)$ and $g(x)$ rather than spatial structures, and the output around the maximum is broad [Chen, Defrise and Deconinck, 1994].

One method to address this condition is to develop an expression that evaluates only the phase of the Fourier transform. This is accomplished by eliminating the amplitude of $F(u)$:

$$\mathcal{F}^{-1}\{[F'(u)/|F(u)|]*G(u)\} \quad [5.19]$$

This expression is known as the phase-only filter. The output of this expression provides a sharper peak than the correlation value of the two functions. The output is still dependent on the amplitude of $g(x)$ but is less sensitive to the amplitudes of the Fourier coefficients.

Further improvement on the output may be obtained by correlating the phases of both $f(x)$ and $g(x)$ and eliminating the amplitude of $F(u)$ and $G(u)$:

$$\mathcal{F}^{-1}\{[F'(u)/|F(u)|]*G(u)/|G(u)|\} \quad [5.20]$$

This expression is known as symmetric phase-only matched filter or SPOMF. The advantages of the phase only filters lie with their high discriminating power, numerical efficiency and robustness against noise [Chen, Defrise and Deconick, 1994]. A major drawback is that the spectral phase of an image is not invariant for rotation and scaling. Therefore, phase-only matched filtering is efficient only when rotation and scaling are small and can be ignored. Chen, Defrise, and Deconick [1994] use the Fourier-Mellin Invariant

descriptors which are translation-invariant and represent rotation and scaling as translations along corresponding axes in parameter space. They use a two-dimensional matching technique based on the symmetric phase-only matched filtering of the Fourier-Mellin invariant descriptors of the images. Since translation, rotation, and scaling have been addressed through the use of a spatial transform to achieve translation, rotation, and scale invariance, the use of Fourier-Mellin Invariant Descriptors is not a requirement.

Implementation of the correlation, the phase-only filter, and the symmetric phase-only matched filter requires that the Fourier Transforms of the two functions, $F(u)$ and $G(u)$, be based on the same number of sampled points.

The implementation of the symmetric phase-only matched filter is with the following process:

1. Compute the Fourier transform $G(u)$ of the template image and the Fourier transform $F(u)$ of a database image.
2. Extract the phase $\exp(-i*\phi_G(u))$ of $G(u)$ and the phase $\exp(-i*\phi_F(u))$ of $F(u)$.
3. Determine the output of the symmetric phase-only matched filter:

$$Q(u) = \exp[-i*\phi_G(u) - i*\phi_F(u)] \quad [5.21]$$

4. Compute the inverse Fourier transform:

$$q(x) = \mathcal{F}^{-1}[Q(u)] \quad [5.22]$$

5. Identify the maximum value $q(x)$. The larger the maximum of $q(x)$, the better the match between the functions.

An evaluation of the Fourier descriptors may also be focused on the absolute difference in the amplitude and phase of the descriptors. The difference in the amplitude of the Fourier descriptors may be evaluated by:

$$M(u) = \sum ||F(u)| - |G(u)|| \quad [5.23]$$

Where:

$$M(u) = \text{Sum of amplitude difference}$$

The phase of the Fourier descriptor will have a impact on matching solutions which is related to the magnitude of the Fourier descriptor. A difference in phase with a Fourier descriptor that has a value close to zero will have little effect on the construction of each solution. The difference in phase with a Fourier descriptor that has the largest magnitude will have a large effect on the construction of each solution. Thus, one method to address this condition is to multiply the phase by the magnitude of the Fourier descriptor being evaluated.

$$P(u) = \sum |F(u) * [F(u) / |F(u)|] - G(u) * [G(u) / |G(u)|]| \quad [5.24]$$

Where:

$$P(u) = \text{Sum of weighted phase difference}$$

The total measure of the difference between the amplitude and phase of the Fourier descriptors may be written:

$$Fd(u) = m * M(u) + n * P(u) \quad [5.25]$$

Where:

$$Fd(u) = \text{Sum of amplitude and phase difference}$$

$$n = \text{Weighting applied to phase difference}$$

$$m = 1 - n = \text{Weighting applied to amplitude difference}$$

The weightings are used to address the difference in the contribution that the amplitude difference and phase differences have to the total difference measure.

Solution Matching using Moments

Invariant moments have been used to extract invariant features from an image and applied to two-dimensional pattern recognition [Hu, 1962]. Applications using invariant moments are many and include recognition of letters and numerals of a particular font [Hu, 1962], categorization of profusion of opacities in medical

chest X, identification of aircraft [Dudani, Bredding and McGhee, 1977], and scene matching [Wong and Hall, 1978].

The set of seven invariant moments defined by Hu [1962], which are invariant to translation, rotation, and scale change, were proved for continuous functions. When invariant moments were used with discrete data and computed by a computer, variations are to be expected based on the size of the rotation, translation, and scale change [Wong and Hall, 1978]. Analysis has shown that the effects of a scale change by a factor up to two and a rotation of up to 45 degrees maintain reasonably good results [Hall, Wong, Chen, Sadjade and Frei, 1976].

Wong and Hall [1978] used a product correlator based on the following equation to correlate the seven invariant moments of radar sub-images with those computed at each of the test locations in an optical search scene:

$$R_k(u, v) = \frac{\sum_j M_j N_j(u, v)}{[\sum_j M_j^2 * \sum_j N_j^2(u, v)]^{0.5}} \quad [5.26]$$

Where:

$R_k(u, v)$ = Moment correlation

M_j = jth Invariant moment of image

N_j = jth Invariant moment of database image

The highest correlation values identify the most likely matches.

Wong and Hall also suggest other weighting factors be applied to

each of the seven moments before correlation. The values of the weighting factors could relate to the information content of the frequency distribution of the gray levels of the images. Such a method, they suggest, could generate a better and more efficient match.

CHAPTER 6. FUNCTION GENERATION

Function generation is where the functional requirement is the relative motion between links which are connected to the ground pivots, or where a specific input position will result in a specific output position. The output position of the follower crank is typically viewed as the output function with the input function being the input position of the drive crank. Other function outputs could be the output angle of the connecting rod. The output angle of the connecting rod will be discussed in Chapter 8 - Motion Generation.

Figure 6.1 is a plot of the follower crank angle for the example four-bar mechanism defined in Chapter 4. The follower crank angle and the drive crank angle are measured from a reference line which passes through the drive crank pivot and the follower crank pivot (Figure 6.2).

The initial follower crank angle and the average follower crank angle are dictated by the definition of the reference line which passes through the drive crank pivot and the follower crank pivot. Any reference line may be used for the definition of the follower crank angle. Therefore, the value of the follower crank

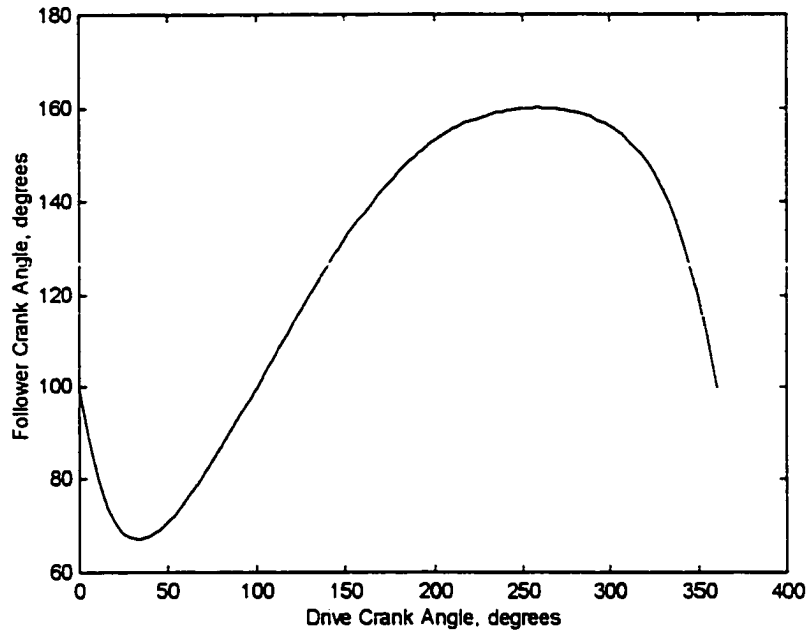


Figure 6.1: Follower crank angle as a function of drive crank angle

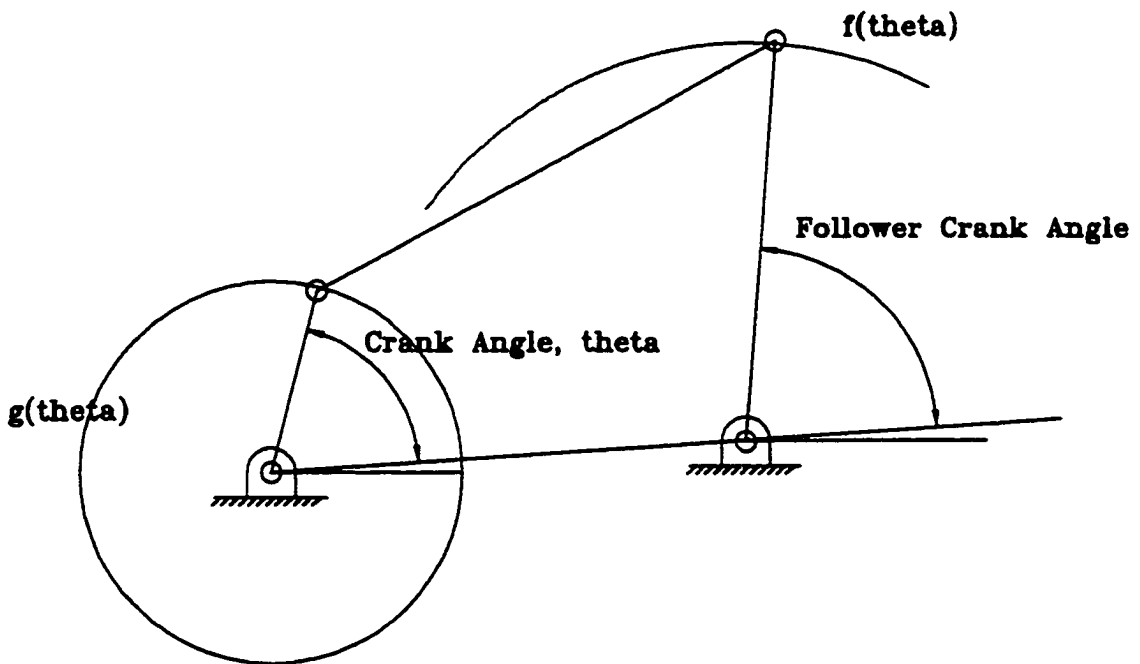


Figure 6.2: Drive crank angle and follower crank angle

angle may be shifted so the average of the follower crank angle over the range of motion is zero.

$$\sum_{x=0}^N f(x) = 0 \quad [6.1]$$

This will normalize the average value of the curve.

The initial angle of the follower crank is dictated by the initial angle of the drive crank and the reference line that passes through the ground pivots. The drive crank angle may be set at any initial position and the reference line through the ground pivots is arbitrary. Therefore, when the drive crank rotates through a complete cycle, the curve may be shifted so the largest positive angle of the curve resides at a crank angle of zero.

$$f(0) = f_{\max}(x) \big|_{x=c} \quad [6.2]$$

This will normalize the phase of the curve. Normalizing for the average value and the phase for each curve will allow the development of a database of curves and the process of matching a desired function with the stored database of curves. An important aspect to remember is that the number of discrete points used in defining the curve and in generating transforms must be consistent. Figure 6.3 graphs the follower crank angle after normalization for the average value. Figure 6.4 graphs the

follower crank angle after normalization for the average value and for the phase shift due to the initial drive crank angle.

A one-dimensional Fourier transform is taken of the invariant follower crank angle using 128 discrete points. The discrete points are taken at each of 128 crank positions ranging from 0 to 360 degrees. Figure 6.5 is a plot of the magnitude of the Fourier transform using equation 4.8.

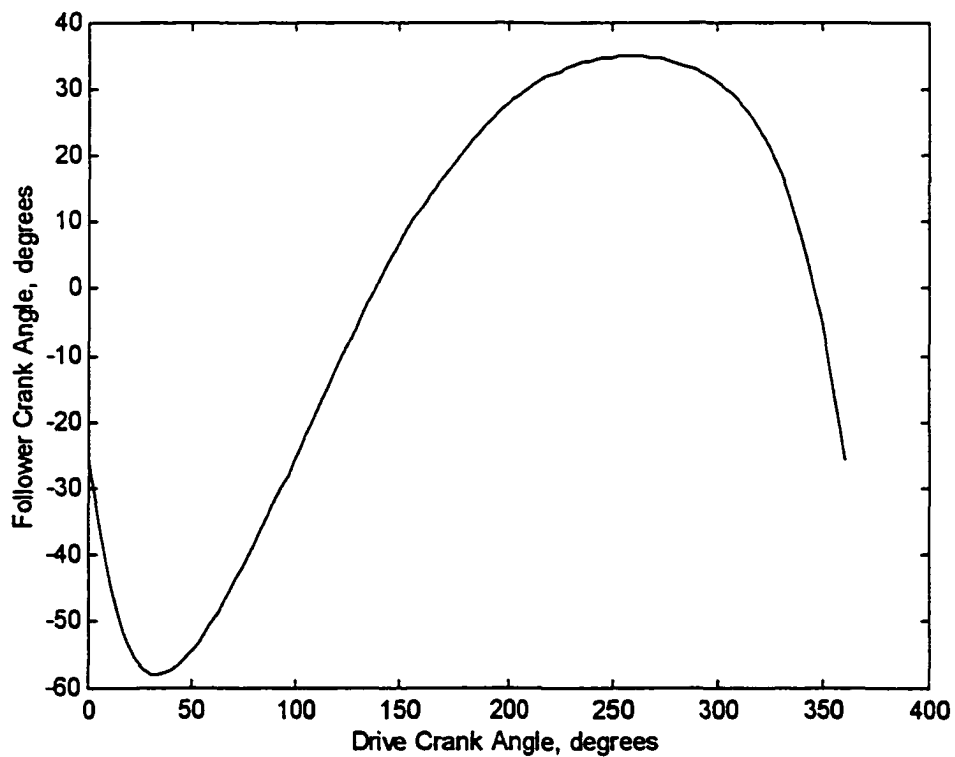


Figure 6.3: Follower crank angle normalized for average value

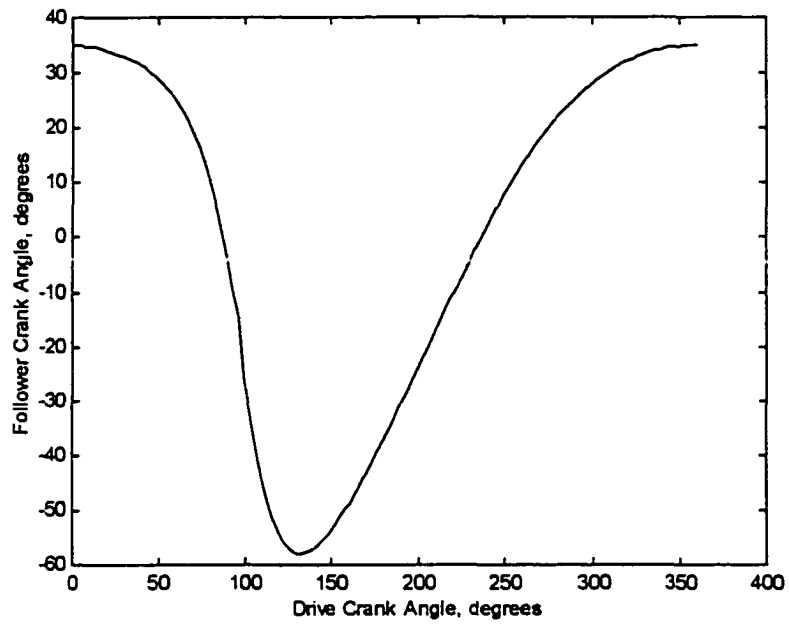


Figure 6.4: Follower crank angle normalized for average value and for phase shift

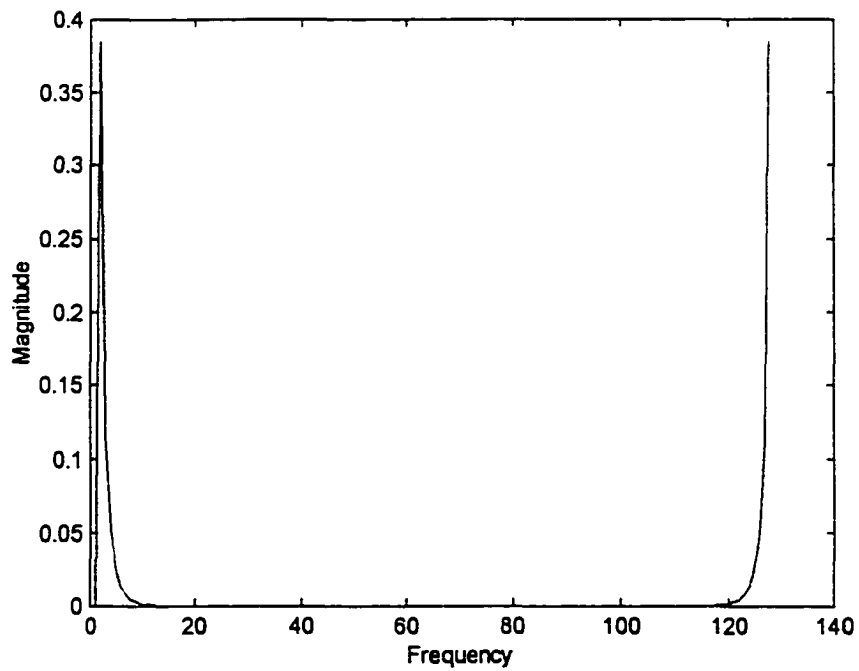


Figure 6.5: Fourier transform of normalized follower crank angle

The crank-rocker four-bar mechanisms defined in Hrones and Nelson are used To develop a database of curves for testing the performance of the various matching techniques. A summary of the four-bar mechanisms is found in Tables 6.1, 6.2, 6.3 and 6.4.

Table 6.1: Summary of database four-bar mechanisms

Drive Crank Length	Connecting Rod Length	Follower Crank Length	Ground Pivot Distance
1.0	1.5	1.5	1.5
1.0	1.5	2.0	2.0
1.0	1.5	2.5	2.5
1.0	1.5	3.0	3.0
1.0	1.5	3.5	3.5
1.0	1.5	4.0	4.0
1.0	2.0	1.5	2.0
1.0	2.0	2.0	1.5
1.0	2.0	2.0	2.0
1.0	2.0	2.0	2.5
1.0	2.0	2.5	2.0
1.0	2.0	2.5	2.5
1.0	2.0	2.5	3.0
1.0	2.0	3.0	2.5
1.0	2.0	3.0	3.0
1.0	2.0	3.0	3.5
1.0	2.0	3.5	3.0
1.0	2.0	3.5	3.5
1.0	2.0	3.5	4.0
1.0	2.0	4.0	3.5
1.0	2.0	4.0	4.0
1.0	2.0	4.0	4.5
1.0	2.5	1.5	2.5
1.0	2.5	2.0	2.0
1.0	2.5	2.0	2.5
1.0	2.5	2.0	3.0
1.0	2.5	2.5	1.5
1.0	2.5	2.5	2.0
1.0	2.5	2.5	2.5
1.0	2.5	2.5	3.0
1.0	2.5	2.5	3.5
1.0	2.5	3.0	2.0
1.0	2.5	3.0	2.5
1.0	2.5	3.0	3.0
1.0	2.5	3.0	3.5

Table 6.2: Summary of database four-bar mechanisms

Drive Crank Length	Connecting Rod Length	Follower Crank Length	Ground Pivot Distance
1.0	2.5	3.0	4.0
1.0	2.5	3.5	2.5
1.0	2.5	3.5	3.0
1.0	2.5	3.5	3.5
1.0	2.5	3.5	4.0
1.0	2.5	3.5	4.5
1.0	2.5	4.0	3.0
1.0	2.5	4.0	3.5
1.0	2.5	4.0	4.0
1.0	2.5	4.0	4.5
1.0	2.5	4.0	5.0
1.0	3.0	1.5	3.0
1.0	3.0	2.0	2.5
1.0	3.0	2.0	3.0
1.0	3.0	2.0	3.5
1.0	3.0	2.5	2.0
1.0	3.0	2.5	2.5
1.0	3.0	2.5	3.0
1.0	3.0	2.5	3.5
1.0	3.0	2.5	4.0
1.0	3.0	3.0	1.5
1.0	3.0	3.0	2.0
1.0	3.0	3.0	2.5
1.0	3.0	3.0	3.0
1.0	3.0	3.0	3.5
1.0	3.0	3.0	4.0
1.0	3.0	3.0	4.5
1.0	3.0	3.5	2.0
1.0	3.0	3.5	2.5
1.0	3.0	3.5	3.0
1.0	3.0	3.5	3.5
1.0	3.0	3.5	4.0
1.0	3.0	3.5	4.5
1.0	3.0	3.5	5.0
1.0	3.0	4.0	2.5
1.0	3.0	4.0	3.0
1.0	3.0	4.0	3.5
1.0	3.0	4.0	4.0
1.0	3.0	4.0	4.5
1.0	3.0	4.0	5.0
1.0	3.5	1.5	3.5
1.0	3.5	2.0	3.0
1.0	3.5	2.0	3.5
1.0	3.5	2.0	4.0

Table 6.3: Summary of database four-bar mechanisms

Drive Crank Length	Connecting Rod Length	Follower Crank Length	Ground Pivot Distance
1.0	3.5	2.5	2.5
1.0	3.5	2.5	3.0
1.0	3.5	2.5	3.5
1.0	3.5	2.5	4.0
1.0	3.5	2.5	4.5
1.0	3.5	3.0	2.0
1.0	3.5	3.0	2.5
1.0	3.5	3.0	3.0
1.0	3.5	3.0	3.5
1.0	3.5	3.0	4.0
1.0	3.5	3.0	4.5
1.0	3.5	3.0	5.0
1.0	3.5	3.5	1.5
1.0	3.5	3.5	2.0
1.0	3.5	3.5	2.5
1.0	3.5	3.5	3.0
1.0	3.5	3.5	3.5
1.0	3.5	3.5	4.0
1.0	3.5	3.5	4.5
1.0	3.5	3.5	5.0
1.0	3.5	3.5	5.5
1.0	3.5	4.0	2.0
1.0	3.5	4.0	2.5
1.0	3.5	4.0	3.0
1.0	3.5	4.0	3.5
1.0	3.5	4.0	4.0
1.0	3.5	4.0	4.5
1.0	3.5	4.0	5.0
1.0	3.5	4.0	5.5
1.0	3.5	4.0	6.0
1.0	4.0	1.5	4.0
1.0	4.0	2.0	3.5
1.0	4.0	2.0	4.0
1.0	4.0	2.0	4.5
1.0	4.0	2.5	3.0
1.0	4.0	2.5	3.5
1.0	4.0	2.5	4.0
1.0	4.0	2.5	4.5
1.0	4.0	2.5	5.0
1.0	4.0	3.0	2.5
1.0	4.0	3.0	3.0
1.0	4.0	3.0	3.5
1.0	4.0	3.0	4.0
1.0	4.0	3.0	4.5

Table 6.4: Summary of database four-bar mechanisms

Drive Crank Length	Connecting Rod Length	Follower Crank Length	Ground Pivot Distance
1.0	4.0	3.0	5.0
1.0	4.0	3.0	5.5
1.0	4.0	3.5	2.0
1.0	4.0	3.5	2.5
1.0	4.0	3.5	3.0
1.0	4.0	3.5	3.5
1.0	4.0	3.5	4.0
1.0	4.0	3.5	4.5
1.0	4.0	3.5	5.0
1.0	4.0	3.5	5.5
1.0	4.0	3.5	6.0
1.0	4.0	3.5	6.5

One hundred and forty five curves were generated with the listed configurations and stored in a database on a Personal Computer with a Pentium® 350 MHz processor running WindowsNT® as an operating system. The generation of the solution curves and the implementation of the solution comparison and matching algorithms were implemented using MATLAB®. The time to generate the 145 curves was 251 seconds. Stored in the database were the following variables defining the four-bar mechanism and the output function:

Drive Crank Length - Floating point, 32 bits

Connecting Rod Length - Floating point, 32 bits

Follower Crank Length - Floating point, 32 bits

Ground Pivot Distance - Floating point, 32 bits

Number of Crank Positions - Integer, 16 bits
 Number of Fourier Descriptors - Integer, 16 bits
 Follower Crank Angle [] - Floating point, 32 bits
 Fourier Descriptors [] - Floating point, 32 bits

Where:

[] - Denotes a vector with a defined length

For each of the 145 curves stored, there were 128 drive crank positions, 16 Fourier Descriptors, and 128 Follower Crank positions. A desired curve was selected to search the database and to evaluate the performance of each solution comparison and matching methods. The desired curve had the following configuration:

Drive Crank Length	=	1.0 units
Connecting Rod Length	=	1.5 units
Follower Crank Length	=	2.5 units
Ground Pivot Distance	=	2.5 units

This curve is stored as the third numbered database curve. The graph of the normalized follower crank angle is found in Figure 6.6. The desired curve was compared with each of the database curves and evaluated with the following matching techniques:

- Normalized cross-correlation
- Sum of absolute differences

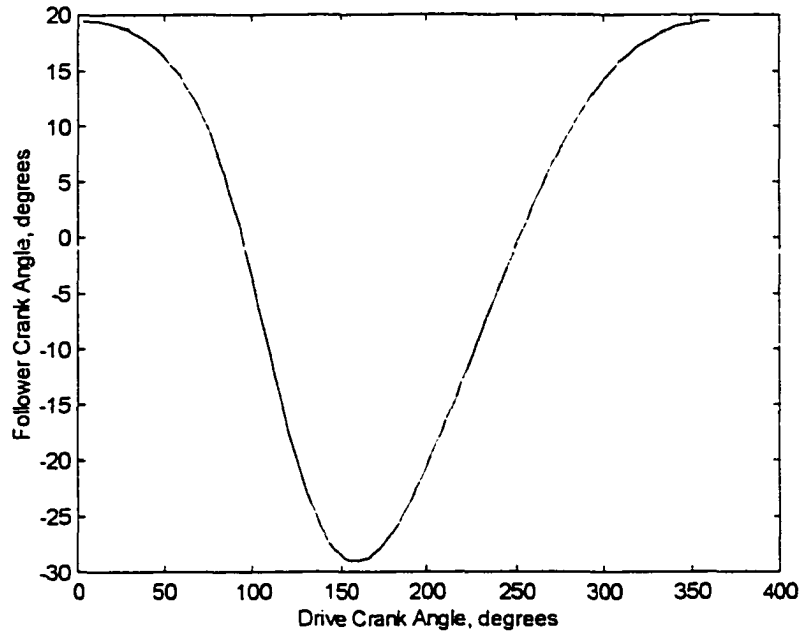


Figure 6.6: Plot of normalized follower crank angle of desired curve

- Sum of squared differences
- Correlation using Fourier transforms
- Phase-only filter using Fourier transforms
- Symmetric phase-only matched filter
- Amplitude difference of Fourier descriptors
- Amplitude and phase difference of Fourier descriptors

Normalized Cross Correlation

Normalized Cross Correlation is a similarity measure and is defined by the following equation:

$$C(x) = P(x)/Q(x) \quad [6.3]$$

Where:

$$P(x) = \sum f(x) * g(x)$$

$$Q(x) = (\sum f(x)^2 * g(x)^2)^{0.5}$$

As the cross-correlation is processed, if two functions are very similar and match in being either positive or negative then value of the denominator will be close to the numerator. Evaluation of two functions that match exactly will generate a cross-correlation value close of one. Two functions that do not match in sign will have a cross correlation less than one. Those functions that are positive and negative at each discrete sample will have a cross correlation value of one. Figure 6.7 is a graph of the cross-correlation of the desired function with the 145 database functions. Note the total number of functions that are close to the value of 1.000. There are 13 database functions which had a cross-correlation greater than 0.9999. These 13 database functions crossed the ordinate axis at essentially the same location as the desired function (database curve number 3). The 15 database functions which had the largest cross-correlation values are listed in Table 6.5. The top 5 matching database functions are plotted in Figure 6.8. The desired curve is plotted using a point at each of the 128 follower crank positions using a *.

The cross-correlation function defined above identified the functions that crossed the ordinate axis most closely with the desired function. Obviously the cross-correlation will not

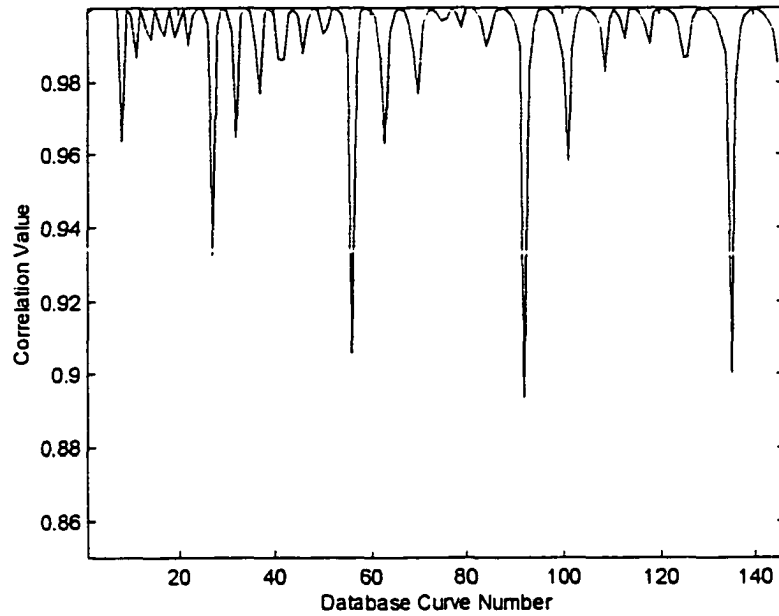


Figure 6.7: Graph of cross-correlation of desired function with 145 database functions.

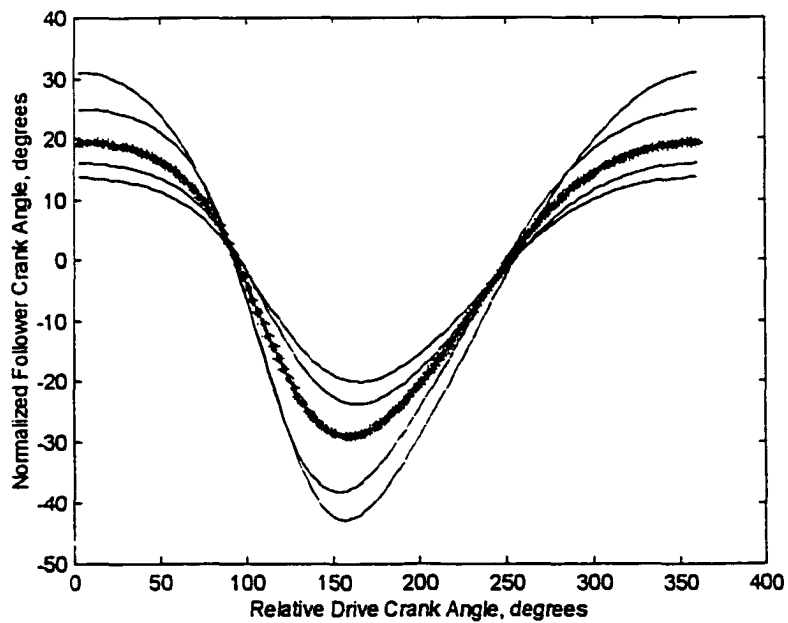


Figure 6.8: Graph of top 5 cross-correlated functions

Table 6.5: Summary of database search using cross-correlation

 Desired Curve - Database Curve #3

Search Rank	Database Curve Number	Cross-Correlation Value
1	3	1.0000
2	2	1.0000
3	5	1.0000
4	48	1.0000
5	4	1.0000
6	15	0.9999
7	6	0.9999
8	12	0.9999
9	77	0.9999
10	18	0.9999
11	34	0.9999
12	81	0.9999
13	39	0.9999
14	25	0.9998
15	59	0.9998

identify optimum solutions for function generation. The database search took 7.04 seconds of CPU time and 133591 FLOPS. A FLOPS is a measure of the cumulative number of floating point operations. Generally, with MATLAB, additions and subtractions are one flop if real and two if complex. Multiplication and division count one flop each if the result is real and six flops if it is not. Elementary functions count one if real and more if complex.

Sum of Absolute Differences

The sum of absolute differences is a difference measure and is defined by the following equation:

$$A(x) = \sum |f(x) - g(x)| \quad [6.4]$$

As the sum of absolute differences is processed, if two functions are very similar the difference will be small. The summing the absolute value of the difference eliminates the effect of one function being negative and one being positive. Evaluating of two functions which match will generate an absolute difference value of zero. Two functions which are not similar will generate an absolute difference greater than zero. Those functions that are very close, regardless of sign - positive or negative, at each discrete sample will have a value closer to zero. Figure 6.9 is a graph of the absolute difference measure of the desired function with the 145 database functions.

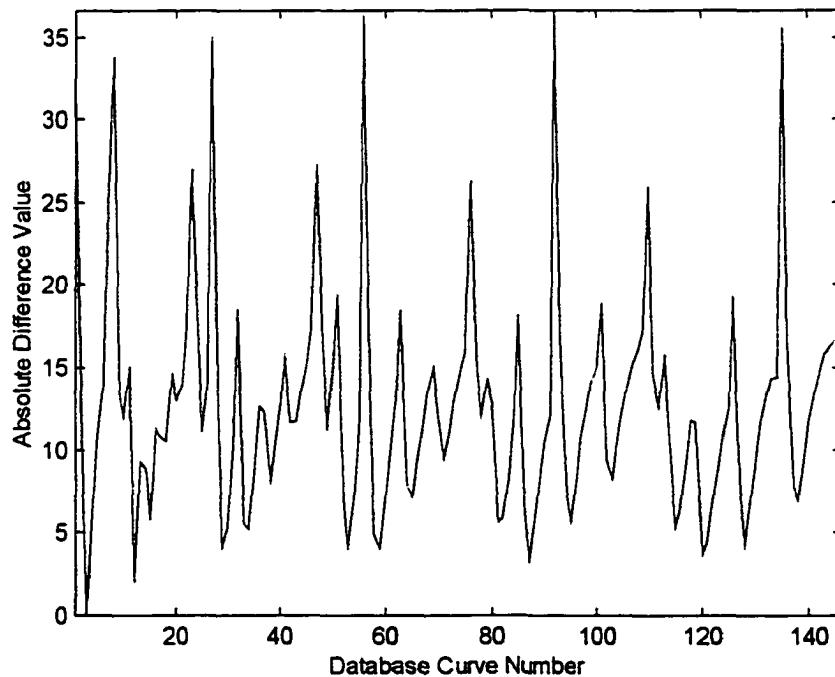


Figure 6.9: Graph of absolute difference of desired function with 145 database functions.

The top 5 matching database functions are plotted in Figure 6.10. The 15 database functions which had the smallest absolute differences values are listed in Table 6.6.

The absolute difference function defined above identified the functions which matched point by point most closely with the desired function. The database search took 4.016 seconds of CPU time and 40646 FLOPS.

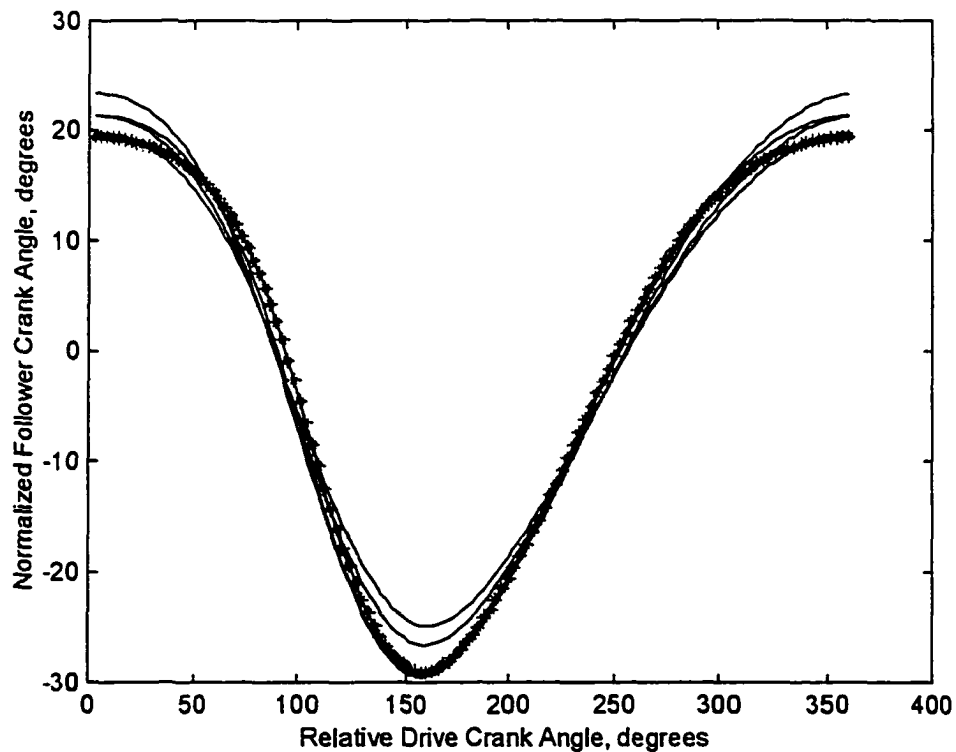


Figure 6.10: Graph of top 5 absolute difference functions

Table 6.6: Summary of database search using absolute difference

Desired Curve - Database Curve #3

Search Rank	Database Curve Number	Absolute Difference Value
1	3	0.0000
2	12	1.9543
3	87	3.3235
4	120	3.6927
5	59	4.0137
6	53	4.0946
7	29	4.1520
8	128	4.2274
9	121	4.3854
10	58	4.9319
11	34	5.1648
12	30	5.2951
13	115	5.3070
14	33	5.5669
15	95	5.6249

Sum of Squared Differences

The sum of squared differences is a difference measure and is defined by the following equation:

$$S(x) = \sum [f(x) - g(x)]^2 \quad [6.5]$$

This difference function is very similar to absolute difference function. Squaring the difference prior to the summation will reduce the sum for differences less than one and increase the sum for differences greater than one.

Figure 6.11 is a graph of the squared difference measure of the desired function with the 145 database functions. The 15 database functions which had the smallest squared differences values are listed in Table 6.7. A comparison of the absolute difference and squared difference top 15 database functions show that 13 of the top 15 functions are the same, but with a slightly different order. The database search took 4.22 seconds and 59206 FLOPS.

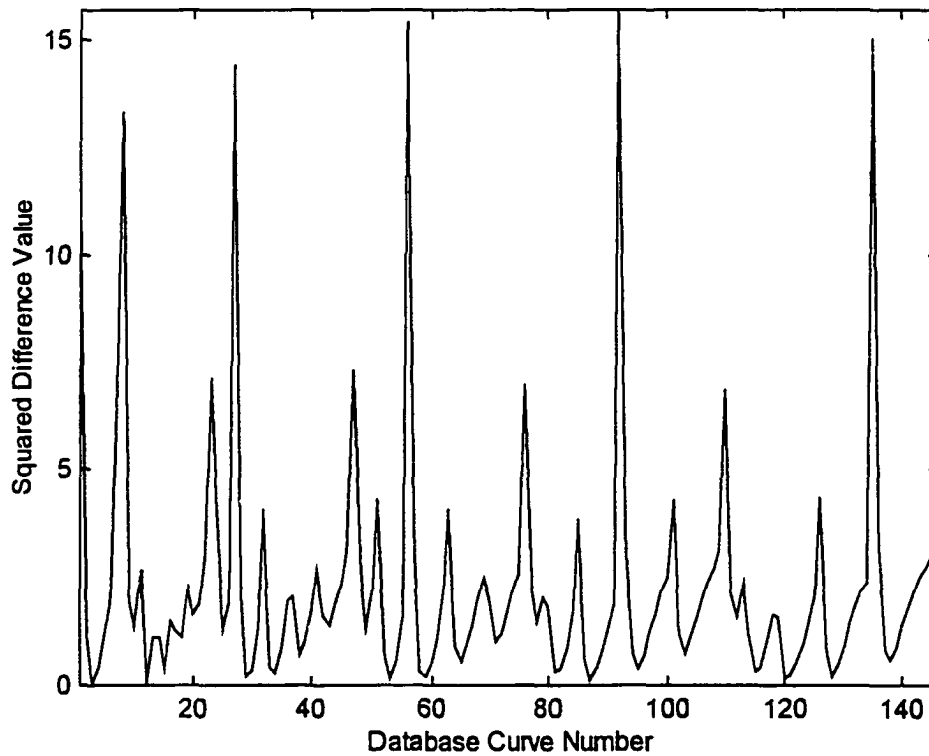


Figure 6.11: Graph of squared difference of desired function with 145 database functions.

Table 6.7: Summary of database search using squared differences

Desired Curve - Database Curve #3

Search Rank	Database Curve Number	Squared Difference Value
1	3	0.0000
2	12	0.0508
3	87	0.1108
4	120	0.1620
5	53	0.1697
6	59	0.1889
7	128	0.2046
8	29	0.2050
9	121	0.2187
10	34	0.2838
11	115	0.3016
12	58	0.3186
13	81	0.3189
14	30	0.3337
15	15	0.3553

Correlation Using Fourier Descriptors

Correlation in the Fourier frequency domain is evaluated by taking the maximum value of:

$$C(x) = \mathcal{J}^{-1} [F^*(u) * G(u)] \quad [6.6]$$

Where:

$C(x)$ = Correlation value of $f(x)$ and $g(x)$

$F^*(u)$ = Complex conjugate of Fourier transform of $f(x)$

$G(u)$ = Fourier transform of $g(x)$

Figure 6.12 is a graph of the frequency correlation of the desired function with the 145 database functions. Note the database functions that are similar to the desired curve have a larger correlation value. The 15 database functions which had the largest correlation values are listed in Table 6.8. The top 5 matching database functions are plotted in Figure 6.13. The database search took 2.48 seconds of CPU time and 1562564 FLOPS.

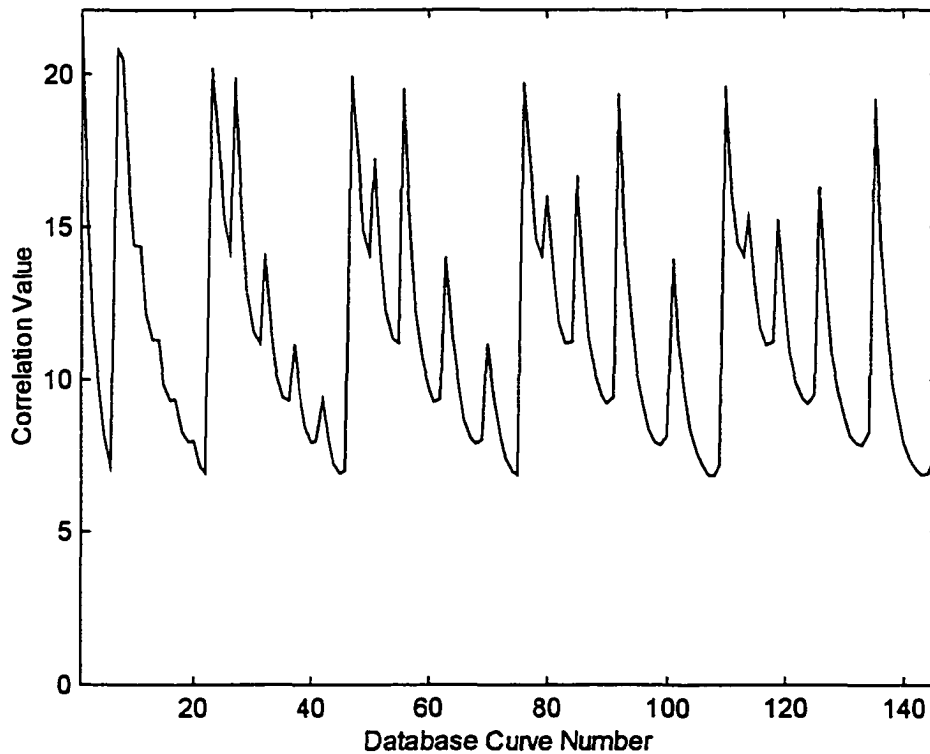


Figure 6.12: Graph of correlation using Fourier descriptors

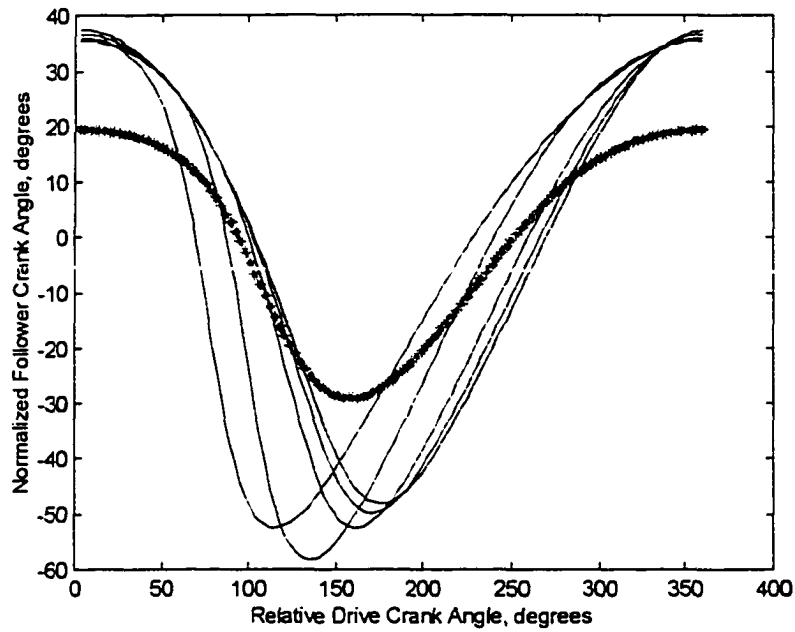


Figure 6.13: Graph of top 5 functions using correlation

Table 6.8: Summary of database search using frequency correlation

Desired Curve - Database Curve #3

Search Rank	Database Curve Number	Correlation Value
1	1	22.1263
2	7	20.8103
3	8	20.5168
4	23	20.2539
5	47	19.9499
6	27	19.8894
7	76	19.7546
8	110	19.6276
9	56	19.5617
10	92	19.3566
11	135	19.2255
12	24	18.3472
13	48	17.3493
14	51	17.2822
15	77	16.7653

Phase-Only Filter

Phase-only filtering in the Fourier frequency domain is evaluated by taking the maximum value of:

$$C(x) = \mathcal{F}^{-1} \{ [F^*(u)/|F(u)|] * G(u) \} \quad [6.7]$$

Where:

$|F(u)|$ = Magnitude of Fourier transform of $f(x)$

Figure 6.14 is a graph of the phase-only filter correlation of the desired function with the 145 database functions. The 15 database functions which had the largest correlation values are listed in Table 6.9. The top 5 matching database functions are plotted in Figure 6.15. The database search took 2.41 seconds of CPU time and 1107991 FLOPS.

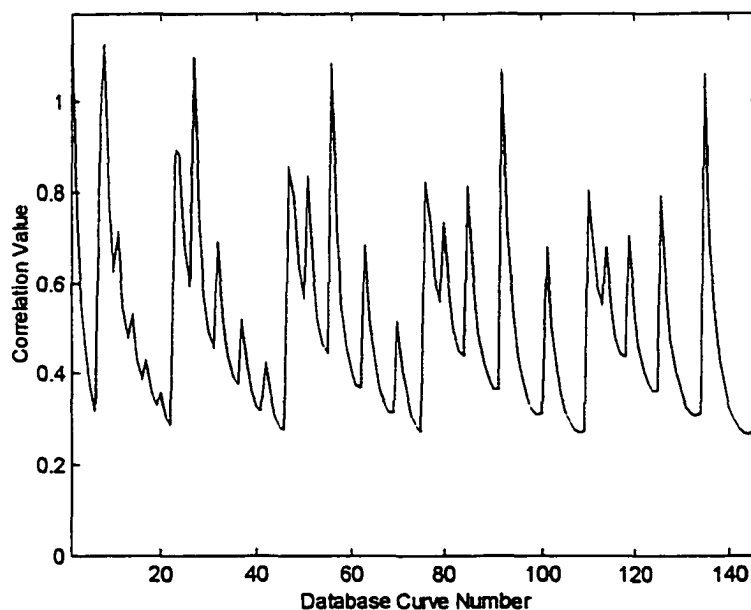


Figure 6.14: Graph of phase-only filter using Fourier descriptors

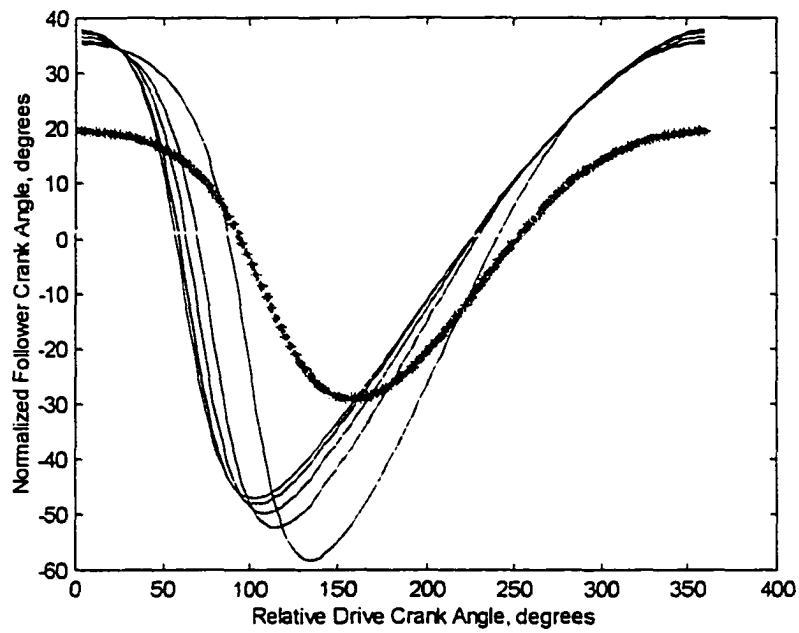


Figure 6.15: Graph of top 5 functions identified using phase-only filter

Table 6.9: Summary of database search using phase-only filter

Desired Curve - Database Curve #3

Search Rank	Database Curve Number	Correlation Value
1	1	1.1922
2	8	1.1277
3	27	1.1001
4	56	1.0835
5	92	1.0722
6	135	1.0640
7	7	0.9720
8	23	0.8924
9	24	0.8810
10	47	0.8504
11	51	0.8384
12	76	0.8242
13	85	0.8128
14	110	0.8064
15	126	0.7953

Symmetric Phase-Only Matched Filter

Symmetric phase-only matched filtering in the Fourier frequency domain is evaluated by taking the maximum value of:

$$C(x) = \mathfrak{F}^{-1} \{ [F^*(u)/|F(u)|] * G(u)/|G(u)| \} \quad [6.8]$$

Figure 6.16 is a graph of the phase-only filter correlation of the desired function with the 145 database functions. The 15 database functions which had the largest correlation values are listed in Table 6.10. The top 5 matching database functions are plotted in Figure 6.17. The database search took 2.56 seconds of CPU time and 1252131 FLOPS.

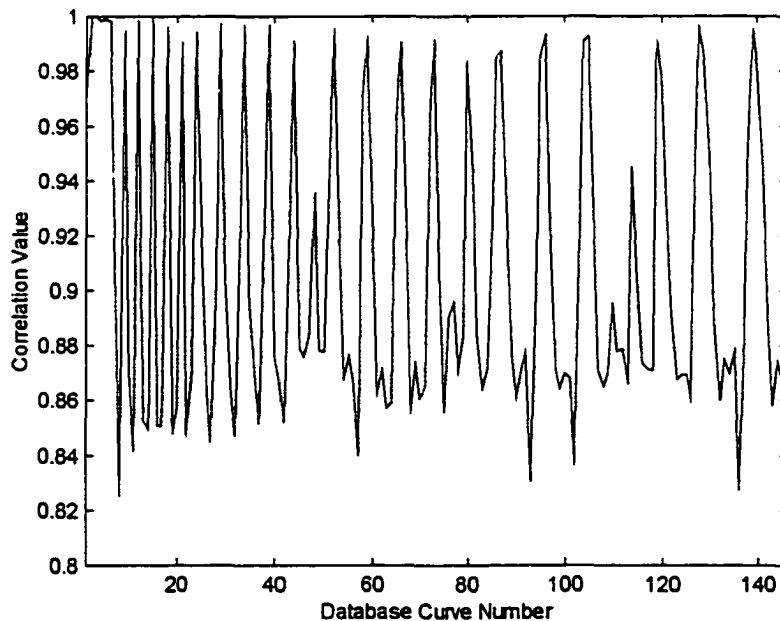


Figure 6.16: Graph of symmetric phase-only matched filtering

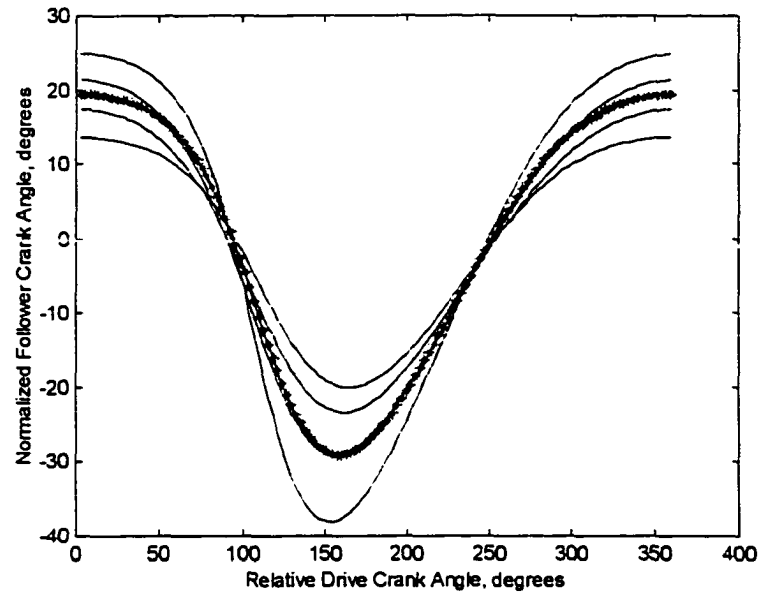


Figure 6.17: Graph of top 5 functions using symmetric phase-only matched filtering

Table 6.10: Summary of database search using symmetric phase-only matched filtering

Desired Curve - Database Curve #3

Search Rank	Database Curve Number	Cross-Correlation Value
1	3	1.0000
2	15	0.9996
3	2	0.9994
4	12	0.9992
5	5	0.9992
6	6	0.9981
7	4	0.9980
8	29	0.9978
9	39	0.9973
10	34	0.9971
11	18	0.9959
12	128	0.9959
13	52	0.9955
14	139	0.9954
15	9	0.9952

Amplitude Difference of Fourier Descriptors

The difference of the magnitude of the Fourier descriptors is defined by the following equation:

$$A(u) = \sum |F(u) - G(u)| \quad [6.9]$$

Figure 6.18 is a graph of the Fourier descriptor amplitude difference of the desired function with the 145 database functions. The 15 database functions which had the smallest amplitude difference are listed in Table 6.11. The top 5 matching database functions are plotted in Figure 6.19. The database search took 6.23 seconds of CPU time and 266212 FLOPS.

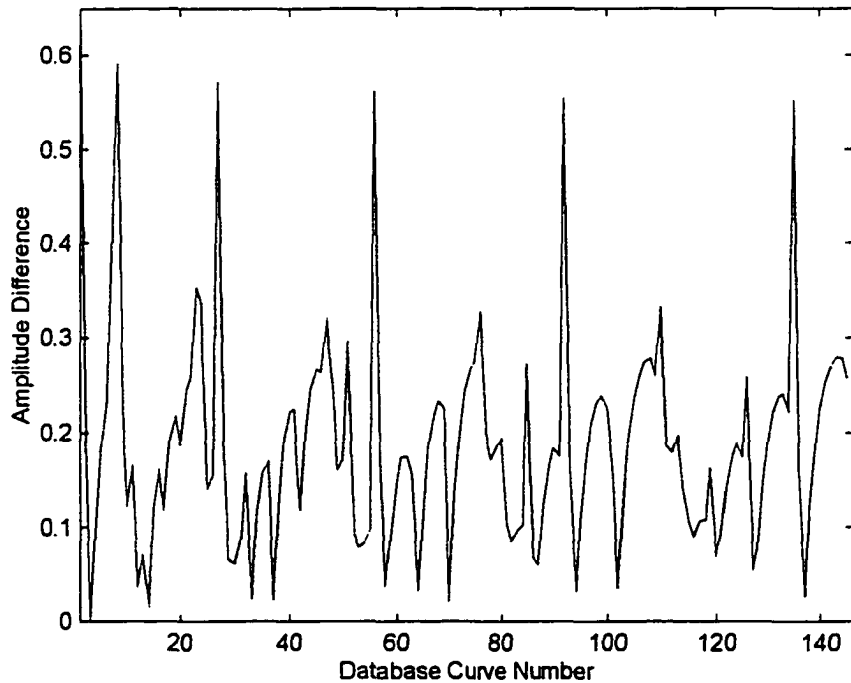


Figure 6.18: Graph of amplitude difference of Fourier descriptors

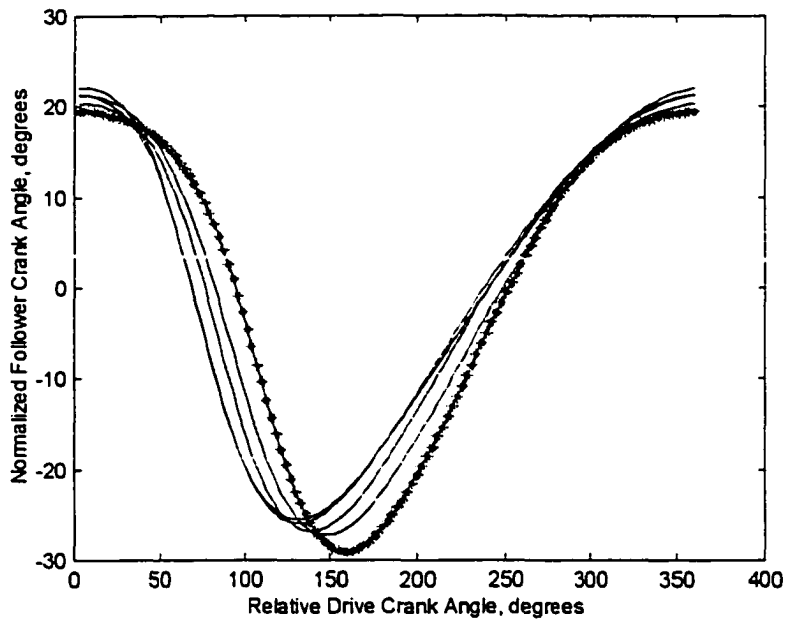


Figure 6.19: Graph of top 5 functions using amplitude difference of Fourier descriptors

Table 6.11: Summary of database search using amplitude difference of Fourier descriptors

Desired Curve - Database Curve #3

Search Rank	Database Curve Number	Amplitude Difference
1	3	0.0000
2	70	0.0201
3	14	0.0204
4	37	0.0220
5	33	0.0235
6	137	0.0249
7	64	0.0311
8	94	0.0318
9	102	0.0344
10	12	0.0386
11	58	0.0433
12	127	0.0548
13	87	0.0548
14	30	0.0624
15	29	0.0657

Amplitude and Phase Difference of Fourier Descriptors

The difference of the magnitude of the Fourier descriptors is defined by the following equation:

$$Fd = \sum m * |F(u) - G(u)| + n * |\text{ang}(F(u)*F(u) - \text{ang}(G(u)*G(u))| \quad [6.10]$$

The value used for n was 0.3 and m was 0.7 (see Appendix A). Figure 6.20 is a graph of the Fourier descriptor amplitude and phase difference of the desired function with the 145 database functions. The 15 database functions which had the smallest amplitude and phase difference are listed in Table 6.12. The top 5 matching database functions are plotted in Figure 6.21. The database search took 6.33 seconds of CPU time and 266212 FLOPS.

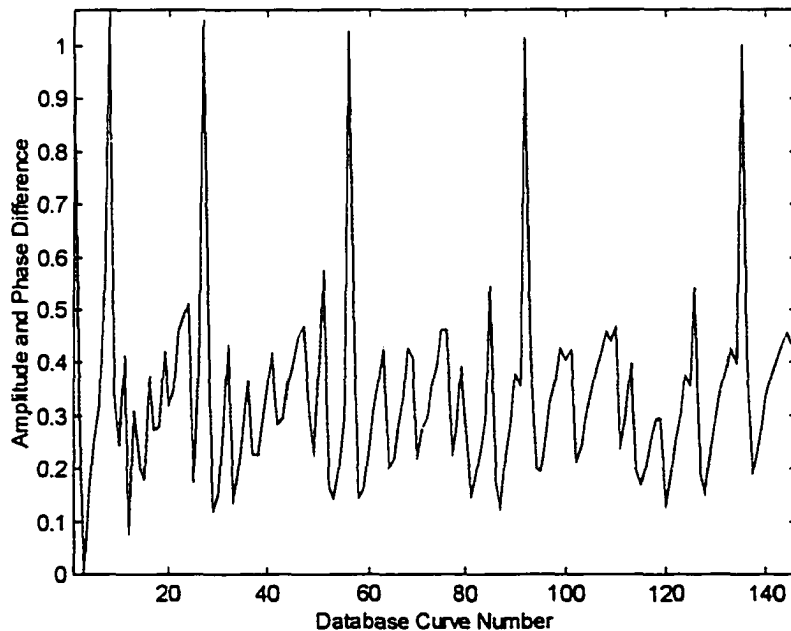


Figure 6.20: Graph of amplitude and phase difference of Fourier descriptors

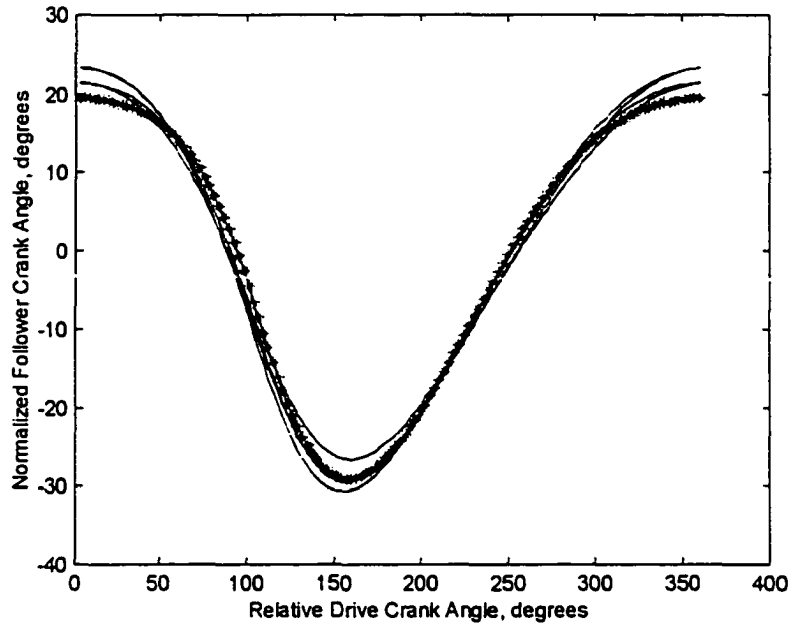


Figure 6.21: Graph of top 5 functions using amplitude and phase difference of Fourier descriptors

Table 6.12: Summary of database search using amplitude and phase difference of Fourier descriptors

Desired Curve - Database Curve #3

Search Rank	Database Curve Number	Amplitude and Phase Difference
1	3	0.0000
2	12	0.0741
3	29	0.1208
4	87	0.1238
5	120	0.1307
6	33	0.1406
7	58	0.1432
8	53	0.1435
9	81	0.1473
10	30	0.1521
11	128	0.1521
12	4	0.1541
13	59	0.1630
14	52	0.1673
15	115	0.1705

Partial Curves

A complete rotation of the drive crank and the resulting function output has been evaluated and is applicable only to four-bar mechanisms where the crank rotates through a full 360 degrees. To consider a crank-rocker, a double-crank, or a double-rocker four-bar mechanism that rotates through a specified angle, a different methodology is required to characterize the output function.

Consider the exemple four-bar mechanism where the drive crank only rotates from an angle of 0 degrees to 90 degrees. Figure 6.22 is a graph of the follower crank angle. Compare this output graph to that of Figure 6.1.

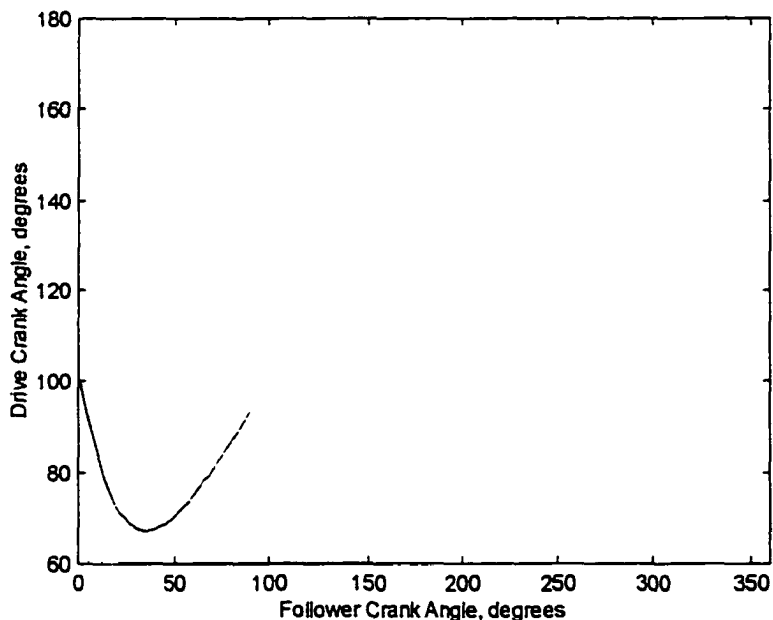


Figure 6.22: Follower crank angle as a function of drive crank angle from 0 to 90 degrees.

The initial follower crank angle and the average follower crank angle are again affected by the definition of the reference line that passes through the drive crank pivot and the follower crank pivot. Any reference line may be used for the definition of the follower crank angle. Therefore, the value of the follower crank angle may be shifted so the average of the follower crank angle over the range of motion is zero (equation 6.1). This will normalize the average value of the curve.

With a partial rotation of the drive crank, the relative change in the follower crank angle is related to the minimum and maximum angular position of the drive crank. Therefore, the curve may not be shifted so the largest positive angle of the curve resides at a crank angle of zero. As a result, the phase of the curve may not be normalized. Figure 6.23 is a graph of the follower crank output angle normalized for the average value only.

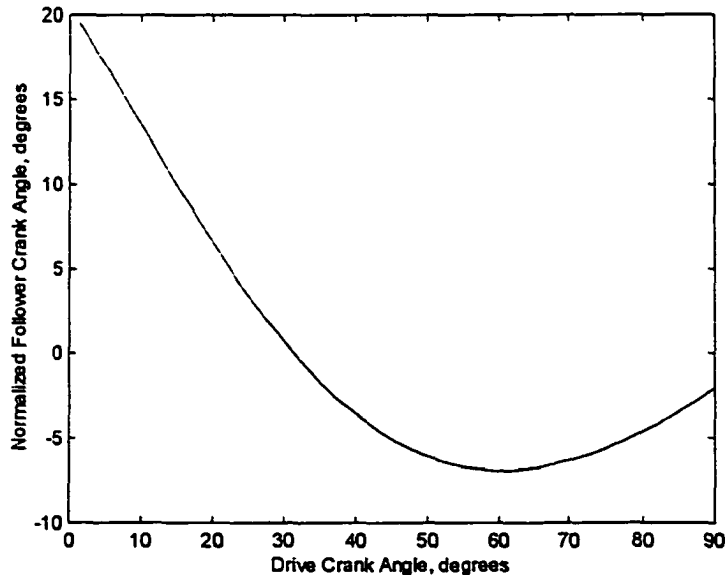


Figure 6.23: Follower crank angle normalized for average value

Discrete points were sampled defining the follower crank output from the initial drive crank angle to the final drive crank angle. The discrete points are based on a constant step, or change, of the drive crank angle. The movement of the drive crank is assumed to move through a full cycle from the minimum angular drive crank position, to the maximum angular drive crank position, and back to the minimum drive crank position. This generates a series of follower crank output points that is cyclic. A total of 128 discrete points are used to sample the complete output function.

One hundred and forty five curves were generated with the configurations listed in Tables 6.1 through 6.4 with the minimum angular drive crank position of 0 degrees and the maximum angular drive crank position of 90 degrees. The database structure and stored information is the same as with the crank rocker with full drive crank motion. A desired curve was selected as the third numbered database curve and the configuration is the same as detailed on page 127.

The desired curve was compared with each of the database curves and evaluated with the following matching techniques:

- Sum of absolute differences
- Fourier descriptor amplitude and phase difference measure

Partial Curves - Sum of Absolute Differences

The sum of absolute differences is a difference measure and is defined by the following equation:

$$A(x) = \sum |f(x) - g(x)| \quad [6.11]$$

Figure 6.24 is a graph of the absolute difference of the partial curve with the 145 database functions. The 15 database functions which had the smallest absolute difference values are listed in Table 6.13. The top 5 matching database functions are plotted in Figure 6.25. The database search took 3.97 seconds of CPU time and 40647 FLOPS.

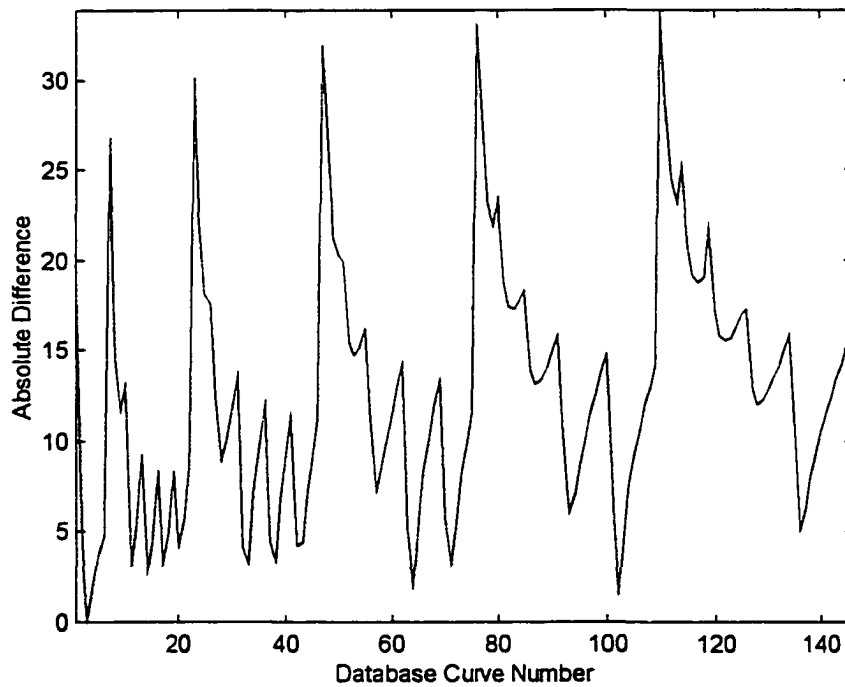


Figure 6.24: Graph of absolute difference of partial curve with 145 database functions

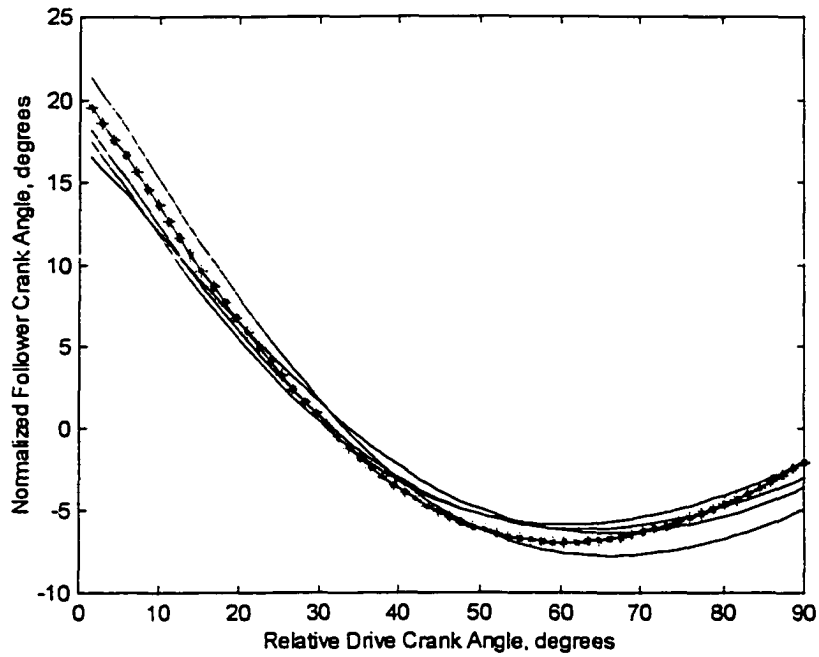


Figure 6.25: Graph of top 5 functions using absolute difference

Table 6.13: Summary of database search using absolute difference

Desired Curve - Database Curve #3

Search Rank	Database Curve Number	Absolute Difference Value
1	3	0.0000
2	102	1.4768
3	64	1.9818
4	4	2.2210
5	14	2.7834
6	11	3.0770
7	71	3.1209
8	17	3.1972
9	33	3.2152
10	38	3.2800
11	5	3.6844
12	20	4.1269
13	32	4.1439
14	42	4.2463
15	2	4.2734

Partial Curves - Amplitude and Phase Difference of Fourier Descriptors

The difference of the magnitude of the Fourier descriptors is defined by the following equation:

$$Fd = \sum |F(u) - G(u)| + m * |\text{ang}(F(u)*F(u) - \text{ang}(G(u)*G(u))| \quad [6.12]$$

The value used for n was 0.3. Figure 6.26 is a graph of the Fourier descriptor amplitude and phase difference of the desired function with the 145 database functions. The 15 database functions which had the smallest amplitude and phase difference are listed in Table 6.14. The top 5 matching database functions are plotted in Figure 6.27. The database search took 6.21 seconds of CPU time and 267123 FLOPS.

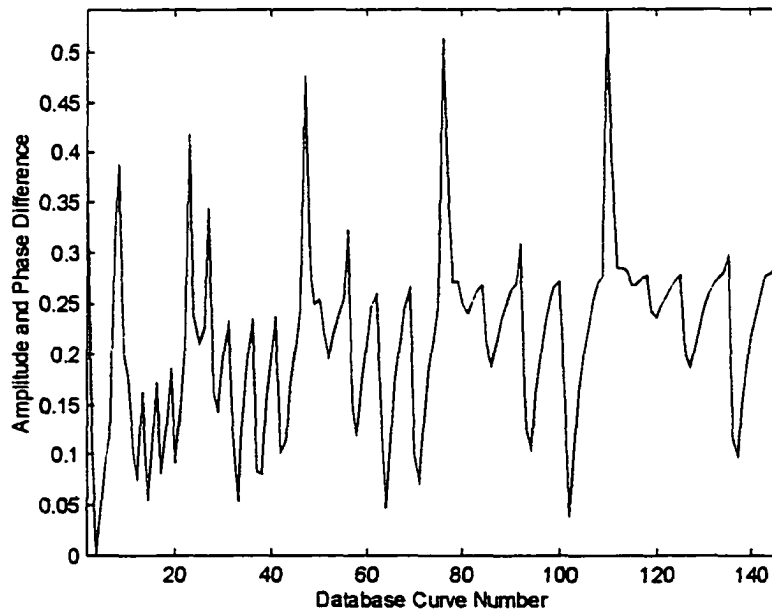


Figure 6.26: Graph of amplitude and phase difference of Fourier descriptors

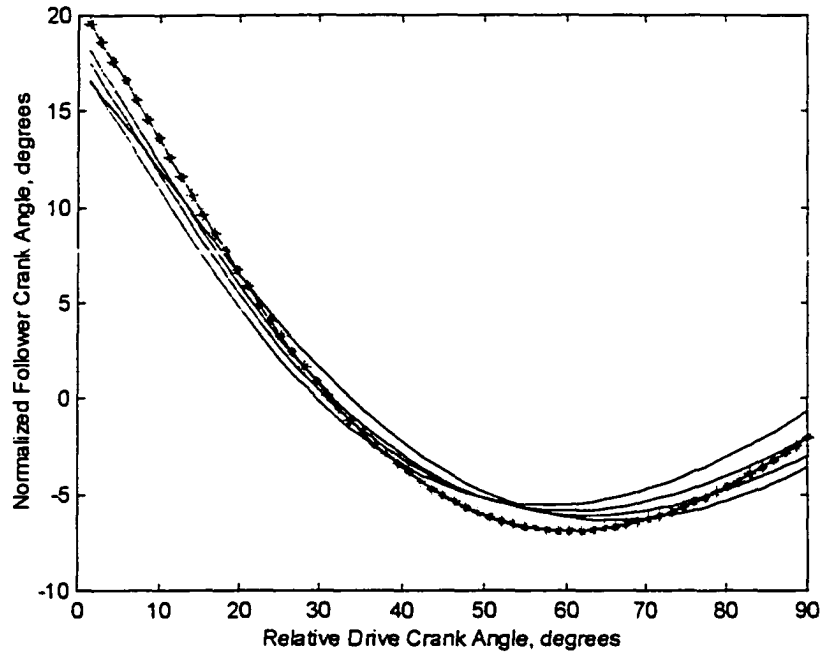


Figure 6.27: Graph of top 5 functions using amplitude and phase difference of Fourier descriptors

Table 6.14: Summary of database search using amplitude and phase difference of Fourier descriptors

Desired Curve - Database Curve #3

Search Rank	Database Curve Number	Amplitude and Phase Difference
1	3	0.0000
2	102	0.0387
3	64	0.0469
4	4	0.0502
5	33	0.0524
6	14	0.0543
7	71	0.0733
8	12	0.0764
9	17	0.0800
10	38	0.0810
11	37	0.0828
12	5	0.0891
13	20	0.0918
14	137	0.0975
15	15	0.0999

Summary

A comparison of the various techniques for the use of invariant characterization, storage and search methods for function generation of four-bar mechanisms was generated. Table 6.15 and Table 6.16 are summaries of the top ten functions identified when using file number 3 as a desired solution. Entries in Table 6.15 and 6.16 are bold if the identified functions are in the top 10 functions identified and match one of the top 10 functions identified by the absolute difference measure. Entries in Table 6.15 and 6.16 are underlined if the identified functions are in the top 5 function identified and match one of the top 5 functions identified by the absolute difference measure. Table 6.16 is a summary of the time to search and compare a desired solution with 145 database curves and the number of FLOPS to run the various search methods. The following are the various file search methods:

- SCC - Spatial transform, normalized cross correlation
- SAD - Spatial transform, absolute difference
- SSS - Spatial transform, sum squared difference
- F1C - One-dimensional Fourier correlation
- F1P - One-dimensional Fourier phase only filter
- F1SP - One-dimensional Fourier descriptors, symmetric phase-only matched filter
- F1A - One-dimensional Fourier transform, amplitude difference of Fourier descriptors

FlAP - One-dimensional Fourier transform, amplitude and phase difference of Fourier descriptors

The amplitude and phase difference of Fourier descriptors was the measure of similarity that identified database functions with a desired solution that correlated most closely to the spatial absolute difference measure. This was found for both full drive crank rotation and for partial drive crank rotation. Four of the top five solutions were the same as identified with the absolute difference measure and 12 of the top 15 curves were the same as identified with the absolute difference measure for functions generated by full rotation of the drive crank. Four of the top five solutions were the same as identified with the absolute difference measure and 11 of the top 15 curves were the same as identified with the absolute difference measure for functions generated by partial rotation of the drive crank.

The spatial matching techniques required the largest database file space while the Fourier transforms required a fraction of the spatial file space. The Fourier transform matching techniques required slightly less time to generate database files and required more time for searching a database.

Table 6.15: Performance of various methods to measure the similarity of a desired solution to 145 filed solutions - full drive crank rotation

Top Ranked File No.	1	2	3	4	5	6	7	8	9	10
SCC	<u>3</u>	2	5	48	4	15	6	12	77	18
SAD	<u>3</u>	<u>12</u>	<u>87</u>	<u>120</u>	<u>59</u>	53	29	128	121	58
SSS	<u>3</u>	<u>12</u>	<u>87</u>	<u>120</u>	53	59	128	29	121	34
F1C	1	7	8	23	47	27	76	110	56	92
F1P	1	8	27	56	92	135	7	23	24	47
F1SP	<u>3</u>	15	2	<u>12</u>	5	6	4	29	39	34
F1A	<u>3</u>	70	14	37	33	137	64	94	102	12
F1AP	<u>3</u>	<u>12</u>	29	<u>87</u>	<u>120</u>	33	58	53	81	30

Table 6.16: Performance of various methods to measure the similarity of a desired solution to 145 filed solutions - partial drive crank rotation

Top Ranked File No.	1	2	3	4	5	6	7	8	9	10
SAD	<u>3</u>	<u>102</u>	<u>64</u>	<u>4</u>	<u>14</u>	11	71	17	33	38
F1AP	<u>3</u>	<u>102</u>	<u>64</u>	<u>4</u>	33	14	71	12	17	38

Table 6.17: Performance of various methods to generate 145 solutions and to search and identify similar solutions

Top Ranked File No.	Time to Generate 145 Files (sec)	Time to Search 145 Files (sec)	FLOPS to Search 145 Files
SCC	260	6.54	133591
SAD	260	3.10	40646
SSS	260	3.28	59206
F1C	275	1.53	1562564
F1P	275	1.51	1107991
F1SP	275	1.59	1252131
F1A	275	5.40	266212
F1AP	275	5.40	266212

CHAPTER 7. PATH GENERATION

Path generation is where the functional requirement is the output path of a trace point that is typically on a coupler link. The path, or position, velocity and acceleration of the trace point is typically viewed as the output with the input being the position, velocity and/or acceleration of the drive crank.

Figure 7.1 is a plot of the trace point path for the example crank-rocker four-bar mechanism that was been defined in Chapter 4. The position and orientation of the trace point path is based off the position of the drive crank ground pivot and the reference line which passes through the drive crank pivot and the follower crank pivot (Figure 6.2).

The initial drive crank angle has an effect on the starting point for the trace point curve. As the drive crank rotates through its complete cycle, the trace point is driven through a path that is cyclical with the drive crank. The trace point path will generate a closed curve. The initial drive crank angle does not have an effect on the form of the trace point path.

The position, rotation and scale of the trace point curve are affected by the position of the drive crank ground pivot, the

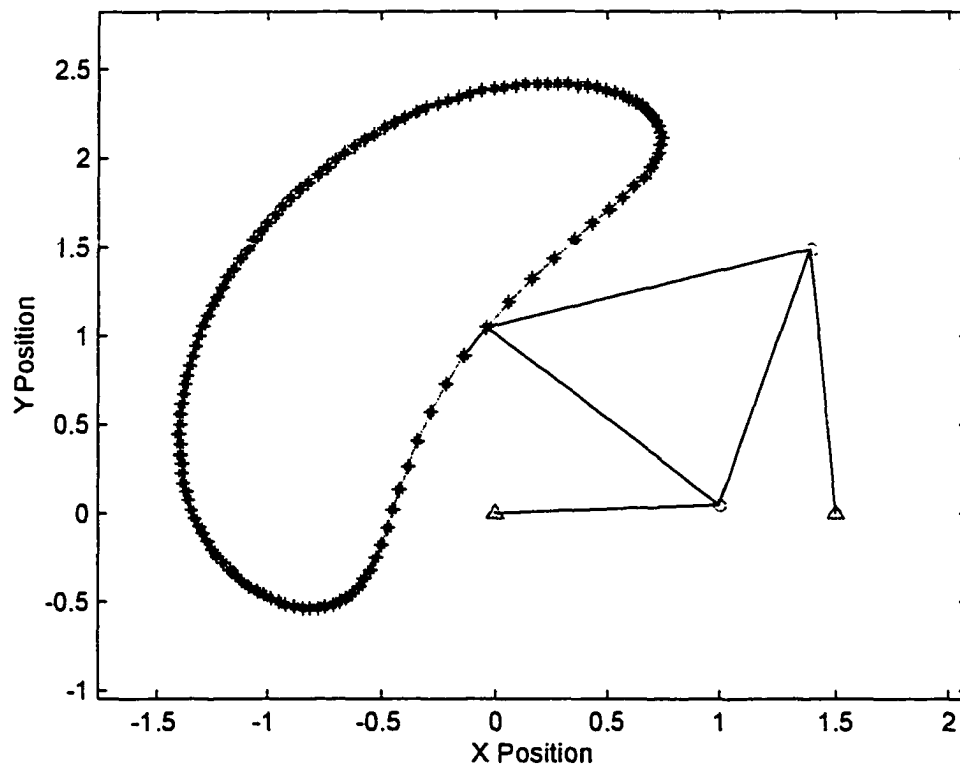


Figure 7.1: Example four-bar mechanism trace point path

angle of the reference line which passes through the drive crank pivot and the follower crank pivot, and the relative size of the four-bar linkage. The relative size of the four bar linkage may be scaled, larger or smaller, if all five of the link dimensions - drive crank length, connecting rod length, follower crank length, ground pivot length, and trace point distance, are scaled by the same factor.

To normalize the trace point path for position, each of the points in the path are translated through the application of the following spatial transformation:

$$P_{i_x}' = P_{i_x} - X_{cen} \quad [7.1]$$

$$P_{i_y}' = P_{i_y} - Y_{cen} \quad [7.2]$$

To normalize the trace point path for scale, each of the points in the path are scaled through the application of the following scaling transformation:

$$P_{i_x}'' = P_{i_x}' / R_{max} \quad [7.3]$$

$$P_{i_y}'' = P_{i_y}' / R_{max} \quad [7.4]$$

Where:

$$R_{max} = \text{Maximum} [(P_{i_x}' - X_{cen})^2 + (P_{i_y}' - Y_{cen})^2]^{0.5} \quad [7.5]$$

To normalize the trace point path for rotation, each of the points in the path are rotated through the application of the following spatial transformation:

$$P_{i_x}''' = P_{i_x}'' * \cos\theta + P_{i_y}'' * \sin\theta \quad [7.6]$$

$$P_{i_y}''' = P_{i_x}'' * \sin\theta - P_{i_y}'' * \cos\theta \quad [7.7]$$

After the application of these spatial transformations, the trace point path is invariant to the original path position, rotation and scale. As with function generation, an important aspect is that the number of discrete points used in defining the curve and in generating transforms must be consistent. The distances

between discrete points on the trace point path are defined by a constant rotation of the drive crank angle. As a result, the points on the trace point path are not spaced equally. Therefore, the distances between the points are normalized to establish a consistent distance between each point; this was not the case with function generation. Figure 7.2 graphs the trace point path after normalization for position, rotation, scale and point distribution.

Normalizing the trace point path for each four-bar mechanism will allow the development of a database of curves and the establishment of a process of matching a desired path $g(x,y)$ with the stored database of curves. Each of the database curves are

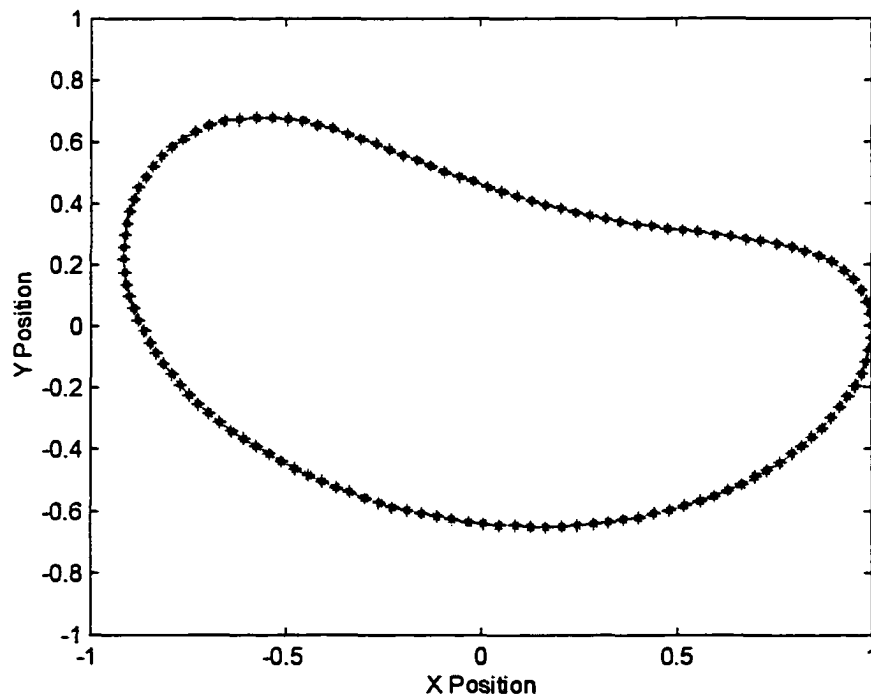


Figure 7.2: Normalized trace point path

generated with a consistent number of discrete points. The number of Fourier descriptors are also consistent for each of the database curves and the desired curve defined.

A one dimensional Fourier transform, equation 4.8, is taken of the trace point path using 128 discrete points viewing each of the path points as a complex number. In this study, there will be 16 Fourier descriptors stored for each curve. Figure 3.22 is a plot of the Fourier spectrum of the invariant trace point path. Table 7.1 is a listing of the top 16 Fourier descriptors of the invariant trace point path for the example.

To develop a database of paths for testing the performance of the various matching techniques, the crank-rocker, four-bar

Table 7.1: Top 16 Fourier descriptors of example trace point path

Fourier Coefficient Number	F(u)	
	Real	Imaginary
2	0.6495	0.0314i
3	-0.0075	-0.0501i
4	0.0671	-0.0241i
5	0.0045	0.0075i
6	0.0121	-0.0110i
7	0.0079	0.0058i
8	0.0010	-0.0022i
9	0.0053	0.0013i
11	0.0021	-0.003i
12	0.0006	0.0016i
122	0.0001	-0.0016i
123	-0.0014	-0.0038i
124	0.0058	-0.0035i
125	-0.0058	-0.0063i
126	0.0380	-0.0513i
127	0.2204	0.1040i

mechanisms defined in Hrones and Nelson [1951] are used. A summary of the drive crank length, connecting rod length, follower crank length and ground pivot distance is given in Tables 6.1, 6.2, 6.3, and 6.4.

In addition to the base configuration of the four-bar mechanism, a grid configuration is fixed to each of the 145 four-bar configurations. The grid configuration generates a set of trace points for each four-bar configuration (see Figure 3.2). The distance between each of the grid points is defined by the number of grid points located from the ends of the connecting rod. In Figure 3.2, there are 6 grid points located from each end of the connecting rod. If the connecting rod had a length 5 units, the minimum distance between each grid point would be one unit.

Each grid is consistent in the fact that there are 5 rows of grid points. What varies with each of the four-bar mechanisms is the number of columns of grid points. The number of columns will be evaluated with the following equation:

$$TC = GPL + GPC + GPR \quad [7.8]$$

Where:

TC = Total number of columns

GPL = Grid points to the left of connecting rod

GPC = Grid points between each end of the connecting rod

GPR = Grid points to the right of the connecting rod

For Figure 3.2 there are 10 columns, with 2 grid points to the left of the connecting rod, 6 points between each end of the connecting rod, and 2 grid points to the right of the connecting rod.

Table 7.2 lists the grid point configuration for each of the database four-bar mechanisms.

Each grid point for a four bar mechanism generates a database file. A database file is not generated for the end of the drive crank as a simple circle will be generated for the path. In addition, a database file is not generated for the end of the follower crank as a simple arc is generated for the path. Therefore, for a four-bar mechanism with a connecting rod with a length of 1.5, there will be $5*(2+4+2)-2 = 38$ database files generated. For the 145 four-bar mechanisms listed in Tables 6.1, 6.2, 6.3, and 6.4, there will be a total of 7,475 database files generated.

Table 7.2: Summary of grid configuration of database four-bar mechanisms

Connecting Rod Length	GPL	GPC	GPR
1.5	2	4	2
2.0	2	5	2
2.5	2	6	2
3.0	2	7	2
3.5	2	8	2
4.0	2	9	2

Seven thousand four hundred and seventy five database files were generated with the listed configuration and stored in a database on a personal computer with a Pentium® 350 MHz processor running WindowsNT® as an operating system. The time to generate the 7,475 database files varied greatly depending on the information required for each matching technique. Stored in the databases were the following variables defining the four-bar mechanism and the output path:

Drive Crank Length - Floating point, 32 bits
 Connecting Rod Length - Floating point, 32 bits
 Follower Crank Length - Floating point, 32 bits
 Ground Pivot Distance - Floating point, 32 bits
 Trace Point Distance - Floating point, 32 bits
 Trace Point Angle - Floating point, 32 bits
 Number of Crank Positions - Integer, 16 bits
 Number of Fourier Descriptors - Integer, 16 bits
 Trace Point Path [] - Floating point, 2 x 32 bits
 Fourier Descriptors [] - Floating point, 32 bits
 Invariant Moments [] - Floating point, 32 bits

Where:

[] - Denotes a vector with a defined length

A desired curve was selected to search the database and to evaluate performance of each of the solution matching measures. The desired curve had the following configuration:

Drive Crank Length	=	1.0 units
Connecting Rod Length	=	1.5 units
Follower Crank Length	=	1.5 units
Ground Pivot Distance	=	1.5 units
Trace Point Distance	=	1.802 units
Trace Point Angle	=	0.588 radians

This curve was stored as the third numbered database curve. The graph of the normalized trace point path is found in Figure 7.3.

The desired path will be taken and compared with each of the database solutions and evaluated with the following matching measures:

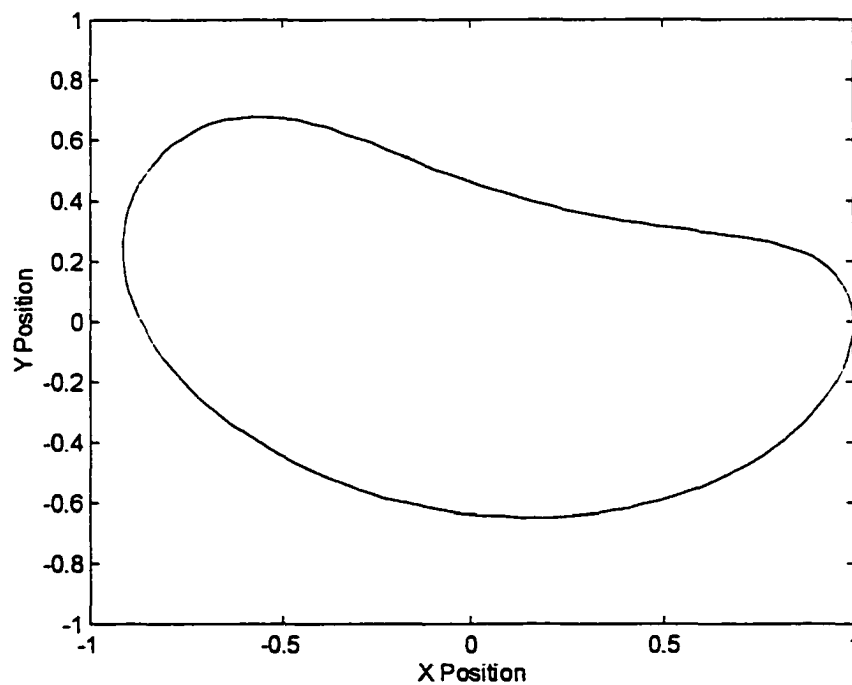


Figure 7.3: Plot of normalized desired trace point path

- Sum of absolute differences
- Sum of squared differences
- Correlation using Fourier descriptors
- Phase-only filter using Fourier descriptors
- Symmetric phase-only matched filter using one-dimensional Fourier descriptors
- Symmetric phase-only matched filter using two-dimensional Fourier descriptors
- Amplitude and phase difference using Fourier descriptors
- Product correlation based on invariant moments

Sum of Absolute Differences

The sum of the absolute difference when used with the trace point path is defined by the following equation:

$$A(x, y) = \sum \{ [(f_x(\theta) - g_x(\theta))^2 + (f_y(\theta) - g_y(\theta))^2]^{0.5} \} \quad [7.9]$$

Where:

$f_x(\theta)$ = X position of database path at a point

$f_y(\theta)$ = Y position of database path at a point

$g_x(\theta)$ = X position of desired path at a point

$g_y(\theta)$ = Y position of desired path at a point

As the sum of the absolute differences is processed, the absolute distance between a specified point in the database path and the

desired path is evaluated. Evaluation of two trace point paths that match will generate an absolute difference value close to zero. Two paths that are not similar have an absolute difference value greater than zero. Figure 7.4 is a graph of the absolute difference measure of the desired trace point path with the first 145 of the total 7,425 database paths. The top 5 matching database paths are plotted in Figure 7.5. The 15 database paths which had the smallest absolute difference values are listed in Table 7.3.

The absolute difference measure, defined for a two dimensional path, analyzed point by point the curves that most closely matched the desired trace point path. The database search took 6.34 seconds of CPU time and 133,447 FLOPS.

Table 7.3: Summary of database search of trace point paths using absolute differences

Desired Curve - Database Curve #3

Search Rank	Database Curve Number	Absolute Difference Value
1	3	0.0000
2	2	1.9380
3	40	2.7016
4	47	3.6223
5	85	3.8841
6	123	4.1691
7	9	4.5882
8	55	4.9861
9	93	5.0443
10	131	5.1391
11	77	6.3275
12	17	6.3615
13	115	6.4063
14	39	6.6065
15	137	6.9945

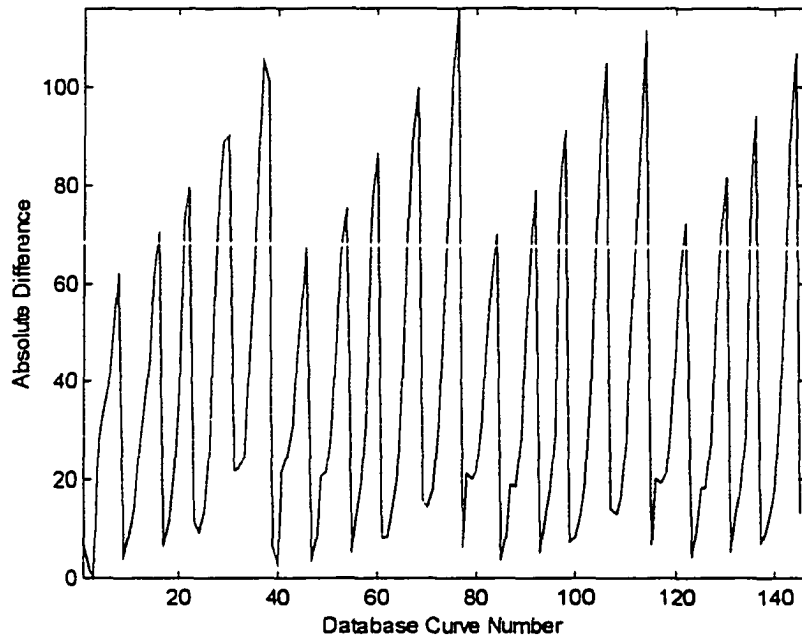


Figure 7.4: Graph of absolute difference of desired trace point path with 145 database trace point paths

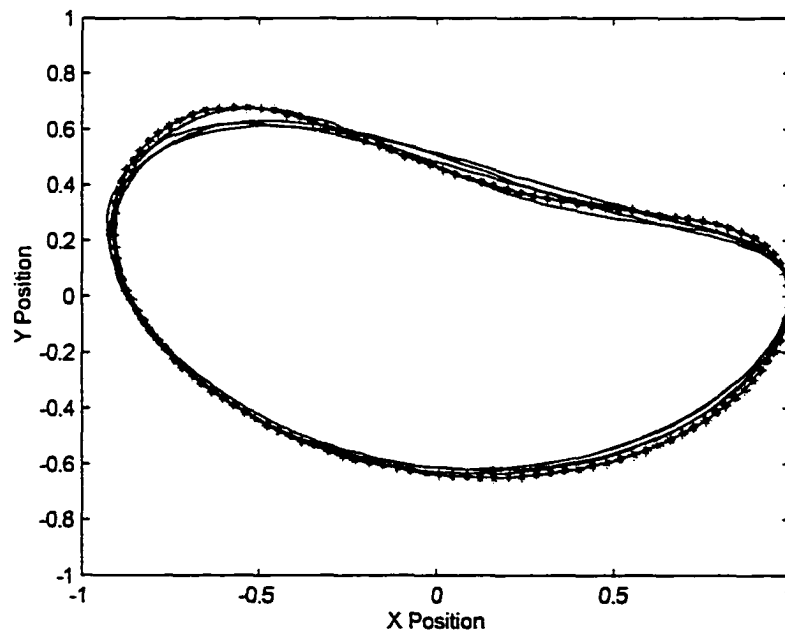


Figure 7.5: Graph of the top 5 database trace point paths identified by absolute differences

Sum of Squared Differences

The sum of the squared differences when used with the trace point path is defined by the following equation:

$$A(x,y) = \sum \{ [(f_x(\theta) - g_x(\theta))^2 + [(f_y(\theta) - g_y(\theta))^2] \} \quad [7.10]$$

Where:

$f_x(\theta)$ = X position of database path at a point

$f_y(\theta)$ = Y position of database path at a point

$g_x(\theta)$ = X position of desired path at a point

$g_y(\theta)$ = Y position of desired path at a point

As the sum of the squared differences is processed, the absolute distance between a specified point in the database path and the desired path is evaluated and squared. Evaluation of two trace point paths that match will generate a squared difference value close to zero. Two paths that are not similar have a squared difference value greater than zero.

Figure 7.6 is a graph of the squared difference measure of the desired trace point path with the first 145 of the total 7,450 database paths. The top 5 matching database paths are plotted in

Figure 7.7. The 15 database paths which had the smallest squared difference values are listed in Table 7.4.

The squared difference measure, defined for a two dimensional path, analyzed point by point the curves that most closely matched the desired trace point path and squared the difference. The top 15 trace point paths identified using squared difference measure were the same as the top 15 trace point paths identified using the absolute difference measure although there were several paths that had a different rank. The database search took 7.42 seconds of CPU time and 114,887 FLOPS.

Table 7.4: Summary of database search of trace point paths using squared difference

Desired Curve - Database Curve #3

Search Rank	Database Curve Number	Squared Difference Value
1	3	0.0000
2	2	0.0380
3	40	0.0752
4	47	0.1334
5	85	0.1588
6	123	0.1936
7	9	0.2471
8	55	0.2525
9	93	0.2636
10	131	0.2850
11	77	0.3987
12	39	0.4279
13	115	0.4414
14	1	0.4766
15	17	0.4890

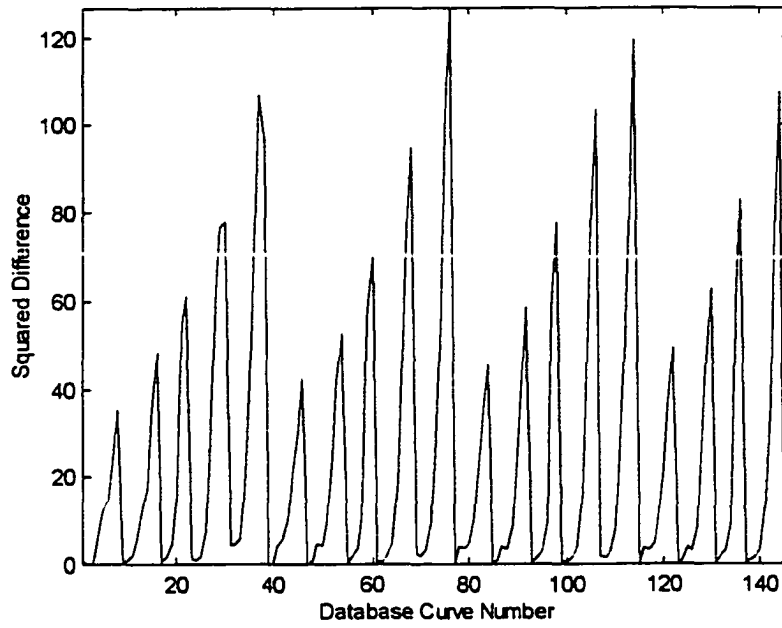


Figure 7.6: Graph of squared difference of desired trace point path with 145 database trace point paths

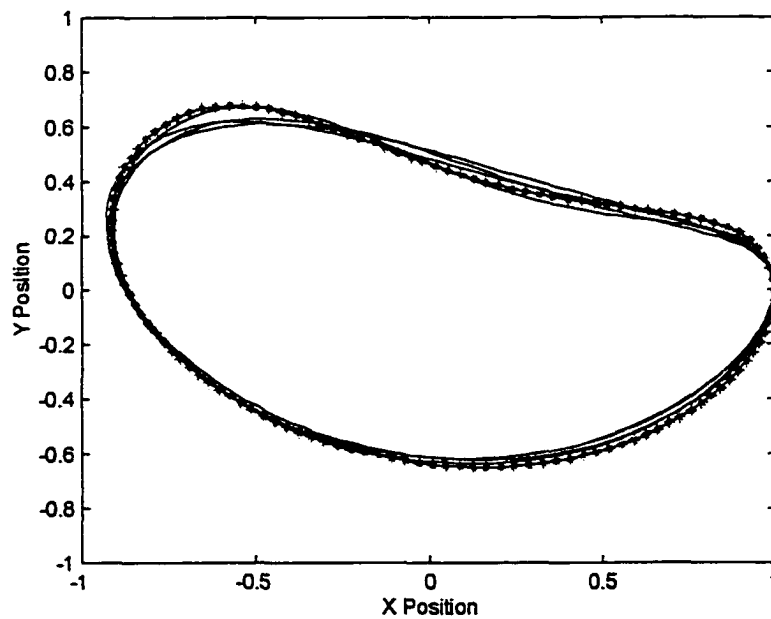


Figure 7.7: Graph of the top 5 database trace point paths identified by squared difference

One-Dimensional Correlation using Fourier Descriptors

Correlation in the Fourier frequency domain is evaluated by taking the maximum value of:

$$C(x) = \mathfrak{F}^{-1} [F^*(u) * G(u)] \quad [7.11]$$

Where:

$F^*(u)$ = Complex conjugate of Fourier transform of $f(x)$

$G(u)$ = Fourier transform of $g(x)$

$C(x)$ = Correlation value of $f(x)$ and $g(x)$

Each point of the trace path curve (x,y) defines a complex number $x + iy$ to support the evaluation of the two dimensional trace point plot by a one-dimensional Fourier transform. The top 16 Fourier descriptors were identified and then stored with the file of the four-bar mechanism configuration.

Figure 7.8 is a graph of the frequency correlation of the desired trace point path with the 145 database trace point paths. The 15 database trace point paths which had the largest correlation values are listed in Table 7.5. The top 5 matching database trace point paths are plotted in Figure 7.9. The database search took 5.33 seconds of CPU time and 113,868 FLOPS.

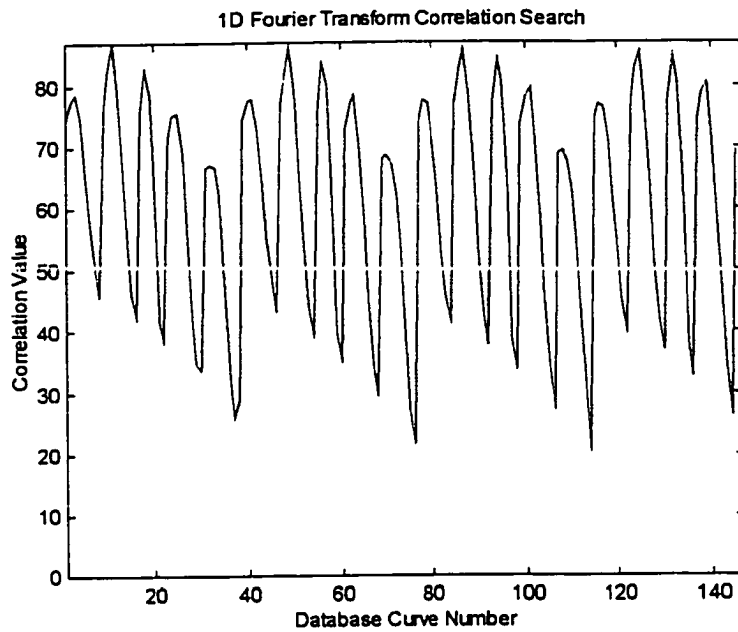


Figure 7.8: Graph of the correlation using Fourier descriptors of the desired trace point path with 145 database trace point paths

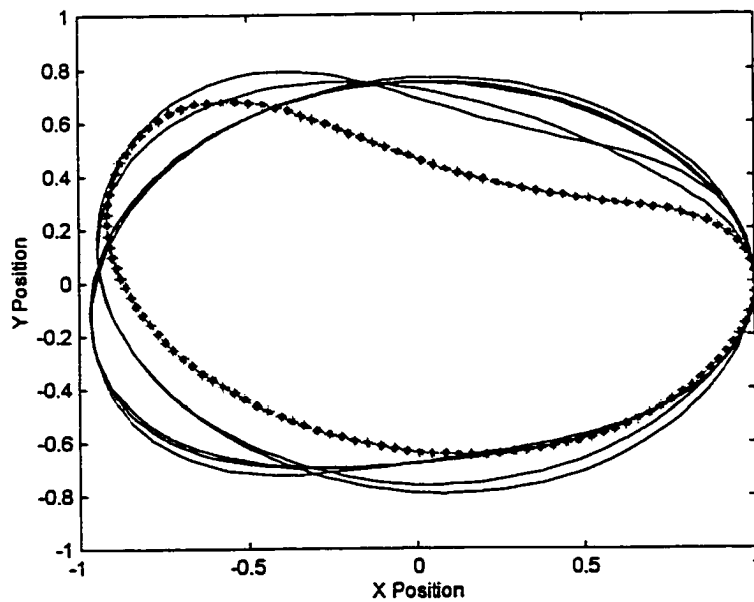


Figure 7.9: Graph of the top 5 database trace point paths identified using correlation of Fourier descriptors

Table 7.5: Summary of database search of trace point paths using correlation of Fourier descriptors

Desired Curve - Database Curve #3

Search Rank	Database Curve Number	Correlation Value
1	11	86.93
2	49	86.35
3	87	85.81
4	125	85.44
5	132	84.88
6	94	84.49
7	56	83.90
8	124	82.88
9	18	82.82
10	86	82.69
11	48	82.49
12	10	82.19
13	133	80.80
14	95	80.54
15	139	80.51

One-Dimensional Phase-Only Filter

Phase-only filtering in the Fourier frequency domain is evaluated by taking the maximum value of:

$$C(x) = \mathcal{J}^{-1} \{ [F^*(u)/|F(u)|] * G(u) \} \quad [7.12]$$

Where:

$$|F(u)| = \text{Magnitude of Fourier transform of } f(x)$$

Figure 7.10 is a graph of the phase-only filter correlation of the desired trace point path with the 145 database trace point

paths. The 15 database paths which had the largest correlation values are listed in Table 7.6. The top 5 matching database trace point paths are plotted in Figure 7.11. The database search took 2.32 seconds of CPU time and 1,126,553 FLOPS.

Table 7.6: Summary of database search of trace point paths using phase-only filter

Desired Curve - Database Curve #3

Search Rank	Database Curve Number	Correlation Value
1	4	1.1330
2	3	1.1260
3	1	1.1251
4	2	1.1218
5	9	1.1084
6	31	1.0977
7	12	1.0966
8	5	1.0961
9	13	1.0954
10	17	1.0902
11	23	1.0862
12	39	1.0861
13	10	1.0859
14	40	1.0858
15	41	1.0807

One-Dimensional Symmetric Phase-Only Matched Filter

Symmetric phase-only matched filtering in the Fourier frequency domain is evaluated by taking the maximum of:

$$C(x) = \mathcal{F}^{-1} \{ [F^*(u)/|F(u)|] * [G(u)/|G(u)|] \} \quad [7.13]$$

Where:

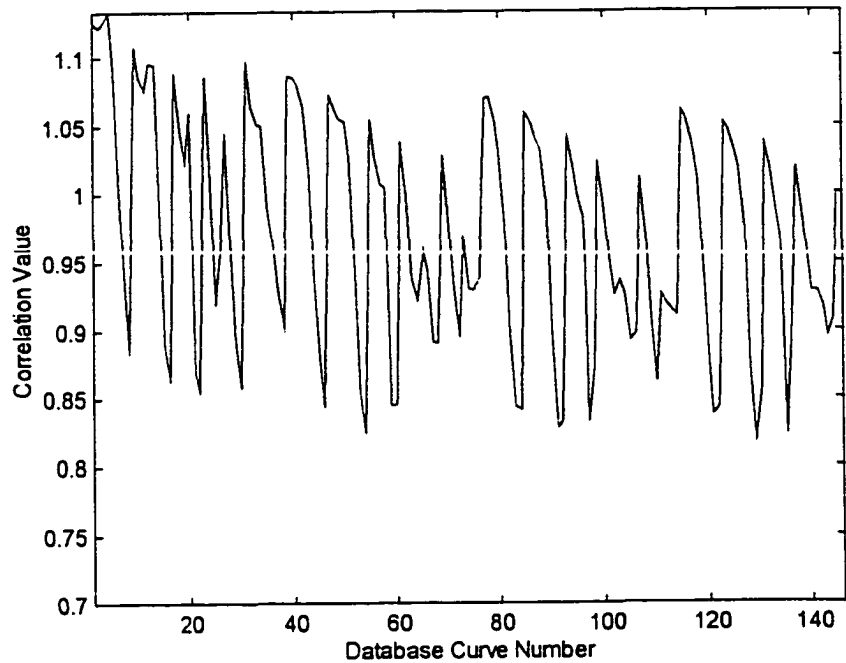


Figure 7.10: Graph of the correlation using phase-only filter

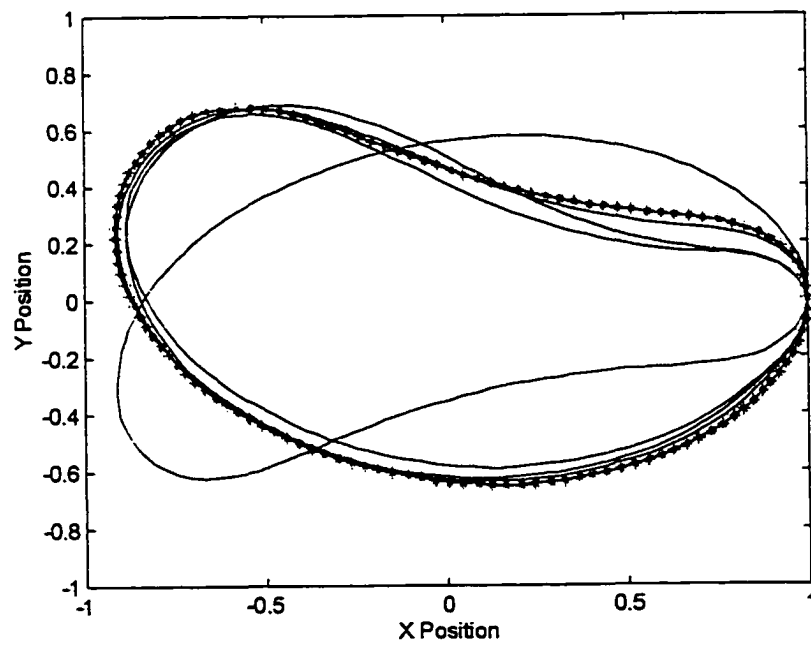


Figure 7.11: Graph of the top 5 database trace point paths identified by using a phase-only filter

$|F(u)|$ = Magnitude of Fourier transform of $f(x)$

$|G(u)|$ = Magnitude of Fourier transform of $g(x)$

Figure 7.12 is a graph of the symmetric phase-only filter correlation of the desired trace point path with the 145 database paths. The 15 database trace point paths that had the largest correlation values are listed in Table 7.7. The top 5 matching database paths are plotted in Figure 7.13. Note should be taken of the one trace point path that appears to be a mirror image; this path is from database curve number 4. This path has the largest radius, R_{max} , approximately 180 degrees from curve number 3. The database search took 2.37 seconds of CPU time and 1,252,133 FLOPS.

Table 7.7: Summary of database search of trace point paths using symmetric phase-only matched filter

Desired Curve - Database Curve #3

Search Rank	Database Curve Number	Correlation Value
1	3	1.0000
2	2	0.9959
3	86	0.9916
4	48	0.9883
5	10	0.9860
6	40	0.9854
7	47	0.9791
8	39	0.9791
9	1	0.9763
10	85	0.9744
11	9	0.9715
12	123	0.9713
13	124	0.9703
14	93	0.9701
15	131	0.9668

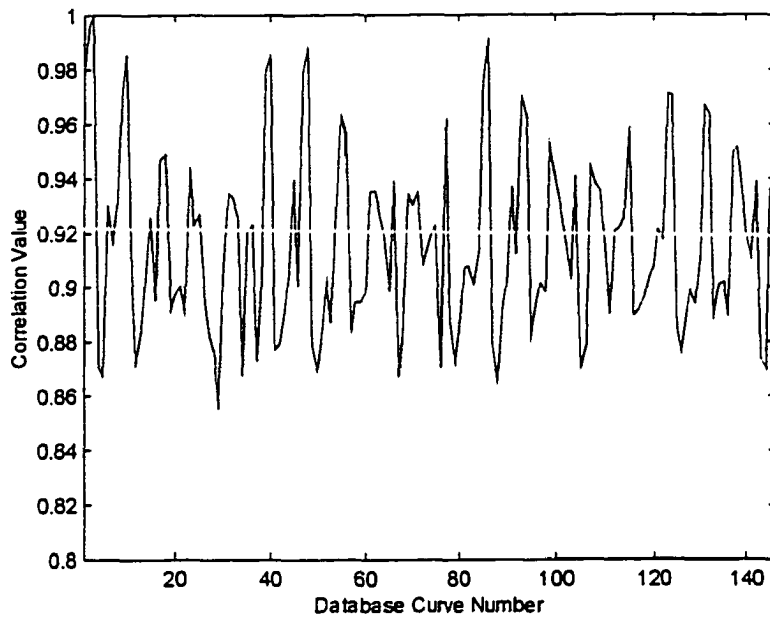


Figure 7.12: Graph of the correlation using symmetric phase-only matched filter

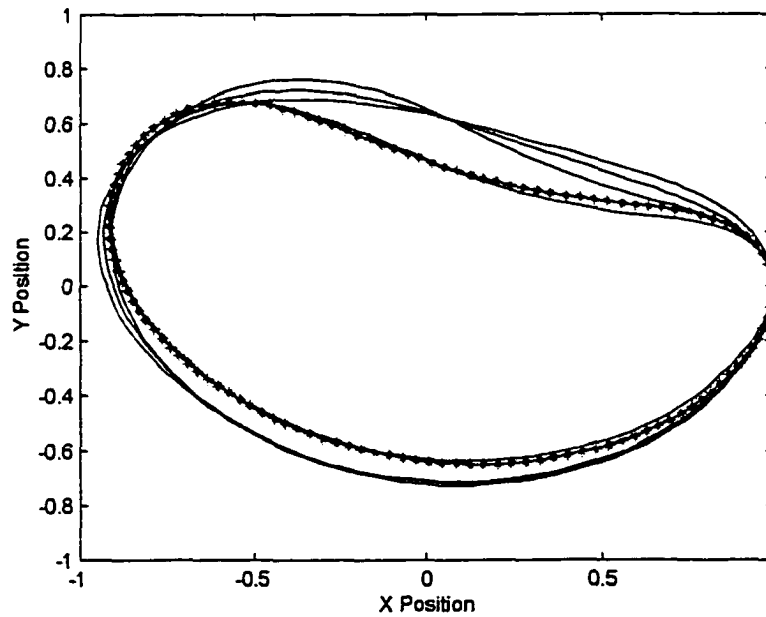


Figure 7.13: Graph of the top 5 database trace point paths identified using a symmetric phase-only matched filter

Amplitude Difference of Fourier Descriptors

The difference of the magnitude of the Fourier descriptors is defined by the following equation:

$$A(u) = \sum |F(u) - G(u)| \quad [7.14]$$

Figure 7.14 is a graph of the Fourier descriptor amplitude phase difference of the desired trace point path with the 145 database functions. The 15 database trace point paths that had the smallest amplitude difference are listed in Table 7.8. The top 5 matching database paths are plotted in Figure 7.15. Note the trace point paths 180° out of phase, Curves 12 and 41. The database search took 6.44 seconds of CPU time and 267,309 FLOPS.

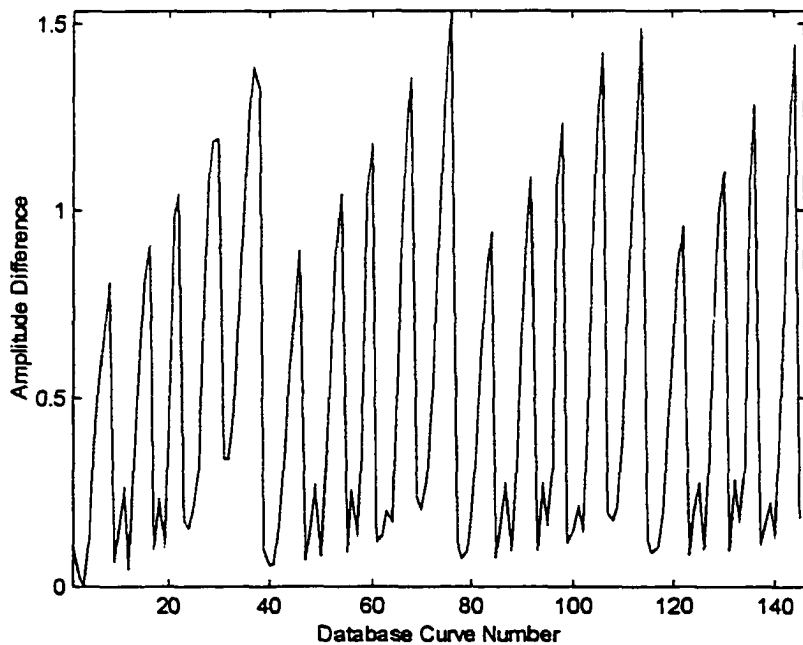


Figure 7.14: Graph of amplitude difference of Fourier descriptors

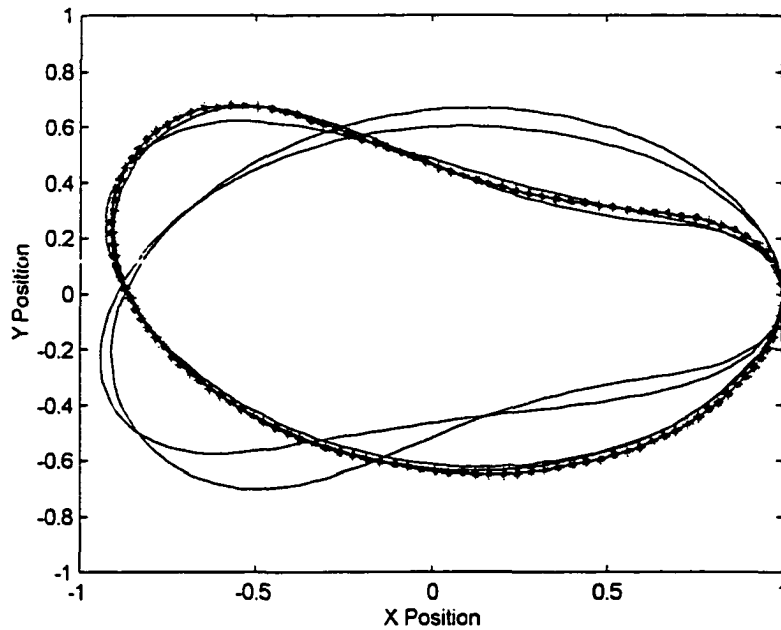


Figure 7.15: Graph of top 5 database trace point paths using amplitude difference of Fourier descriptors

Table 7.8: Summary of database search using amplitude difference of Fourier descriptors

Desired Curve - Database Curve #3

Search Rank	Database Curve Number	Amplitude Difference Value
1	3	0.000
2	2	3.293
3	12	5.821
4	40	7.257
5	41	7.829
6	9	8.348
7	47	8.622
8	78	9.445
9	85	9.749
10	50	10.217
11	123	10.342
12	55	11.249
13	116	11.280
14	79	11.726
15	88	11.826

Amplitude and Phase Difference of Fourier Descriptors

The difference of the magnitude of the Fourier descriptors is defined by the following equation:

$$Fd = \sum m * |F(u) - G(u)| + n * |\text{ang}(F(u) * F(u) - \text{ang}(G(u) * G(u))| \quad [7.15]$$

The value used for n was 0.3 and m was 0.7. Figure 7.16 is a graph of the Fourier descriptor amplitude and phase difference of the desired trace point path with the 145 database functions. The 15 database trace point paths that had the smallest amplitude and phase difference are listed in Table 7.9. The top 5 matching database trace point paths are plotted in Figure 7.17. The database search took 6.20 seconds of CPU time and 267,309 FLOPS.

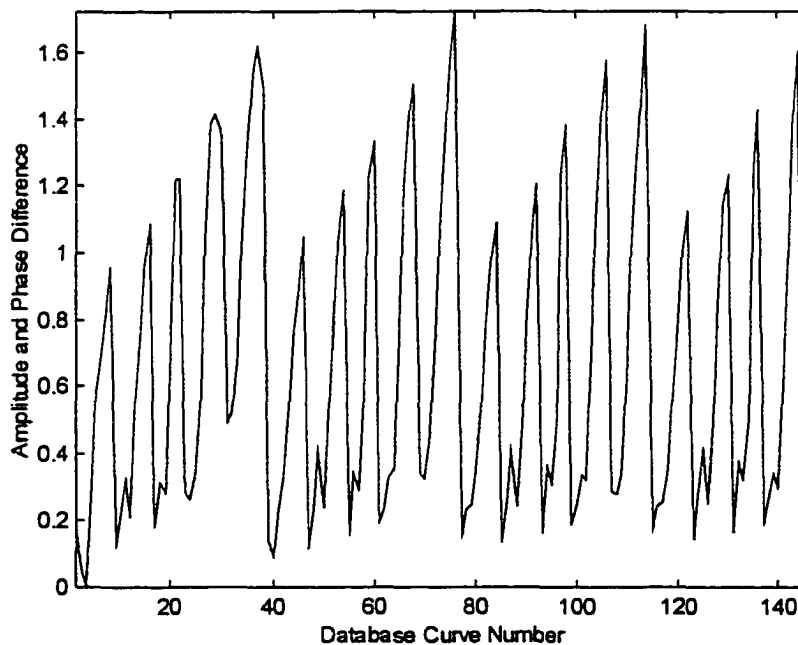


Figure 7.16: Graph of amplitude and phase difference of Fourier descriptors

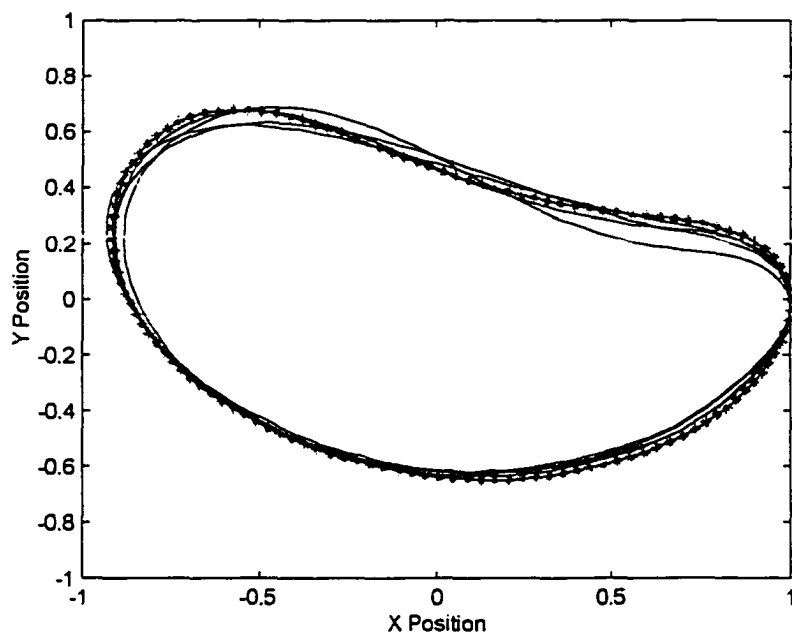


Figure 7.17: Graph of top 5 trace point paths using amplitude and phase difference of Fourier descriptors

Table 7.9: Summary of database search using amplitude and phase difference of Fourier descriptors

Desired Curve - Database Curve #3

Search Rank	Database Curve Number	Amplitude and Phase Difference
1	3	0.000
2	2	4.564
3	40	9.157
4	47	11.144
5	9	11.652
6	85	12.696
7	123	13.582
8	55	14.742
9	12	15.021
10	39	15.026
11	93	15.529
12	131	15.997
13	77	16.823
14	41	16.835
15	17	16.888

Correlation with Two-Dimensional Fourier Transform

Correlation in the Fourier frequency domain using a two-dimensional Fourier Transform, equation 4.11, is evaluated by taking the maximum value of:

$$C(x) = \mathcal{F}^{-1} [F^*(u) * G(u)] \quad [7.16]$$

The top 16 Fourier Descriptors are stored in the database to compare with the one-dimensional Fourier transforms.

Figure 7.18 is a graph of the frequency correlation of the desired trace point path with the 145 database functions. The 15 database paths that had the largest correlation values are listed in Table 7.10. The top 5 matching database trace point paths are plotted in Figure 7.19. The database search took 11.43 seconds of CPU time and 207,808,187 FLOPS.

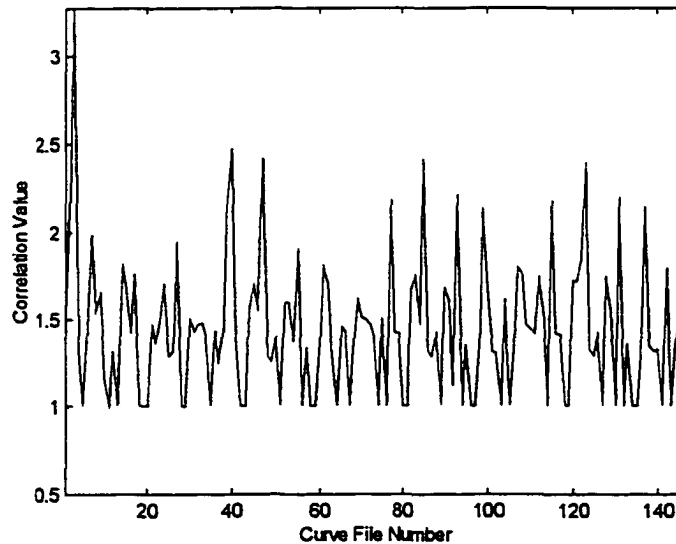


Figure 7.18: Graph of the correlation using Fourier descriptors of the desired trace point path with 145 database trace point paths

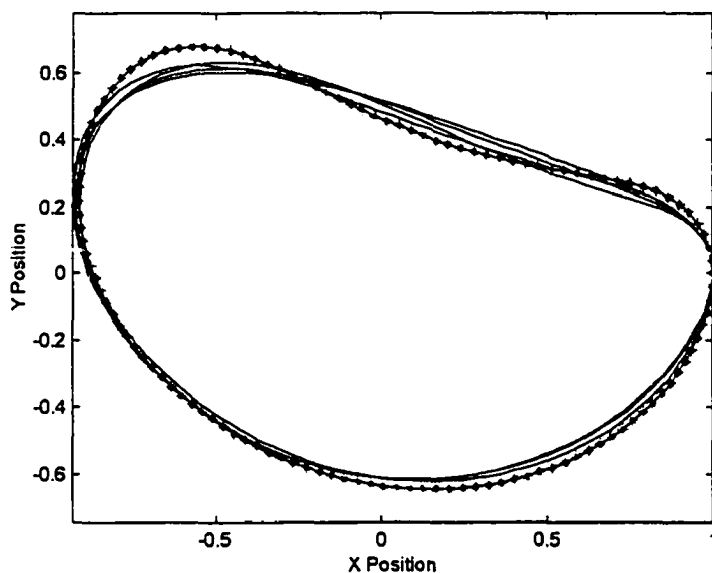


Figure 7.19: Graph of the top 5 database trace point paths identified using correlation of Fourier descriptors

Table 7.10: Summary of database search of trace point paths using correlation of Fourier descriptors

Desired Curve - Database Curve #81

Search Rank	Database Curve Number	Correlation Value
1	3	3.2803
2	40	2.4811
3	47	2.4177
4	85	2.4168
5	123	2.3956
6	2	2.2615
7	93	2.2167
8	131	2.1988
9	77	2.1872
10	115	2.1828
11	39	2.1749
12	137	2.1466
13	99	2.1407
14	7	1.9855
15	27	1.9537

Phase-Only Filter with Two-Dimensional Fourier Transform

Phase-only filtering in the Fourier frequency domain is evaluated by taking the maximum value of:

$$C(x) = \mathcal{F}^{-1} \{ (|F^*(u)|/|F(u)|) * G(u) \} \quad [7.17]$$

Figure 7.20 is a graph of the phase-only filter correlation of the desired trace point path with the 145 database trace point paths. The 15 database paths that had the largest correlation values are listed in Table 7.11. The top 5 matching database trace point paths are plotted in Figure 7.21. The database search took 11.56 seconds of CPU time and 208,068,283 FLOPS.

Table 7.11: Summary of database search of trace point paths using phase-only filter

Desired Curve - Database Curve #3

Search Rank	Database Curve Number	Correlation Value
1	3	0.0530
2	40	0.0352
3	85	0.0340
4	47	0.0340
5	123	0.0336
6	2	0.0307
7	93	0.0301
8	131	0.0297
9	77	0.0287
10	115	0.0286
11	39	0.0284
12	137	0.0280
13	99	0.0278
14	7	0.0263
15	27	0.0248

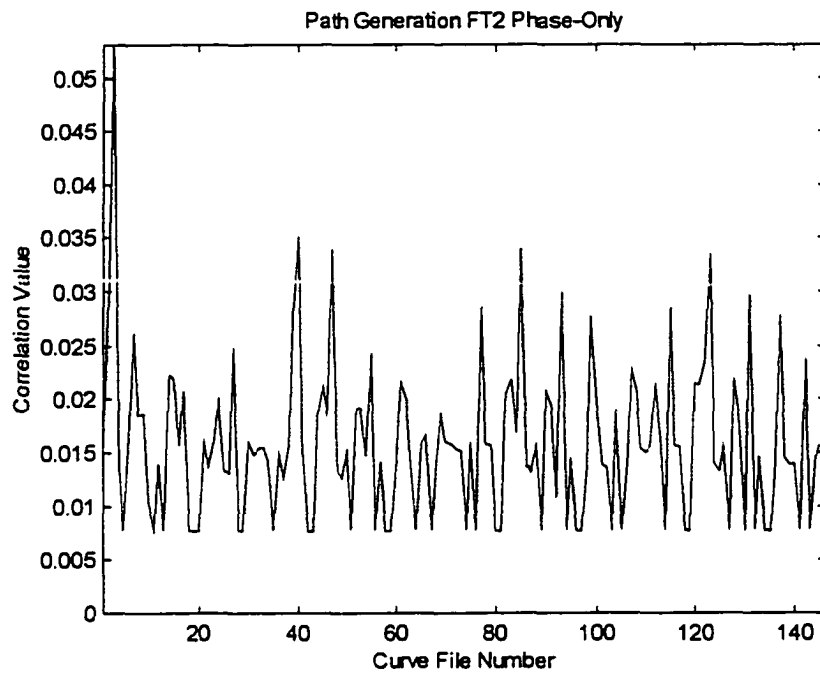


Figure 7.20: Graph of correlation using phase-only filter

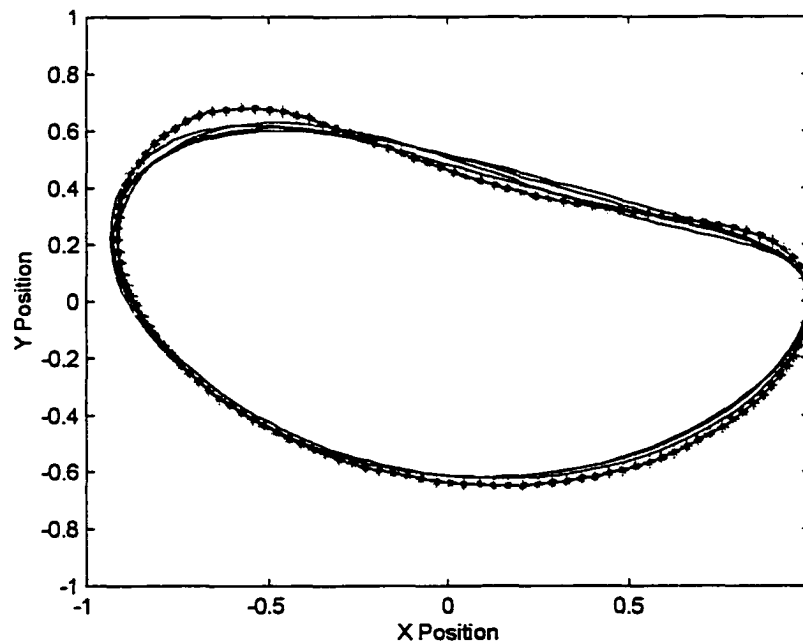


Figure 7.21: Graph of top 5 database trace point paths identified by using a phase-only filter

**Symmetric Phase-Only Matched Filter with Two-Dimensional
Fourier Transforms**

Symmetric phase-only matched filtering in the Fourier frequency domain is evaluated by taking the maximum of:

$$C(x) = \mathcal{F}^{-1} \{ [F'(u)/|F(u)|] * [G(u)/|G(u)|] \} \quad [7.18]$$

Figure 7.22 is a graph of the symmetric phase-only filter correlation of the desired trace point path with the 145 database paths. The 15 database trace point paths that had the largest correlation values are listed in Table 7.12. The top 5 matching database paths are plotted in Figure 7.23. The database search took 20.89 seconds of CPU time and 251,050,075 FLOPS.

Table 7.12: Summary of database search of trace point paths using symmetric phase-only matched filter

Desired Curve - Database Curve #3

Search Rank	Database Curve Number	Correlation Value
1	3	1.0000
2	47	0.9996
3	93	0.9994
4	85	0.9994
5	40	0.9994
6	131	0.9993
7	115	0.9993
8	99	0.9992
9	117	0.9992
10	77	0.9992
11	123	0.9992
12	139	0.9991
13	106	0.9991
14	25	0.9991
15	78	0.9991

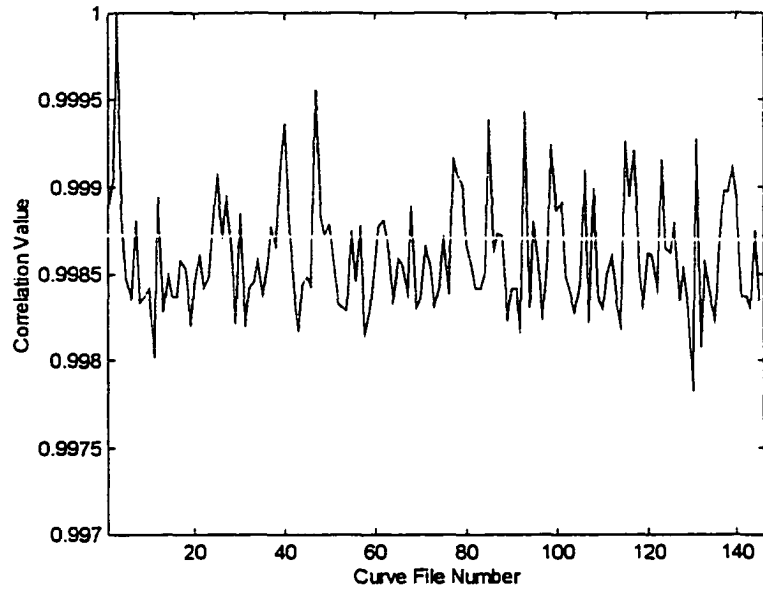


Figure 7.22: Graph of the correlation using symmetric phase-only matched filter

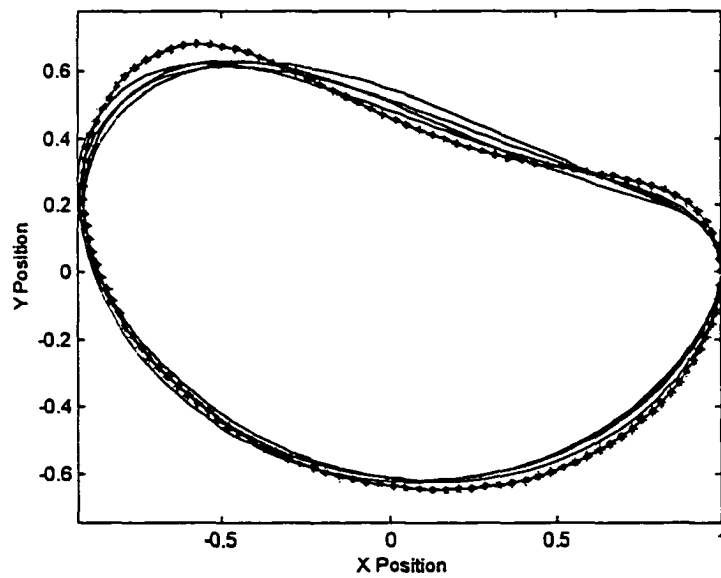


Figure 7.23: Graph of the top 5 database trace point paths identified using symmetric phase-only matched filter

Moment Normalized Cross Correlation

Pattern matching using seven invariant moments may be evaluated by the following [Wong and Hall, 1978]:

$$R_k = \frac{\sum_j M_j N_j}{[\sum_j M_j^2 * \sum_j N_j^2]^{0.5}} \quad [7.19]$$

Where:

R = Moment correlation

M_j = jth Invariant moment of desired image

N_j = jth Invariant moment of database image

There were seven invariant moments stored in the database for each of the trace point paths (Chapter 4, equations 4.56-4.62).

Figure 7.24 is a graph of the moment correlation of the desired trace point path with the 145 database trace point paths. The 15 database paths that had the largest correlation values are listed in Table 7.13. The top 5 matching database trace point paths are plotted in Figure 7.25. The database search took 1.97 seconds of CPU time and 10051 FLOPS.

Table 7.13: Summary of database search of trace point paths using invariant moments and normalized cross correlation

Desired Curve - Database Curve #3

Search Rank	Database Curve Number	Moment Correlation Value
1	3	1.0000
2	133	0.9989
3	50	0.9957
4	12	0.9900
5	70	0.9766
6	137	0.9708
7	107	0.9548
8	69	0.9437
9	75	0.9412
10	61	0.9248
11	145	0.9185
12	116	0.9165
13	23	0.9152
14	31	0.9102
15	29	0.8917

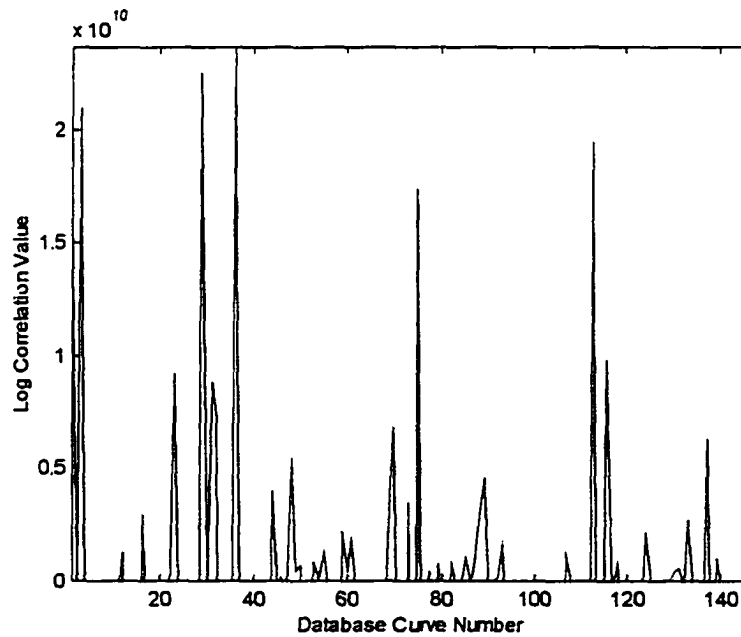


Figure 7.24: Graph of the correlation using invariant moments and normalized cross correlation

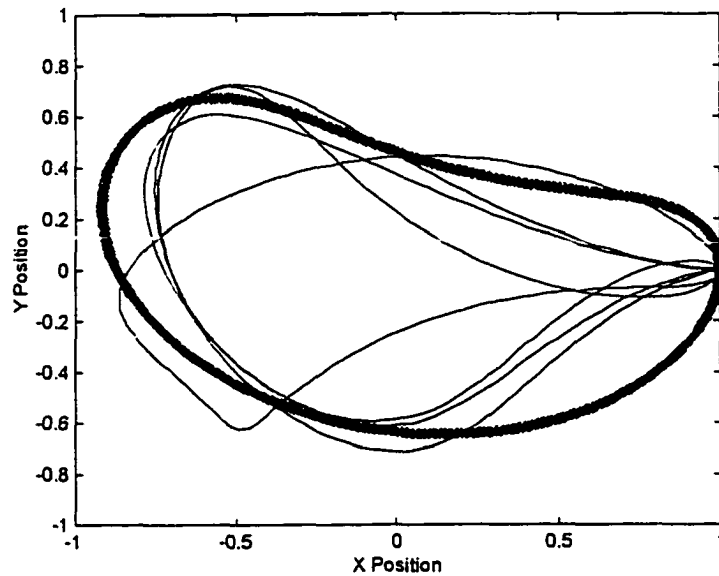


Figure 7.25: Graph of the top 5 database trace point paths identified using invariant moments and normalized cross correlation

Moment Sum of Percentage Difference

Pattern matching using the seven invariant moments may be evaluated by the following:

$$S = \exp \left[\sum_j (|M_j - N_j|/M_j) \right] \quad [7.20]$$

Where:

S = Moment correlation

M_j = j th Invariant moment of image

N_j = j th Invariant moment of database image

The highest correlation values identify the most likely matches. This type of matching technique provides a correlation number that is between zero and one. A perfect match will have a correlation of 1.0. Each invariant moment has an effect on the correlation.

Figure 7.26 is a graph of the moment correlation of the desired trace point path with the 145 database functions. The 15 database trace point paths that had the largest correlation values are listed in Table 7.14. The top 5 matching database trace point paths are plotted in Figure 7.27. The database search took 1.96 seconds of CPU time and 6427 FLOPS.

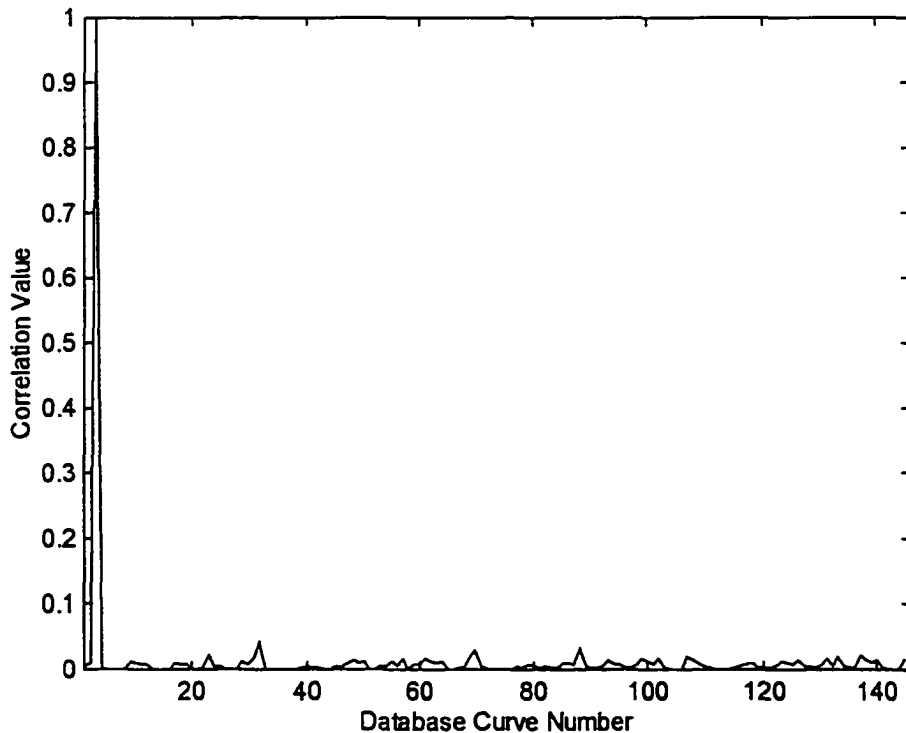


Figure 7.26: Graph of the correlation using invariant moments and sum of percentage difference

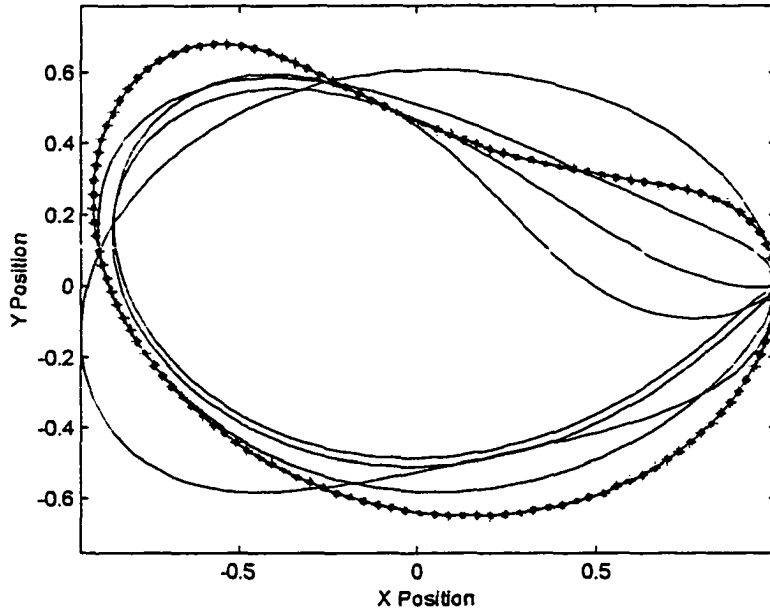


Figure 7.27: Graph of the top 5 database trace point paths identified using invariant moments and sum of percentage difference

Table 7.14: Summary of database search of trace point paths using invariant moments and sum of percentage difference

Desired Curve - Database Curve #3

Search Rank	Database Curve Number	Moment Correlation Value
1	3	1.0000
2	32	0.0403
3	88	0.0308
4	70	0.0295
5	137	0.0226
6	23	0.0223
7	133	0.0202
8	107	0.0189
9	69	0.0188
10	31	0.0184
11	131	0.0173
12	145	0.0173
13	102	0.0172
14	61	0.0172
15	57	0.0169

Partial Curves

A complete rotation of the drive crank and the resulting trace point path has been evaluated for path generation four-bar mechanisms. The trace point path has been a closed curve and is applicable only to four-bar mechanisms where the drive crank rotates a complete 360 degrees. A different methodology is required to characterize the output path of a crank-rocker, a double-crank, or double-rocker four-bar mechanisms that only rotate through a specified angle and generate trace point paths that are not closed.

Consider the example four-bar mechanism where the drive crank only rotates from an angle of 0 degrees to 90 degrees. Figure 7.28 is a graph of the trace point path. Compare this trace point path to that of Figure 7.1.

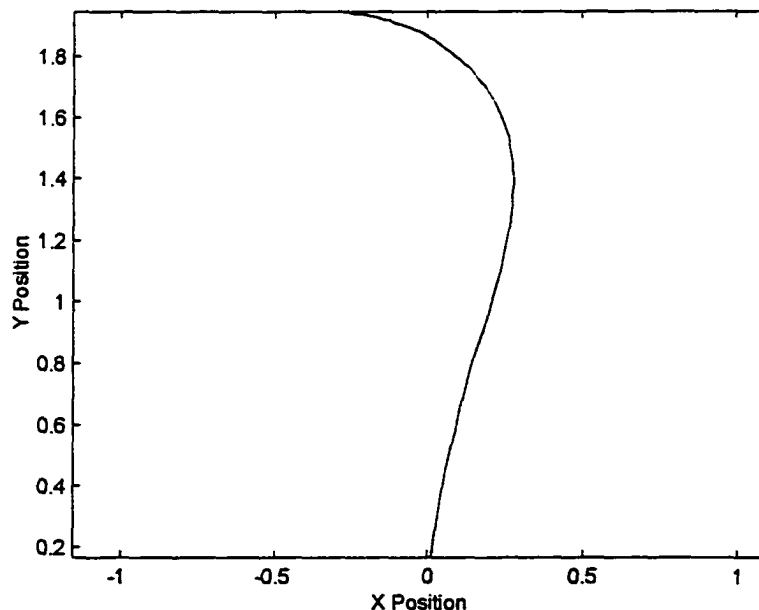


Figure 7.28: Trace point path resulting from the drive crank angle from moving from 0 to 90 degrees.

The trace point path and its relationship to the drive crank angle are not of interest when searching for trace point paths stored in a database. As a result the trace point path is sampled from one end of the path, end point "A", to the other end of the path, end point "B" in equal segments. The trace point path is then sampled from end point "B" back to end point "A" in equal steps. This generates a series of x and y coordinates that are cyclic. A total of 128 discrete points were used to sample the complete trace point path. This process generates a series of points that may be normalized for translation, rotation and scale in the same manner that a closed trace point path. Figure 7.29 is a graph of the trace point path normalized for position, rotation, scale and point distribution. Note that while there are only 64 discrete points that may be visually identified on the trace point path, there are actually 128 discrete points used in the definition of the path.

A database of 7,475 trace point paths was generated with the configurations described earlier in this chapter. The drive crank angle was a minimum of 0 degrees and a maximum of 90 degrees. The database structure and information stored is the same as with the crank rocker with full drive crank motion. A desired curve was selected as the third numbered database curve and the configuration is the same as defined on page 145.

The desired curve was compared with each of the first 150 database curves and evaluated with the following matching techniques:

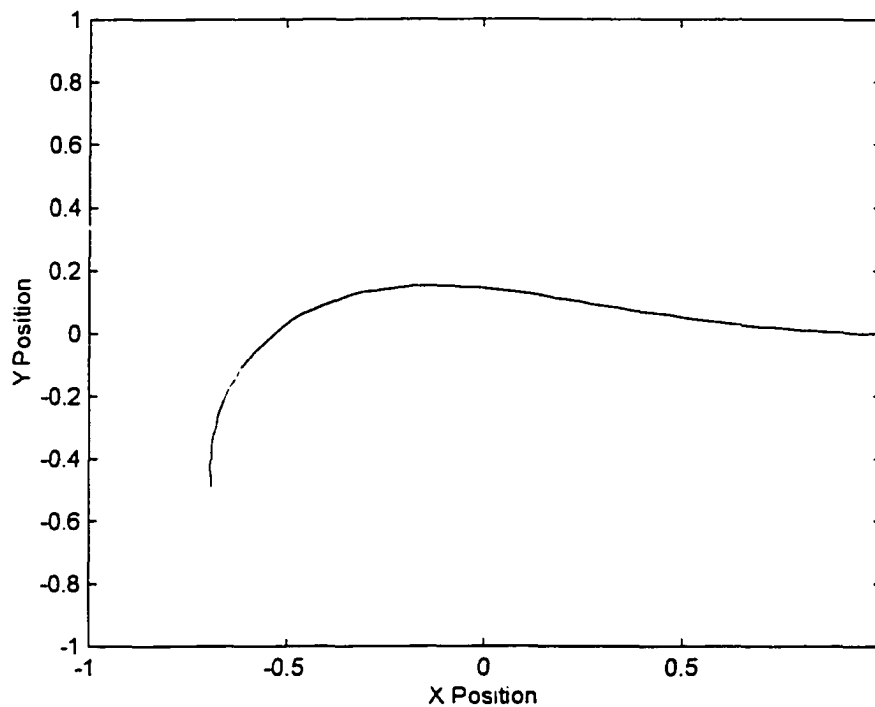


Figure 7.29: Trace point path normalized for position, rotation, and scale

- Sum of absolute differences
- Fourier descriptor amplitude and phase difference measure
- Two-dimensional Fourier descriptors with symmetric phase only matched filtering.

Partial Curves - Sum of Absolute Differences

The sum of absolute differences is a difference measure and is defined by equation 7.8. The starting point for evaluating the absolute difference is always at the point on the curve that lies

on the X-axis and has a x and y value of 1.0 and 0.0 respectively. Figure 7.30 is a graph of the absolute difference of the partial trace point path with the 145 database partial trace point paths. The 15 database partial trace point paths that had the smallest absolute difference values are listed in Table 7.15. The top 5 matching database partial trace point curves are plotted in Figure 7.31. The database search took 6.41 seconds of CPU time and 133,447 FLOPS.

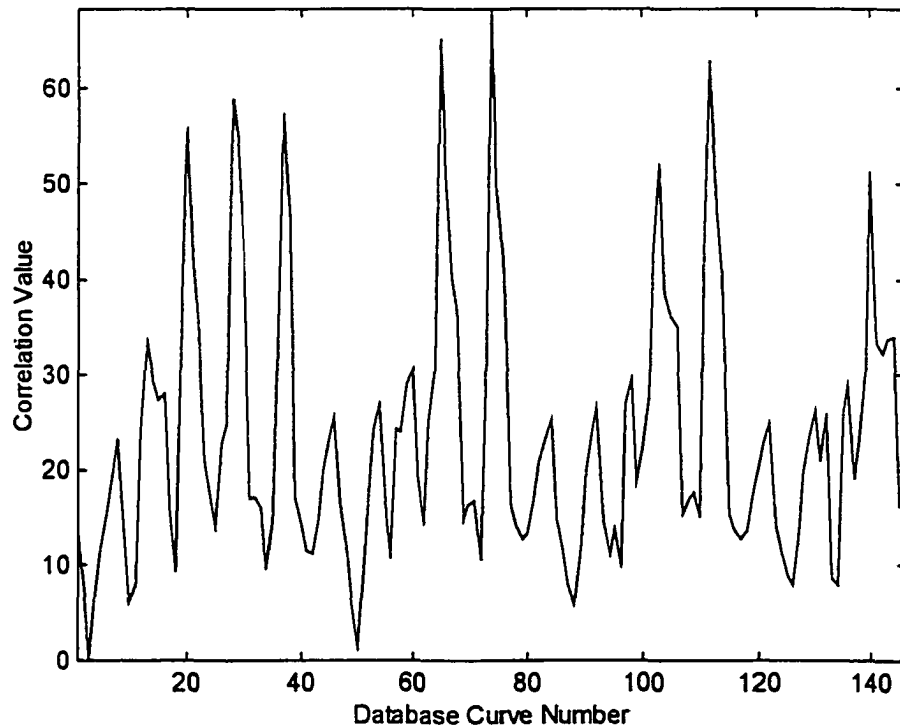


Figure 7.30: Graph of absolute difference of partial curve path with 145 database trace point paths

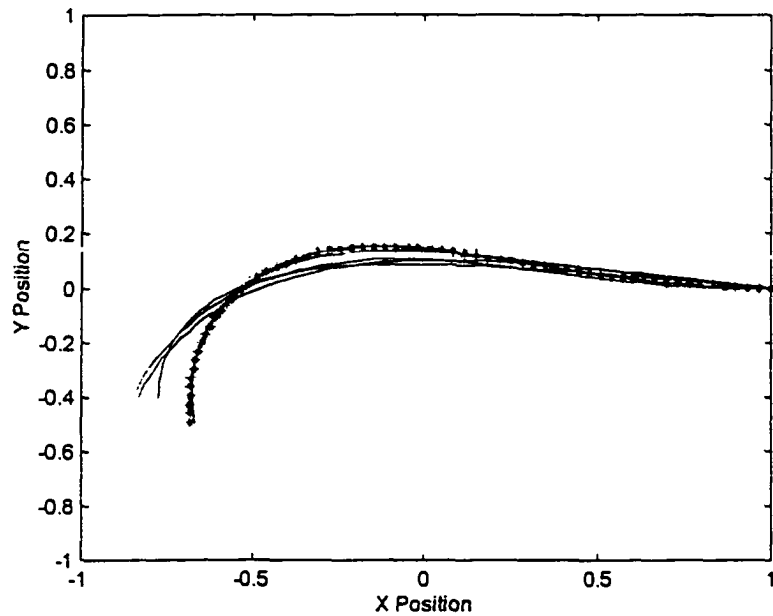


Figure 7.31: Graph of the top 5 database partial trace point paths identified by absolute difference

Table 7.15: Summary of database search of partial trace point paths using absolute difference

Desired Curve - Database Curve #3

Search Rank	Database Curve Number	Absolute Difference Value
1	3	0.0000
2	50	1.3375
3	49	5.7995
4	88	5.8419
5	10	5.9706
6	4	7.2782
7	2	7.4143
8	134	7.8362
9	126	7.8481
10	87	7.9162
11	51	7.9202
12	11	8.0683
13	133	8.6225
14	125	8.7809
15	18	9.2137

Partial Curves - Amplitude and Phase Difference of Fourier Descriptors

The difference of the magnitude and phase of the Fourier descriptors is defined by equation 7.13. The value used for "n" was 0.3. Figure 7.32 is a graph of the Fourier descriptor amplitude and phase difference of the desired partial trace point path with the 145 database partial trace point paths. The 15 database partial trace point paths that had the smallest amplitude and phase difference are listed in Table 7.16. The top 5 matching database partial trace point paths are plotted in Figure 7.33. The database search took 6.64 seconds of CPU time and 267,614 FLOPS.

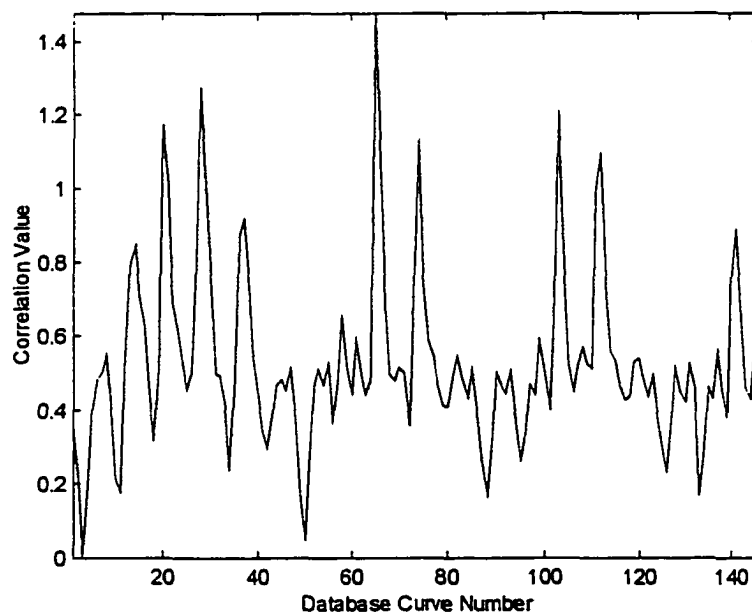


Figure 7.32: Graph of amplitude and phase difference of Fourier descriptors

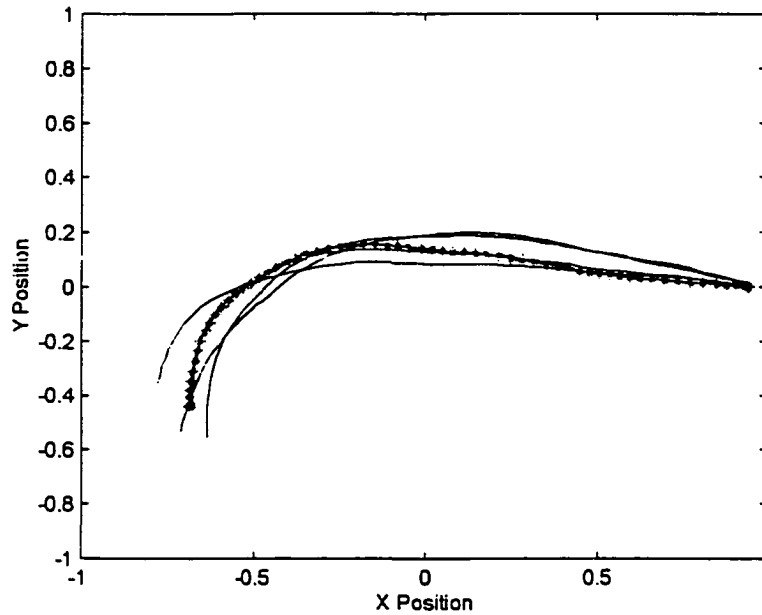


Figure 7.33: Graph of top 5 partial trace point paths identified using amplitude and phase difference

Table 7.16: Summary of database search of partial trace point paths using amplitude and phase difference

Desired Curve - Database Curve #3

Search Rank	Database Curve Number	Amplitude and Phase Difference
1	3	0.0000
2	50	0.0430
3	133	0.1652
4	88	0.1698
5	11	0.1780
6	49	0.1794
7	4	0.2063
8	10	0.2106
9	2	0.2132
10	126	0.2301
11	34	0.2325
12	51	0.2566
13	95	0.2616
14	87	0.2640
15	134	0.2811

**Partial Curves - Symmetric Phase-Only Matched Filter with
Two-Dimensional Fourier Transforms**

Symmetric phase-only matched filtering in the Fourier frequency domain is evaluated by taking the maximum of equation 7.15. Figure 7.34 is a graph of the symmetric phase-only filter correlation of the desired partial trace point path with the 145 database partial trace point paths. The 15 database partial trace point paths that had the largest correlation values are listed in Table 7.17. The top 5 matching database partial trace point paths are plotted in Figure 7.35. The database search took 2.41 seconds of CPU time and 1,252,133 FLOPS.

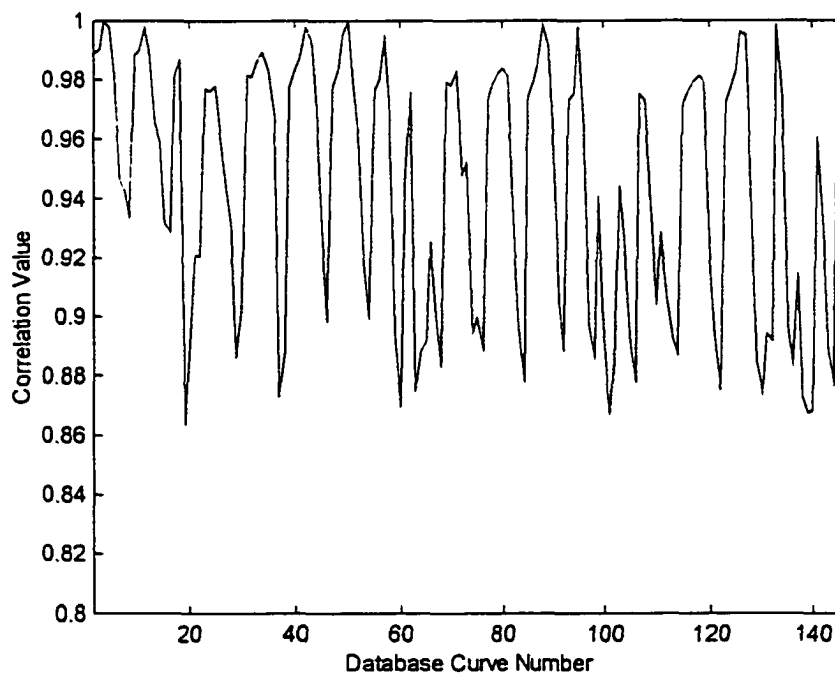


Figure 7.34: Graph of correlation using symmetric phase only matched filter correlation

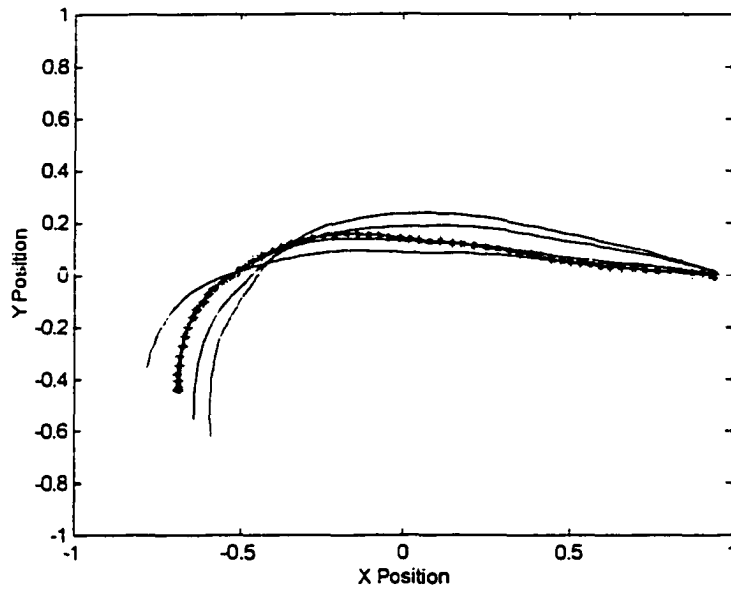


Figure 7.35: Graph of top 5 partial trace point paths identified using symmetric phase only matched filter

Table 7.17: Summary of database search of partial trace point paths using symmetric phase only matched filter

Desired Curve - Database Curve #3

Search Rank	Database Curve Number	Correlation Value
1	3	1.0000
2	50	0.9999
3	133	0.9989
4	88	0.9985
5	95	0.9981
6	4	0.9978
7	11	0.9975
8	42	0.9973
9	126	0.9962
10	49	0.9951
11	127	0.9950
12	57	0.9949
13	43	0.9932
14	89	0.9916
15	2	0.9904

Summary

A comparison of the various techniques for the use of invariant characterization, storage, and search methods for path generation of four-bar mechanisms was generated. Tables 7.18 and 7.19 are summaries of the top ten trace point paths identified when using file number 3 as a desired solution. Entries in table 7.18 and 7.19 are bold if the identified trace point paths are in the top 10 trace point paths identified by the absolute difference measure. Entries in table 7.18 and 7.19 are underlined if the identified trace point paths are in the top 5 trace point paths identified and match one of the top 5 trace point paths identified by the absolute difference measure. Table 7.20 is a summary of the time to generate 145 solutions to be filed, the time to search 145 curves and the number of FLOPS to run the various search techniques. The following are the various file search methods:

- SAD - Spatial transform, absolute difference
- SSS - Spatial transform, sum squared
- F1C - One-dimensional Fourier correlation
- F1P - One-dimensional Fourier phase only filter
- F1SP - One-dimensional Fourier descriptors, symmetric phase only matched filter
- F1A - One-dimensional Fourier transform, amplitude difference of Fourier descriptors
- F1AP - One-dimensional Fourier transform, amplitude and phase difference of Fourier descriptors
- F2 - Two-dimensional Fourier correlation

- F2P - Two-dimensional Fourier phase only filter
 F2SP - Two-dimensional Fourier descriptors, symmetric phase only matched filter
 MCC - Moment normalized cross correlation
 MPD - Moment percentage difference

Table 7.18: Performance of various methods to measure the similarity of a desired solution to 145 filed solutions - full drive crank rotation

Top Ranked File No.	1	2	3	4	5	6	7	8	9	10
SAD	<u>3</u>	<u>2</u>	<u>40</u>	<u>47</u>	<u>85</u>	123	9	55	93	131
SSS	<u>3</u>	<u>2</u>	<u>40</u>	<u>47</u>	<u>85</u>	123	9	55	93	131
F1C	11	49	87	125	132	94	56	124	18	86
F1P	4	<u>3</u>	1	<u>2</u>	9	31	12	5	13	12
F1SP	<u>3</u>	<u>2</u>	86	48	10	<u>40</u>	<u>47</u>	39	1	<u>85</u>
F1A	<u>3</u>	<u>2</u>	12	<u>40</u>	41	9	<u>47</u>	78	<u>85</u>	50
F1AP	<u>3</u>	<u>2</u>	<u>40</u>	<u>47</u>	9	<u>85</u>	<u>123</u>	<u>55</u>	12	39
F2C	<u>3</u>	<u>40</u>	<u>47</u>	<u>85</u>	123	2	<u>93</u>	<u>131</u>	77	115
F2P	<u>3</u>	<u>40</u>	<u>85</u>	<u>47</u>	123	2	<u>93</u>	<u>131</u>	77	115
F2SP	<u>3</u>	<u>47</u>	<u>93</u>	<u>85</u>	<u>40</u>	<u>131</u>	115	99	117	77
MCC	<u>3</u>	133	50	12	70	137	107	69	75	61
MPD	<u>3</u>	32	88	70	137	23	133	107	69	31

The amplitude and phase difference of Fourier descriptors was the measure of similarity that identified database trace point paths with a desired solution that correlated most closely to the spatial absolute difference measure. This was found for both full drive crank rotation and for partial drive crank rotation. Four of the top five solutions were the same and the order identified matched with the absolute difference measure. Of the top 10 curves identified by the absolute difference measure, eight were also identified by the amplitude and phase difference of Fourier descriptors. By modifying the weighting value of "m" in the amplitude and phase difference measure, trace point paths which were "mirror" images of the desired solution were also identified.

The spatial matching techniques required the largest database file space while the two-dimensional Fourier transform matching techniques and the moment invariants required the most time to generate a database of solutions.

Table 7.19: Performance of various methods to measure the similarity of a desired solution to 145 filed solutions - partial drive crank rotation

Top Ranked File No.	1	2	3	4	5	6	7	8	9	10
SAD	<u>3</u>	<u>50</u>	<u>49</u>	<u>88</u>	<u>10</u>	4	2	134	126	87
F1AP	<u>3</u>	<u>50</u>	133	<u>88</u>	11	49	4	10	2	126
F2SP	<u>3</u>	<u>50</u>	133	<u>88</u>	95	4	11	42	126	49

The one-dimensional Fourier transform amplitude difference was the only matching technique that identified both candidate curves similar to the absolute difference measure and candidate curves were rotated 180° from the desired trace point path. Depending on the database generation and search technique, this matching technique is the only technique that will identify those solutions 180° out of phase. The one-dimensional Fourier transform amplitude and phase difference matching technique showed the best performance in identifying solutions in the same rank and order when compared to the absolute difference measure while having smaller database space storage requirements and faster search times. The one-dimensional Fourier transform amplitude, and amplitude and phase difference, matching techniques showed much lower times to generate a database of candidate curves when compared to the two-dimensional Fourier transforms and moments. The one-dimensional amplitude, and amplitude and phase difference, showed the overall best performance. Appendix A details performance of these two methods with a variety of trace point paths.

Table 7.20: Performance of various methods to generate 145 solutions and to search and identify similar solutions

Top Ranked File No.	Time to Generate 145 Files (sec)	Time to Search 145 Files (sec)	FLOPS to Search 145 Files
SAD	260	5.52	133447
SSS	260	5.48	114887
F1C	275	1.57	113868
F1P	275	1.55	1125442
F1SP	275	1.62	1252133
F1A	275	5.48	267309
F1AP	275	5.46	267309
F2C	2202	10.64	207808187
F2P	2202	10.72	208068283
F2SP	2202	20.89	251050075
MCC	2100	1.55	10051
MPD	2100	1.53	6427

CHAPTER 8. MOTION GENERATION

Motion generation is where the functional requirements are the output path of a trace point and angle of the connecting rod. The trace point is rigidly fixed to the connecting rod and the change in angle of the connecting rod is defined by the relative angle change of the connecting rod. The path and angle are typically viewed as the output function with the input function being the input position, velocity and/or acceleration of the drive crank.

Figure 8.1 is the normalized two dimensional plot of the trace point path for the defined example crank-rocker, four-bar mechanism. The trace point path is normalized for translation, rotation and scale in the same manner as outlined in Chapter 7.

Figure 8.2 is the plot of the connecting rod angle. The connecting rod angle has been normalized for the average value of the angle through the entire cycle of the path. The connecting rod angle is not normalized with respect to phase as the angle is based upon the path position. The angular displacement in the connecting rod angle is not dependent on the initial drive crank position or a defined reference line. The relative change in the connecting rod angle will not vary based upon the location,

rotation or scale of the mechanism or the starting point of the drive crank. As a result, the connecting rod angle is not normalized in the same manner as the output angle for the follower crank for function generation (see Chapter 6).

Figure 8.3 is a three dimensional plot of the output motion for the example crank-rocker, four-bar mechanism. The trace point path is laid out in the x-y plane and the normalized connecting rod angle is plotted in radians on the z-axis. In this form the output motion of the four-bar mechanism is in a form that a two-dimensional Fourier transform may be taken of the image. Figure 8.4 shows the two-dimensional Fourier transform of the trace point path. Figure 8.5 show the Fourier transform of the trace point path when the connecting rod angle is placed on the z-axis of the trace point path (Figure 8.3).

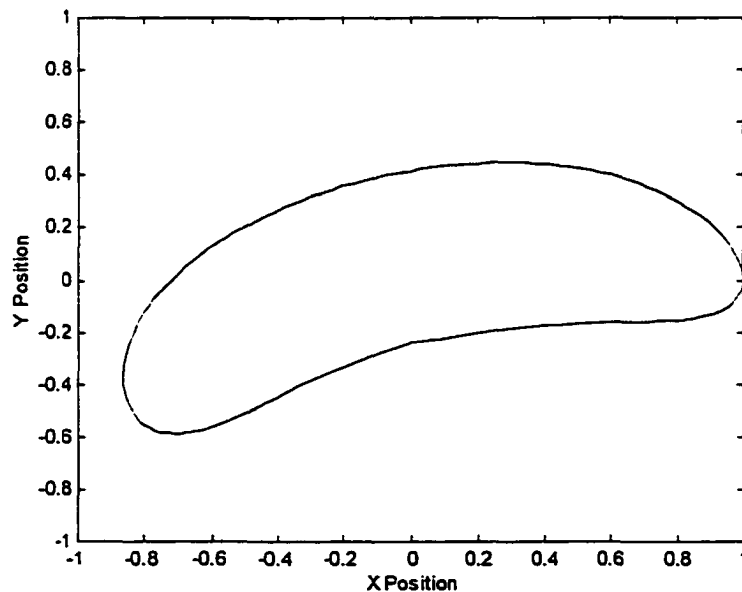


Figure 8.1 Two dimensional plot of the trace point path

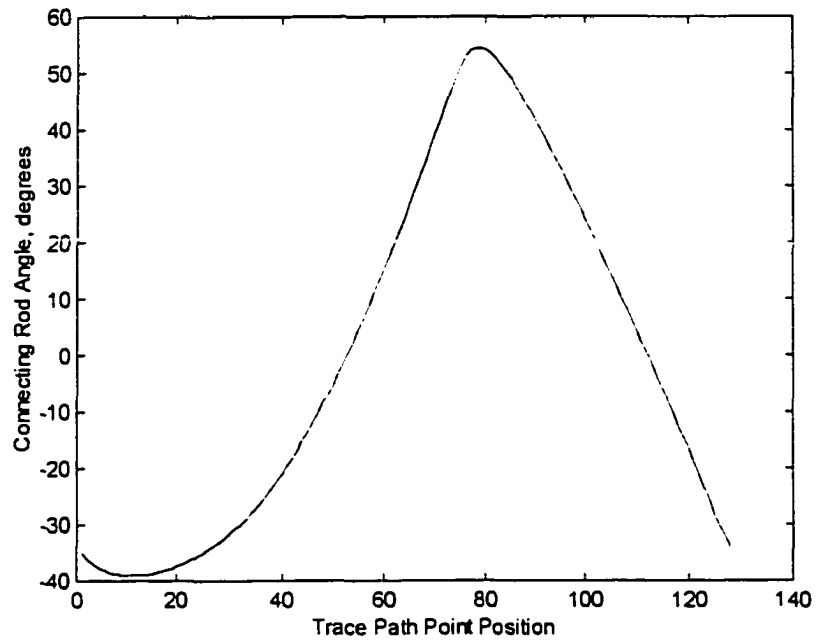


Figure 8.2 Normalized plot of the connecting rod relative angle

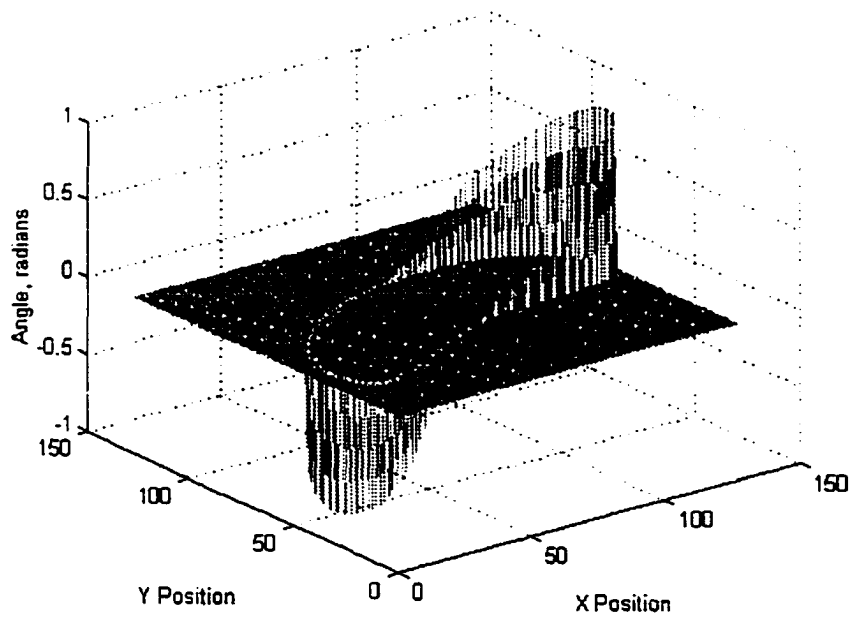


Figure 8.3 Three dimensional plot of the trace point path and connecting rod angle for the example crank-rocker

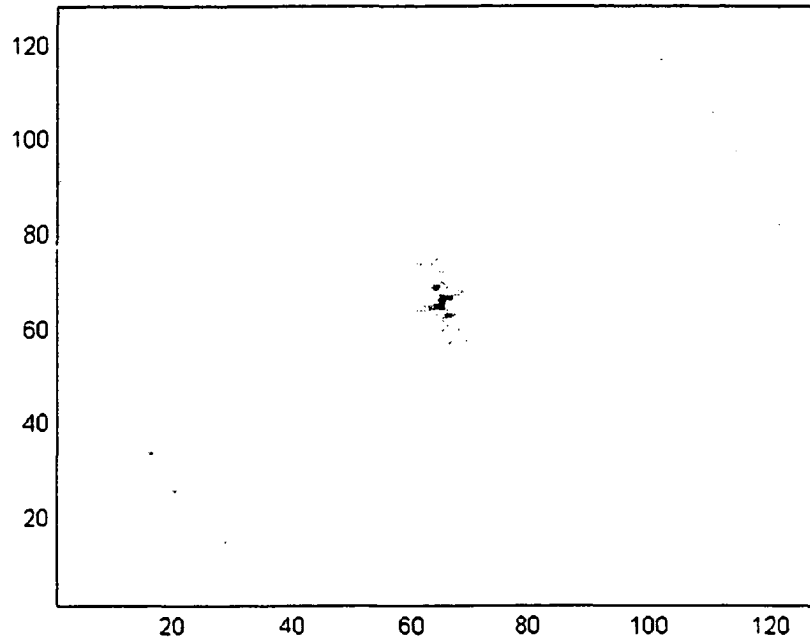


Figure 8.4: Two-Dimensional Fourier transform of trace point path

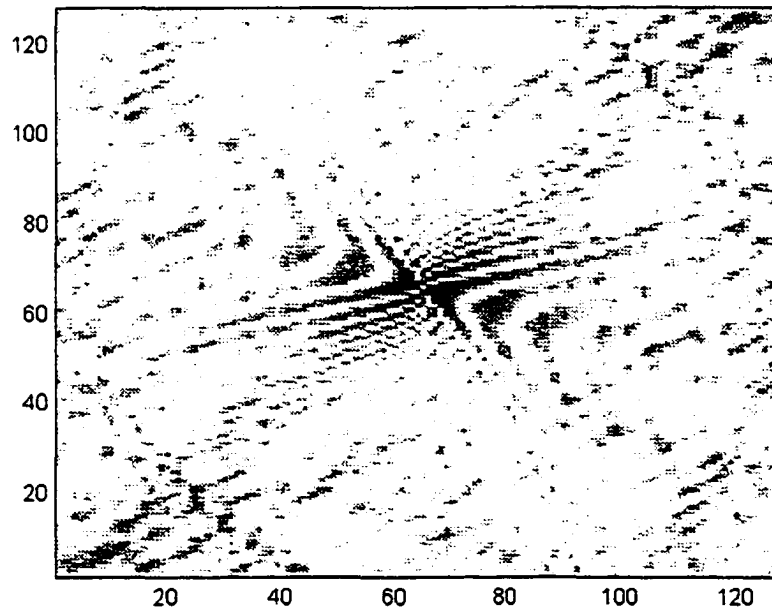


Figure 8.5: Two-Dimensional Fourier transform of trace point path and connecting rod angle

The output path and the output motion must be evaluated to develop a similarity expression between motion generation four-bar mechanisms. A desired curve was selected to search the database and to evaluate performance of each of the following solution matching measures. The desired curve was the same as previously defined on page 166 and was stored as the third numbered database four-bar mechanism. The graph of the normalized trace point path and angle is found in Figure 8.6. The desired path was compared with each of the database mechanisms and evaluated with the following matching measures:

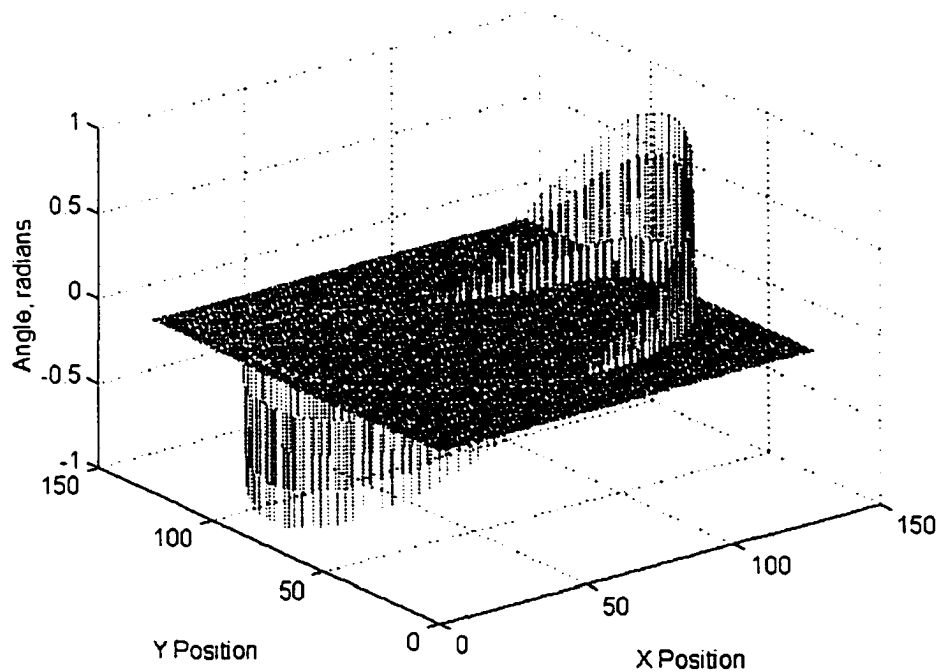


Figure 8.6: Normalized plot of desired motion

- Sum of absolute difference
- Amplitude and phase difference using Fourier descriptors
- Symmetric phase-only matched filter using two-dimensional Fourier descriptors

Sum of Absolute Differences

The sum of the absolute difference when used with the trace point path is defined by:

$$A_p = \sum \{ [(f_x - g_x)^2 + [(f_y - g_y)^2]^{0.5} \} \quad [8.1]$$

The sum of the absolute difference when used with the connecting rod angle is defined by:

$$A_a = \sum | f_\theta - g_\theta | \quad [8.2]$$

The overall scale for the trace point path and the connecting rod angle are not the same. As a result, a weight factor may be applied to each of the correlation values to address the overall influence that each correlation may have to the overall similarity measure. An overall measure may be evaluated by the following:

$$A_t = p \cdot A_p + q \cdot A_a \quad [8.3]$$

Where:

A_t = Total absolute difference measure

A_p = Absolute difference measure of trace point path

A_a = Absolute difference measure of connecting rod angle

p, q = Weighting factor where $p + q = 1.0$

For evaluating the motion of the desired four-bar mechanism, the weighting factors were each given values of: $p = 0.7$, $q = 0.3$ (See Appendix B). If p is equal to one the expression reduces to a path generation process. If q is equal to one the expression reduces to a function generation process. The configuration of the four-bar mechanism taken for the desired motion is defined on page 165 (file number 3).

Figure 8.7 is a graph of the absolute difference measure of the desired trace point motion with the 145 database functions. The top 5 matching trace point paths are plotted in Figure 8.8. The top 5 matching connecting rod angles are plotted in Figure 8.9. The 15 database trace point motion which had the smallest absolute differences values are listed in Table 8.1. The absolute difference function defined above identified the functions that matched point by point most closely with the desired function. The database search took 8.86 seconds of CPU time and 171292 FLOPS.

Amplitude and Phase Difference of Fourier Descriptors

For evaluating the amplitude and phase difference using Fourier descriptors, equation 7.15 was used to evaluate the

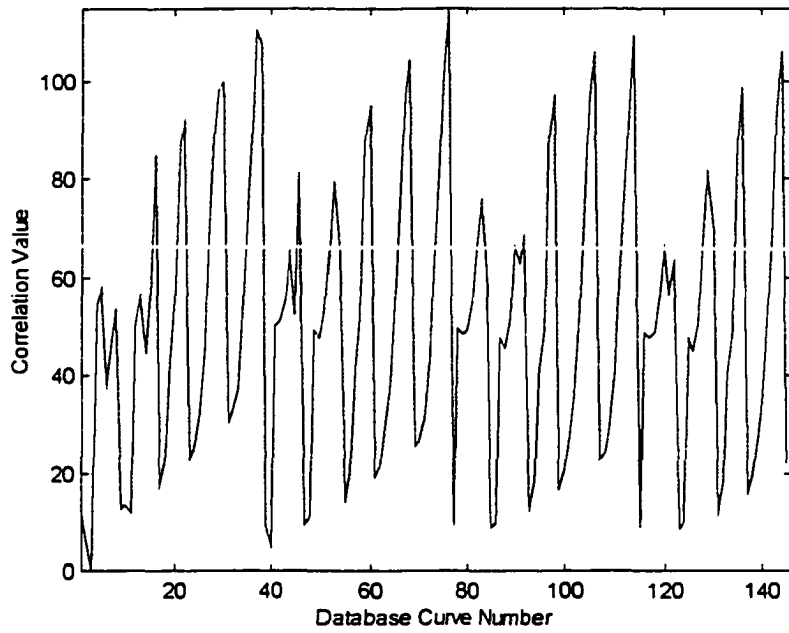


Figure 8.7: Graph of absolute difference of desired motion with 145 database candidate solutions

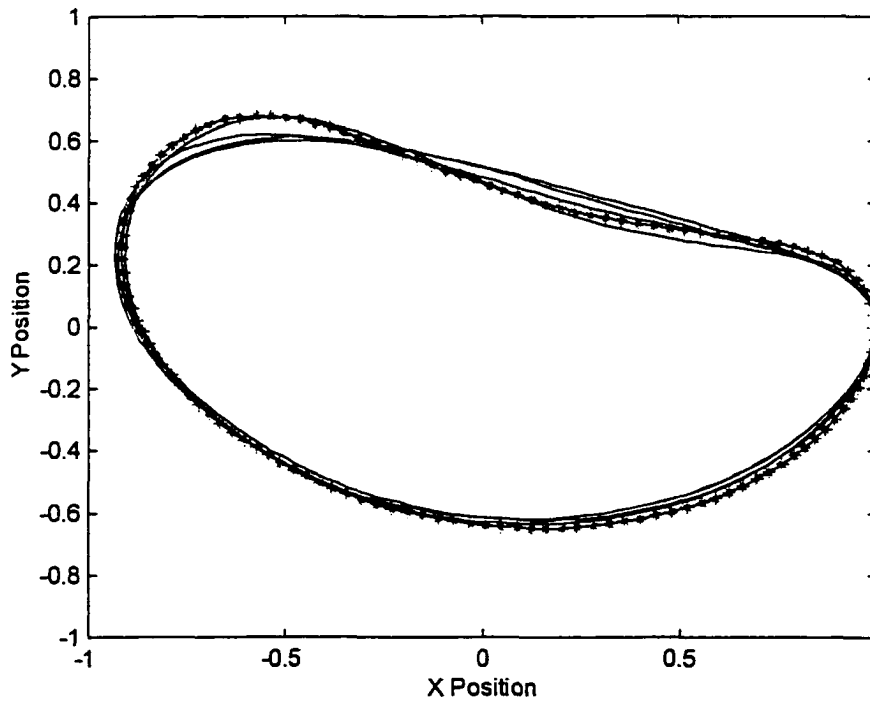


Figure 8.8: Graph of the top 5 filed trace point paths identified by absolute difference (motion generation)

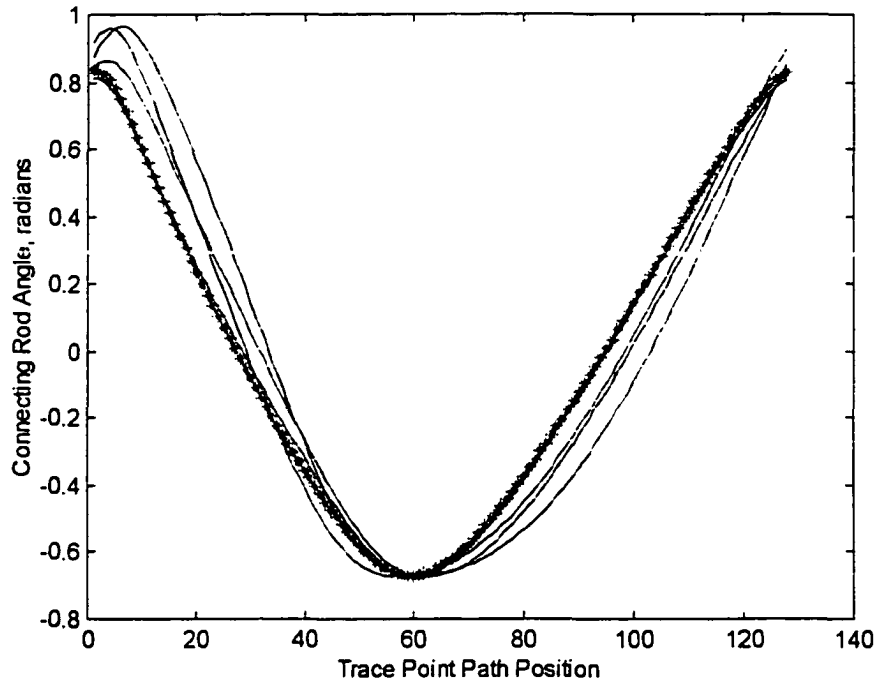


Figure 8.9: Graph of the top 5 filed connecting rod angle identified by absolute difference (motion generation)

Table 8.1: Summary of database search using absolute difference

Desired Curve - Database Curve #3

Search Rank	Database Curve Number	Absolute Difference Value
1	3	0.0000
2	40	4.6490
3	2	5.1333
4	123	8.3977
5	85	8.6192
6	115	8.6804
7	77	8.8434
8	39	8.8927
9	47	9.2172
10	124	9.7638
11	86	9.8140
12	48	11.1558
13	1	11.5304
14	11	11.7555
15	131	11.8905

difference measure for the desired trace point path and connecting rod angle with each of the database solutions. The value used for n was 0.3 for each difference measure.

An overall measure may be evaluated by the following:

$$AP_t = p_{AP} * AP_p + q_{AP} * AP_a \quad [8.4]$$

Where:

AP_t = Total amplitude and phase difference measure

AP_p = Amplitude and Phase difference measure of trace point path

AP_a = Amplitude and Phase difference measure of connecting rod angle

p_{AP}, q_{AP} = Weighting factor where $p_{AP} + q_{AP} = 1.0$

For evaluating the motion of the desired four-bar mechanism, the weighting factors were each assigned a values of: $p_{AP} = 0.6$ and $q_{AP} = 0.4$ (See Appendix B).

Figure 8.10 is a graph of the absolute difference measure of the desired trace point motion with the 145 database candidate solutions. The top 5 database candidates were identified: the trace point paths are plotted in Figure 8.11 and the connecting rod angles are plotted in Figure 8.12. The 15 database solutions which had the smallest absolute differences values are listed in Table 8.2. The absolute difference function defined above identified the motions that matched point by point most closely with the desired solution. The database search took 6.23 seconds of CPU time and 267454 FLOPS.

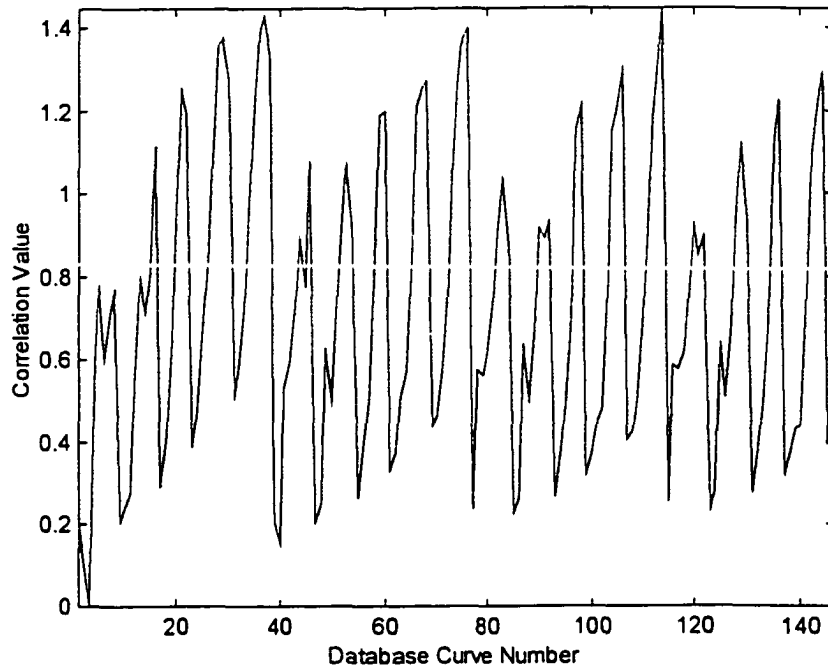


Figure 8.10: Graph of amplitude and phase difference of desired motion with 145 database candidate solutions

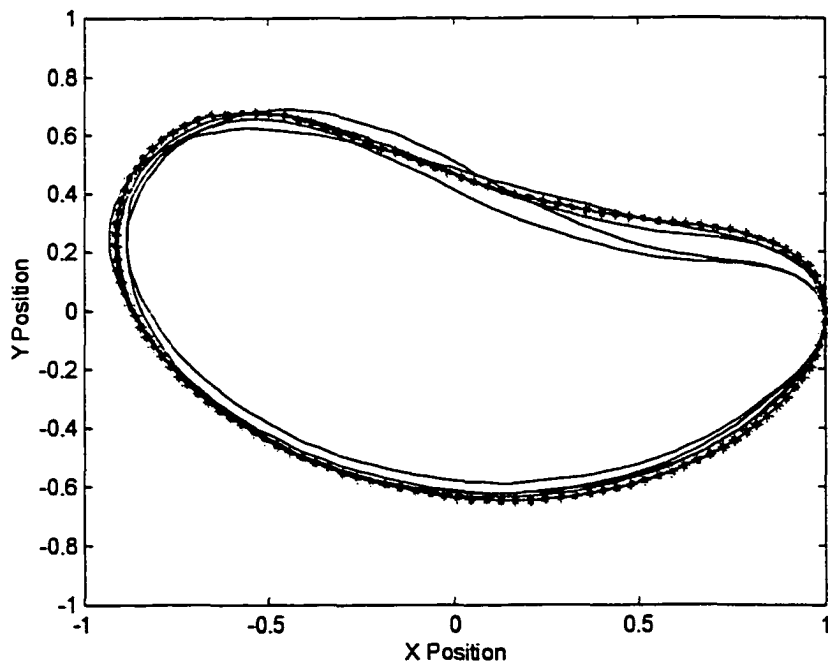


Figure 8.11: Graph of the top 5 filed trace point paths identified by amplitude and phase difference (motion generation)

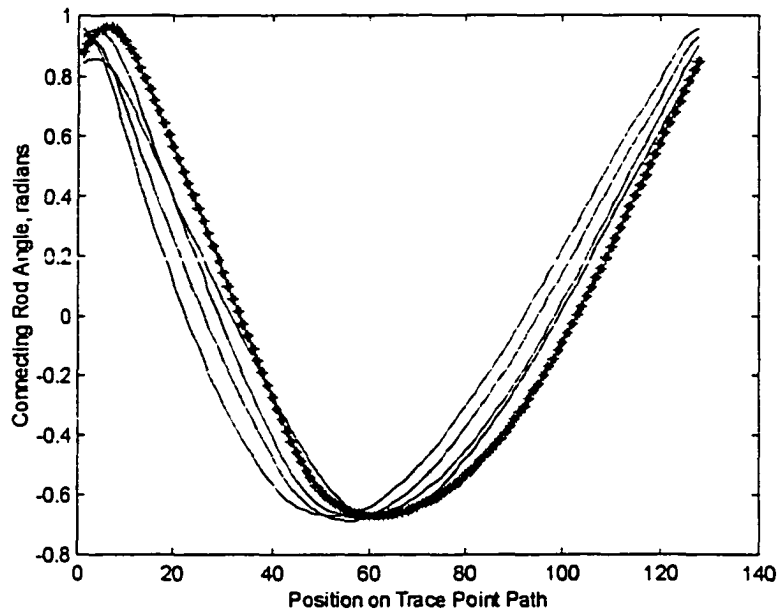


Figure 8.12: Graph of the top 5 filed connecting rod angle identified by amplitude and phase difference of Fourier descriptors

Table 8.2: Summary of database search using amplitude and phase difference of Fourier descriptors

Desired Curve - Database Curve #3

Search Rank	Database Curve Number	Amplitude and Phase Difference
1	3	0.0000
2	2	0.0845
3	40	0.1500
4	1	0.2004
5	9	0.2030
6	47	0.2035
7	39	0.2045
8	85	0.2245
9	77	0.2339
10	123	0.2366
11	10	0.2369
12	48	0.2489
13	115	0.2496
14	55	0.2621
15	86	0.2640

Symmetric Phase-Only Matched Filter

Symmetric phase-only matched filtering using two-dimensional Fourier transforms was shown to be the effect in matching a desired solution with a candidate solution with path generation. The trace point path is laid out in the x-y plane and the normalized connecting rod angle is plotted in radians on the z-axis (Figure 8.3). A two-dimensional Fourier transform of the trace point path and the connecting rod angle is then generated. The top 16 Fourier coefficients are retained and stored in the database for each candidate solution. When a symmetric phase-only matched filter when comparing a desired motion with each of the database candidate solutions, the maximum value of the resulting correlation is retain. The correlation value of a perfect match will have a value of 1.0.

This type of database search does not require weighting factors be applied to the trace point path difference and the connecting rod angle difference as was implemented with the absolute difference measure and the amplitude and phase difference of the one-dimensional Fourier descriptors. Information regarding both the connecting rod angle and the trace point path are contained in the two-dimensional Fourier transform.

Figure 8.13 is a graph of the symmetric phase-only matched filter correlation of the desired trace point motion with the 145 database solutions. The top 5 database candidates were identified: the trace point paths are plotted in Figure 8.14 and the connecting rod angles are plotted in Figure 8.15.

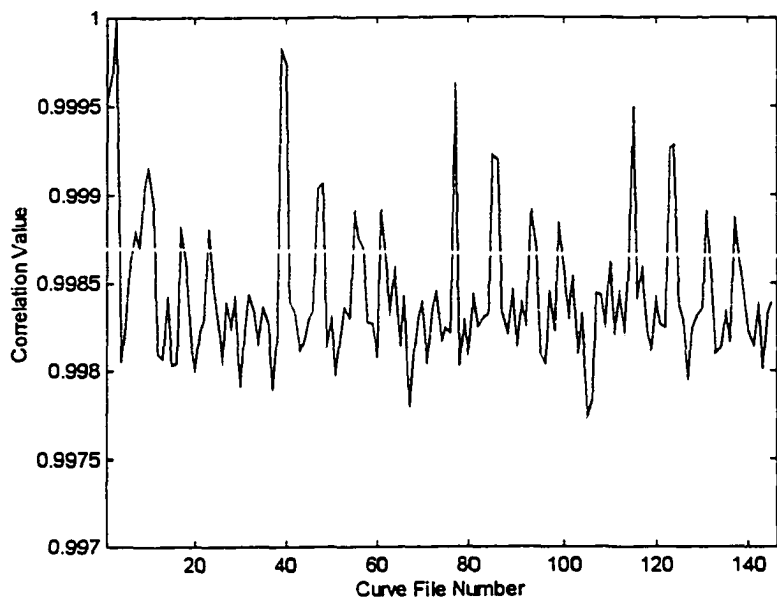


Figure 8.13: Graph of symmetric phase only filter correlation of desired motion with 145 database candidate solutions

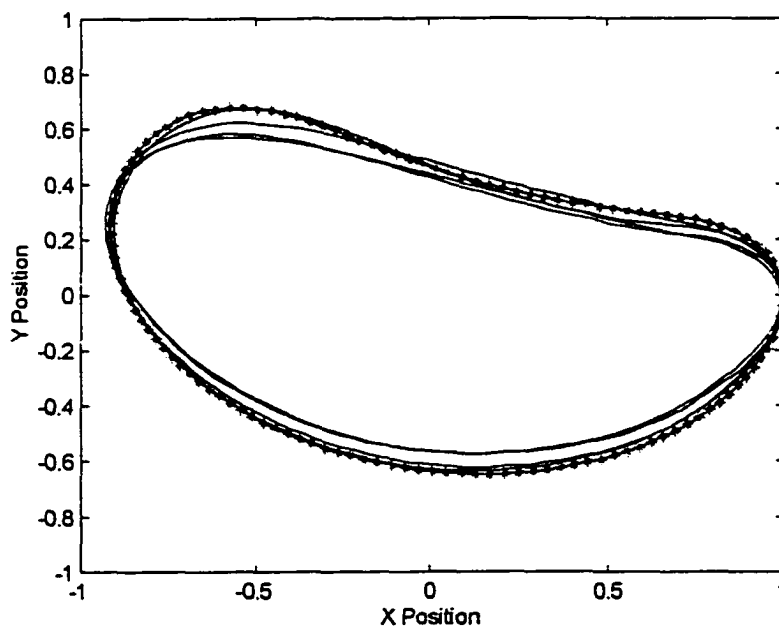


Figure 8.14: Graph of the top 5 filed trace point paths identified by symmetric phase only filter (motion generation)

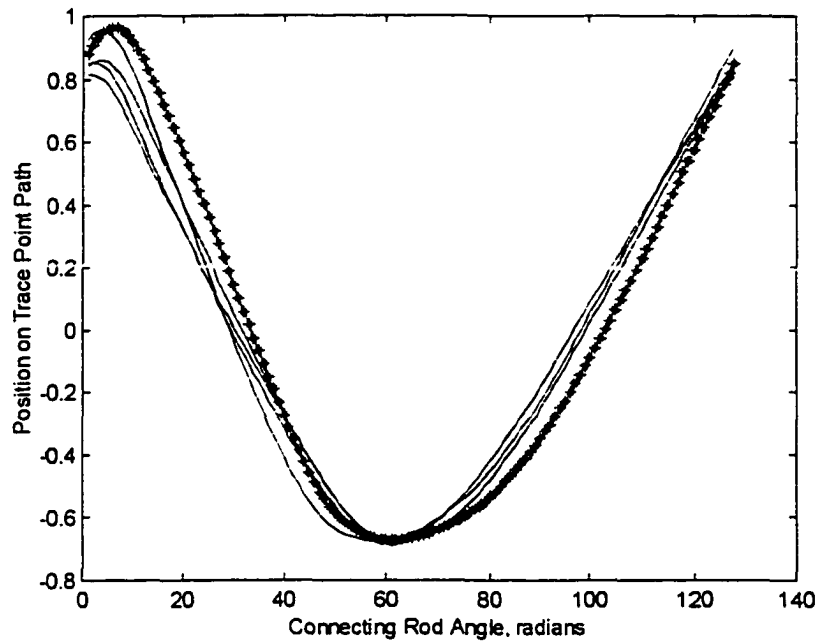


Figure 8.15: Graph of the top 5 filed connecting rod angle identified by symmetric phase only filter (motion generation)

Table 8.3: Summary of database search using symmetric phase only matched filtering

Desired Curve - Database Curve #3

Search Rank	Database Curve Number	Correlation Value
1	3	1.0000
2	39	0.9998
3	40	0.9997
4	2	0.9997
5	77	0.9996
6	1	0.9995
7	115	0.9995
8	124	0.9993
9	123	0.9993
10	85	0.9992
11	86	0.9992
12	10	0.9992
13	48	0.9991
14	9	0.9990
15	47	0.9990

The 15 database functions which had the highest correlation values are listed in Table 8.3. The database search took 20.63 seconds of CPU time and 251050075 FLOPS.

Partial Curves

A complete rotation of the drive crank and the resulting trace point motion has been evaluated for motion generation four-bar mechanisms. The trace point path and angle have been closed curves and is applicable only to four-bar mechanisms where the drive crank rotates through a complete 360 degrees. Once again, to consider a crank-rocker, a double-crank, or a double-rocker, four bar mechanism that only rotates through a specified angle, a different methodology is required to characterize the output path.

As with function and path generation, consider the example four-bar mechanism where the drive crank only rotates from an angle of 0 degrees to 90 degrees. Figure 8.16 is a graph of the trace point motion. Compare this trace point motion to that of Figure 8.1.

The trace point motion and its relationship to the drive crank angle is not of interest when searching for trace point motions stored in a database. As a result the trace point motion is sampled from one end of the path, end point "A", to the other end of the path, end point "B" in equal segments. The trace point motion is then sampled from end point "B" back to end point "A" in equal steps. This generates a series of x and y coordinates that are cyclic. A total of 128 discrete points were used to sample the complete trace point motion. This process generated a series

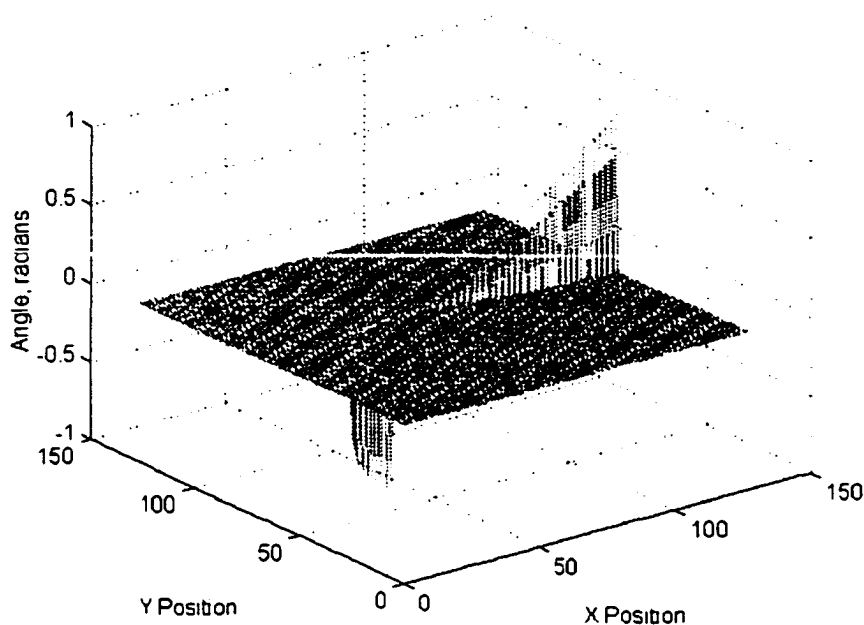


Figure 8.16: Three-dimensional plot of the trace point motion

of points that may be normalized for translation, rotation, scale, and discrete point distribution in the same manner as the closed trace point motion.

Figure 8.17 is a graph of the trace point motion normalized for position, rotation, scale, and discrete point distribution. Note that while there are only 64 discrete points that may be visually identified on the trace point path, there are actually 128 discrete points used in the definition of the path. A database of 7,475 trace point paths was generated with the configurations described earlier in this chapter. The drive crank angle was a minimum of 0 degrees and a maximum of 90 degrees. The database structure and information stored is the same as with the

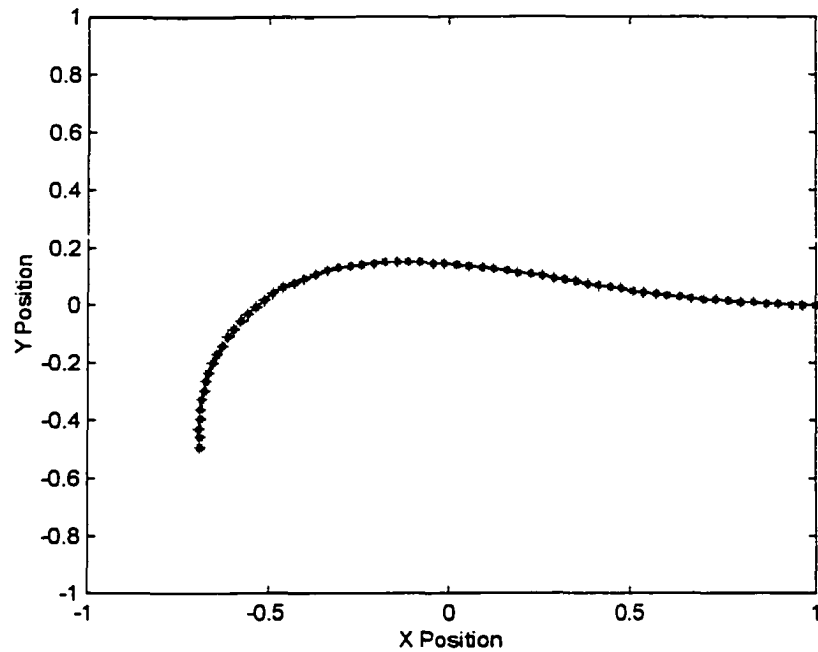


Figure 8.17: Normalized trace point path

crank rocker with full drive crank motion. A desired curve was selected as the third numbered database curve and the configuration is the same as defined on page 165.

The desired curve was compared with each of the first 150 database curves and evaluated with the following matching techniques:

- Sum of absolute differences
- Fourier descriptor amplitude and phase difference measure
- Two-dimensional Fourier descriptors with symmetric phase only matched filtering.

Partial Curves - Sum of Absolute Differences

The sum of absolute differences is a difference measure and is defined by equation 8.3. The starting point for evaluating the absolute difference is always at the point on the curve that lies on the X-axis and has a x and y value of 1.0 and 0.0 respectively. Figure 8.18 is a graph of the absolute difference of the partial trace point motion with the 145 database candidate solutions. The 15 database partial trace point paths that had the smallest absolute difference values are listed in Table 8.4. The top 5 database candidates were identified: the partial trace point paths are plotted in Figure 8.19 and the connecting rod angles are plotted in Figure 8.20. The database search took 8.47 seconds of CPU time and 171292 FLOPS.

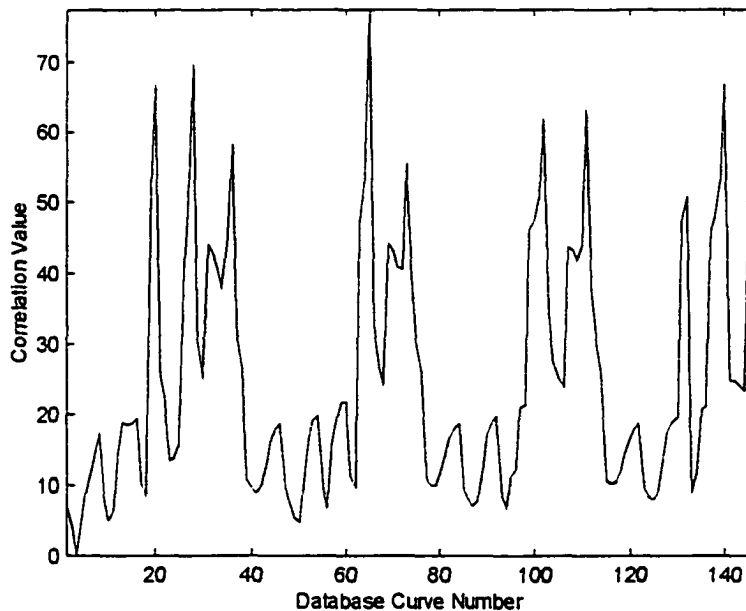


Figure 8.18: Graph of absolute difference of partial curve motion with 145 database candidate solutions

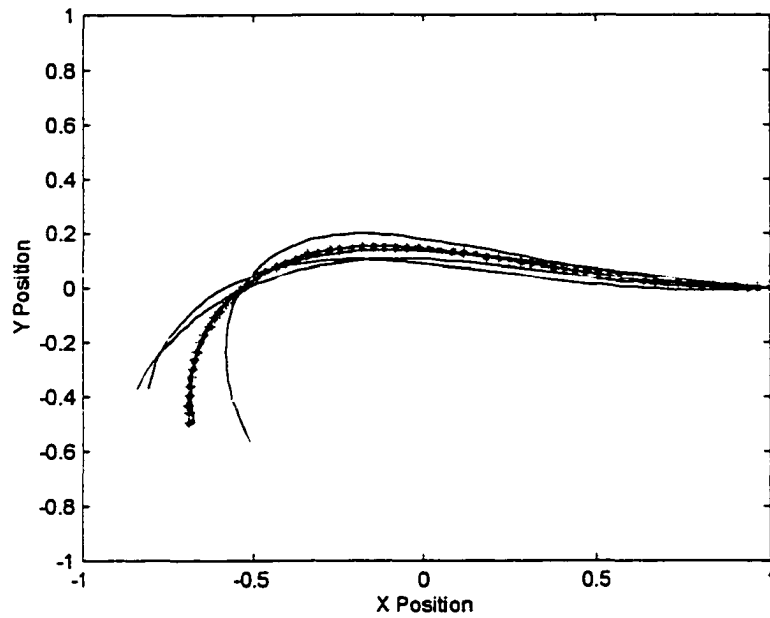


Figure 8.19: Graph of the top 5 database trace point paths identified by absolute difference

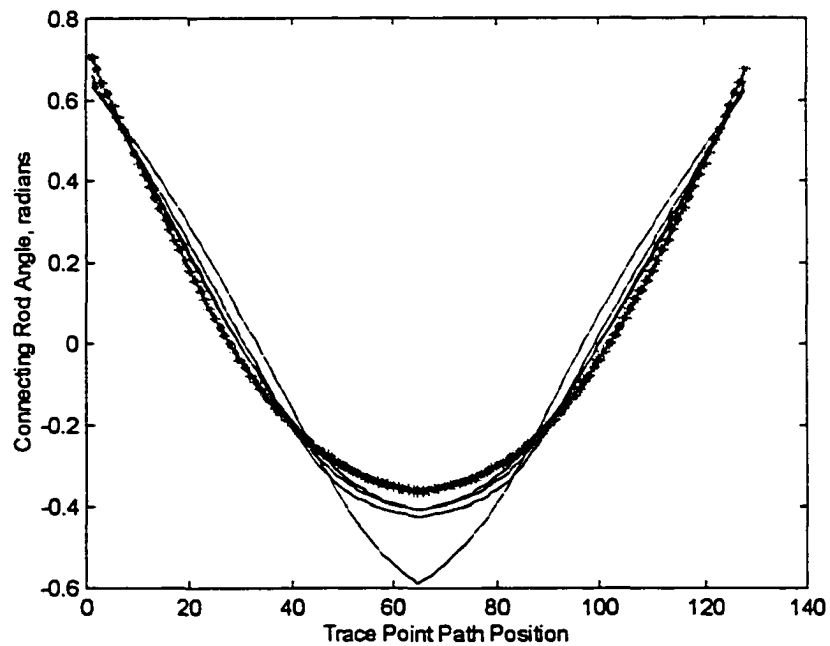


Figure 8.20: Graph of the top 5 database connecting rod angle identified by absolute difference (motion generation)

Table 8.4: Summary of database search of trace point paths using absolute difference

Desired Curve - Database Curve #3

Search Rank	Database Curve Number	Absolute Difference Value
1	3	0.0000
2	50	3.3613
3	10	5.3301
4	2	5.4727
5	49	5.5905
6	4	5.6992
7	88	6.9226
8	11	7.1162
9	87	7.3730
10	125	8.2644
11	56	8.2936
12	94	8.4384
13	126	8.5693
14	18	8.7384
15	48	8.8194

Partial Curves - Amplitude and Phase Difference of Fourier Descriptors

The difference of the magnitude and phase of the Fourier descriptors is defined by the equation 7.15. The equation was used for both analysis of the path and the angle. The value used for "n" was 0.3. Figure 8.21 is a graph of the Fourier descriptor amplitude and phase difference of the desired partial trace point motion with the 145 database solutions. The 15 database candidates that had the smallest correlation values are listed in Table 8.5. The top 5 database candidates were identified: the partial trace point paths are plotted in Figure 8.22 and the connecting rod angles are plotted in Figure 8.23. The database search took 6.44 seconds of CPU time and 267614 FLOPS.

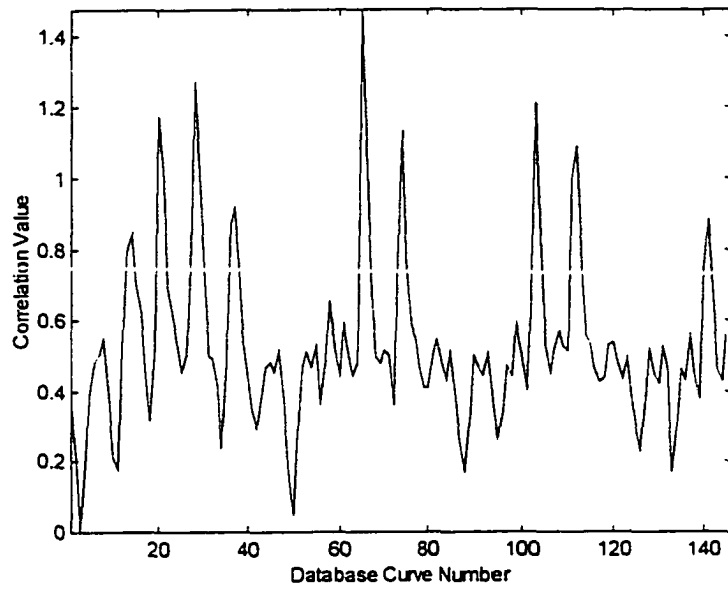


Figure 8.21: Graph of amplitude and phase difference of partial curve motion with 145 database candidate solutions

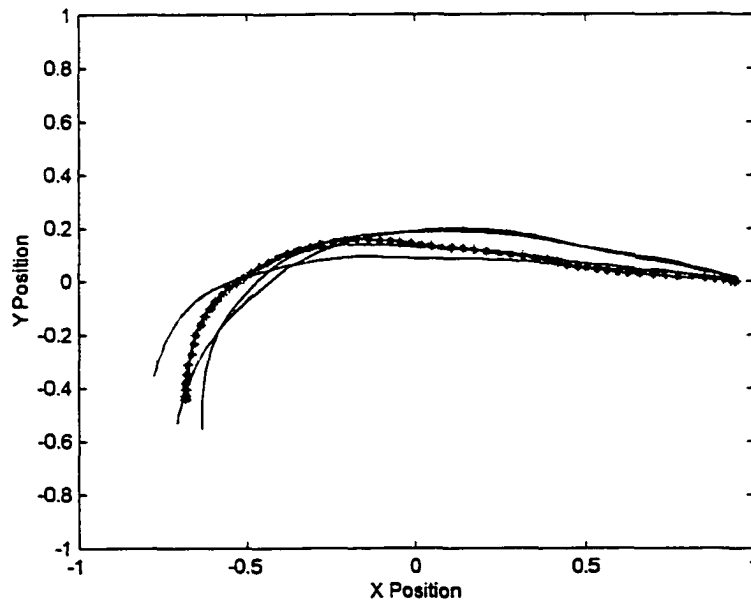


Figure 8.22: Graph of top 5 partial trace point paths identified using amplitude and phase difference of Fourier descriptors

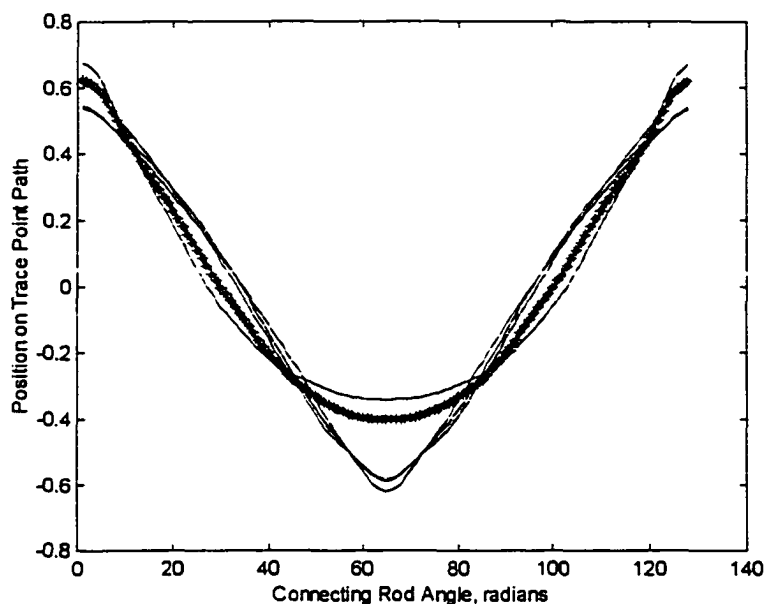


Figure 8.23: Graph of the top 5 database connecting rod angle identified using amplitude and phase difference measure

Table 8.5: Summary of database search of partial trace point paths using amplitude and phase difference

Desired Curve - Database Curve #3

Search Rank	Database Curve Number	Amplitude and Phase Difference
1	3	0.0000
2	50	0.1009
3	2	0.1360
4	4	0.1426
5	11	0.1489
6	49	0.1616
7	10	0.1629
8	133	0.1718
9	88	0.1808
10	126	0.2097
11	87	0.2281
12	1	0.2316
13	95	0.2352
14	125	0.2370
15	94	0.2492

Partial Curves - Symmetric Phase-Only Matched Filter

Two-dimensional symmetric phase-only matched filtering in the Fourier frequency domain is evaluated by taking the maximum of equation 7.15. Figure 8.24 is a graph of the symmetric phase-only filter correlation of the desired motion with the 145 database candidate solutions. The 15 database candidates that had the largest correlation values are listed in Table 8.6. The top 5 database candidates were identified: the matching database partial trace point paths are plotted in Figure 8.25, and the connecting rod angles in Figure 8.26. The database search took 20.55 seconds of CPU time and 251,050,075 FLOPS.

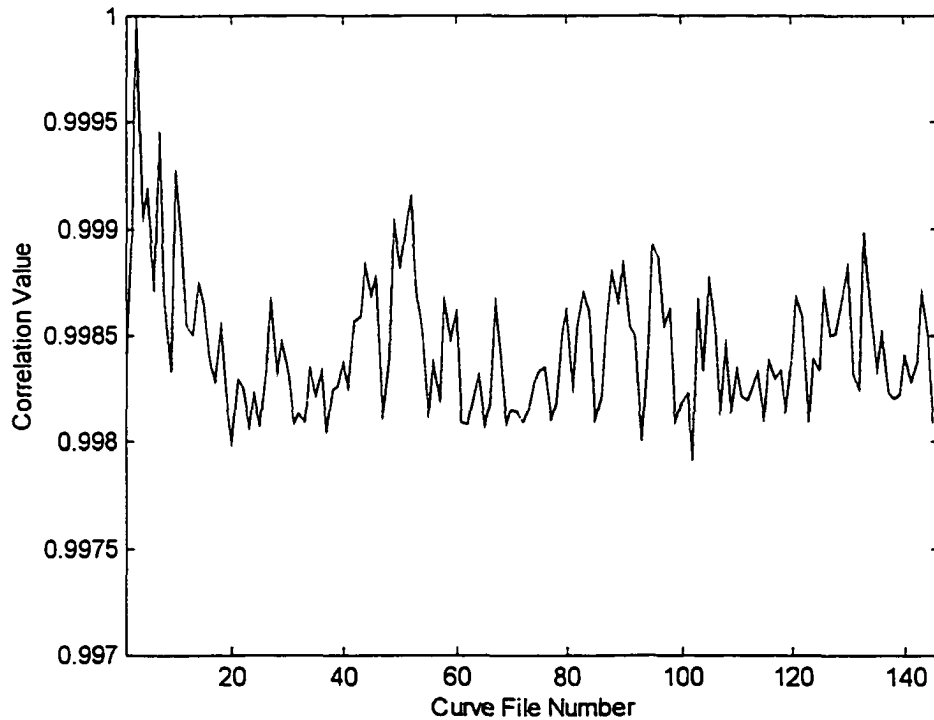


Figure 8.24: Graph of Fourier two-dimensional symmetric phase only matched filter correlation of partial curve motion with 145 database candidate solutions

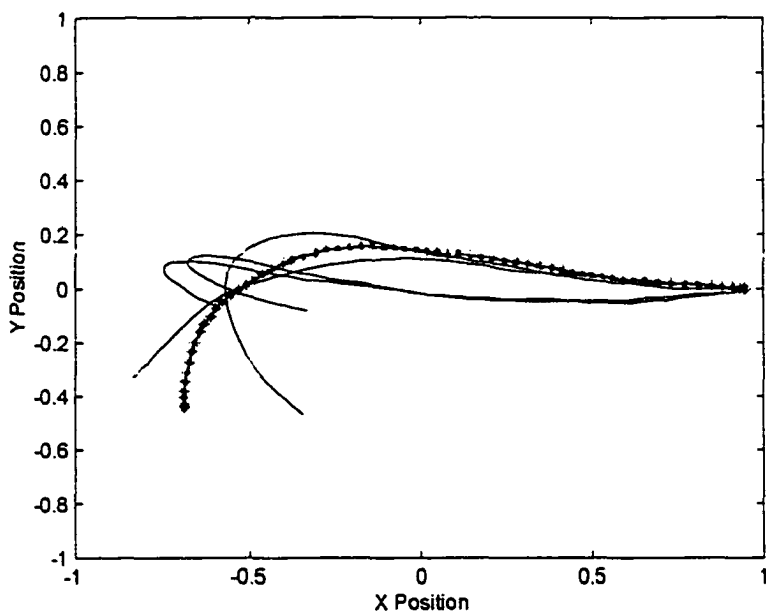


Figure 8.25: Graph of the top 5 database partial trace point paths identified using symmetric phase only matched filter

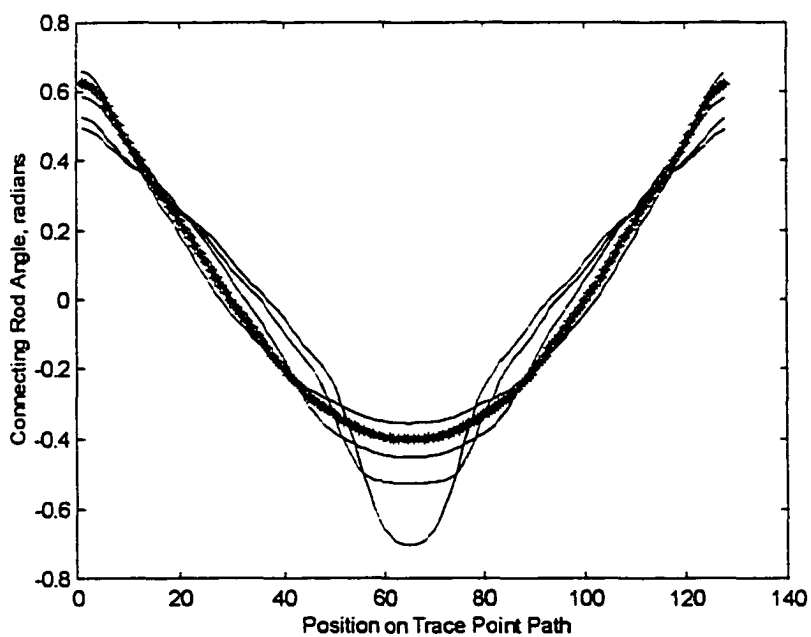


Figure 8.26: Graph of the top 5 database connecting rod angle identified by symmetric phase only filter (motion generation)

Table 8.6: Summary of database search of partial trace point paths using symmetric phase only matched filter

Desired Curve - Database Curve #3

Search Rank	Database Curve Number	Correlation Value
1	3	1.0000
2	7	0.9995
3	10	0.9993
4	5	0.9992
5	52	0.9991
6	4	0.9991
7	49	0.9990
8	133	0.9990
9	2	0.9990
10	51	0.9990
11	11	0.9989
12	95	0.9989
13	96	0.9989
14	90	0.9988
15	44	0.9988

Summary

A comparison of the various techniques for the use of invariant characterization, storage and search methods for motion generation of four-bar mechanisms was developed. Tables 8.7 and 8.8 are summaries of the top ten database solutions identified when using file number 3 as a desired solution. Entries in Table 8.7 and 8.8 are bold if the identified solutions are in the top 10 trace point motions identified and match one of the top 10 solutions identified by the absolute difference measure. The absolute difference measure is used as a benchmark. Entries in Table 8.7 and 8.8 are underlined if the identified solution are in

the top 5 solutions identified by the absolute difference measure. Table 8.9 is a summary of the time to search and compare a desired solution with 145 database curves and the number of FLOPS to run the various search methods. The following are the various file search methods:

SAD - Spatial transform, sum of absolute difference

F1AP - One-dimensional Fourier descriptors, amplitude and phase difference measure

F2SF - Two-dimensional Fourier descriptors, symmetric phase-only matched filter

For full drive crank rotation, the amplitude and phase difference of Fourier descriptors and two-dimensional symmetric phase-only matched filtering showed good performance in identifying database motion generation solutions with a desired solution. For symmetric phase-only matched filtering, three of the top five solutions were the same as with the absolute difference measure. Eight of the top ten solutions were the same as with the absolute difference measure. For amplitude and phase difference, three of the top five solutions were the same as the absolute difference measure and eight of the top ten were the same.

For partial drive crank rotation, the amplitude and phase difference of Fourier descriptors was the measure of similarity that identified database trace point motion generation solutions with a desired solution that correlated most closely to the spatial absolute difference measure. For amplitude and phase

difference, three of the top five solutions were the same as the absolute difference measure and eight of the top ten were the same.

Database file space, time to generate solutions to be stored in a database and time to search the database were similar to previous results.

Table 8.7: Performance of various methods to measure the similarity of a desired solution to 145 filed solutions - full drive crank rotation

Top Ranked File No.	1	2	3	4	5	6	7	8	9	10
SAD	<u>3</u>	<u>40</u>	<u>2</u>	<u>123</u>	<u>85</u>	115	77	39	47	124
F1AD	<u>3</u>	<u>2</u>	<u>40</u>	1	9	47	39	85	77	123
F2SF	<u>3</u>	39	<u>40</u>	<u>2</u>	77	1	115	124	85	86

Table 8.8: Performance of various methods to measure the similarity of a desired solution to 145 filed solutions - partial drive crank rotation

Top Ranked File No.	1	2	3	4	5	6	7	8	9	10
SAD	<u>3</u>	<u>50</u>	<u>10</u>	<u>2</u>	<u>49</u>	4	88	11	87	125
F1AD	<u>3</u>	<u>50</u>	<u>2</u>	4	11	49	10	133	88	126
F2SF	<u>3</u>	7	<u>10</u>	5	52	4	49	133	2	51

Table 8.9: Performance of various methods to generate 145 solutions and to search and identify similar solutions

Top Ranked File No.	Time to Generate 145 Files (sec)	Time to Search 145 Files (sec)	FLOPS to Search 145 Files
SAD	260	7.67	171292
F1AP	275	9.80	267454
F2SP	2202	20.63	251050075

CHAPTER 9. DESIRED SOLUTION GENERATION

A framework has been established to store, search and match invariant characteristics of four-bar mechanisms for function, path and motion generation. A method is required to allow a designer to define the function, path or motion of a desired solution so that a database of solutions may be searched. The use of precision points are used in many of the synthesis methods for four-bar mechanisms but the number of points are limited based on the type of synthesis selected. The number of points used to represent a desired solution may range from two, representing a straight line, to as many as may be required to adequately define a solution.

There are many methods to create curves based on the specification of precision points. In geometric modeling the most common form of curve representation has been a parametric form due to its ease of programming and computation [Anand, 1993]. The parametric representation of a three dimensional curve which may be applied for function, path or motion generation of four-bar mechanisms is:

$$x = x(t) \quad [9.1]$$

$$y = y(t) \quad [9.2]$$

$$z = z(t) \quad [9.3]$$

Where:

$$t = \text{Parametric variable, } 0 \leq t \leq 1$$

All functions of the parameter t are polynomials and describe a curve directly. Some techniques for finding an arbitrary curve that fit a set of data points include the Lagrange polynomial, parametric cubic curve, cubic splines, Bezier curves and B-splines.

The Lagrange polynomial has a degree of polynomial that is related to the number of precision points used to define the curve. An attribute with the Lagrange polynomial is that the curve oscillates about the defined precision points. In addition, as the number of points is increased, the polynomial generated is of a higher degree. This typically results in a curve with excessive oscillations between the precision points.

Parametric Cubic Curve

A parametric cubic curve is defined as:

$$P(t) = \sum_{i=1}^3 a_i t^i \quad 0 \leq t \leq 1 \quad [9.4]$$

Where:

$P(t)$ = Points on the curve

t = Parametric variable, $0 \leq t \leq 1$

Separating the equation into the three components of $P(t)$ results in:

$$x(t) = a_{3x}t^3 + a_{2x}t^2 + a_{1x}t + a_{0x} \quad [9.5]$$

$$y(t) = a_{3y}t^3 + a_{2y}t^2 + a_{1y}t + a_{0y} \quad [9.6]$$

$$z(t) = a_{3z}t^3 + a_{2z}t^2 + a_{1z}t + a_{0z} \quad [9.7]$$

Boundary conditions are required to permit the twelve unknown coefficients a_{ij} to be evaluated. The boundary conditions relate to specific geometric constraints of the curve. Assuming that the solution curve is specified by the designer in a fashion where the sequence of the precision points is known, then two precision points may be sequentially interpolated segment by segment. This provides six of the twelve boundary conditions needed to evaluate a_{ij} .

Additional boundary conditions may be established by imposing geometric requirements on the curve. Parametric continuity is one method of imposing geometric constraints. No parametric continuity is where two line segments are discontinuous and do not meet at an endpoint. A parametric continuity of C^0 is where two line segments meet at a precision point, but do not have the same slope. Parametric continuity of C^0 essentially ensures there are no gaps in a curve. A parametric continuity of C^1 is where two

line segments meet at a precision point and both line segments have the same slope at the precision point. A parametric continuity of C^2 is where two line segments meet at a precision point and the second derivative of each line segment at the precision point are equal. A parametric cubic curve has a C^3 level of continuity and each meeting line segment has the same tangent vector at a specific precision point. Requiring the slope of each line segment that terminates at a precision point to be equal places an additional three boundary conditions on the system of equations. Substituting $t = 0$ and $t = 1$ into the equation [9.4] results in:

$$P(0) = a_0 \quad [9.8]$$

$$P(1) = a_3 + a_2 + a_1 + a_0 \quad [9.9]$$

$$P'(0) = a_1 \quad [9.10]$$

$$P'(1) = 3a_3 + 2a_2 + a_1 \quad [9.11]$$

Solving for $P(t)$ results in:

$$P(t) = (2t^3 - 3t^2 + 1)P(0) + (-2t^3 + 3t^2)P(1) \quad [9.12]$$

$$+ (t^3 - 2t^2 + t)P'(0) + (t^3 - t^2)P'(1)$$

The polynomial coefficients are known as blending functions. By varying the parameter t from 0 to 1, points on the curve segment between two precision points are defined. This process of using endpoints and tangent vectors is one form of the Hermite interpolation.

In matrix form the parametric equation may be written:

$$P(t) = [t^3 \ t^2 \ t \ 1] \begin{bmatrix} 2 & -2 & 1 & 1 \\ -3 & 3 & -2 & -1 \\ 0 & 0 & 1 & 0 \\ 1 & 0 & 0 & 0 \end{bmatrix} \begin{bmatrix} P(0) \\ P(1) \\ P'(0) \\ P'(1) \end{bmatrix} \quad [9.13]$$

or

$$P(t) = [t][M]_H[G]_H \quad [9.14]$$

Where:

$[t]$ = Parametric variable matrix, $0 \leq t \leq 1$

$[M]_H$ = Hermite matrix

$[G]_H$ = Geometric coefficient matrix

Matrices $[t]$ and $[M]_H$ are used for any cubic curve, while $[G]_H$ is unique in specifying the geometric constraints of the position of the precision points and tangents at the precision points.

Cubic Spline Function

With a cubic spline function additional geometric constraints are placed on the system of equations by requiring a level of C^2 parametric continuity. The second derivative of each line segment that meets at a precision point is the same. This requirement establishes the following relationship:

$$P''_{i-1}(1) = P''_i(0) \quad [9.15]$$

Substituting this equation into the cubic polynomial equation 9.4 results in the following:

$$P'_{i-1} + 4P'_i + P'_{i+1} = 3(P_{i+1} - P_{i-1}) \quad [9.16]$$

This equation supports a solution for all segments that are internal to a curve, but does not support a solution for the end line segments. The development of curves for function, path and motion generation has assumed that all curves are cyclic closed curves. Therefore, an additional constraint on the system of equations to support a solution for the end line segments is the fact that the last line segment meets at the first precision point of the first line segment.

Solving the system of equations established by equation 9.16 results in the following matrix equation:

$$\begin{bmatrix} 4 & 1 & . & . & . & . & 0 & 1 \\ 1 & 4 & 1 & . & . & . & 0 & 0 \\ . & . & . & . & . & . & . & . \\ . & . & . & . & . & . & . & . \\ 0 & 0 & . & . & . & 1 & 4 & 1 \\ 1 & 0 & 0 & . & . & . & 1 & 4 \end{bmatrix} \begin{bmatrix} P'_0 \\ P'_1 \\ . \\ . \\ P'_N \end{bmatrix} = \begin{bmatrix} 3(P_1 - P_N) \\ 3(P_2 - P_0) \\ . \\ . \\ 3(P_N - P_{N-2}) \\ 3(P_0 - P_{N-1}) \end{bmatrix} \quad [9.17]$$

This set of equations provides the solution of the values of the tangent vectors at each of the precision points. The system of equations defined by equation 9.13 may now be solved knowing a series of precision points.

This cubic spline function was used to generate curves and was evaluated with the databases of path and motion generation

solutions. The precision points used for the cubic spline function were 16 precision points sampled from a four-bar mechanism. The four-bar mechanism used to generate a desired solution is defined on page 125 and is saved in the database as curve number 3.

The spacing of the sixteen precision points was defined by 16 equal rotations of the drive crank. As a result, the precision points are not spaced an equal distance from one another. To generate a function, path or motion solution using the cubic spline function, the parametric variable "t" was varied from 0 to 1 in eight equal steps.

Figure 9.1 is a graph of the trace point path (path generation) generated by the cubic spline function using sixteen precision points. Compare this to the trace point path in Figure 9.2.

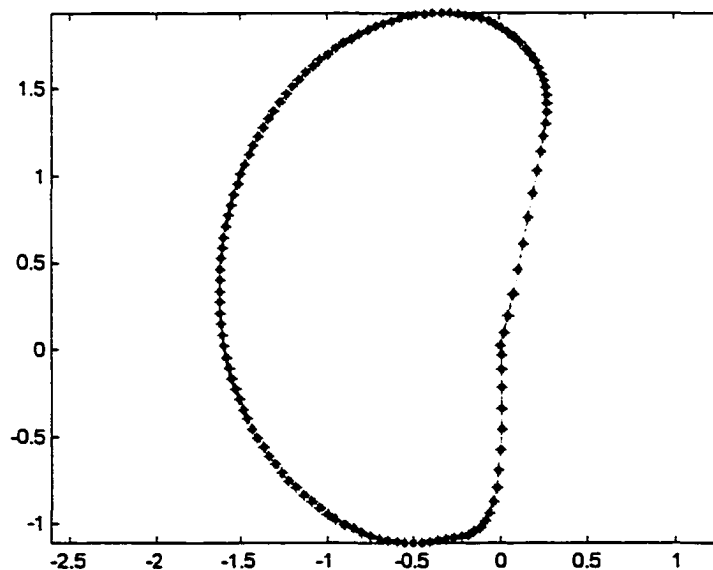


Figure 9.1: Trace point path generated by cubic spline

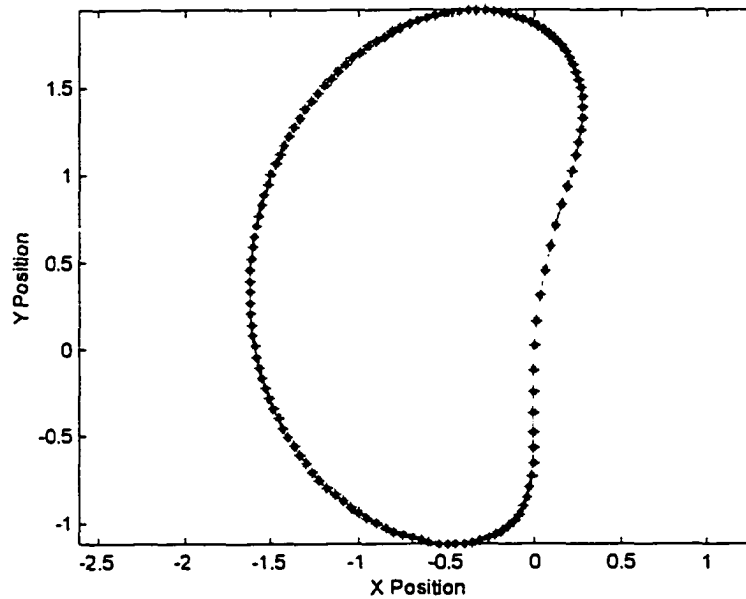


Figure 9.2: Trace point path generated by four-bar mechanism

The trace point path defined by the cubic spline function was then normalized for position, rotation, scale and discrete point distribution as described in Chapter 7. The normalized trace point path was then compared with each of the database solutions and evaluated with the following matching measures:

- Sum of absolute differences
- Amplitude and phase difference using Fourier descriptors

Sum of Absolute Differences - Path Generation

The sum of the absolute difference when used with the trace point path is defined by the equation 7.8. Figure 9.3 is a graph

of the absolute difference measure of the desired trace point path with the first 145 of the total 7,425 database paths. The top 5 matching database paths are plotted in Figure 9.4. The 15 database paths which had the smallest absolute difference values are listed in Table 9.1.

The absolute difference measure, defined for a two dimensional path, analyzed point by point the curves that most closely matched the desired trace point path. Comparing the results with Table 7.3 shows that nine of the top ten candidate solutions are the same.

Table 9.1: Summary of database search of trace point paths using absolute difference - Cubic Spline

Desired Curve - Database Curve #3

Search Rank	Database Curve Number	Absolute Difference Value
1	3	3.9698
2	2	4.8024
3	9	5.2065
4	40	5.2442
5	47	5.6456
6	55	5.8289
7	85	6.0895
8	17	6.4090
9	123	6.5965
10	93	6.9381
11	131	7.1118
12	10	7.5212
13	48	7.9584
14	77	8.1376
15	137	8.4825

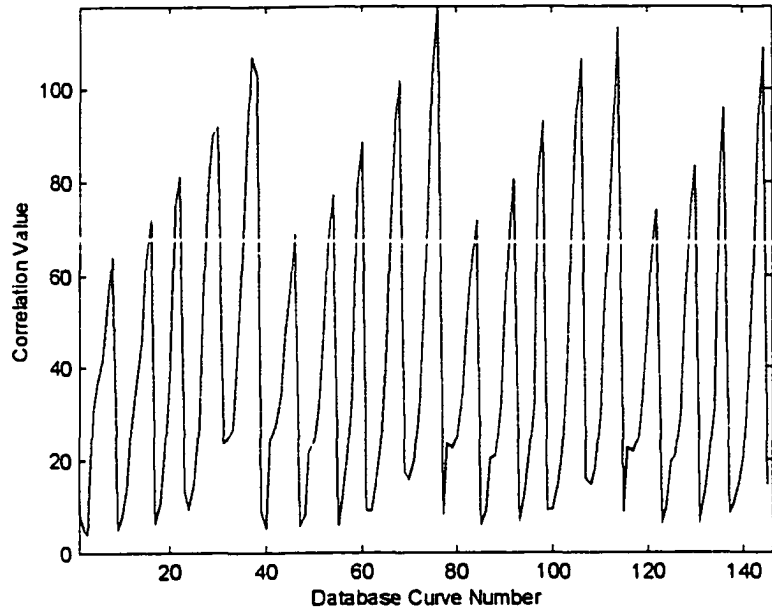


Figure 9.3: Graph of absolute difference of desired trace point path with 145 database trace point paths - cubic spline

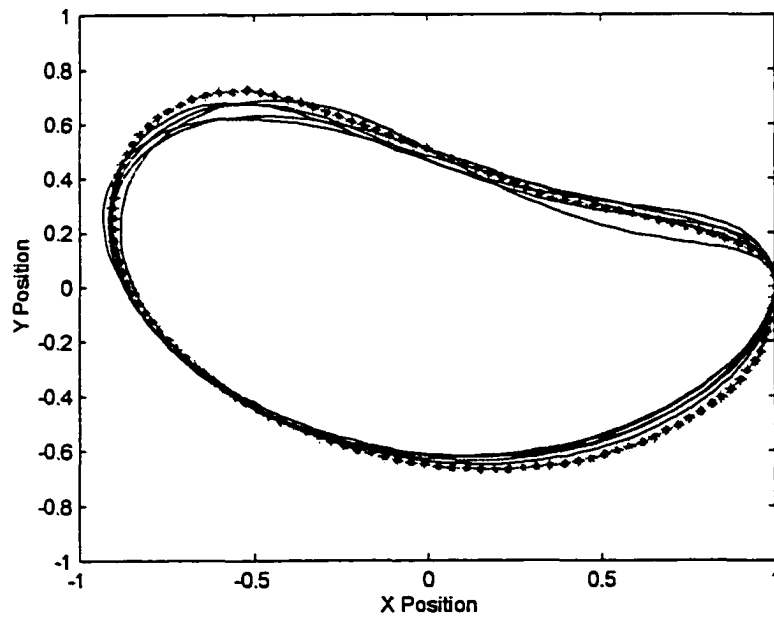


Figure 9.4: Graph of the top 5 database trace point paths identified by absolute difference measure - cubic spline

Fourier Descriptor Amplitude and Phase Difference Measure - Path Generation

The difference of the amplitude and phase of the Fourier descriptors is defined by equation 7.15. The value used for n was 0.3. Figure 9.5 is a graph of the Fourier descriptor amplitude and phase difference of the desired trace point path with the 145 database functions. The top 5 matching database paths are plotted in Figure 9.6. The 15 database trace point paths that had the largest correlation values are listed in Table 9.2. Comparing the results with Table 7.9 shows that nine of the top ten candidate solutions are the same.

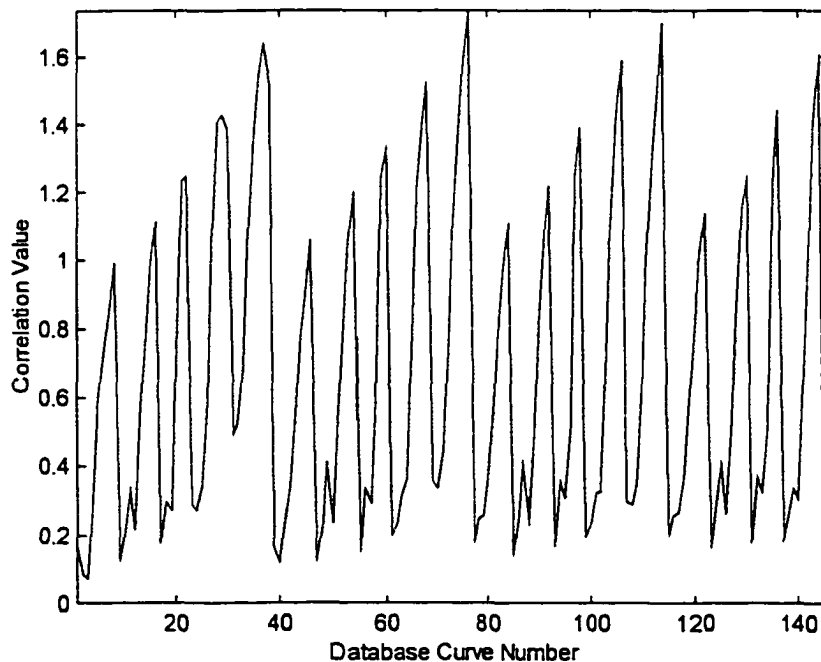


Figure 9.5: Graph of Fourier descriptor amplitude and phase difference measure of desired trace point path with 145 database trace point paths - cubic spline

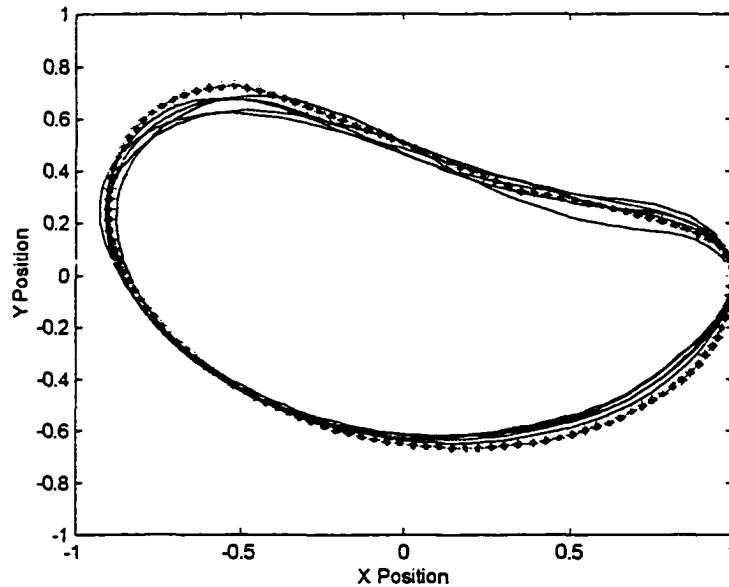


Figure 9.6: Graph of the top 5 database trace point paths identified by amplitude and phase difference of Fourier descriptors - cubic spline

Table 9.2: Summary of database search of trace point paths using amplitude and phase difference measure of Fourier descriptors - Cubic Spline

Desired Curve - Database Curve #3

Search Rank	Database Curve Number	Amplitude and Phase Difference
1	3	0.0738
2	2	0.0854
3	40	0.1165
4	9	0.1222
5	47	0.1227
6	85	0.1427
7	55	0.1497
8	123	0.1561
9	93	0.1629
10	39	0.1660
11	1	0.1679
12	131	0.1695
13	17	0.1732
14	77	0.1791
15	137	0.1895

Sum of Absolute Differences - Partial Path Generation

The sum of the absolute difference when used with the trace point path is defined by the following equation 7.8. Figure 9.7 is a graph of the absolute difference measure of the desired trace point path with the first 145 of the total 7,425 database paths. The top 5 matching database paths are plotted in Figure 9.8. The 15 database paths which had the smallest absolute difference values are listed in Table 9.3. Comparing the results with Table 7.15 shows that ten of the top ten candidate solutions are the same.

Table 9.3: Summary of database search of partial trace point paths using absolute difference - Cubic Spline

Desired Curve - Database Curve #3

Search Rank	Database Curve Number	Absolute Difference Value
1	3	0.2955
2	50	1.1905
3	49	5.6966
4	88	5.7403
5	10	6.0701
6	4	7.2308
7	2	7.5286
8	126	7.7445
9	87	7.8028
10	134	7.9114
11	11	7.9408
12	51	8.0036
13	133	8.4858
14	125	8.6653
15	18	9.3127

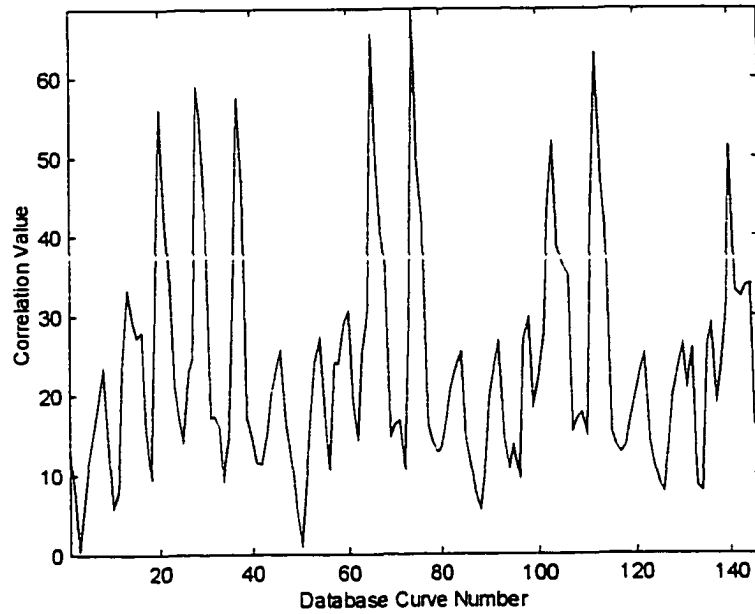


Figure 9.7: Graph of absolute difference of desired partial trace point path with 145 database trace point paths - cubic spline

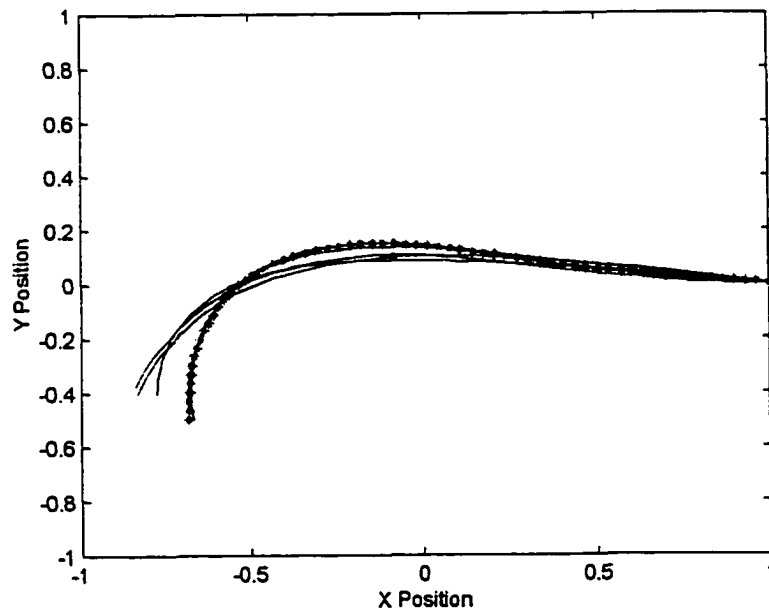


Figure 9.8: Graph of the top 5 database partial trace point paths identified by absolute difference measure - cubic spline

Fourier Descriptor Amplitude and Phase Difference Measure - Partial Path Generation

The difference of the magnitude of the Fourier descriptors is defined by equation 7.13. The value used for n was 0.3. Figure 9.9 is a graph of the Fourier descriptor amplitude and phase difference of the desired trace point path with the 145 database functions. The top 5 matching database paths are plotted in Figure 9.10. The 15 database trace point paths that had the largest correlation values are listed in Table 9.4. Comparing the results with Table 7.16 shows that nine of the top 10 candidate solutions are the same.

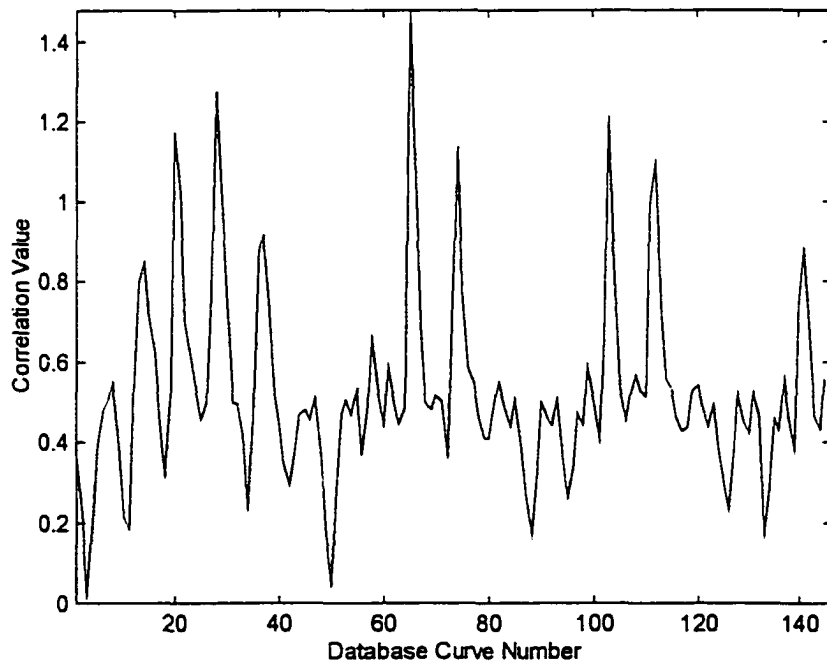


Figure 9.9: Graph of Fourier descriptor amplitude and phase difference measure of desired partial trace point path with 145 database trace point paths - cubic spline

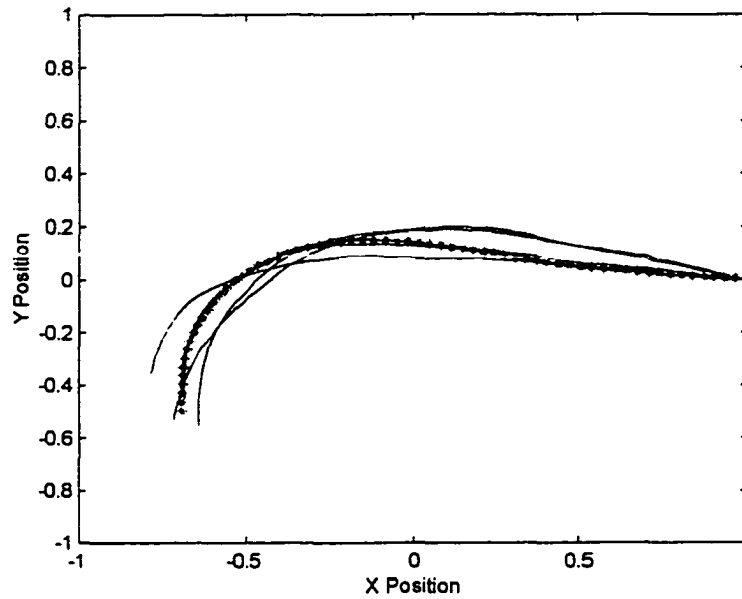


Figure 9.10: Graph of the top 5 database partial trace point paths identified by amplitude and phase difference of Fourier descriptors - cubic spline

Table 9.4: Summary of database search of partial trace point paths using amplitude and phase difference measure of Fourier descriptors - cubic spline

Desired Curve - Database Curve #3

Search Rank	Database Curve Number	Amplitude and Phase Difference
1	3	0.0126
2	50	0.0383
3	133	0.1646
4	88	0.1695
5	11	0.1818
6	49	0.1819
7	4	0.2053
8	10	0.2116
9	2	0.2153
10	34	0.2284
11	126	0.2318
12	51	0.2549
13	95	0.2607
14	87	0.2666
15	134	0.2793

Figure 9.11 is a graph of the normalized trace point motion (motion generation) generated by the cubic spline function using sixteen precision points. Compare this to the normalized trace point path in Figure 9.12.

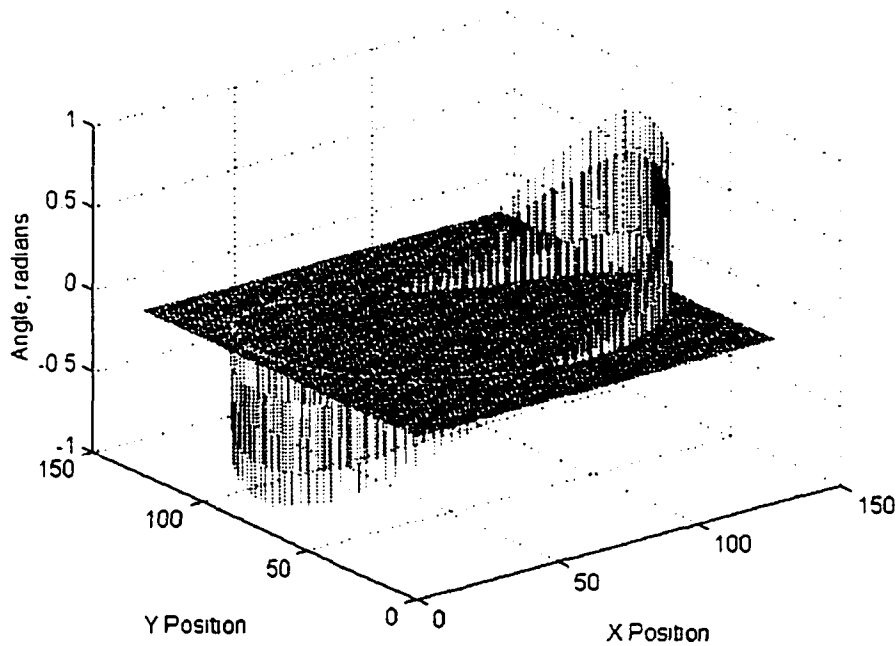


Figure 9.11: Normalized path and angle generated by cubic spline

The trace point motion defined by the cubic spline function was then normalized for position, rotation, scale and point spacing as described in Chapter 8. The normalized trace point motion was then compared with each of the database solutions and evaluated with the following matching measures:

- Sum of absolute differences
- Amplitude and phase difference using Fourier descriptors

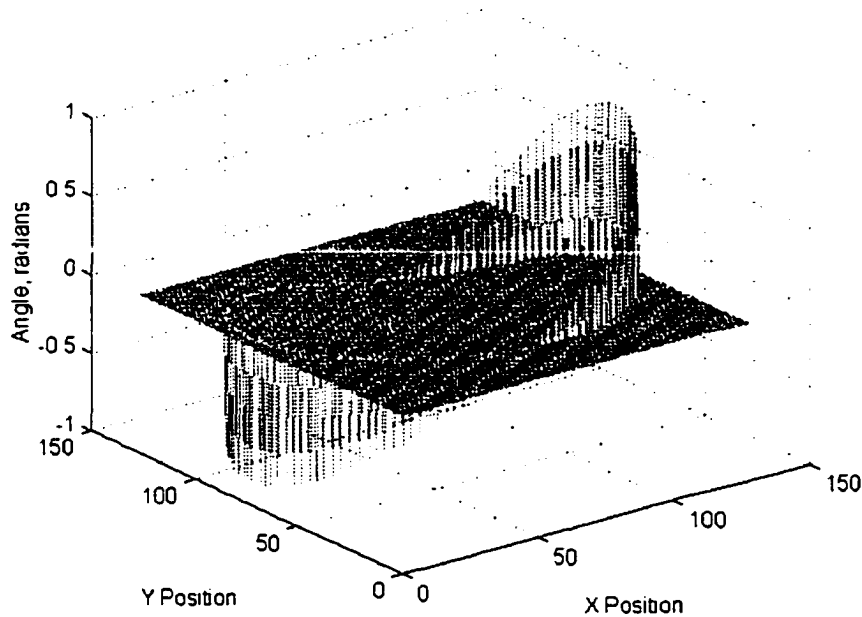


Figure 9.12: Normalized path and angle generated by four-bar mechanism

Sum of Absolute Differences - Motion Generation

The sum of the absolute difference when used with the trace point path is defined by equation 8.3. For evaluating the motion of the desired four-bar mechanism, the weighting factors, p and q , were each assigned a value of 0.5.

Figure 9.13 is a graph of the absolute difference measure of the desired trace point motion with the 145 database functions. The top 5 matching candidate solutions were identified; the trace point paths are plotted in Figure 9.14 and the connecting rod angles are plotted in Figure 9.15. The 15 database candidate solutions which had the smallest absolute differences values are listed in Table 9.5. Comparing the results with Table 8.1 shows that nine of the top 10 candidate solutions are the same.

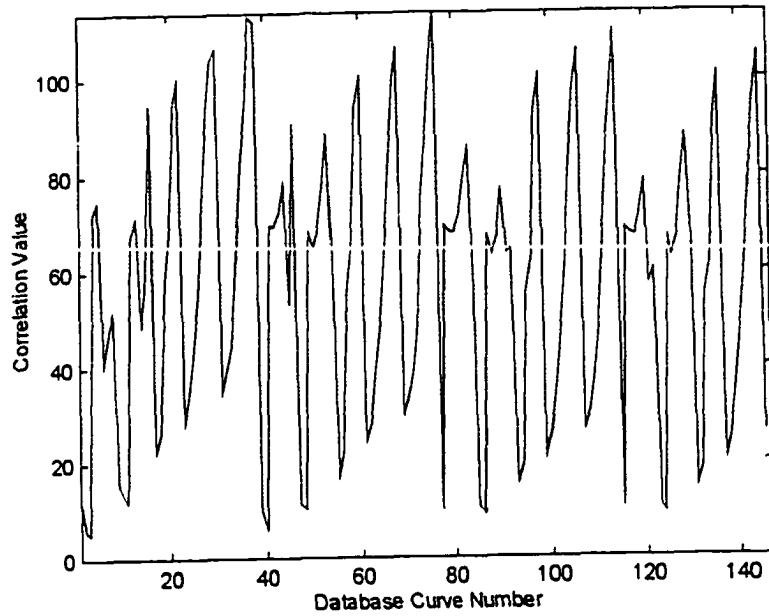


Figure 9.13: Graph of absolute difference of desired motion with 145 database candidate solutions - cubic spline

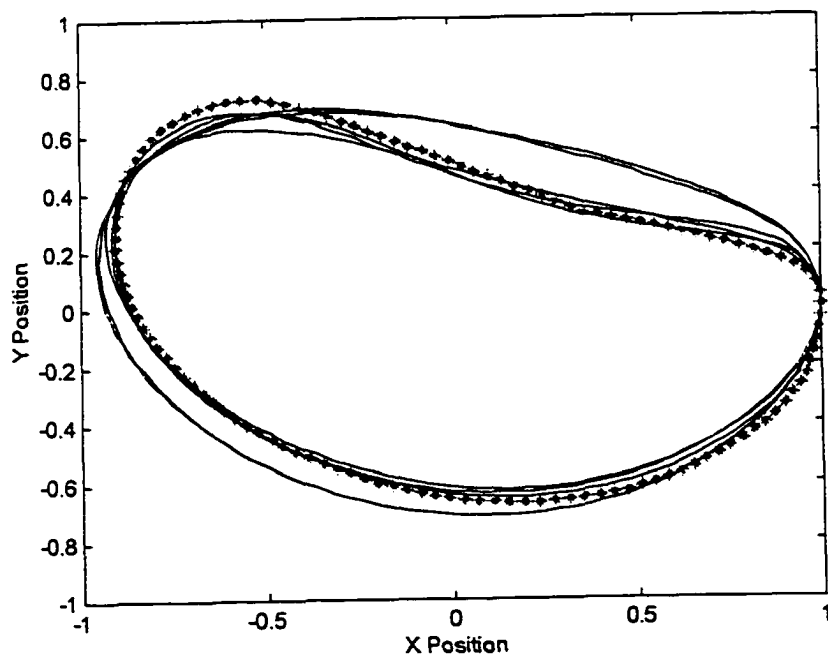


Figure 9.14: Graph of the top 5 database trace point paths identified by absolute difference measure (motion generation) - cubic spline

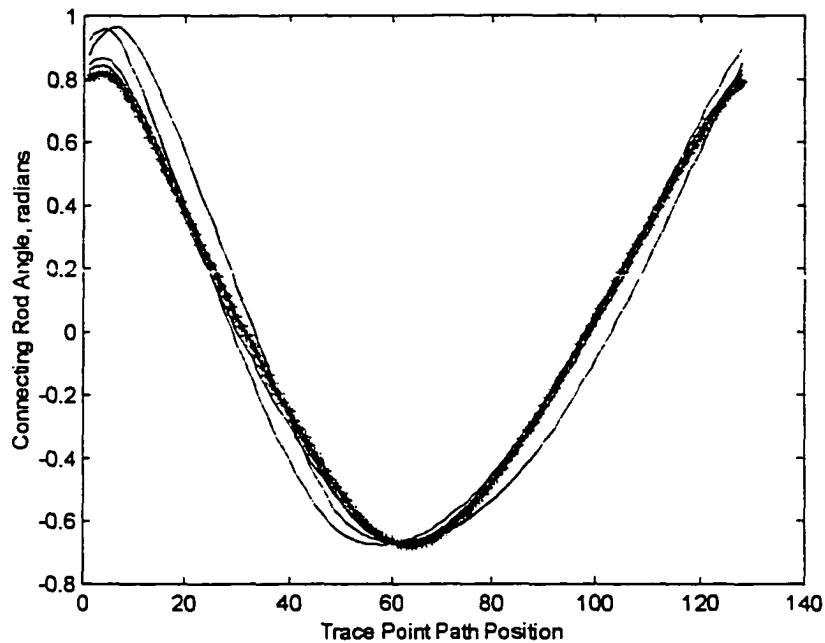


Figure 9.15: Graph of the top 5 database connecting rod angles identified by absolute difference measure (motion generation) - cubic spline

Table 9.5: Summary of database search of trace point motion using absolute difference - cubic spline

Desired Curve - Database Curve #3

Search Rank	Database Curve Number	Absolute Difference Value
1	3	5.0845
2	2	5.7332
3	40	5.8566
4	86	8.8740
5	124	9.1336
6	39	9.6029
7	77	9.7859
8	115	10.0576
9	48	10.0918
10	123	10.4217
11	85	10.5758
12	47	11.2253
13	11	11.4290
14	1	12.3757
15	10	13.4673

Amplitude and Phase Difference Using Fourier Descriptors - Motion Generation

For evaluating the amplitude and phase difference using Fourier descriptors equation 7.13 was used to evaluate the difference measure for the desired motion with each of the database solutions. The value used for n was 0.3 and the value used for m was 0.7. Equation 7.13 was used to evaluate a difference measure for the connecting rod angle of the desired connecting rod angle with each of the database solutions. The value used for n was 0.3. An overall measure was evaluated using equation 8.4. For evaluating the motion of the desired four-bar mechanism, the weighting factors, p and q , were each addressed a value of 0.5.

Figure 9.16 is a graph of the absolute difference measure of the desired motion with the 145 database candidate solutions. The top 5 matching candidate solutions were identified; the trace point paths are plotted in Figure 9.17, and the connecting rod angles are plotted in Figure 9.18. The 15 database trace point motion which had the smallest amplitude and phase difference are listed in Table 9.6. Comparing the results with Table 8.2 shows that nine of the top 10 candidate solutions are the same.

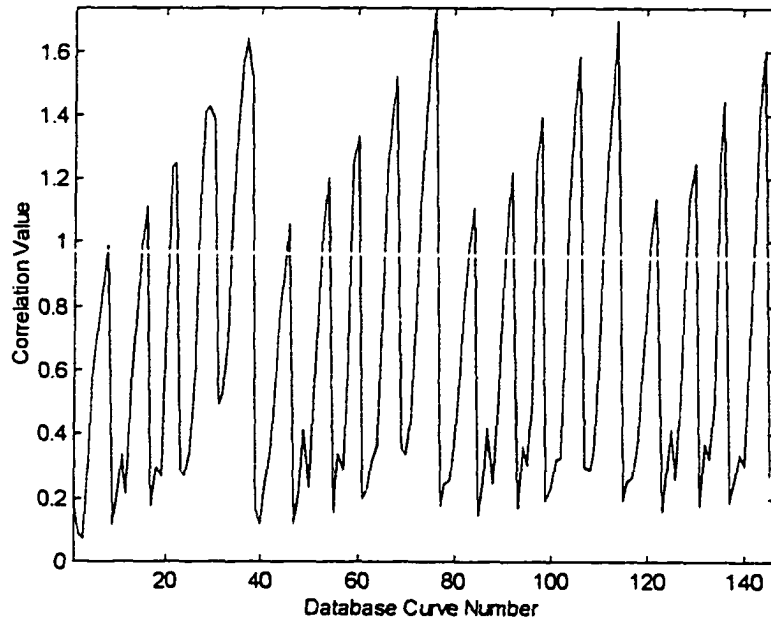


Figure 9.16: Graph of Fourier descriptor amplitude and phase difference measure of desired motion with 145 database candidate solutions - cubic spline

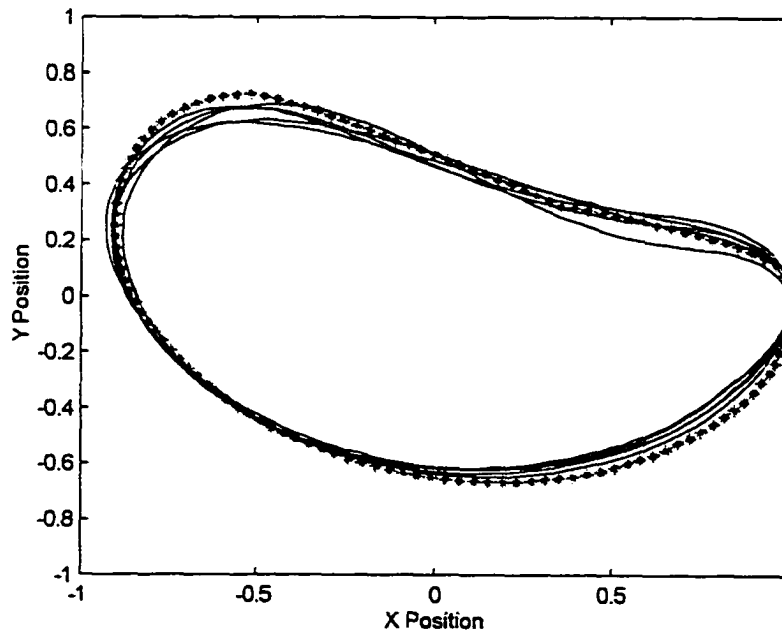


Figure 9.17: Graph of the top 5 database trace point paths identified by amplitude and phase difference of Fourier descriptors (motion generation) - cubic spline

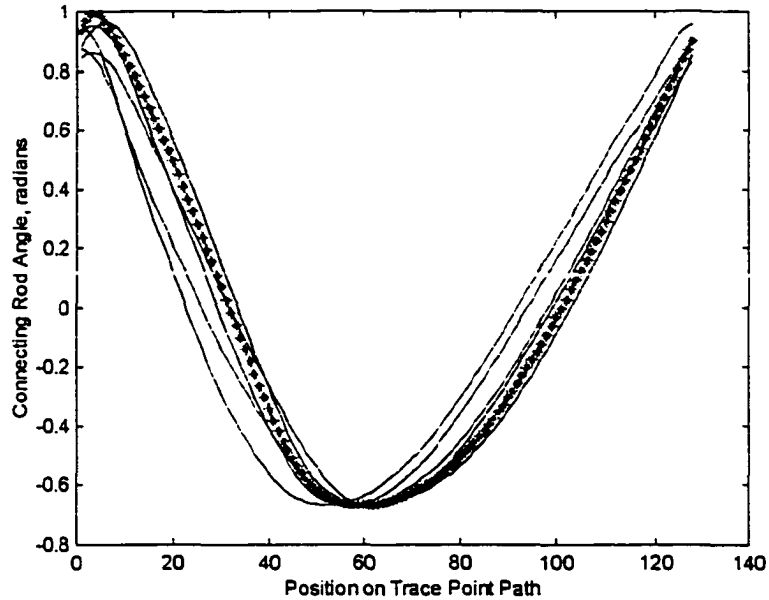


Figure 9.18: Graph of the top 5 database connecting rod angles identified by amplitude and phase difference of Fourier descriptors (motion generation) - cubic spline

Table 9.6: Summary of database search of trace point motion using amplitude and phase difference measure of Fourier descriptors - Cubic Spline

Desired Curve - Database Curve #3

Search Rank	Database Curve Number	Amplitude and Phase Difference
1	3	0.0738
2	2	0.0854
3	40	0.1165
4	9	0.1222
5	47	0.1227
6	85	0.1427
7	55	0.1497
8	123	0.1561
9	93	0.1629
10	39	0.1660
11	1	0.1679
12	131	0.1695
13	17	0.1732
14	77	0.1791
15	137	0.1895

Sum of Absolute Differences - Partial Curve Motion Generation

The sum of the absolute difference when used with the trace point path is defined by equation 8.3. For evaluating the motion of the desired four-bar mechanism, the weighting factors, p and q , were each addressed a value of 0.5.

Figure 9.19 is a graph of the absolute difference measure of the desired trace point motion with the 145 database candidate solutions. The top 5 matching candidate solutions were identified; the trace point paths are plotted in Figure 9.20 and the connecting rod angles are plotted in Figure 9.21. The 15 database candidate solutions which had the smallest absolute differences values are listed in Table 9.7. Comparing the results with Table 8.4 shows that ten of the top ten candidate solutions are the same.

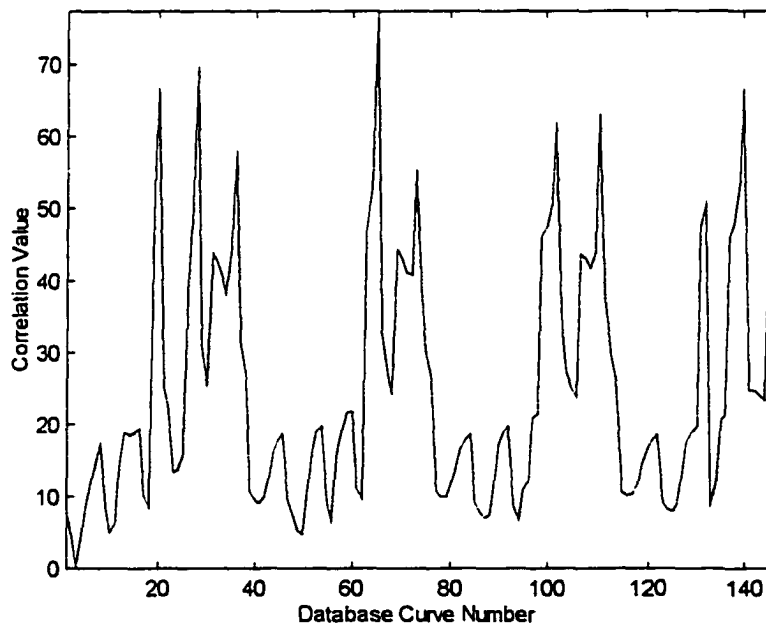


Figure 9.19: Graph of absolute difference of desired partial trace point motion with 145 database trace point paths - cubic spline

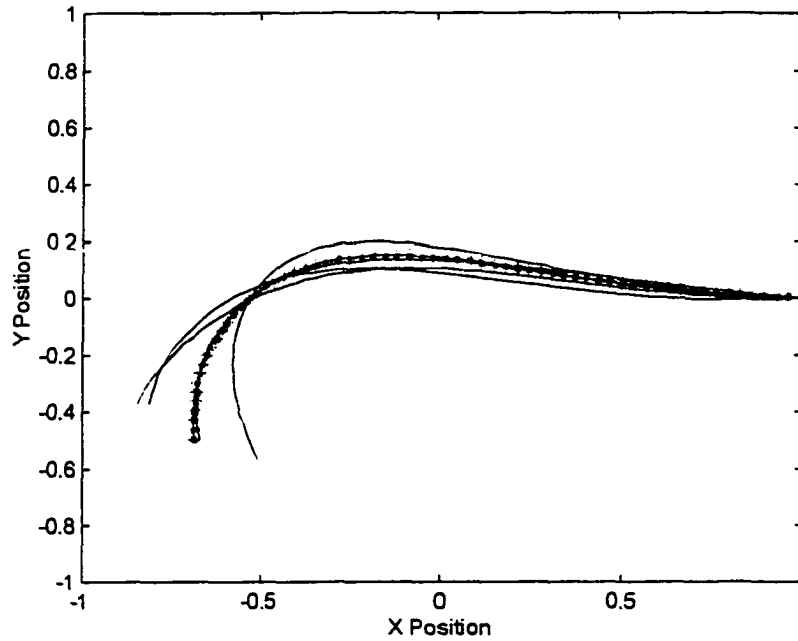


Figure 9.20: Graph of the top 5 database partial trace point paths identified by absolute difference measure (motion generation) - cubic spline

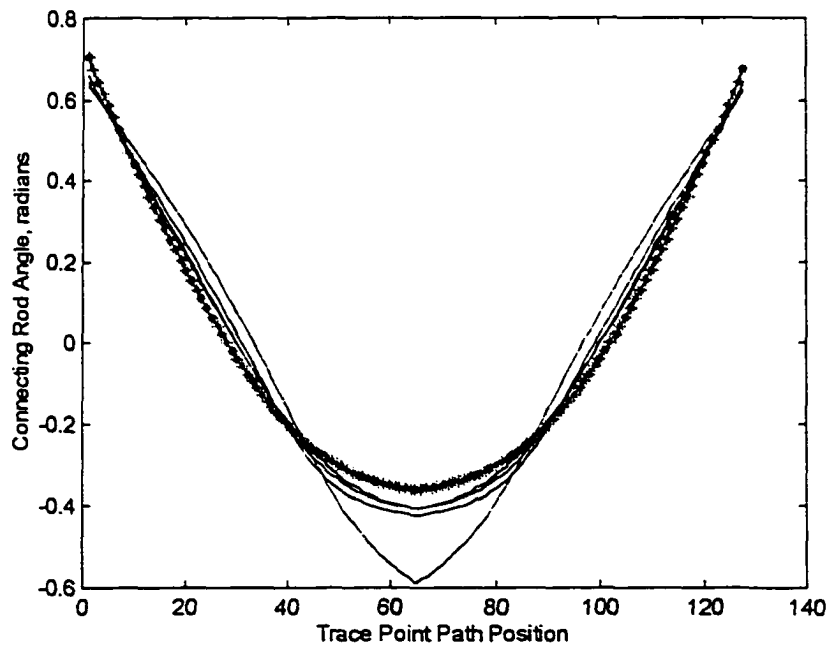


Figure 9.21: Graph of the top 5 database connecting rod angles identified by absolute difference measure (motion generation) - cubic spline

Table 9.7: Summary of database search of trace point motion using absolute difference - Cubic Spline

Desired Curve - Database Curve #3

Search Rank	Database Curve Number	Absolute Difference Value
1	3	0.1629
2	2	4.2256
3	4	4.6283
4	50	4.6449
5	10	4.9489
6	49	5.4087
7	11	6.4159
8	56	6.6696
9	94	6.7109
10	87	6.9554
11	48	7.3766
12	1	7.4202
13	88	7.5909
14	86	7.7782
15	125	7.8591

Amplitude and Phase Difference using Fourier Descriptors - Partial Curve Motion Generation

For evaluating the amplitude and phase difference using Fourier descriptors equation 7.13 was used to evaluate the difference measure for the desired motion with each of the database solutions. The value used for n was 0.3. Equation 7.13 was used to evaluate a difference measure for the connecting rod angle of the desired connecting rod angle with each of the database solutions. The value used for n was 0.3. An overall measure was evaluated using equation 8.4. For evaluating the

motion of the desired four-bar mechanism, the weighting factors, p and q , were each addressed a value of 0.5.

Figure 9.22 is a graph of the absolute difference measure of the desired motion with the 145 database candidate solutions. The top 5 matching candidate solutions were identified; the trace point paths are plotted in Figure 9.23 and the connecting rod angles are plotted in Figure 9.24. The 15 database trace point motion which had the smallest absolute differences values are listed in Table 9.8. Comparing the results with Table 8.5 shows that nine of the top 10 candidate solutions are the same.

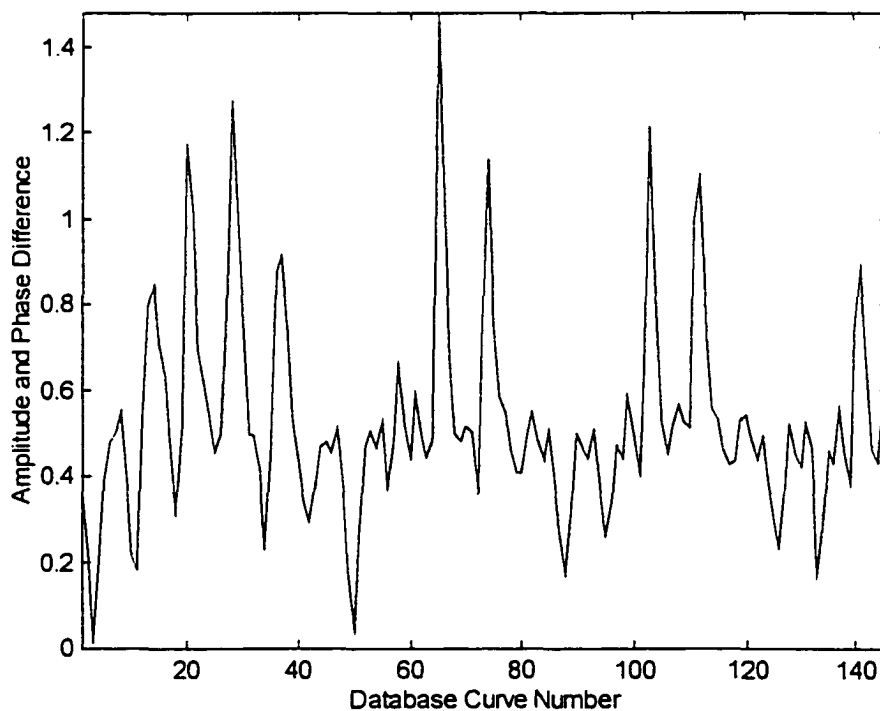


Figure 9.22: Graph of Fourier descriptor amplitude and phase difference measure of desired motion with 145 database candidate solutions - cubic spline

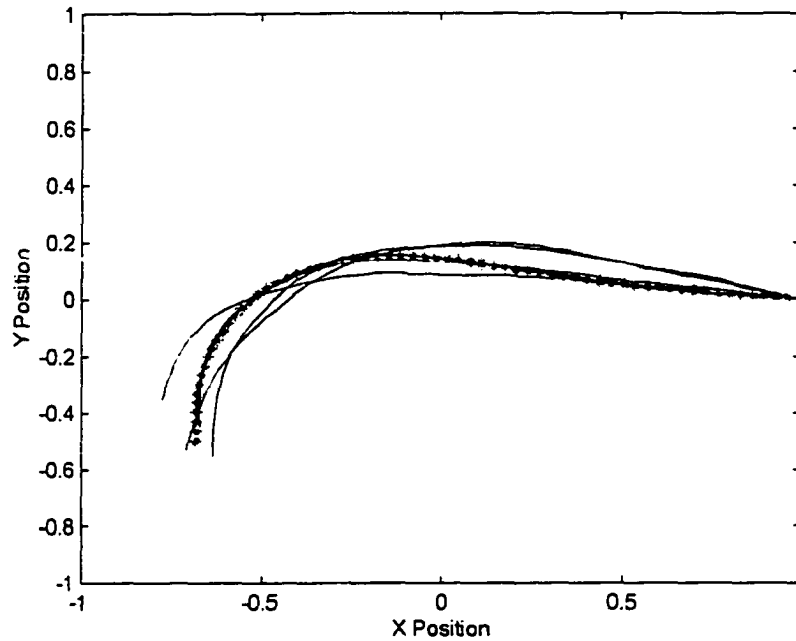


Figure 9.23: Graph of the top 5 database partial trace point paths identified by amplitude and phase difference of Fourier descriptors (motion generation) - cubic spline

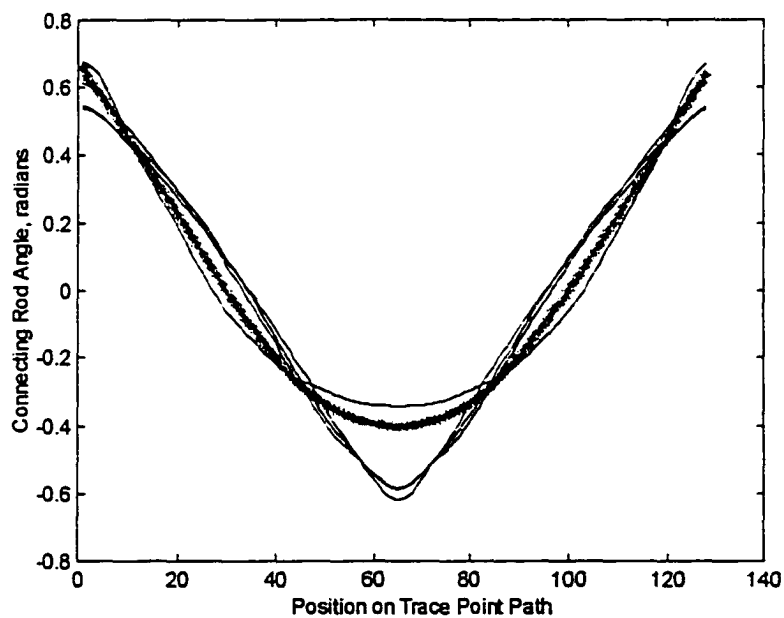


Figure 9.24: Graph of the top 5 database connecting rod angles identified by amplitude and phase difference of Fourier descriptors (motion generation) - cubic spline

Table 9.8: Summary of database search of trace point motion using amplitude and phase difference measure of Fourier descriptors - cubic spline

Desired Curve - Database Curve #3

Search Rank	Database Curve Number	Amplitude and Phase Difference
1	3	0.0126
2	50	0.0383
3	133	0.1646
4	88	0.1695
5	11	0.1818
6	49	0.1819
7	4	0.2053
8	10	0.2116
9	2	0.2153
10	36	0.2284
11	126	0.2318
12	51	0.2549
13	95	0.2607
14	87	0.2666
15	134	0.2793

B-Splines

A B-spline blending function generates a parametric polynomial curve through any number of "control points." The benefits of B-splines includes the fact that the designer may select the degree of the polynomial used in generating the curve, and that the redefinition of the location of a control affects only a few of the curve segments which are close to the control point. The remainder of the curve remains unchanged when one control point is moved. Uniform cubic B-splines is a specific implementation of a B-spline blending function and will be evaluated for use in defining solutions for function, path, and motion generation.

Uniform cubic B-splines have C^2 parametric continuity and the parametric intervals of t are equal. A uniform cubic B-spline curve is defined by the following equation:

$$P_i(t) = N_{0,3}(t)V_i + N_{1,3}(t)V_i + N_{2,3}(t)V_i + N_{3,3}(t)V_i \quad [9.18]$$

Where:

P_i = B-spline curve points

V_i = Control Points

$N_{j,3}$ = Cubic Polynomials

t = Parametric variable, $0 \leq t \leq 1$

The cubic polynomial is defined by:

$$N_{j,3}(t) = a_j + b_j t + c_j t^2 + d_j t^3 \quad [9.19]$$

Where:

a, b, c, d = Polynomial coefficients

$j = 0, 1, 2, 3$

There are 16 unknown polynomial coefficients. The geometric constraints of having the curve segments first and second derivative equal to zero results in six constraints. Parametric continuity C^0 , C^1 , and C^2 result in defining 9 more constraints. The last constraint is obtained by the following normalizing condition:

$$N_{0,3}(t) + N_{1,3}(t) + N_{2,3}(t) + N_{3,3}(t) = 1$$

This condition force the curve to lie within a convex figure established by the extreme points of a polygon formed by the control points (known as the convex hull). Solving the equations results in the following polynomials for $0 \leq t \leq 1$.

$$N_{0,3}(t) = t^3/6 \quad [9.20]$$

$$N_{1,3}(t) = (-3t^3 + 3t^2 + 3t + 1)/6 \quad [9.21]$$

$$N_{2,3}(t) = (3t^3 - 6t^2 + 4)/6 \quad [9.22]$$

$$N_{3,3}(t) = (-t^3 + 3t^2 - 3t + 1)/6 \quad [9.23]$$

Substituting equations 9.20, 9.21, 9.22, and 9.23 into equation 9.18 and placing into matrix form yields:

$$P_i(t) = [t^3 \ t^2 \ t \ 1] \begin{bmatrix} -1 & 3 & -3 & 1 \\ 3 & -6 & 3 & 0 \\ -3 & 0 & 3 & 0 \\ 1 & 4 & 1 & 0 \end{bmatrix} \begin{bmatrix} V_{i-1} \\ V_i \\ V_{i+1} \\ V_{i+2} \end{bmatrix} \quad [9.24]$$

or

$$P_i(t) = (1/6) [t] [M]_{BS} [G]_{BS} \quad [9.25]$$

Where:

$[t]$ = Parametric variable matrix, $0 \leq t \leq 1$

$[M]_{BS}$ = B-spline Cubic polynomial matrix

$[G]_{BS}$ = B-spline control point matrix

With a set of defined precision points equation 9.24 may be solved for the closed curves which have been established for function, path and motion generation.

$$P_0(0) = (1/6) [1 \ 4 \ 1 \ 0] [V_N \ V_0 \ V_1 \ V_2]^{-1} \quad [9.26]$$

$$P_1(0) = (1/6) [1 \ 4 \ 1 \ 0] [V_0 \ V_1 \ V_2 \ V_3]^{-1} \quad [9.27]$$

.

.

$$P_N(0) = (1/6) [1 \ 4 \ 1 \ 0] [V_{N-1} \ V_N \ V_0 \ V_1]^{-1} \quad [9.28]$$

Or in matrix form:

$$\begin{bmatrix} P_0 \\ P_1 \\ . \\ . \\ P_{N-1} \\ P_N \end{bmatrix} = \begin{bmatrix} 4 & 1 & . & . & . & . & 0 & 1 \\ 1 & 4 & 1 & . & . & . & 0 & 0 \\ . & . & . & . & . & . & . & . \\ . & . & . & . & . & . & . & . \\ 0 & 0 & . & . & . & 1 & 4 & 1 \\ 1 & 0 & 0 & . & . & . & 1 & 4 \end{bmatrix} \begin{bmatrix} V_0 \\ V_1 \\ . \\ . \\ . \\ V_N \end{bmatrix} \quad [9.29]$$

With a set of defined precision points the control points, V_i , may be evaluated.

This B-spline function was used to generate curves and was evaluated with the databases of path and motion generation solutions. The precision points used for the B-spline function were 16 precision points sampled from a four-bar mechanism. The four-bar mechanism was saved in the database as curve number 3.

The spacing of the sixteen precision points was defined by 16 equal rotations of the drive crank. As a result, the precision points are not spaced an equal distance from one another. To

generate a function, path or motion solution using the cubic spline function, the parametric variable "t" was varied from 0 to 1 in eight equal steps.

Figure 9.25 is a graph of the trace point path (path generation) generated by the B-spline function using sixteen precision points. Compare this to the trace point path in Figure 9.26.

The trace point path defined by the cubic spline function was then normalized for position, rotation, scale and point spacing as described in Chapter 7. The normalized trace point path was then compared with each of the database solutions and evaluated with the following matching measures:

- Sum of absolute differences
- Amplitude and phase difference using Fourier descriptors

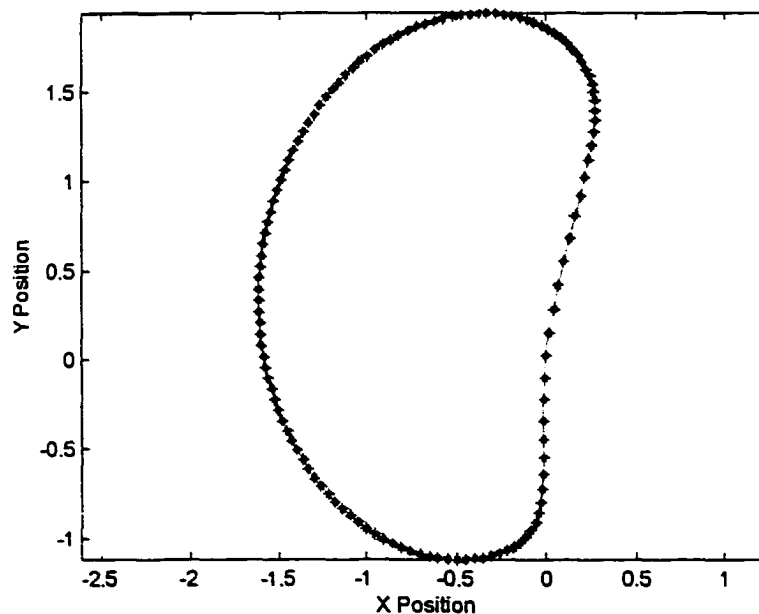


Figure 9.25: Trace point path generated by B-spline

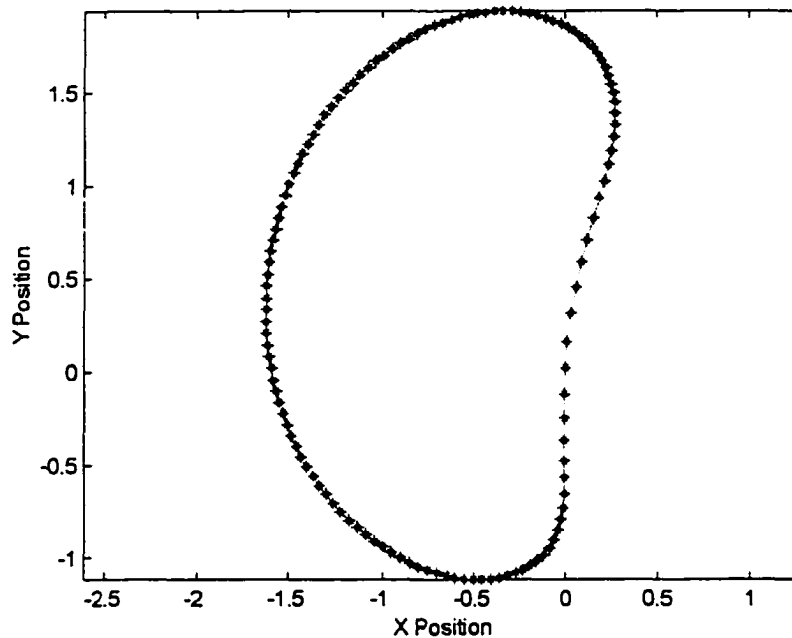


Figure 9.26: Trace point path generated by four-bar mechanism

Sum of Absolute Differences - Path Generation

The sum of the absolute difference when used with the trace point path is defined by the following equation 7.8. Figure 9.27 is a graph of the absolute difference measure of the desired trace point path with the first 145 of the total 7,425 database paths. The top 5 matching database paths are plotted in Figure 9.28. The 15 database paths which had the smallest absolute difference values are listed in Table 9.9. Comparing the results with Table 7.3 shows that ten of the top ten candidate solutions are the same.

Table 9.9: Summary of database search of trace point paths using absolute difference - B-Spline

Desired Curve - Database Curve #3

Search Rank	Database Curve Number	Absolute Difference Value
1	3	0.5555
2	2	2.1544
3	40	2.8699
4	47	3.7063
5	85	4.0331
6	123	4.3619
7	9	4.6417
8	55	5.0259
9	93	5.1518
10	131	5.2764
11	17	6.3783
12	77	6.6063
13	115	6.6620
14	39	6.8923
15	137	7.1318

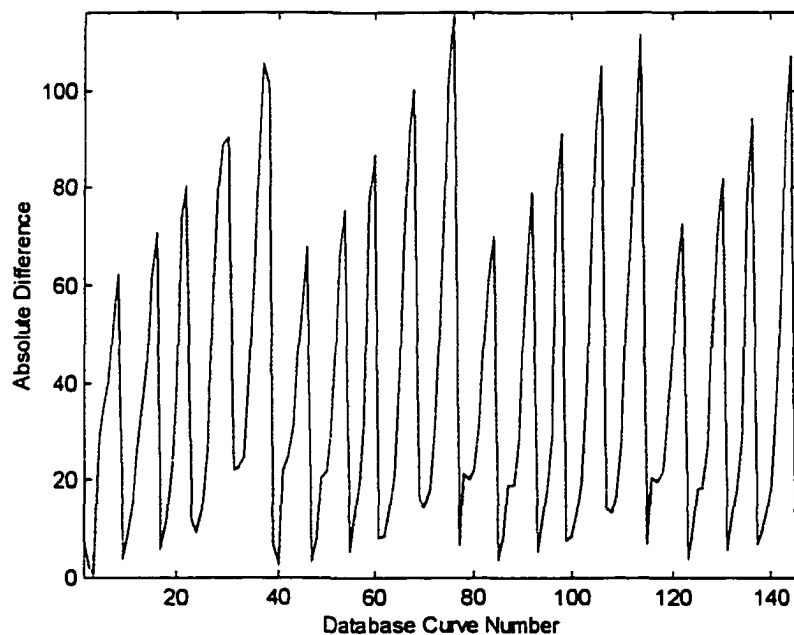


Figure 9.27: Graph of absolute difference of desired trace point path with 145 database trace point paths - B-spline

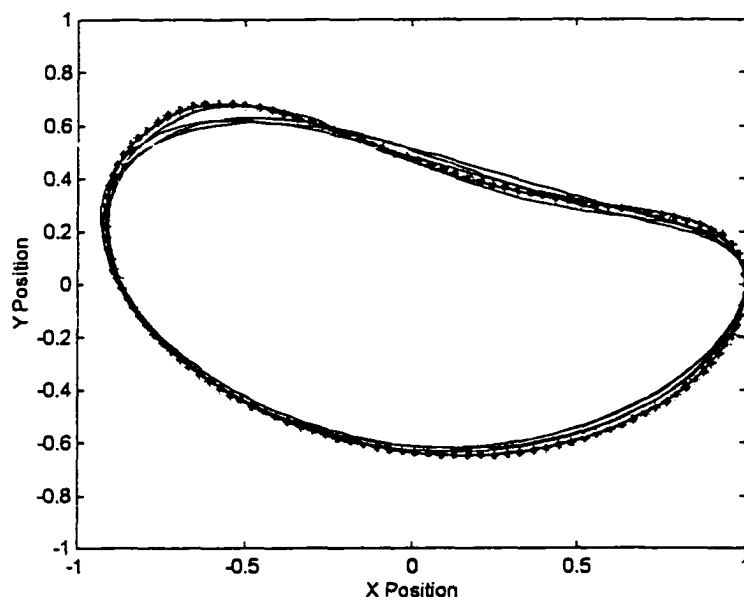


Figure 9.28: Graph of the top 5 database trace point paths identified by absolute difference measure - B-spline

Fourier Descriptor Amplitude and Phase Difference Measure - Path Generation

The difference of the amplitude and phase of the Fourier descriptors is defined by equation 7.15. The value used for n was 0.3. Figure 9.29 is a graph of the Fourier descriptor amplitude and phase difference of the desired trace point path with the 145 database functions. The top 5 matching database paths are plotted in Figure 9.20. The 15 database trace point paths that had the smallest amplitude and phase difference are listed in Table 9.10. Comparing the results with Table 7.9 shows that nine of the top ten candidate solutions are the same.

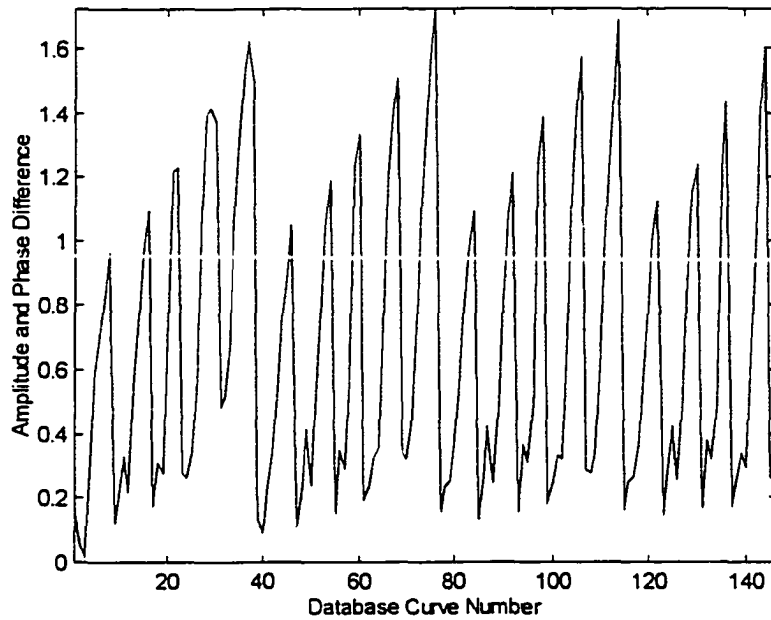


Figure 9.29: Graph of Fourier descriptor amplitude and phase difference measure of desired trace point path with 145 database trace point paths - B-spline

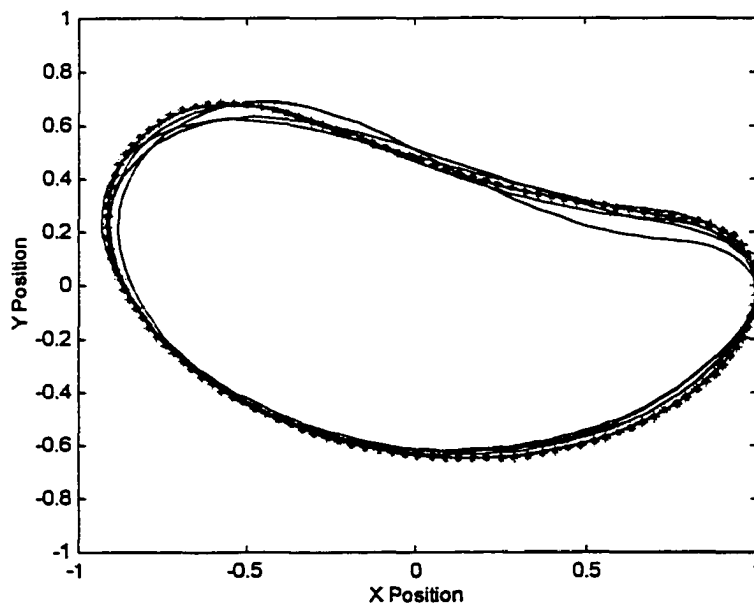


Figure 9.30: Graph of the top 5 database trace point paths identified by amplitude and phase difference of Fourier descriptors - B-spline

Table 9.10: Summary of database search of trace point paths using amplitude and phase difference measure of Fourier descriptors - B-Spline

Desired Curve - Database Curve #3

Search Rank	Database Curve Number	Amplitude and Phase Value
1	3	0.0204
2	2	0.0483
3	40	0.0936
4	47	0.1103
5	9	0.1179
6	85	0.1310
7	39	0.1356
8	123	0.1430
9	55	0.1474
10	77	0.1551
11	93	0.1570
12	1	0.1583
13	131	0.1655
14	17	0.1725
15	115	0.1738

Sum of Absolute Differences - Partial Path Generation

The sum of the absolute difference when used with the trace point path is defined by the following equation 7.8. Figure 9.31 is a graph of the absolute difference measure of the desired trace point path with the first 145 of the total 7,425 database paths. The top 5 matching database paths are plotted in Figure 9.32. The 15 database paths which had the smallest absolute difference values are listed in Table 9.11. Comparing the results with Table 7.15 shows that nine of the top ten candidate solutions are the same.

Table 9.11: Summary of database search of partial trace point paths using absolute difference - B-Spline

Desired Curve - Database Curve #3

Search Rank	Database Curve Number	Absolute Difference Value
1	3	1.3843
2	50	1.8418
3	49	5.7874
4	88	5.8392
5	10	6.2379
6	4	7.5472
7	2	7.6919
8	126	7.7859
9	87	7.8387
10	11	8.0332
11	134	8.2138
12	51	8.2890
13	133	8.5685
14	125	8.6889
15	18	9.4503

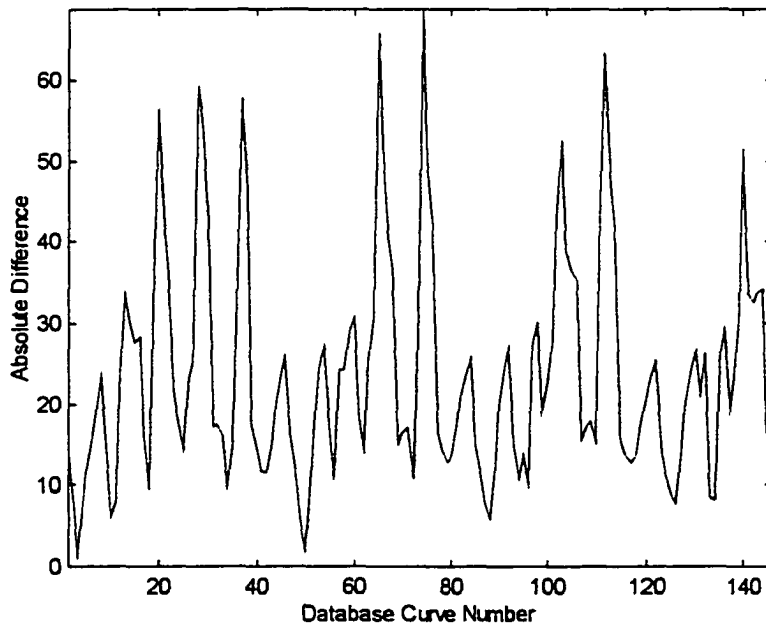


Figure 9.31: Graph of absolute difference of desired partial trace point path with 145 database trace point paths - B-spline

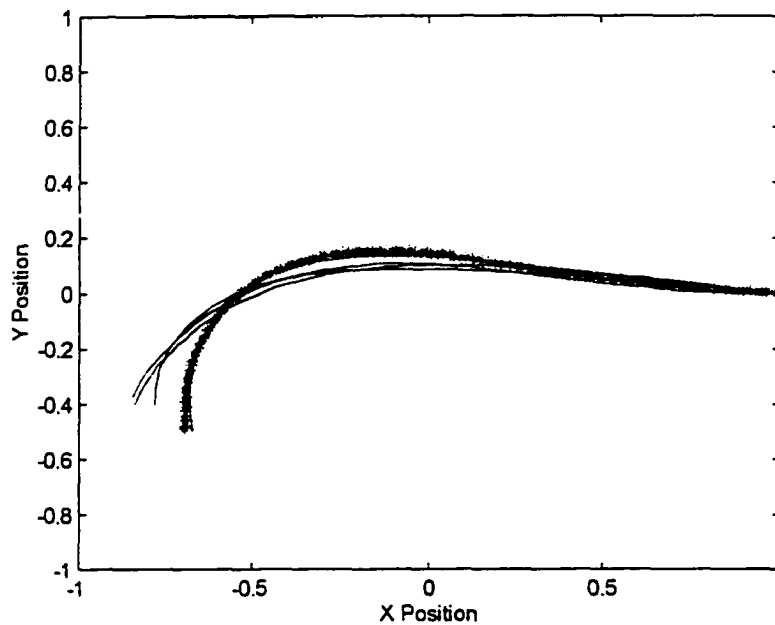


Figure 9.32: Graph of the top 5 database partial trace point paths identified by absolute difference measure - B-spline

Fourier Descriptor Amplitude and Phase Difference Measure - Partial Path Generation

The difference of the magnitude of the Fourier descriptors is defined by equation 7.13. The value used for n was 0.3. Figure 9.33 is a graph of the Fourier descriptor amplitude and phase difference of the desired trace point path with the 145 database functions. The top 5 matching database paths are plotted in Figure 9.34. The 15 database trace point paths that had the smallest amplitude and phase difference are listed in Table 9.12. Comparing the results with Table 7.16 shows that ten of the top ten candidate solutions are the same.

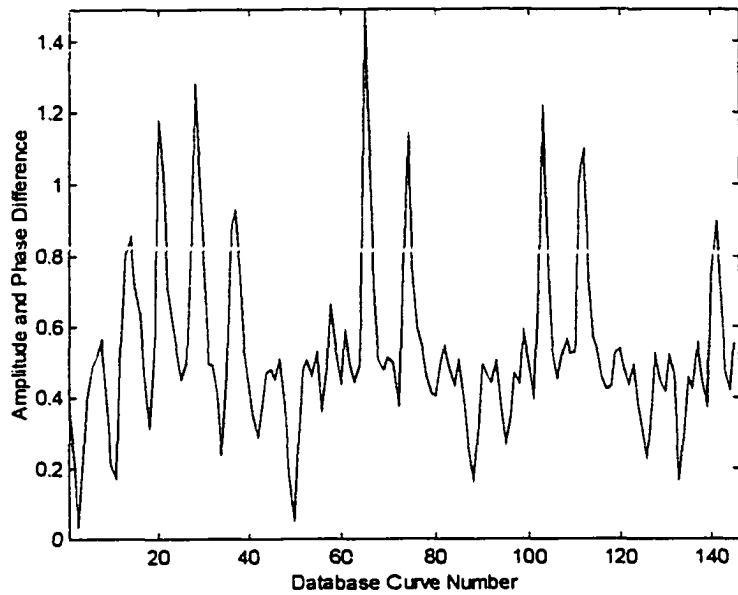


Figure 9.33: Graph of Fourier descriptor amplitude and phase difference measure of desired partial trace point path with 145 database trace point paths - B-spline

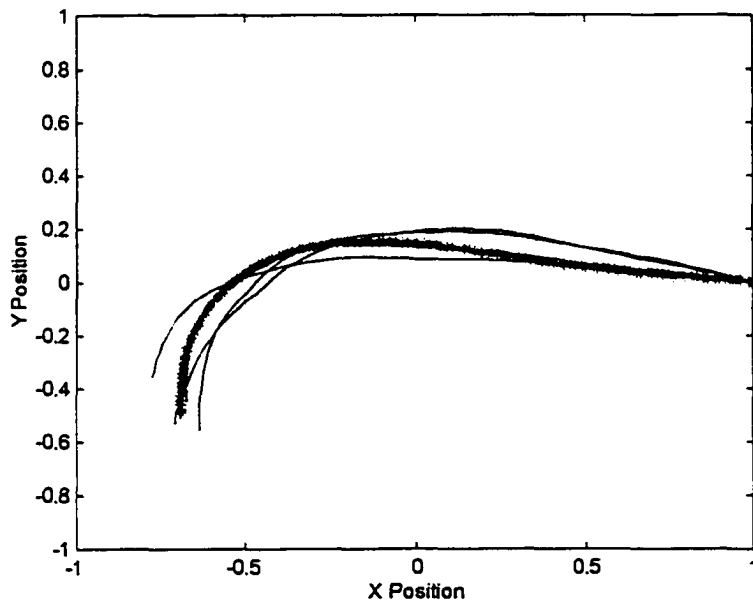


Figure 9.34: Graph of the top 5 database partial trace point paths identified by amplitude and phase difference of Fourier descriptors - B-spline

Table 9.12: Summary of database search of partial trace point paths using amplitude and phase difference measure of Fourier descriptors - B-Spline

Desired Curve - Database Curve #3

Search Rank	Database Curve Number	Amplitude and Phase Value
1	3	0.0317
2	50	0.0468
3	133	0.1631
4	88	0.1675
5	11	0.1741
6	49	0.1805
7	10	0.2102
8	2	0.2119
9	4	0.2124
10	126	0.2301
11	34	0.2368
12	87	0.2640
13	51	0.2658
14	95	0.2688
15	125	0.2874

Figure 9.35 is a graph of the normalized motion (motion generation) generated by the B-spline function using sixteen precision points. Compare this to the normalized trace point path in Figure 9.36.

The motion defined by the B-spline function was then normalized for position, rotation, scale and point spacing as described in Chapter 8. The normalized motion was then compared with each of the database solutions and evaluated with the following matching measures:

- Sum of absolute differences
- Amplitude and phase difference using Fourier descriptors

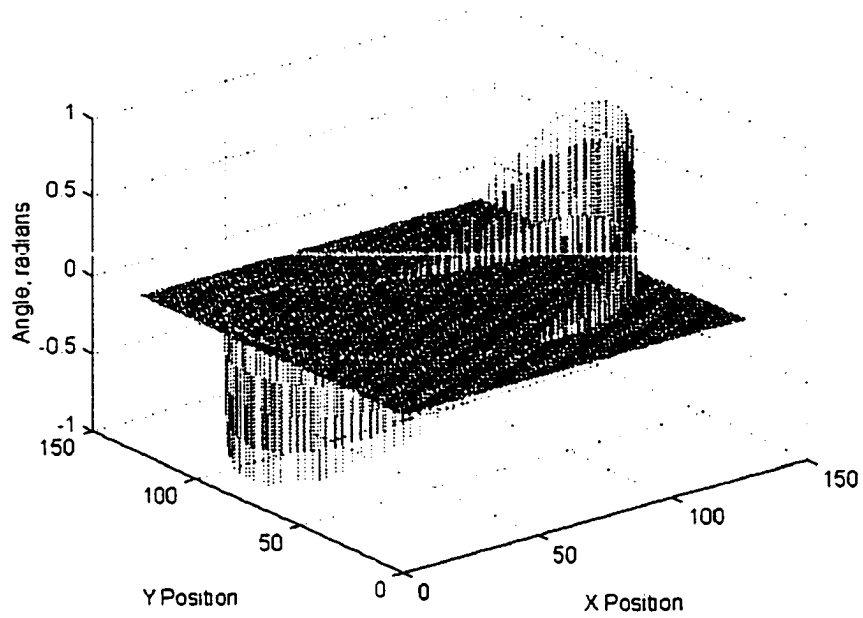


Figure 9.35: Normalized trace point motion generated by B-spline

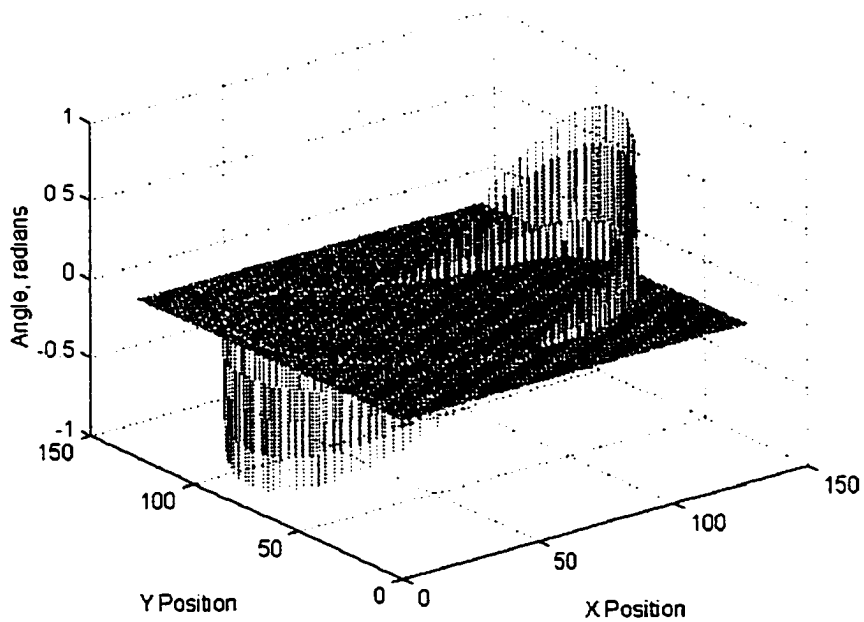


Figure 9.36: Normalized trace point motion generated four-bar mechanism

Sum of Absolute Differences - Motion Generation

The sum of the absolute difference when used with the desired motion is defined by equation 8.3. For evaluating the motion of the desired four-bar mechanism, the weighting factors, p and q , were each addressed a value of 0.5.

Figure 9.37 is a graph of the absolute difference measure of the desired motion with the 145 database candidate solutions. The top 5 matching candidate solutions were identified; the trace point paths are plotted in Figure 9.38, and the connecting rod angles are plotted in Figure 9.39. The 15 database trace point motion which had the smallest absolute differences values are listed in Table 9.13. Comparing the results with Table 8.1 shows that nine of the top ten candidate solutions are the same.

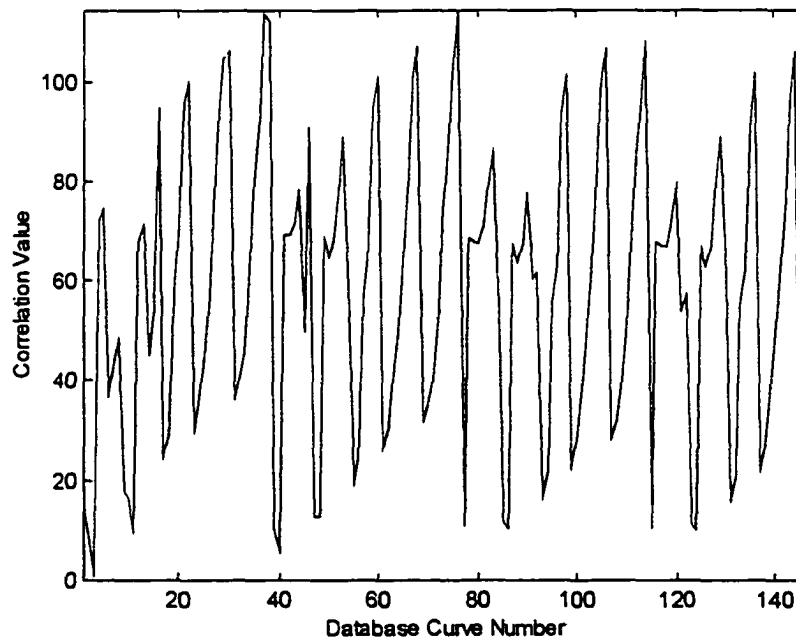


Figure 9.37: Graph of absolute difference of desired with 145 database candidate solutions - B-spline

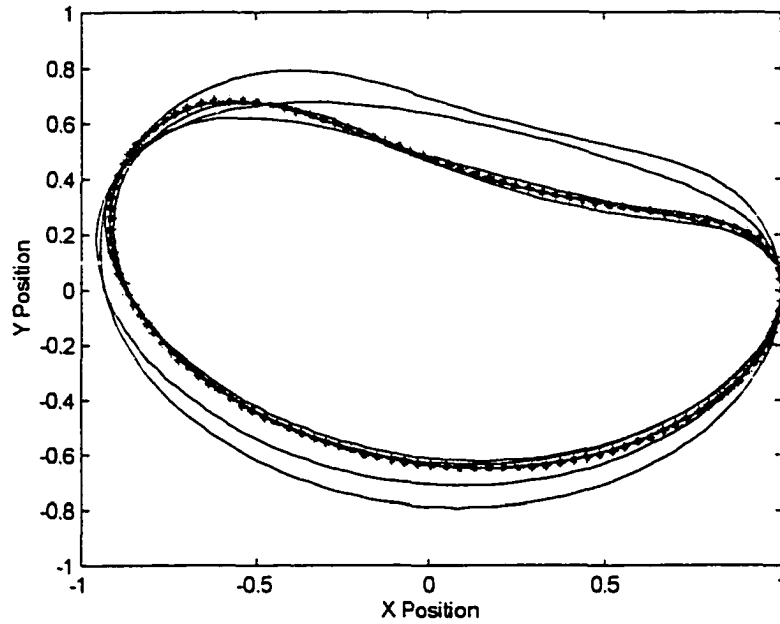


Figure 9.38: Graph of the top 5 database trace point paths identified by absolute difference measure (motion generation) - B-spline

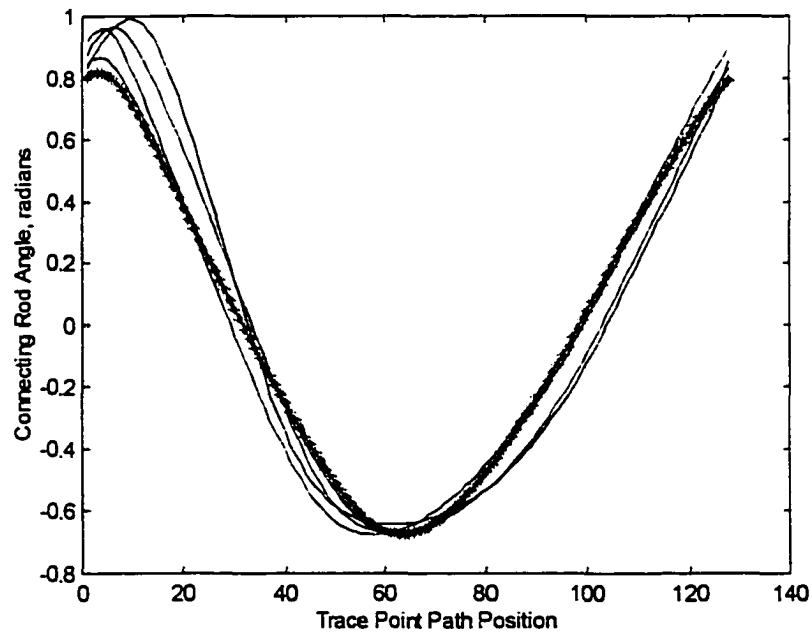


Figure 9.39: Graph of the top 5 database connecting rod angles identified by absolute difference measure (motion generation) - B-spline

Table 9.13: Summary of database search of trace point motion using absolute difference - B-Spline

Desired Curve - Database Curve #3

Search Rank	Database Curve Number	Absolute Difference
1	3	0.5246
2	40	5.9187
3	2	7.1485
4	11	9.8437
5	124	9.9720
6	115	10.2303
7	86	10.2718
8	39	10.4050
9	77	10.5367
10	123	11.1639
11	85	11.6717
12	48	12.6679
13	47	12.7882
14	1	14.4647
15	131	16.2312

Amplitude and Phase Difference Using Fourier Descriptors - Motion Generation

For evaluating the amplitude and phase difference using Fourier descriptors equation 7.15 was used to evaluate the difference measure for the desired motion with each of the database candidate solutions. The value used for n was 0.3. Equation 7.13 was used to evaluate a difference measure for the connecting rod angle of the desired connecting rod angle with each of the database solutions. The value used for n was 0.3. An overall measure was evaluated using equation 8.4. For evaluating the motion of the desired four-bar mechanism, the weighting factors, p and q , were each addressed a value of 0.5.

Figure 9.40 is a graph of the amplitude and phase difference of the desired motion with the 145 database candidate solutions. The top 5 matching candidate solutions were identified; the trace point paths are plotted in Figure 9.41, and the connecting rod angles are plotted in Figure 9.42. The 15 database trace point motion which had the smallest amplitude and phase difference are listed in Table 9.14. Comparing the results with Table 8.2 shows that ten of the top ten candidate solutions are the same.

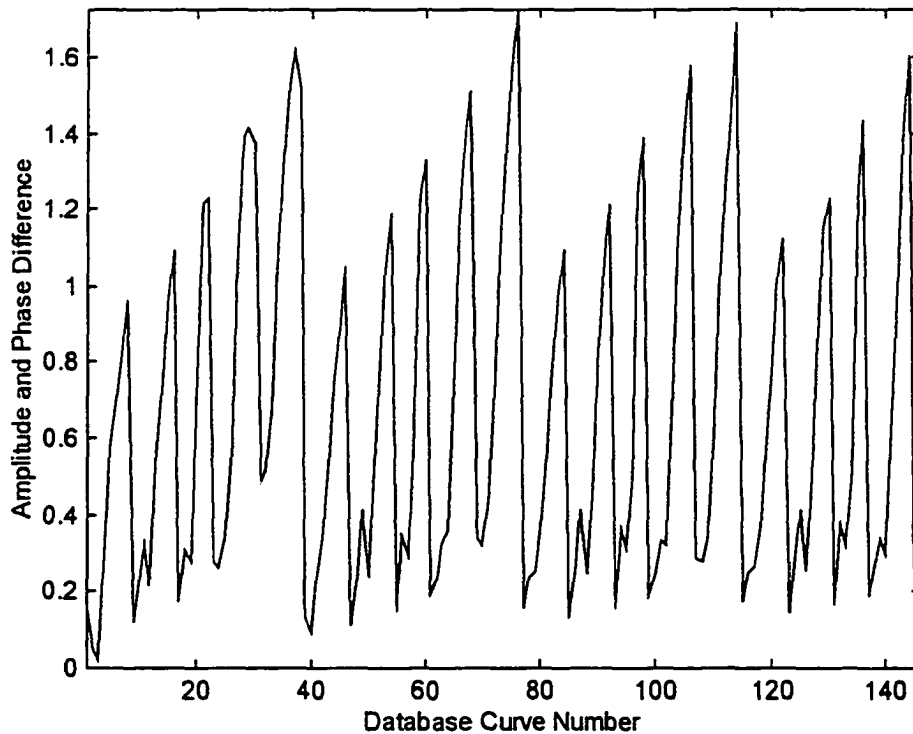


Figure 9.40: Graph of Fourier descriptor amplitude and phase difference measure of desired motion with 145 database trace point paths - B-spline

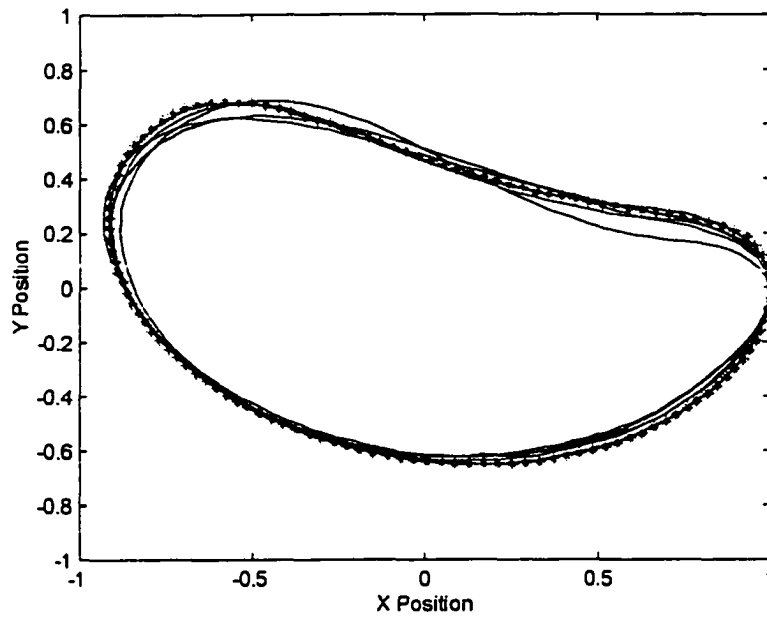


Figure 9.41: Graph of the top 5 database trace point paths identified by amplitude and phase difference of Fourier descriptors (motion generation) - B-spline

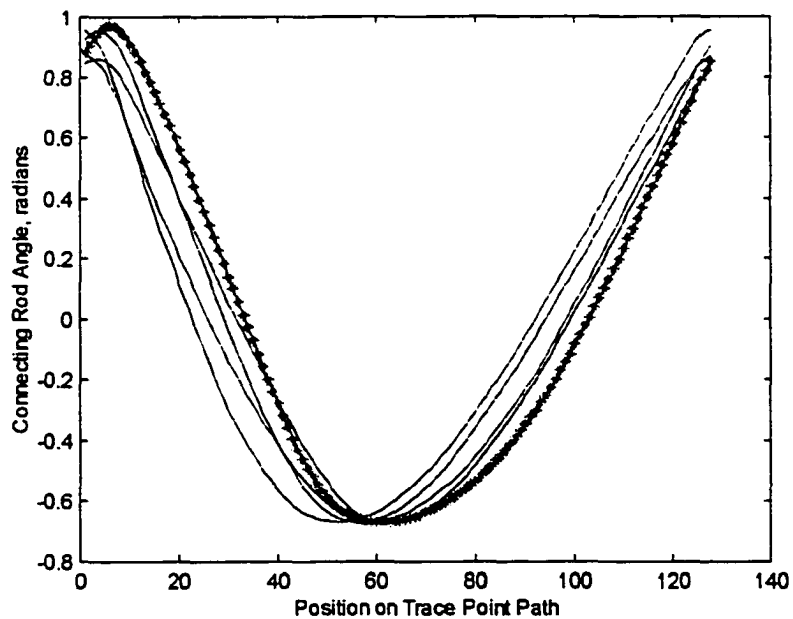


Figure 9.42: Graph of the top 5 database connecting rod angles identified by amplitude and phase difference of Fourier descriptors (motion generation) - B-spline

Table 9.14: Summary of database search of trace point motion using amplitude and phase difference measure of Fourier descriptors - B-Spline

Desired Curve - Database Curve #3

Search Rank	Database Curve Number	Amplitude and Phase Difference
1	3	0.0204
2	2	0.0483
3	40	0.0936
4	47	0.1103
5	9	0.1179
6	85	0.1310
7	39	0.1356
8	123	0.1430
9	55	0.1474
10	77	0.1551
11	93	0.1570
12	1	0.1583
13	131	0.1655
14	17	0.1725
15	115	0.1738

Sum of Absolute Differences - Partial Curve Motion Generation

The sum of the absolute difference when used with the desired motion is defined by equation 8.3. For evaluating the motion of the desired four-bar mechanism, the weighting factors, p and q , were each addressed a value of 0.5.

Figure 9.41 is a graph of the absolute difference measure of the desired motion with the 145 database candidate solutions. The top 5 matching candidate solutions were identified; the trace point paths are plotted in Figure 9.42, and the connecting rod angles are plotted in Figure 9.43. The 15 database trace point motion which had the smallest absolute differences values are listed in Table 9.15. Comparing the results with Table 8.4 shows that ten of the top ten candidate solutions are the same.

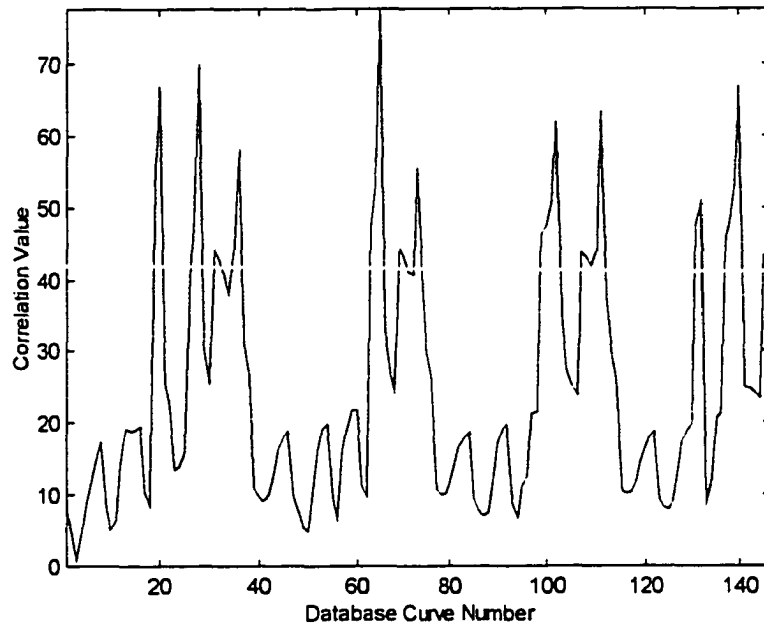


Figure 9.43: Graph of absolute difference of desired motion with 145 database trace point paths - B-spline

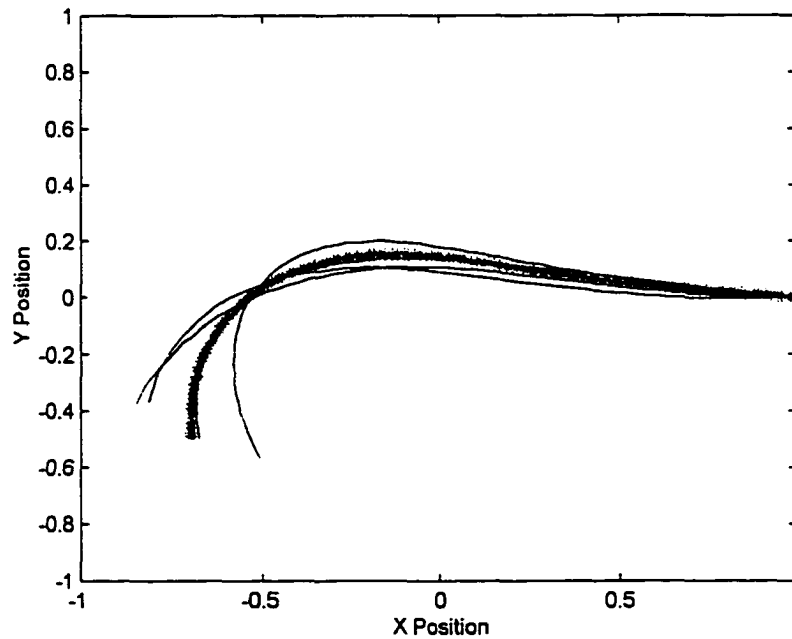


Figure 9.44: Graph of the top 5 database partial trace point paths identified by absolute difference measure (motion generation) - B-spline

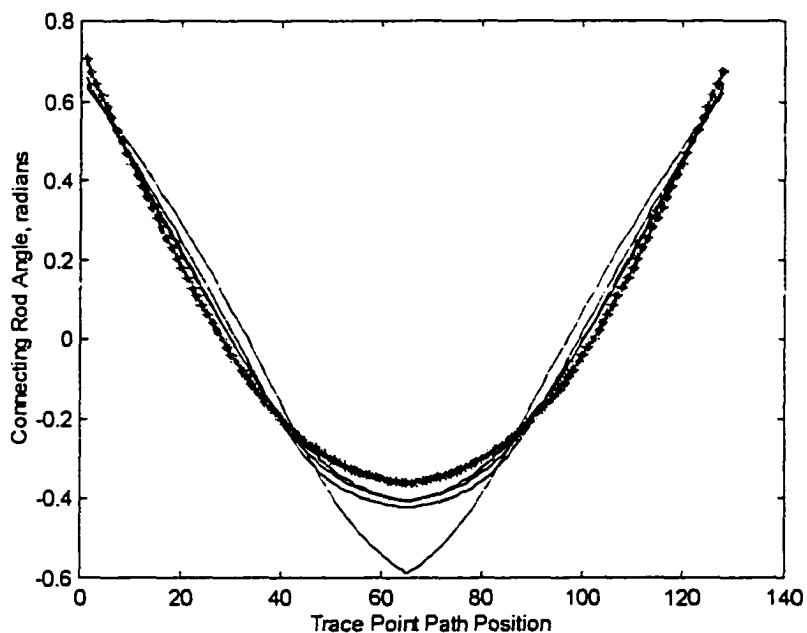


Figure 9.45: Graph of the top 5 database connecting rod angles identified by absolute difference measure (motion generation) - B-spline

Table 9.15: Summary of database search of trace point motion using absolute difference - B-Spline

Desired Curve - Database Curve #3

Search Rank	Database Curve Number	Absolute Difference
1	3	1.0089
2	2	4.3563
3	4	4.8136
4	50	4.9793
5	10	5.0491
6	49	5.4611
7	11	6.4738
8	56	6.6989
9	94	6.7575
10	87	6.9818
11	48	7.4387
12	1	7.5035
13	88	7.6442
14	86	7.8088
15	125	7.8773

.

**Amplitude and Phase Difference using Fourier Descriptors -
Partial Curve Motion Generation**

Equation 7.15 was used to evaluate the amplitude and phase difference for the desired motion with each of the database candidate solutions. The value used for n was 0.3. Equation 7.15 was also used to evaluate a difference measure for the connecting rod angle of the desired solution with each of the database solutions. The value used for n was 0.3. An overall measure was evaluated using equation 8.4. For evaluating the motion of the desired four-bar mechanism, the weighting factors, p and q , were each addressed a value of 0.5.

Figure 9.41 is a graph of the absolute difference measure of the desired motion with the 145 database candidate solutions. The top 5 matching candidate solutions were identified; the trace point paths are plotted in Figure 9.42, and the connecting rod angles are plotted in Figure 9.43. The 15 database trace point motion which had the smallest amplitude and phase difference of the Fourier descriptors are listed in Table 9.16. Comparing the results with Table 8.5 shows that ten of the top ten candidate solutions are the same.

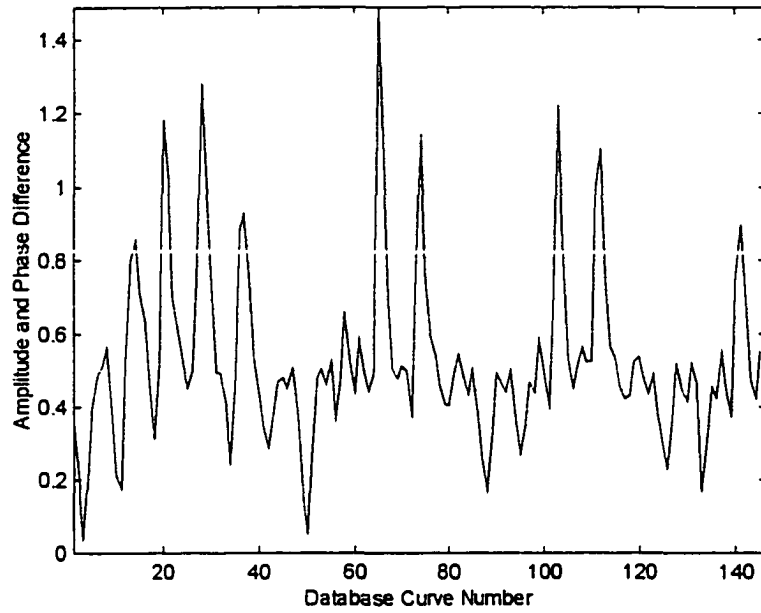


Figure 9.46: Graph of Fourier descriptor amplitude and phase difference measure of desired motion with 145 database candidate solutions - B-spline

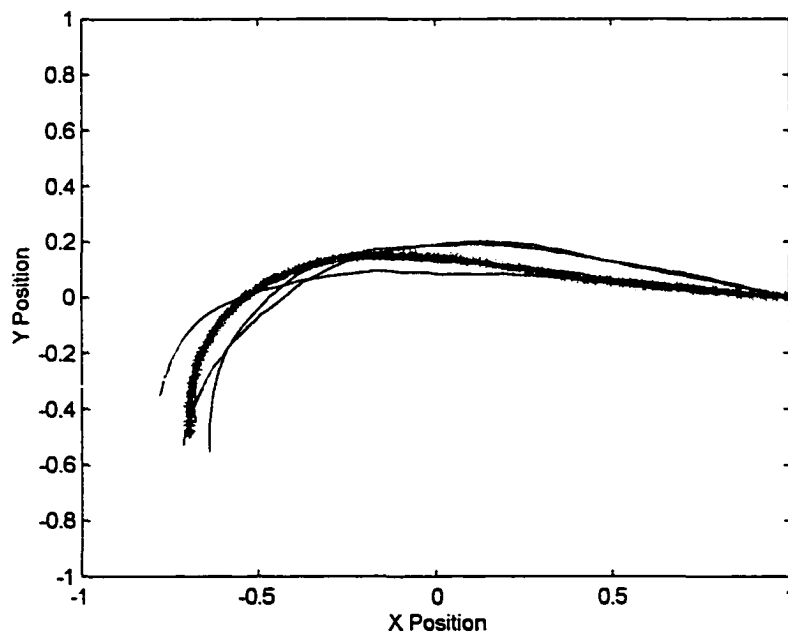


Figure 9.47: Graph of the top 5 database partial trace point paths identified by amplitude and phase difference of Fourier descriptors (motion generation) - B-spline

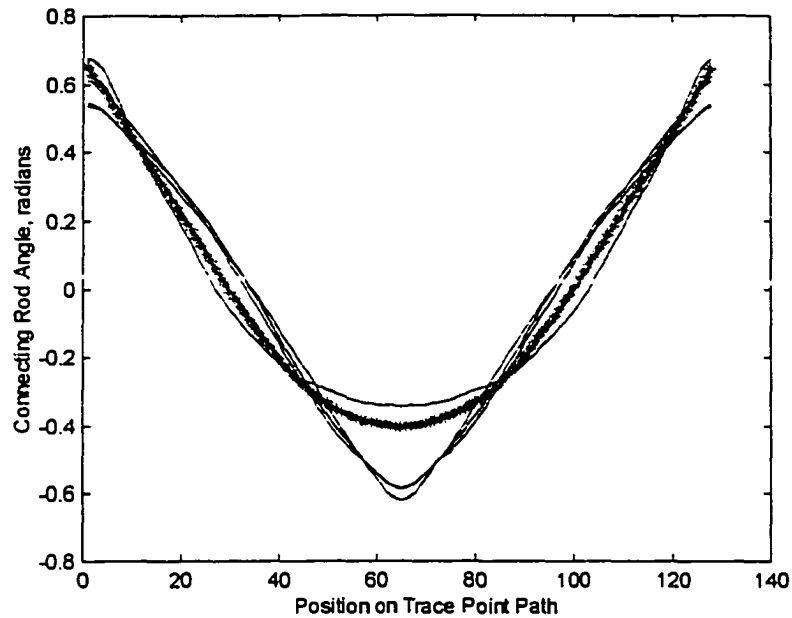


Figure 9.48: Graph of the top 5 database connecting rod angles identified by amplitude and phase difference of Fourier descriptors (motion generation) - B-spline

Table 9.16: Summary of database search of trace point motion using amplitude and phase difference measure of Fourier descriptors - B-Spline

Desired Curve - Database Curve #3

Search Rank	Database Curve Number	Amplitude and Phase Difference
1	3	0.0317
2	50	0.0468
3	133	0.1631
4	88	0.1675
5	11	0.1741
6	49	0.1805
7	10	0.2102
8	2	0.2119
9	4	0.2124
10	126	0.2301
11	34	0.2368
12	87	0.2640
13	51	0.2654
14	95	0.2688
15	125	0.2874

Summary

Cubic splines and B-splines were successfully used to generate partial curves and closed curves to represent desired solutions for the synthesis of four-bar mechanisms. Sixteen points on database curve number 3 were used to generate closed curves and partial curves for path generation and motion generation. The database matching measure was the absolute difference and the amplitude and phase difference measure of Fourier descriptors. Table 9.16 is a summary of the top 10 closed trace point paths identified when using cubic splines and B-splines with the database matching measures. Table 9.17 is a summary of the of the top 10 partial trace point paths identified when using cubic splines and B-splines with the database matching measures. Table 9.18 is a summary of the of the top 10 closed trace point motion solutions identified when using cubic splines and B-splines with the database matching measures. Table 9.19 is a summary of the of the top 10 partial trace point motion solutions identified when using cubic splines and B-splines with the database matching measures.

These results show that both cubic splines and B-splines perform well in representing trace point path and motion solutions using 16 precision points. With closed trace point paths, when using the amplitude and phase difference of Fourier descriptors measure and cubic or B-spline generated curves, four of the top five solutions were the same as identified by using the original

curve and an absolute difference search measure. Nine (cubic spline) and eight (B-Spline) of the top ten were the same.

With partial trace point paths, when using the amplitude and phase difference of Fourier descriptors measure and cubic or B-spline generated curves, three of the top five solutions were the same as identified by using the original curve and an absolute difference search measure. Seven (cubic spline) and eight (B-Spline) of the top ten were the same.

With full crank rotation with motion generation, when using the amplitude and phase difference of Fourier descriptors measure and cubic or B-spline generated curves, three of the top five solutions were the same as identified by using the original curve and an absolute difference search measure. Five (cubic spline) and six (B-Spline) of the top ten were the same.

With partial crank rotation with motion generation, when using the amplitude and phase difference of Fourier descriptors measure and cubic or B-spline generated curves two of the top five were the same as identified by using the original curve and an absolute difference search measure. Seven of the top ten were the same.

Table 9.17: Performance of cubic splines and B-splines for path generation using 16 data points from database curve number 3 - full crank rotation

Top Ranked File No.	1	2	3	4	5	6	7	8	9	10
Four-bar										
SAD	<u>3</u>	<u>2</u>	<u>40</u>	<u>47</u>	<u>85</u>	123	9	55	93	131
Cubic Spline										
SAD	<u>3</u>	<u>2</u>	9	<u>40</u>	<u>47</u>	55	85	17	123	93
FlAP	<u>3</u>	<u>2</u>	<u>40</u>	9	<u>47</u>	85	55	123	93	39
B-Spline										
SAD	<u>3</u>	<u>2</u>	<u>40</u>	<u>47</u>	<u>85</u>	123	9	55	93	131
FlAP	<u>3</u>	<u>2</u>	<u>40</u>	<u>47</u>	9	85	39	123	55	77

Table 9.18: Performance of cubic splines and B-splines for path generation using 16 data points from database curve number 3 - partial crank rotation

Top Ranked File No.	1	2	3	4	5	6	7	8	9	10
Four-bar										
SAD	<u>3</u>	<u>50</u>	<u>49</u>	<u>88</u>	<u>10</u>	4	2	134	126	87
Cubic Spline										
SAD	<u>3</u>	<u>50</u>	<u>49</u>	<u>88</u>	<u>10</u>	4	2	126	87	134
FlAP	<u>3</u>	<u>50</u>	133	<u>88</u>	11	49	4	10	2	34
B-Spline										
SAD	<u>3</u>	<u>50</u>	<u>49</u>	<u>88</u>	<u>10</u>	4	2	126	87	11
FlAP	<u>3</u>	<u>50</u>	133	<u>88</u>	11	49	10	2	4	126

Table 9.19: Performance of cubic splines and B-splines for motion generation using 16 data points from database curve number 3 - full crank rotation

Top Ranked File No.	1	2	3	4	5	6	7	8	9	10
Four-bar										
SAD	<u>3</u>	<u>40</u>	<u>2</u>	<u>11</u>	<u>124</u>	115	39	86	77	123
Cubic Spline										
SAD	<u>3</u>	<u>2</u>	<u>40</u>	86	<u>124</u>	39	77	115	48	123
F1AP	<u>3</u>	<u>2</u>	<u>40</u>	9	47	85	55	123	93	39
B-Spline										
SAD	<u>3</u>	<u>40</u>	<u>2</u>	<u>11</u>	<u>124</u>	115	86	39	77	123
F1AP	<u>3</u>	<u>2</u>	<u>40</u>	47	9	85	39	123	55	77

Table 9.20: Performance of cubic splines and B-splines for motion generation using 16 data points from database curve number 3 - partial crank rotation

Top Ranked File No.	1	2	3	4	5	6	7	8	9	10
Four-bar										
SAD	<u>3</u>	<u>2</u>	<u>4</u>	<u>50</u>	<u>10</u>	49	11	56	94	87
Cubic Spline										
SAD	<u>3</u>	<u>2</u>	<u>4</u>	<u>50</u>	<u>10</u>	49	11	56	94	87
F1AP	<u>3</u>	<u>50</u>	133	88	11	49	4	10	2	36
B-Spline										
SAD	<u>3</u>	<u>2</u>	<u>4</u>	<u>50</u>	<u>10</u>	49	11	56	94	87
F1AP	<u>3</u>	<u>50</u>	133	88	11	49	10	2	4	126

CHAPTER 10. DATABASE GENERATION

The focus of the designer in synthesizing a function, path or motion generation mechanism is to identify the best solution, or solutions, which will fulfill a set of design requirements. This essentially is a nonlinear optimization problem. As has been discussed, the general behavior of the function that describes the function, path or motion of a mechanism within a design space is not known. As a result, the use of numerical techniques to find an optimal solution is dependent on the initial guess of the mechanism. An optimal solution may be identified for a local design space while an optimal global solution remains unidentified. Since the behavior of the function is unknown over the design space, the designer has no way of understanding if a global solution is ever obtained.

Jovanovic and Kazerounian [1998] presented a novel method for locating global minima in nonlinear design optimization problems. The method was based on utilizing fractal areas to locate all the solutions along one direction in variable space. A search was started at an arbitrary point in the design space. A randomly chosen direction in the design space was identified and solutions

along that direction obtained. The process continued until an optimal design was obtained.

In most cases, the designer has an understanding of many of the design constraints that the final design must conform to. Examples of design constraints could be the type of mechanism, space limitations to the overall motion of the system, ground pivot locations, or the minimum transmission angle. The design constraints used in the synthesis process may reduce the scope of the nonlinear optimization problem from identifying a global design space solution(s) to a local design space solution(s).

In this chapter, a method for generating a database of candidate solutions is developed based on a random local design space search and a solution refinement process. The generation of candidate solutions is based on generating random system variables that meet the requirements of a specific type of mechanism (crank-rocker, double-crank or double-rocker) and then ensuring that the mechanism conforms to the design constraints known by the designer. A database of candidate solutions is developed and then a desired solution is compared with the generated database of solutions. The candidate solution that has the best match with the desired solution is then identified. A refinement process is then started by generating a second database of candidate solutions developed around the identified candidate solution using small changes to the system variables of the identified candidate solution. This refinement process is repeated until a limit is reached in the function that measures the similarity between the

candidate solution and the desired solution. The overall process may be repeated to generate additional candidate solutions.

This process was evaluated with a specific example. A crank-rocker mechanism was selected as the "mechanism type" and design constraints defined which allowed a local design space to be specified. A desired trace point path curve was then generated.

For the database generation test the following constraints were implemented which defined the class of operation for the mechanism as a crank-rocker four-bar mechanism:

- The drive crank is one unit of length
- The drive crank is the shortest length:
 - Drive Crank Length (DC) < Ground Pivot Distance (GPD)
 - Drive Crank Length (DC) < Connecting Rod Length (CR)
 - Drive Crank Length (DC) < Follower Crank Length (FC)
- $GPD + DC < CR + FC$
- $GPD - DC > |CR - FC|$

The following constraints were implemented which defined limitations on the size and function of the mechanism:

- The Ground Pivot Distance is between 1 and 5 units
- The Follower Crank is between 1 and 4 units
- The Connecting Rod Length is between 1 and 4 units
- The Trace Point Distance is within the following distance of the center of the Connecting Rod:
 - $TPD = CR/2 + DC$

- The transmission angle is constrained from 40° to 140°

The amplitude and phase difference using one-dimensional Fourier descriptors was used to evaluate the similarity between the desired curve with the generated candidate curves. The desired trace point path used is the same path generated by the B-spline function using sixteen precision points in Chapter 9 (Figure 9.25).

The process was set to generate a database of 500 candidate trace point paths that met the constraint requirements previously defined. Figure 10.1 is a graph of the amplitude and phase difference of the desired trace point path with the paths of the 500 candidate curves.

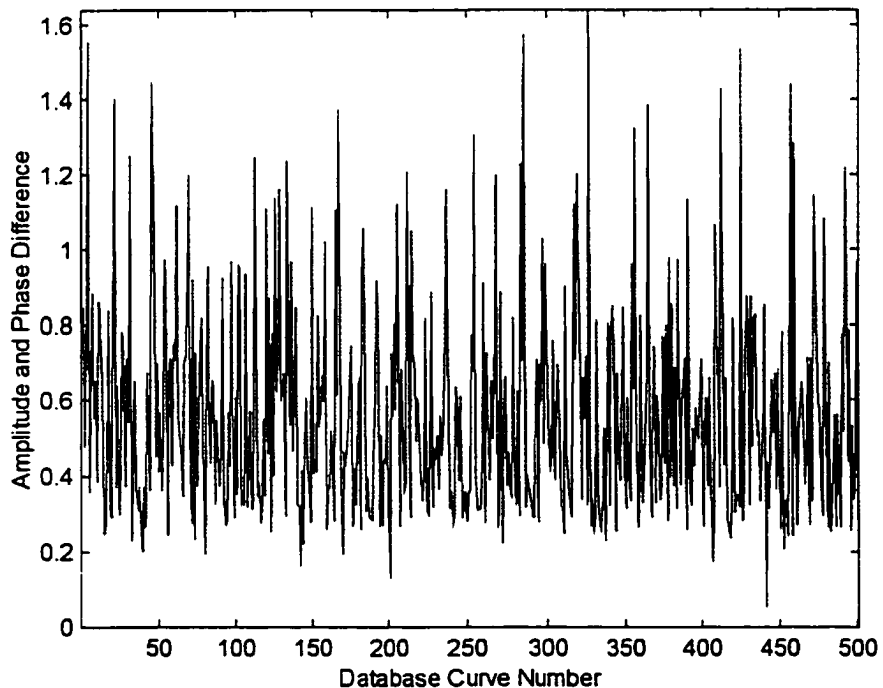


Figure 10.1: Graph of amplitude and phase difference of Fourier descriptors of desired trace point path and 500 candidate paths

The top 15 database trace point paths that had the smallest amplitude and phase difference are listed in Table 10.1. The time to generate the database of 500 curves was 20.4 minutes. The time to search the entire database and generate the amplitude and phase difference of the Fourier descriptors was 22.3 seconds.

Table 10.1: Summary of database search of 500 candidate trace point paths using amplitude and phase difference

Search Rank	Database Curve Number	Amplitude and Phase Difference
1	441	0.0496
2	201	0.1297
3	142	0.1589
4	407	0.1739
5	80	0.1913
6	170	0.1921
7	39	0.2007
8	453	0.2025
9	272	0.2199
10	144	0.2209
11	33	0.2266
12	338	0.2285
13	73	0.2307
14	459	0.2390
15	456	0.2408

Database curve number 441 was identified as the best match with the desired solution. A refinement process then generated a second database of candidate solutions developed around the identified candidate solution. Small random modifications were made to the system variables of the identified candidate solution. The length of the connecting rod, follower crank, ground pivot

distance, trace point distance, and trace point angle were randomly varied within $\pm 10\%$ from the defined value of the candidate solution. A total of 50 database curves were generated during the refinement process. The process was checked to ensure that the constraint requirements previously defined were met. Figure 10.2 is a graph of the amplitude and phase difference of the desired trace point path with the paths of the initially generated 500 candidate curves and the additional 50 database curves generated in the refinement process. The top 15 database trace point paths that had the smallest amplitude and phase difference are listed in Table 10.2. The candidate solution that had the best match with the desired solution was identified as database curve number 522.

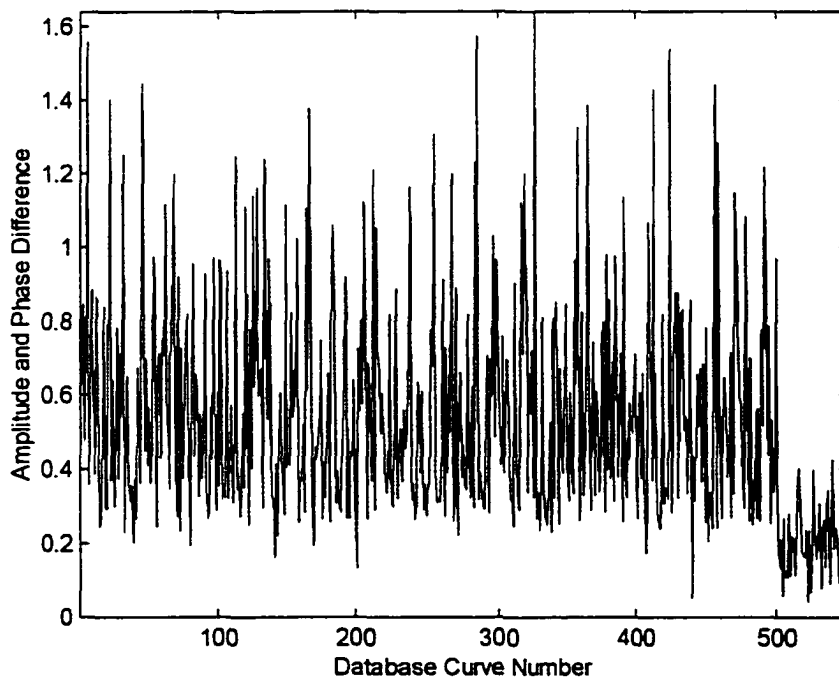


Figure 10.2: Graph of amplitude and phase difference of Fourier descriptors of desired trace point path and 550 candidate paths

Table 10.2: Summary of database search of 550 candidate trace point paths using amplitude and phase difference

Search Rank	Database Curve Number	Amplitude and Phase Difference
1	522	0.0416
2	441	0.0496
3	504	0.0580
4	548	0.0658
5	525	0.0666
6	532	0.0753
7	538	0.0872
8	545	0.0911
9	507	0.1077
10	508	0.1095
11	510	0.1109
12	513	0.1137
13	201	0.1297
14	547	0.1307
15	506	0.1324

A second refinement process was then started by generating a third database of candidate solutions developed around the refined candidate solution. Again, small changes were made to the system variables of the refined candidate solution. The length of the connecting rod, follower crank, ground pivot distance, trace point distance, and trace point angle were allowed to randomly vary $\pm 1\%$ from the defined value of the candidate solution. A total of 50 database curves were generated during the second refinement process. The process was checked to ensure that the constraint requirements previously defined were met. Figure 10.3 is a graph of the amplitude and phase difference of the desired trace point path with the paths of the initially generated 500 candidate curves, the 50 database curves generated in the first refinement process, and the 50 database curves generated in the second

refinement process. The top 15 database trace point paths that had the smallest amplitude and phase difference are listed in Table 10.3. The candidate solution that had the best match with the desired solution was identified as database curve number 597. Figure 10.4 is a graph of the desired curve with the best generated candidate curve. The configuration of the drive-crank mechanisms that generated curve number 597 is:

Drive Crank Length	=	1.0000 units
Connecting Rod Length	=	2.1741 units
Ground Pivot Distance	=	1.5998 units
Follower Crank Length	=	2.4344 units
Trace Point Distance	=	2.4160 units
Trace Point Angle	=	0.4827 radians

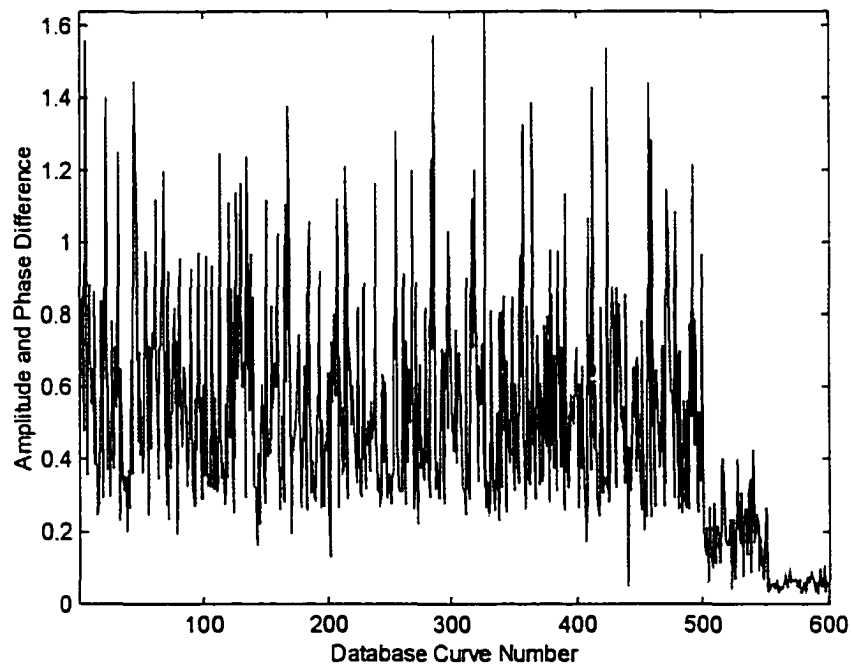


Figure 10.3: Graph of amplitude and phase difference of Fourier descriptors of desired trace point path and 600 candidate paths

Table 10.3: Summary of database search of 600 candidate trace point paths using amplitude and phase difference

Search Rank	Database Curve Number	Amplitude and Phase Difference
1	597	0.0319
2	578	0.0331
3	592	0.0345
4	579	0.0352
5	561	0.0367
6	551	0.0379
7	552	0.0388
8	522	0.0416
9	563	0.0417
10	554	0.0424
11	559	0.0438
12	557	0.0446
13	589	0.0458
14	581	0.0460
15	595	0.0474

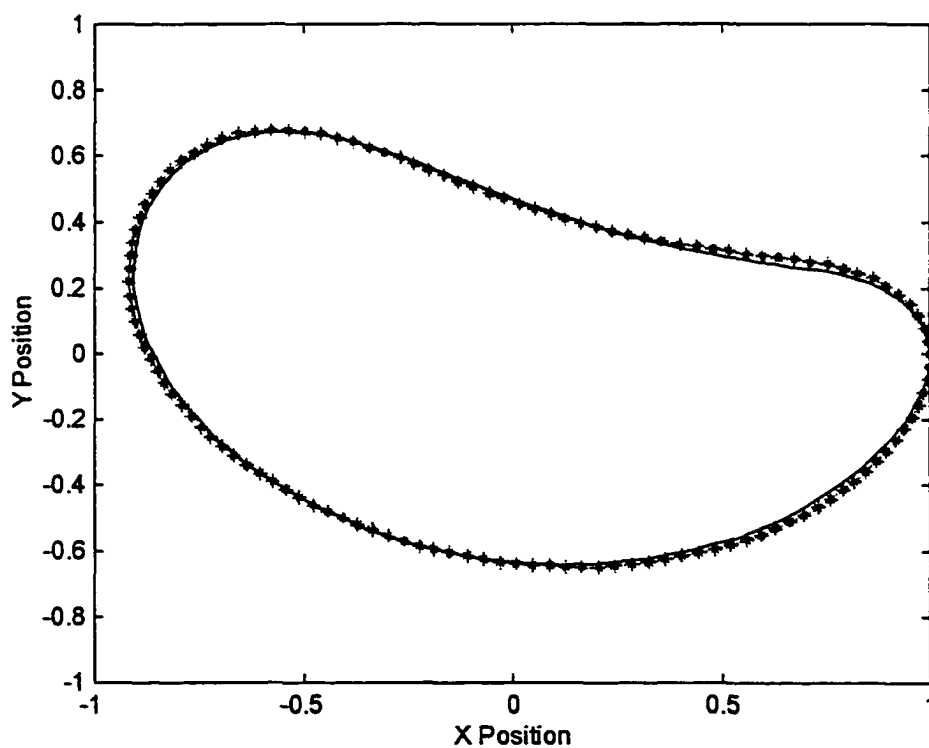


Figure 10.4: Graph of synthesized trace point path using amplitude and phase difference measure of Fourier descriptors

This random search process was repeated ten times to generate a selection of candidate curves. Table 10.4 is a summary of the curves identified, the mechanism configuration and the value of the amplitude and phase difference of the Fourier descriptors. Appendix C contains graphs of each trace point path and four-bar mechanism synthesized.

Table 10.4: Summary of candidate trace point paths generated through the random search and refinement process

Curve	DC	CR	FC	GPD	TPD	TPA	A&P Diff.
1	1.0000	2.1741	2.4344	1.5998	2.4160	0.4827	0.0319
2	1.0000	3.5891	3.4255	1.6354	4.0794	0.3554	0.0308
3	1.0000	2.2816	2.5814	1.7054	2.7172	0.4808	0.0377
4	1.0000	1.9038	2.0929	1.6251	2.4368	0.4962	0.0359
5	1.0000	1.8380	1.6752	1.5498	2.4936	0.4923	0.0325
6	1.0000	2.3015	1.6801	1.8183	2.5273	0.5605	0.0428
7	1.0000	3.1259	2.9017	1.6391	3.3870	0.4192	0.0372
8	1.0000	1.5118	1.8548	1.6616	1.9443	0.5345	0.0271
9	1.0000	1.7446	2.3512	1.9543	2.4541	0.4590	0.0707
10	1.0000	2.9716	2.6252	1.6856	3.2038	0.4497	0.0386

This database generation and search process was evaluated with a partial trace point path example. A crank-rocker mechanism was selected as the "mechanism type" and design constraints defined which allowed a local design space to be specified. A desired partial trace point path curve was then generated.

For the crank-rocker four-bar mechanism the following constraints were implemented which defined the class of operation for the mechanism:

- The drive crank is one unit of length

- The drive crank is the shortest length:
 - Drive Crank Length (DC) < Ground Pivot Distance (GPD)
 - Drive Crank Length (DC) < Connecting Rod Length (CR)
 - Drive Crank Length (DC) < Follower Crank Length (FC)
- $GPD + DC < CR + FC$
- $GPD - DC > |CR - FC|$

The following constraints were implemented which defined limitations on the size and function of the mechanism:

- The Ground Pivot Distance is between 1 and 5 units
- The Follower Crank is between 1 and 4 units
- The Connecting Rod Length is between 1 and 4 units
- The Trace Point Distance is within the following distance of the center of the Connecting Rod:
 - $TPD = CR/2 + DC$
- The transmission angle is constrained from 40° to 140°
- The minimum crank angle rotation was 45°
- The maximum crank angle rotation was 270°

The amplitude and phase difference using one-dimensional Fourier descriptors was used to evaluate the similarity between the desired curve with the generated candidate curves. The desired trace point path used is the same path generated by the B-spline function using sixteen precision points in Chapter 9 (Figure 9.32).

The process was set to generate a database of 500 candidate trace point paths that met the constraint requirements previously defined. Figure 10.6 is a graph of the amplitude and phase difference of the desired trace point path with the paths of the 500 candidate curves.

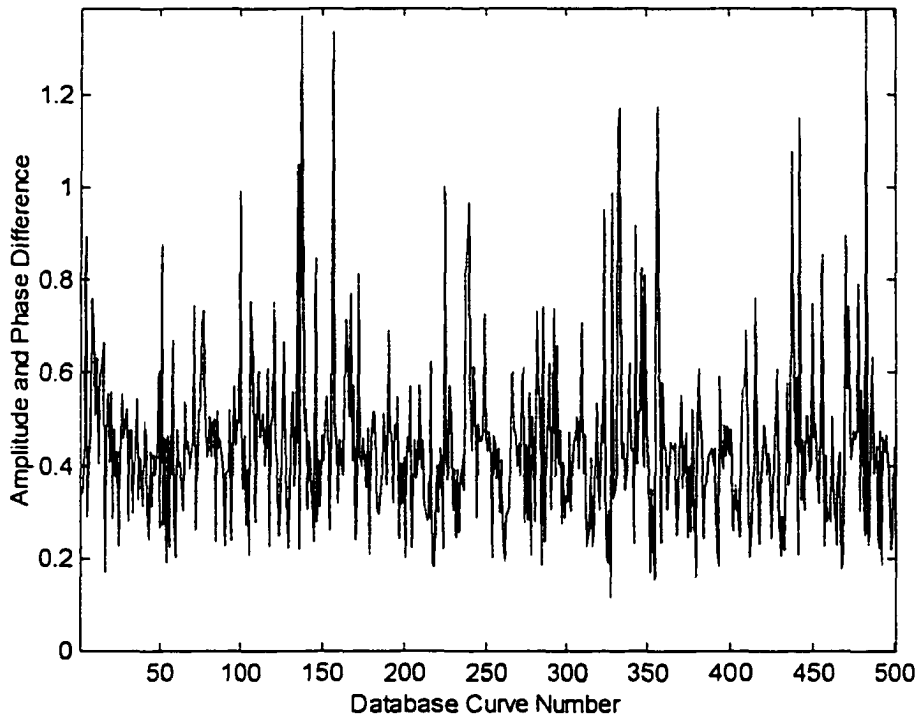


Figure 10.5: Graph of amplitude and phase difference of Fourier descriptors of desired partial trace point path and 500 candidate paths

The top 15 database trace point paths that had the smallest amplitude and phase difference are listed in Table 10.5. The time to generate the database of 500 curves was 19.0 minutes. The time to search the entire database and generate the amplitude and phase difference of the Fourier descriptors was 22.3 seconds.

Table 10.5: Summary of database search of 500 candidate partial trace point paths using amplitude and phase difference

Search Rank	Database Curve Number	Amplitude and Phase Difference
1	113	0.1468
2	262	0.1486
3	203	0.1572
4	37	0.1603
5	383	0.1661
6	346	0.1695
7	75	0.1787
8	391	0.1795
9	277	0.1855
10	340	0.1885
11	61	0.1929
12	358	0.1929
13	461	0.1930
14	433	0.1949
15	197	0.1996

Database curve number 113 was identified as the best match with the desired solution. A refinement process then generated a second database of candidate solutions developed around the identified candidate solution. Small random modifications were made to the system variables of the identified candidate solution. The length of the connecting rod, follower crank, ground pivot distance, trace point distance, trace point angle, drive crank starting angle and drive crank stopping angle were randomly varied within $\pm 10\%$ from the defined value of the candidate solution. A total of 50 database curves were generated during the refinement process. The process was checked to ensure that the constraint requirements previously defined were met. Figure 10.7 is a graph

of the amplitude and phase difference of the desired trace point path with the paths of the initially generated 500 candidate curves and the additional 50 database curves generated in the refinement process. The top 15 database trace point paths that had the smallest amplitude and phase difference are listed in Table 10.6. The candidate solution that had the best match with the desired solution was identified as database curve number 503.

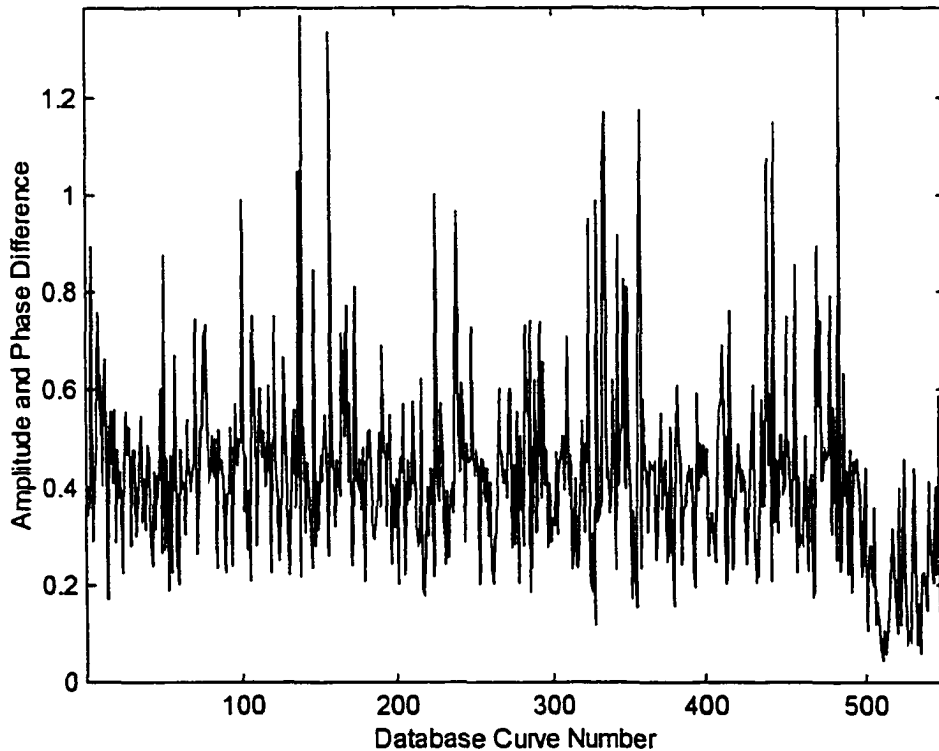


Figure 10.6: Graph of amplitude and phase difference of Fourier descriptors of desired partial trace point path and 550 candidate paths

Table 10.6: Summary of database search of 550 candidate partial trace point paths using amplitude and phase difference

Search Rank	Database Curve Number	Amplitude and Phase Difference
1	503	0.1386
2	530	0.1424
3	113	0.1468
4	292	0.1496
5	526	0.1531
6	523	0.1531
7	203	0.1572
8	521	0.1580
9	37	0.1603
10	508	0.1608
11	514	0.1649
12	383	0.1661
13	550	0.1664
14	346	0.1695
15	512	0.1730

A second refinement process was then started by generating a third database of candidate solutions developed around the refined candidate solution. Again, small changes were made to the system variables of the refined candidate solution. The length of the connecting rod, follower crank, ground pivot distance, trace point angle, drive crank starting angle and drive crank stopping angle were allowed to randomly vary $\pm 1\%$ from the defined value of the candidate solution. A total of 50 database curves were generated during the second refinement process. The process was checked to ensure that the constraint requirements previously defined were met. Figure 10.8 is a graph of the amplitude and phase difference of the desired trace point path with the paths of the initially generated 500 candidate curves, the 50 database curves generated in the first refinement process, and the 50 database curves

generated in the second refinement process. The top 15 database trace point paths that had the smallest amplitude and phase difference are listed in Table 10.7. The candidate solution that had the best match with the desired solution was identified as database curve number 600. Figure 10.9 is a graph of the desired curve with the top candidate curve. The configuration of the drive-crank mechanisms that generated curve number 600 is:

Drive Crank Length	=	1.0000 units
Connecting Rod Length	=	3.3738 units
Ground Pivot Distance	=	2.7472 units
Follower Crank Length	=	2.7892 units
Trace Point Distance	=	1.3096 units

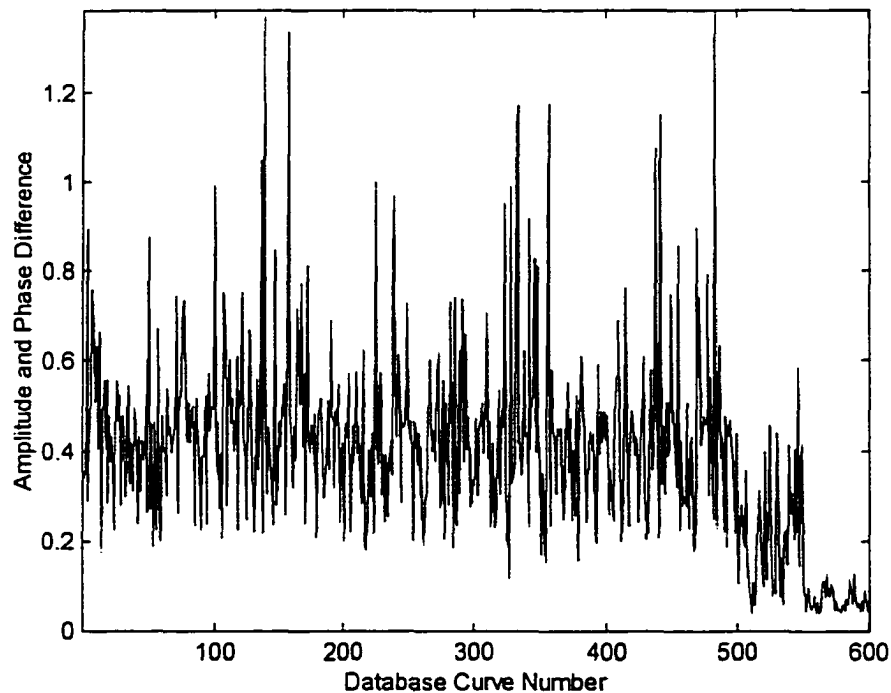


Figure 10.7: Graph of amplitude and phase difference of Fourier descriptors of desired partial trace point path and 600 candidate paths

Table 10.7: Summary of database search of 600 candidate partial trace point paths using amplitude and phase difference

Search Rank	Database Curve Number	Amplitude and Phase Difference
1	600	0.1325
2	557	0.1332
3	581	0.1338
4	565	0.1346
5	583	0.1346
6	561	0.1357
7	596	0.1361
8	597	0.1380
9	503	0.1386
10	564	0.1393
11	553	0.1403
12	595	0.1404
13	598	0.1409
14	530	0.1424
15	554	0.1428

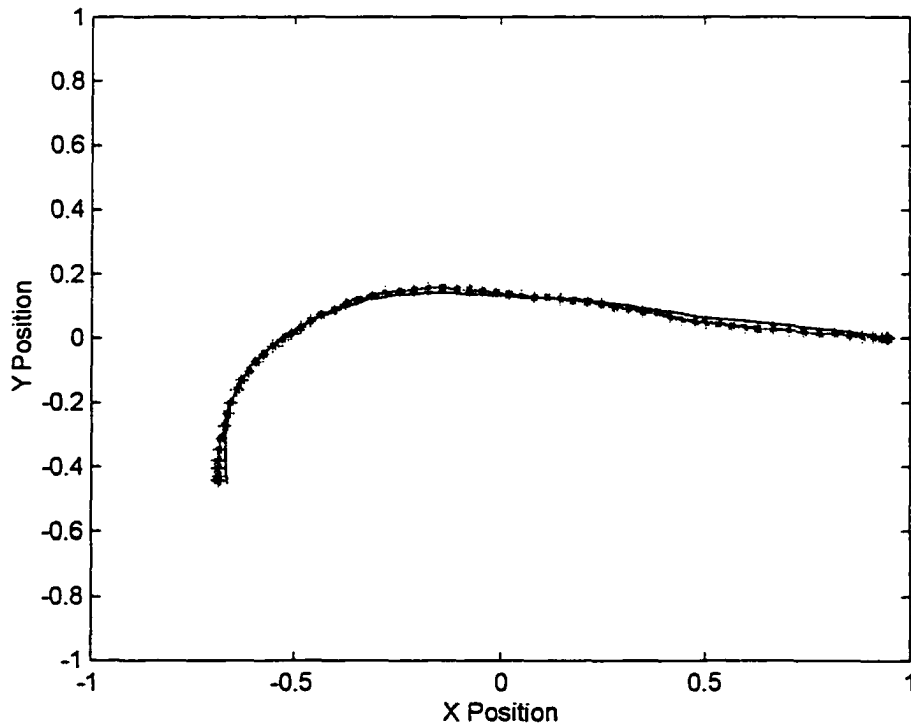


Figure 10.8: Graph of synthesized partial trace point path using amplitude and phase difference measure of Fourier descriptors

Trace Point Angle	=	0.1991 radians
Crank Angle Start	=	187.71 radians
Crank Angle Stop	=	258.79 radians

This random search process was repeated ten times to generate a selection of candidate curves. Table 10.8 is a summary of the curves identified, the mechanism configuration and the value of the amplitude and phase difference of the Fourier descriptors. Appendix C contains graphs of each trace point path and four-bar mechanism synthesized.

Table 10.8: Summary of candidate partial trace point paths generated through the random search and refinement process

Curve	CR	FC	GPD	TPD	TPA	AStart	AStop	A&P Diff.
1	3.0768	3.6118	1.8865	2.9217	0.5282	18	101	0.0404
2	3.2818	2.8000	2.5018	1.6665	0.6599	8	54	0.0725
3	3.3738	2.7892	2.7472	1.3096	0.1991	188	259	0.1325
4	2.7002	3.3017	2.2239	3.4412	-0.3120	8	185	0.0438
5	1.5847	3.6657	3.0871	1.0736	0.0440	12	99	0.0489
6	2.5390	3.3317	3.3517	1.3837	-0.3551	1	55	0.0678
7	1.8043	3.7563	3.0864	1.2497	-0.1399	7	85	0.0491
8	2.0111	4.0014	3.3027	1.4625	0.9476	50	114	0.0854
9	3.3465	2.4488	2.1415	3.1445	-1.0256	1	72	0.0260
10	2.8575	3.6647	2.0471	3.8274	-0.4980	4	115	0.0307

CHAPTER 11. CONCLUSIONS

This dissertation set out to develop an approach for the synthesis of four-bar planar function, path and motion mechanisms based upon the use of invariant descriptors to characterize a solution, to store the characteristic information in a database, and for use in solution comparison and matching methods. In addition, a methodology was developed to allow a designer to investigate a local design space by generating a database of candidate solutions based on the random development of a type of four-bar mechanism that met specified design constraints.

Various methods were developed to characterize solutions to function, path and motion four-bar mechanisms. The methods used to characterize solutions addressed both closed curves, generated by full drive crank rotation of crank-rocker mechanisms, and partial curves generated by the movement of the drive crank through a specified angle. These methods used spatial transformation, Fourier transformations and invariant moments. Each method was implemented and was shown to have the capability to characterize the function, path and motion of a four-bar mechanism.

Various search methods were implemented to evaluate the similarity of a desired solution with candidate solutions. A thorough comparison of each search method was conducted. An application model built upon MATLAB was developed to evaluate the performance of the various transformations, file storage and search methods for function, path and motion generation four-bar mechanisms. Over 8,000 candidate solutions were generated with respect to spatial transformations, one-dimensional Fourier transformations, two-dimensional Fourier transformations, and invariant moments.

Candidate solutions for function generation four-bar mechanisms were generated and characterized with spatial transforms and Fourier transforms. Search methods used to match a desired solution with a database of candidate solutions were: normalized cross correlation, absolute difference measure, sum squared difference measure, correlation using Fourier descriptors, phase only filtering in the frequency domain, symmetric phase-only matched filter, amplitude difference of the Fourier descriptors, and amplitude and phase difference of Fourier descriptors. The measure of similarity that had the lowest error was the absolute difference matching. This comparison and matching method required the largest file space. The use of Fourier transform required least amount of file space. Besides the spatial comparisons of solutions, the amplitude and phase difference of Fourier descriptors showed the best capability to match a desired function generation solution to a database of candidate solutions.

Candidate solutions for path generation four-bar mechanism were generated and characterized with spatial transforms, Fourier transforms, and invariant moments. The following comparison and matching techniques were developed and tested on 145 file solutions.

- SAD - Spatial transform, absolute difference
- SSS - Spatial transform, sum squared
- F1C - One-dimensional Fourier correlation
- F1P - One-dimensional Fourier phase only filter
- F1SP - One-dimensional Fourier descriptors, symmetric phase only matched filter
- F1A - One-dimensional Fourier transform, amplitude difference of Fourier descriptors
- F1AP - One-dimensional Fourier transform, amplitude and phase difference of Fourier descriptors
- F2C - Two-dimensional Fourier correlation
- F2P - Two-dimensional Fourier phase only filter
- F2SP - Two-dimensional Fourier descriptors, symmetric phase only matched filter
- MCC - Moment normalized cross correlation
- MPD - Moment percentage difference

Candidate solutions for motion generation four-bar mechanism were generated and characterized with spatial transforms and Fourier transforms. The measure of similarity that had the lowest error was the absolute difference matching. This comparison and matching method also required the largest file space and was high in processing time for matching filed solutions. The Fourier

transform and invariant moments required less file space. Besides the spatial comparisons of solutions, the amplitude and phase difference of Fourier descriptors showed the best capability to match a desired function generation solution to a database of candidate solutions.

A methodology was developed using Parametric Cubic Curves and B-Splines to allow the generation of a desired solution. The use of cubic curves and B-splines allow the designer to specify any number of precision points for a desired solution and is not limited to a maximum number of precision points as graphical, analytical and numeric methods are.

Based on this developed framework for the characterization, storage and search methods of solutions for function, path and motion generation four-bar mechanisms, a methodology was developed to randomly generate a database of candidate solutions for a specified "local" design space. The local design space is a subspace of a global domain in that the designer specifies the type of mechanisms and any design constraints. This random search methodology was shown to be effective in developing a database of candidate solutions and "synthesizing" mechanisms that were a close match to a desired solution.

This dissertation developed a new method for the synthesis of mechanisms for function, path, and motion generation using invariant characterization, storage and search methods. The methodology supports the synthesis of solutions that have full drive crank rotation and generate closed curves or have partial drive crank rotation and generate partial curves. Synthesis

limitations that were discussed in Chapter 3 that were totally eliminated or reduced were:

- Precision Points are required that define select points of the output path or function. With this methodology, precision points may be used or a solution may be drawn and digitized, or a desired solution may generated by an equation.
- The number of precision points is limited based upon the synthesis technique used. A maximum of nine precision points may be used for path generation and five for motion generation; the lower number of precision points provides more choices to the designer for selection of the mechanisms attributes such as pivot points, link lengths, and angles. With this methodology there is no limitation to the number of precision points.
- An initial guess of a mechanism which is close to the desired solution may be required so numerical techniques may find a local solution; the solution may not be a global solution. This methodology provides a rational approach to generate initial guesses to search a design space based specified design constraints and refines candidate solutions.
- Synthesis of mechanisms using Fourier descriptors has addressed the synthesis of path generation mechanisms and has not addressed motion or function generation mechanisms. This methodology has been shown to address function, path and motion generation mechanisms which are closed curves and partial curves.

Recommendations for Future Work

This dissertation provides a basis for the synthesis of mechanisms for function, path and motion generation using invariant characterizations, storage and search methods. The type of mechanism was focused on the four-bar mechanisms for the generation of the function, path and/or motion. This work may be expanded to focus on any other types and classes of mechanism where the output is of interest such as geared five-bar, cams, spatial mechanisms, etc.

An area of future work could focus on the development of a generalized massive database of candidate solutions that could be searched based on a desired solution. The database could be developed from a large cross section of mechanisms including four-bar, spatial, geared five-bar, etc.

This technique may be expanded to include optimization techniques to refine candidate curves that are generated and identified with the random database generation and search methodology.

APPENDIX A. FOURIER AMPLITUDE & PHASE DIFFERENCE:
WEIGHTING SELECTION AND VARIOUS PATH TYPES

This Appendix investigates two aspects of solution matching using the Fourier amplitude and phase difference measure: 1) the selection weighting applied to the phase difference of the Fourier amplitude and phase difference described in equation 5.25, and 2) application of the technique to various trace point paths. The total measure of the difference between the amplitude and phase of the Fourier descriptors may be written:

$$Fd(u) = m*A(u) + n*P(u)$$

Where:

$Fd(u)$ = Sum of amplitude and phase difference

n = Weighting applied to phase difference

$m = 1 - n$ = Weighting applied to amplitude difference

The weightings are used to address the difference in the contribution that the amplitude difference and phase differences have to the total difference measure. The weighting applied to the phase difference, n , was varied from 0.0 to 0.9. Database solution #3 was used to search the database of 145 candidate

solutions and the database search ranking was compared to the rankings generated with an absolute difference search. The results are found in Table A.1. A phase weighting of 0.2-0.3 demonstrated the best performance.

Ten trace point paths were selected to investigate the performance of the amplitude and phase difference of Fourier descriptors matching technique on various trace point path types. The performance was compared to the absolute difference search.

Ten trace point paths were selected and are graphed in Figures A.1 through A.10. The #1 ranked database solution found

Table A.1: Fourier amplitude and phase difference ranking.
Solutions matching absolute difference ranking. Desired Solution = #3

Rank	Abs Diff	<u>Weighting</u>									
		0.0	0.1	0.2	0.3	0.4	0.5	0.6	0.7	0.8	0.9
#1	3	<u>3</u>	<u>3</u>	<u>3</u>	<u>3</u>	<u>3</u>	<u>3</u>	<u>3</u>	<u>3</u>	<u>3</u>	<u>3</u>
#2	2	<u>2</u>	<u>2</u>	<u>2</u>	<u>2</u>	<u>2</u>	<u>2</u>	<u>2</u>	<u>2</u>	<u>2</u>	<u>2</u>
#3	40	12	<u>40</u>								
#4	47	40	<u>47</u>	<u>47</u>	<u>47</u>	<u>47</u>	<u>47</u>	<u>47</u>	39	39	39
#5	85	41	9	9	9	9	39	39	47	77	77
#6	123	9	12	85	85	85	85	77	77	47	47
#7	9	47	85	123	123	39	9	85	85	85	115
#8	55	78	123	39	39	123	77	9	9	115	85
#9	93	85	41	55	55	77	123	123	115	9	123
#10	131	50	55	93	77	55	55	115	123	123	9

in Table A.2 was used as the desired solution to search the database of 145 solutions. The amplitude and phase difference of Fourier descriptors matching technique identified an average of 3.7 of the top 5 solutions identified by the absolute difference measure, and identified an average of 7.8 of the top 10 solutions identified by the absolute difference measure.

Table A.2: Database Solution Ranking
Weighting applied to Fourier amplitude and phase
difference: $n=0.3$

Matching Measure	Ranking									
	#1	#2	#3	#4	#5	#6	#7	#8	#9	#10
Abs Diff	14	6	7	45	15	142	8	120	73	128
Amp & Ph	<u>14</u>	<u>6</u>	<u>7</u>	44	52	82	120	90	15	128
Abs Diff	28	21	16	59	22	97	53	29	135	143
Amp & Ph	<u>28</u>	<u>21</u>	<u>16</u>	112	66	74	104	59	53	46
Abs Diff	42	80	4	117	79	116	78	41	140	102
Amp & Ph	<u>42</u>	<u>80</u>	118	<u>4</u>	41	117	79	116	78	102
Abs Diff	56	94	132	18	48	10	86	11	124	101
Amp & Ph	<u>56</u>	<u>94</u>	<u>132</u>	<u>18</u>	139	124	86	101	48	11
Abs Diff	70	108	107	145	69	71	23	109	61	99
Amp & Ph	<u>70</u>	<u>108</u>	<u>107</u>	<u>69</u>	<u>145</u>	71	23	61	24	99
Abs Diff	84	122	91	54	129	121	92	46	135	8
Amp & Ph	<u>84</u>	<u>122</u>	<u>91</u>	121	46	129	54	53	92	16
Abs Diff	98	136	60	30	68	38	67	143	130	105
Amp & Ph	<u>98</u>	<u>136</u>	<u>60</u>	<u>30</u>	<u>68</u>	130	92	54	143	135
Abs Diff	112	74	66	104	122	35	84	142	121	8
Amp & Ph	<u>112</u>	<u>74</u>	<u>66</u>	<u>104</u>	84	122	35	8	15	28
Abs Diff	126	88	116	79	78	117	41	50	95	133
Amp & Ph	<u>126</u>	<u>88</u>	50	117	<u>79</u>	116	78	95	133	41
Abs Diff	140	102	64	117	118	80	79	116	126	42
Amp & Ph	<u>140</u>	<u>102</u>	<u>64</u>	<u>117</u>	137	116	79	99	118	126

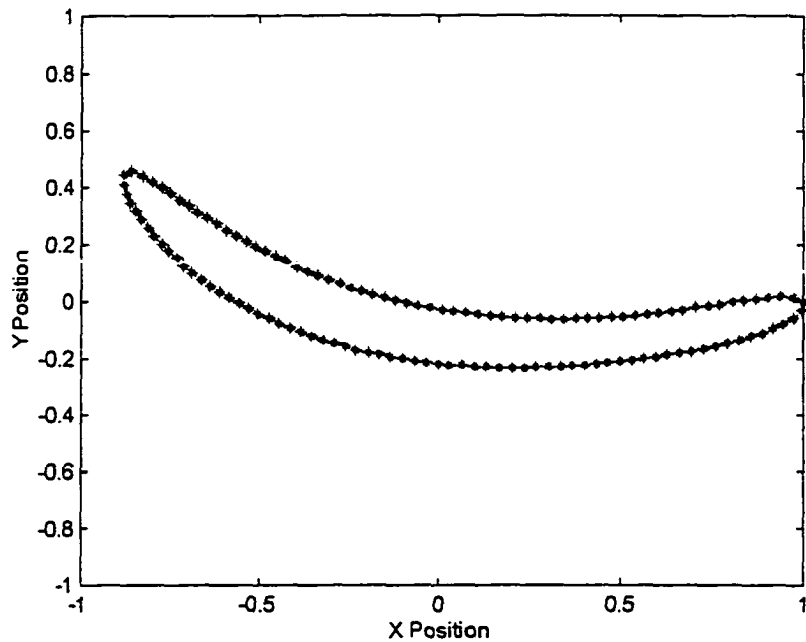


Figure A.1: Database Trace Point Path #14

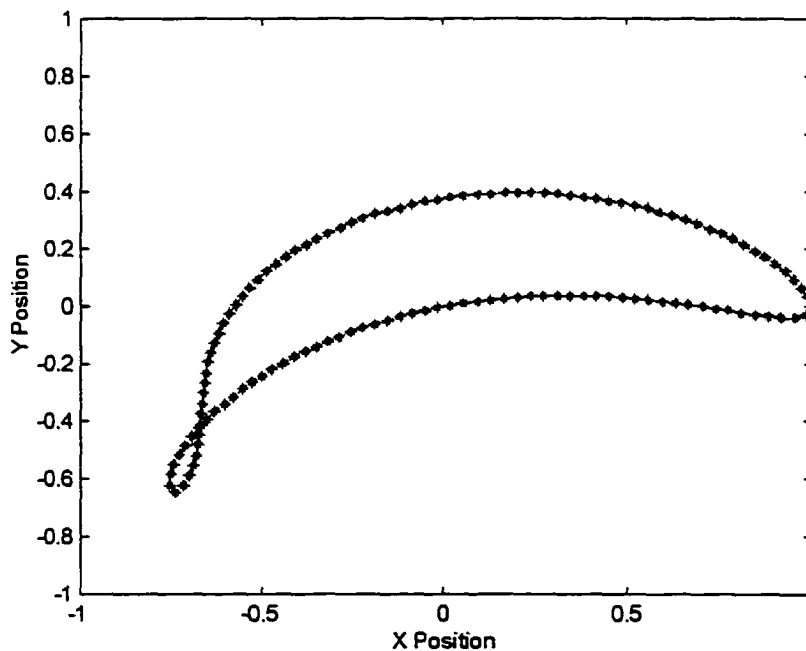


Figure A.2: Database Trace Point Path #28

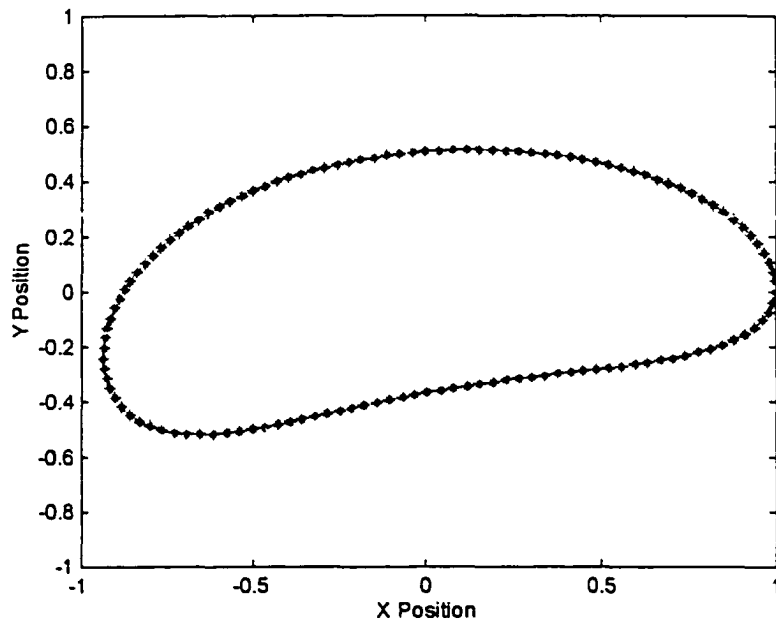


Figure A.3: Database Trace Point Path #42

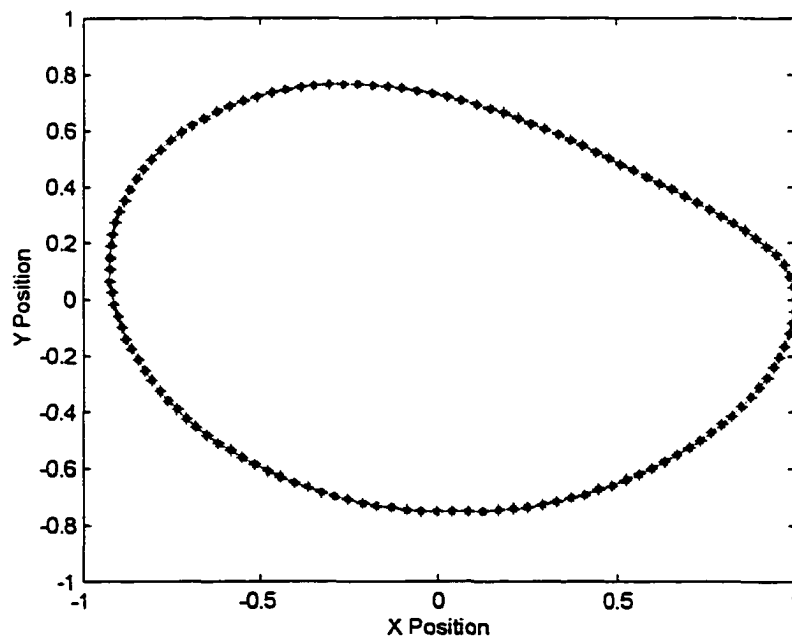


Figure A.4: Database Trace Point Path #56

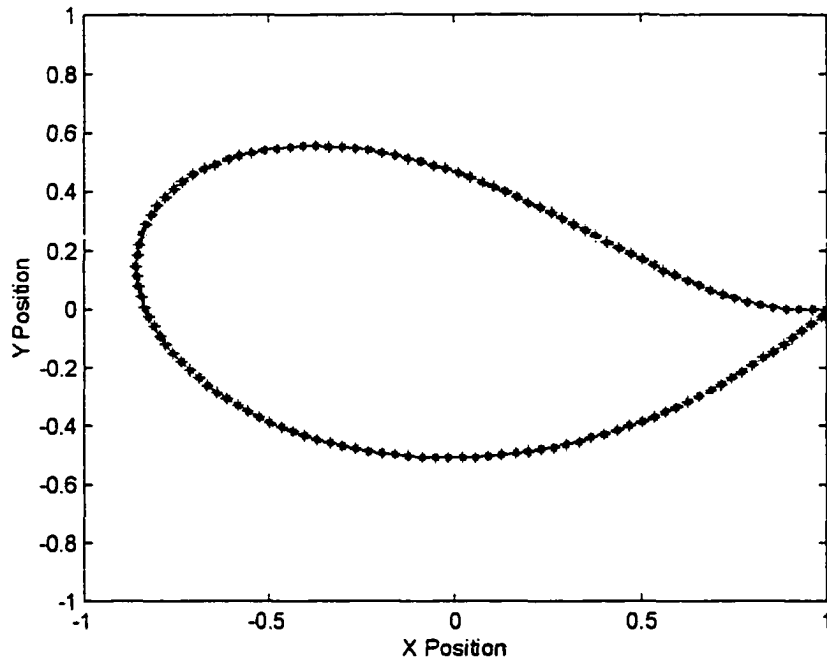


Figure A.5: Database Trace Point Path #70

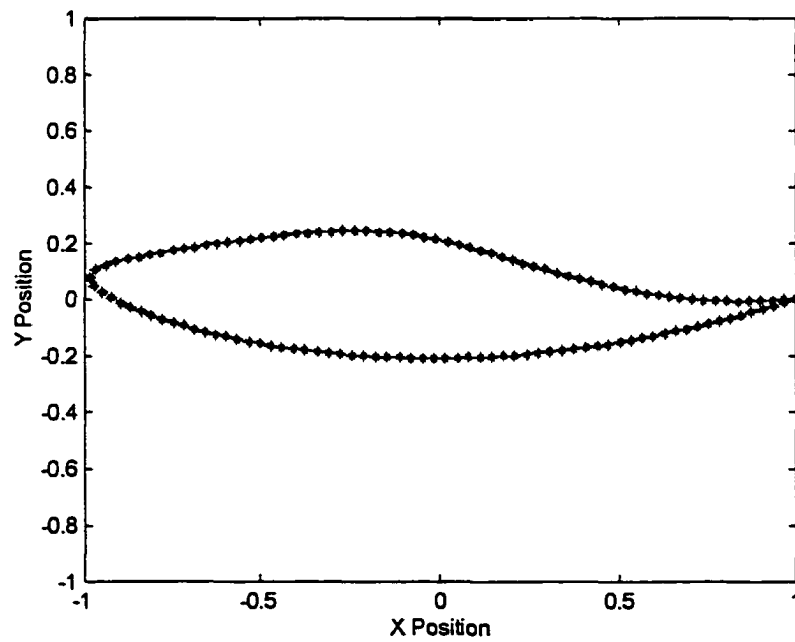


Figure A.6: Database Trace Point Path #84

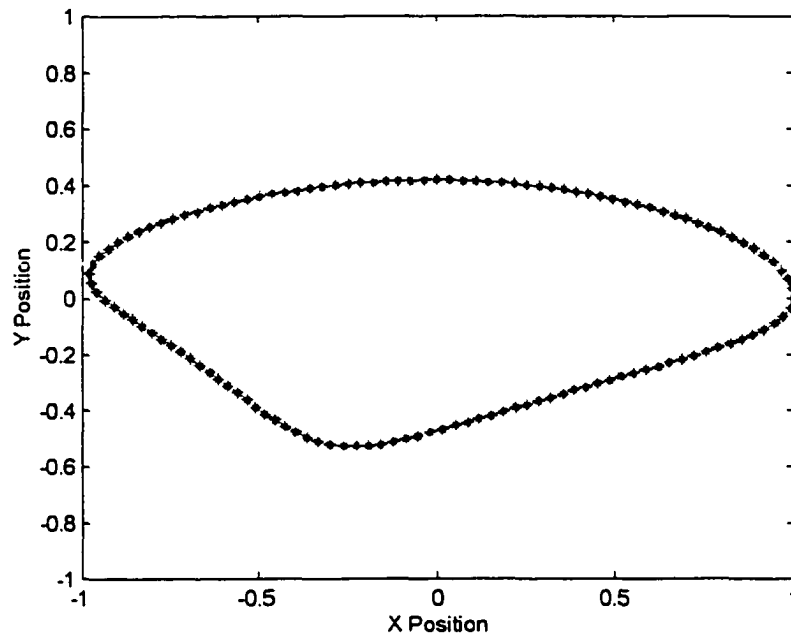


Figure A.7: Database Trace Point Path #98

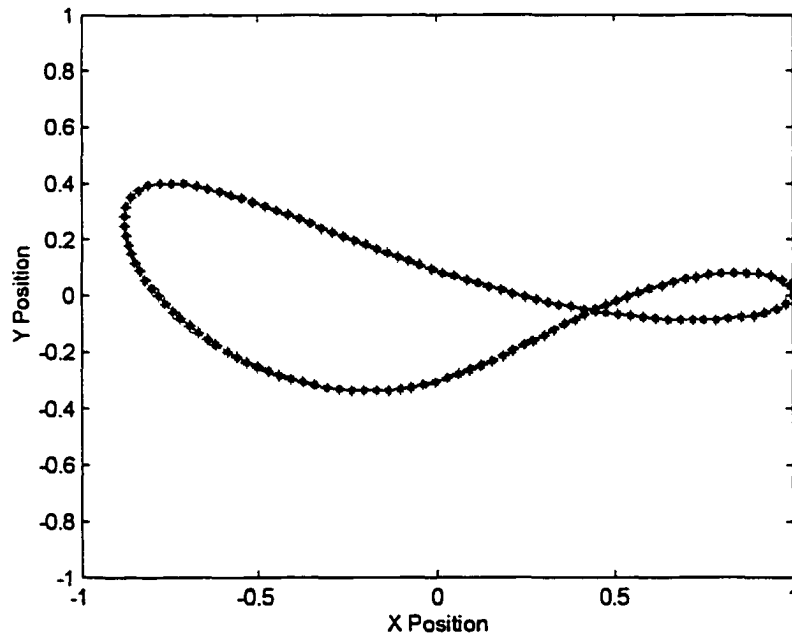


Figure A.8: Database Trace Point Path #112

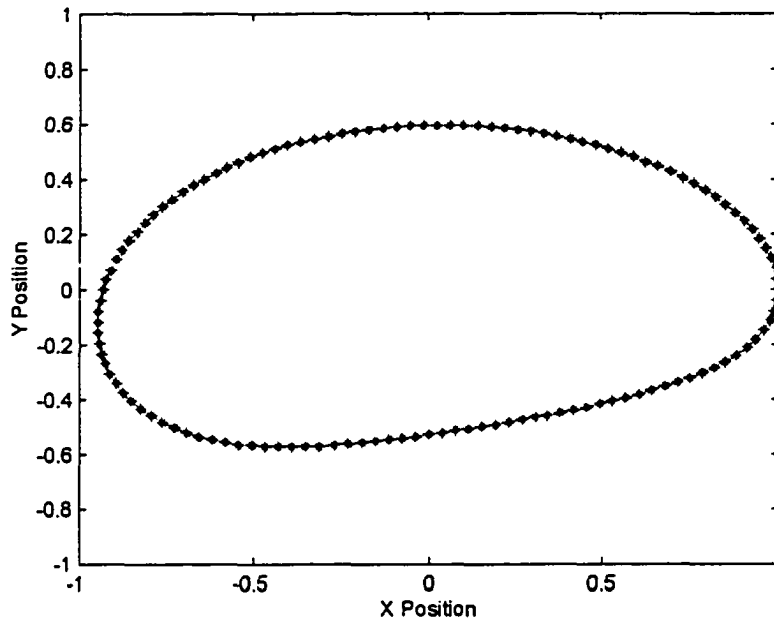


Figure A.9: Database Trace Point Path #126

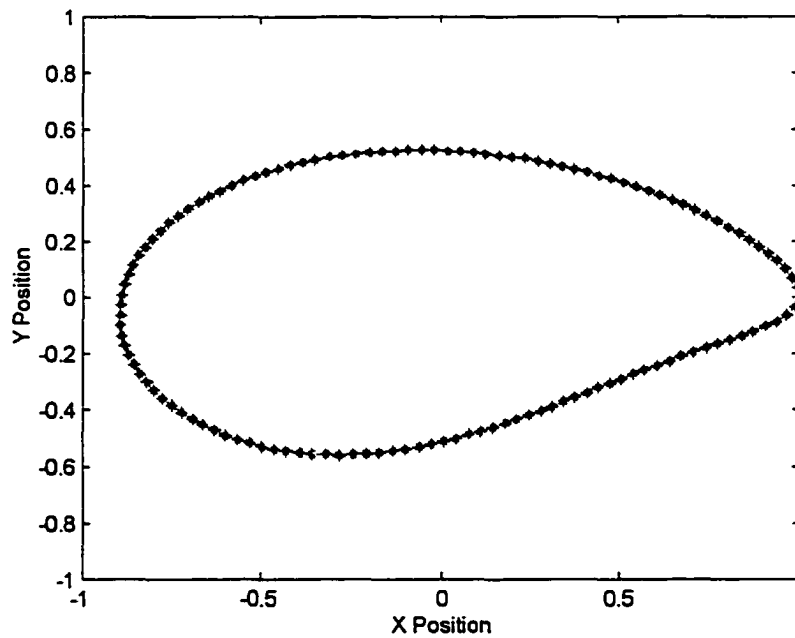


Figure A.10: Database Trace Point Path #140

APPENDIX B. MOTION GENERATION WEIGHTING FACTORS

This Appendix investigates weighting factors used in motion generation. The weighting factors are applied to the trace point path difference measure and the connecting rod angle measure when evaluating the correlation between a desired motion and the motion of a database candidate solutions. The overall measure of similarity when using the sum of absolute differences is found in equation 8.3.

$$A_t = p \cdot A_p + q \cdot A_a$$

Where:

A_t = Total absolute difference measure

A_p = Absolute difference measure of trace point path

A_a = Absolute difference measure of connecting rod angle

p, q = Weighting factor where $p + q = 1.0$

The weightings are used to address the difference in the contribution that the trace point path difference and the connecting rod angle differences have to the total difference

measure. The weighting applied to the trace point path difference, p , was varied from 0.0 to 1.0.

With a weighting value assignment of $p = 1.0$ and $q = 0.0$, the absolute difference measure in searching the database with a desired motion defined by database curve #3. The top 15 database candidate solutions are found in Table B.1 with the total absolute difference measure and the contributions of the path difference and the angle difference. The connecting rod average difference was 4.8 times as great as compared with the trace point path difference when $p = 1.0$ and $q = 0.0$. Figures B.1, B.2 and B.3 contain the graph of the absolute difference measure for the 145 database candidate solutions, the top 5 candidate solution trace point paths, and the top 5 candidate solution connecting rod angles respectively.

With a weighting value assignment of $p = 0.5$ and $q = 0.5$, the absolute difference measure in searching the database with a desired motion defined by database curve #3. The top 15 database candidate solutions are found in Table B.2 with the total absolute difference measure and the contributions of the path difference and the angle difference. The connecting rod average difference was 2.5 times as great as compared with the trace point path difference when $p = 0.5$ and $q = 0.5$. Figures B.4, B.5 and B.6 contain the graph of the absolute difference measure for the 145 database candidate solutions, the top 5 candidate solution trace point paths, and the top 5 candidate solution connecting rod angles respectively.

With a weighting value assignment of $p = 0.0$ and $q = 1.0$, the absolute difference measure in searching the database with a desired motion defined by database curve #3. The top 15 database candidate solutions are found in Table B.3 with the total absolute difference measure and the contributions of the path difference and the angle difference. The connecting rod average difference was 2.4 times as great as compared with the trace point path difference when $p = 0.0$ and $q = 1.0$. Figures B.7, B.8 and B.9 contain the graph of the absolute difference measure for the 145 database candidate solutions, the top 5 candidate solution trace point paths, and the top 5 candidate solution connecting rod angles respectively.

With a weighting value assignment of $p = 0.7$ and $q = 0.3$, the absolute difference measure in searching the database with a desired motion defined by database curve #3. The top 15 database candidate solutions are found in Table B.4 with the total absolute difference measure and the contributions of the path difference and the angle difference. The connecting rod average difference was 2.1 times as great as compared with the trace point path difference when $p = 0.7$ and $q = 0.3$. Figures B.10, B.11 and B.12 contain the graph of the absolute difference measure for the 145 database candidate solutions, the top 5 candidate solution trace point paths, and the top 5 candidate solution connecting rod angles respectively. A weighting value of $p=0.7$ and $q=0.3$ provides for a similar the contribution of the path difference and the angle difference to the total absolute difference measure.

Table B.1: Absolute difference measure, path and angle difference contributions. $p = 1.0$, $q = 0.0$

Desired Curve - Database Curve #3

Database Curve Number	Absolute Difference	Path Difference	Angle Difference
3.0000	0.0000	0.0000	0.0000
2.0000	1.9380	1.9380	12.5890
40.0000	2.7016	2.7016	9.1930
47.0000	3.6223	3.6223	22.2719
85.0000	3.8841	3.8841	19.6676
123.0000	4.1691	4.1691	18.2644
9.0000	4.5882	4.5882	31.1370
55.0000	4.9861	4.9861	33.8637
93.0000	5.0443	5.0443	29.0963
131.0000	5.1391	5.1391	27.6439
77.0000	6.3275	6.3275	14.7138
17.0000	6.3615	6.3615	43.1780
115.0000	6.4063	6.4063	13.9866
39.0000	6.6065	6.6065	14.2272
137.0000	6.9945	6.9945	37.3210

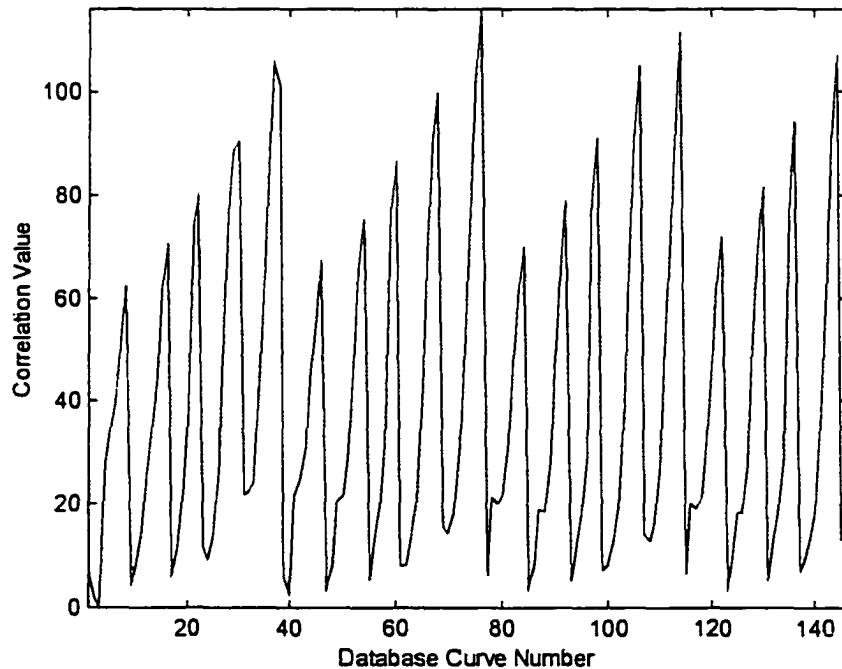


Figure B.1: Graph of absolute difference of desired motion with 145 candidate solutions, $p=1.0$, $q=0.0$

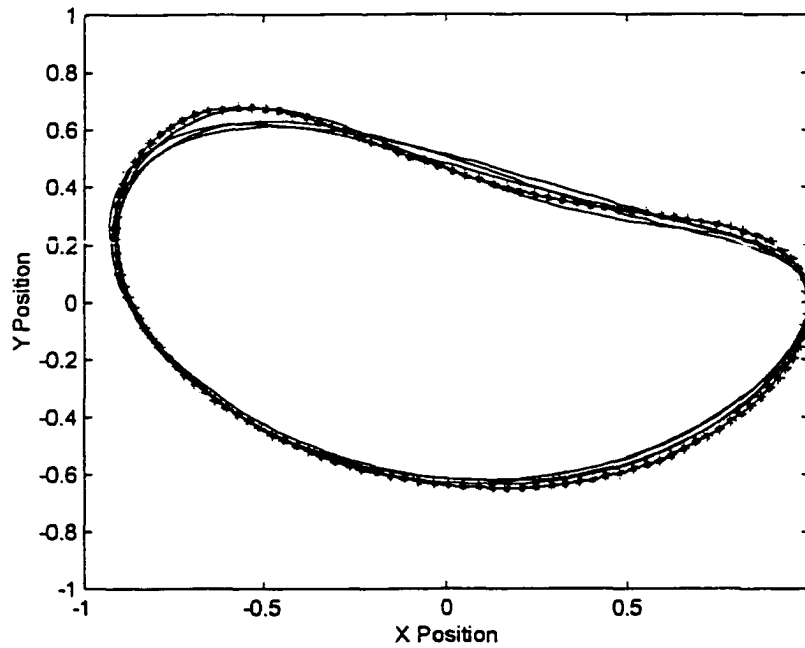


Figure B.2: Graph of the top 5 trace point paths identified by absolute difference (motion generation), $p=1.0$, $q=0.0$

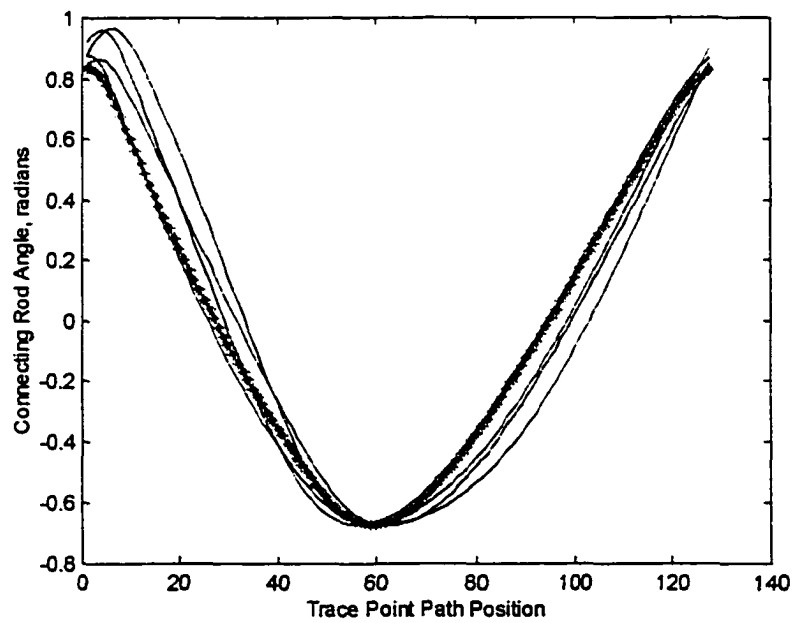


Figure B.3: Graph of the top 5 connecting rod angles identified by absolute difference (motion generation), $p=1.0$, $q=0.0$

Table B.2: Absolute difference measure, path and angle difference contributions. $p = 0.5$, $q = 0.5$

Desired Curve - Database Curve #3

Database Curve Number	Absolute Difference	Path Difference	Angle Difference
3.0000	0	0	0
40.0000	5.9473	2.7016	9.1930
2.0000	7.2635	1.9380	12.5890
11.0000	9.8431	14.6241	5.0621
124.0000	10.1448	9.1921	11.0976
115.0000	10.1965	6.4063	13.9866
39.0000	10.4168	6.6065	14.2272
86.0000	10.4821	8.8120	12.1521
77.0000	10.5206	6.3275	14.7138
123.0000	11.2167	4.1691	18.2644
85.0000	11.7759	3.8841	19.6676
47.0000	12.9471	3.6223	22.2719
48.0000	12.9499	8.4646	17.4352
1.0000	14.5249	7.0387	22.0110
131.0000	16.3915	5.1391	27.6439

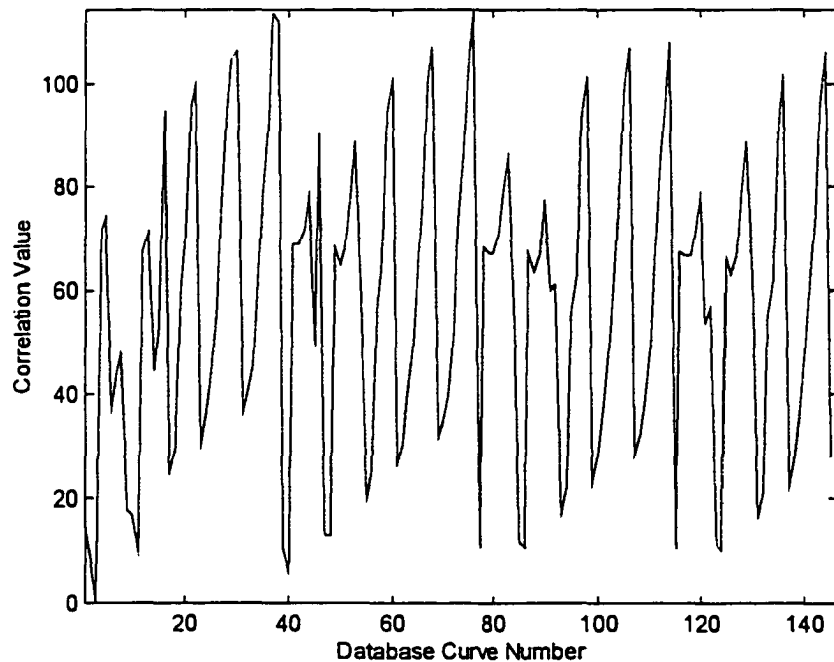


Figure B.4: Graph of absolute difference of desired motion with 145 candidate solutions, $p=0.5$, $q=0.5$

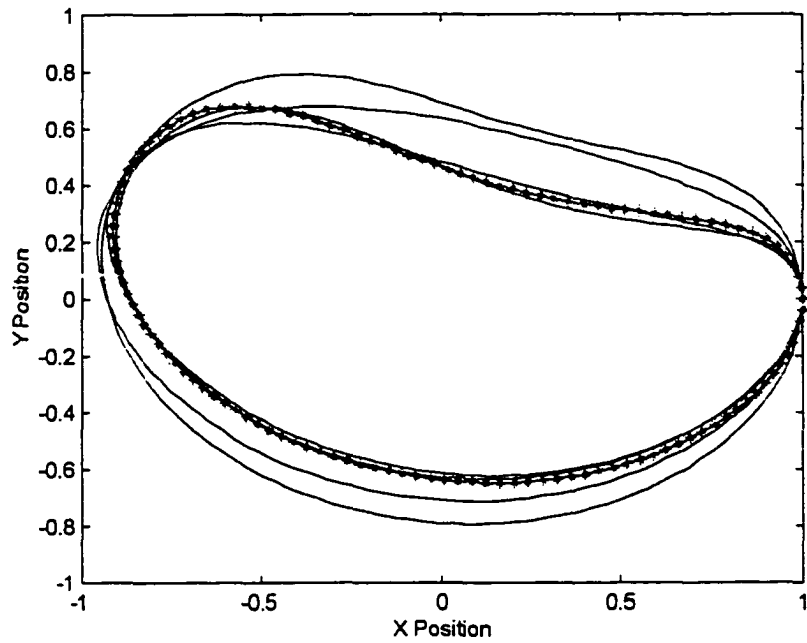


Figure B.5: Graph of the top 5 trace point paths identified by absolute difference (motion generation), $p=0.5$, $q=0.5$

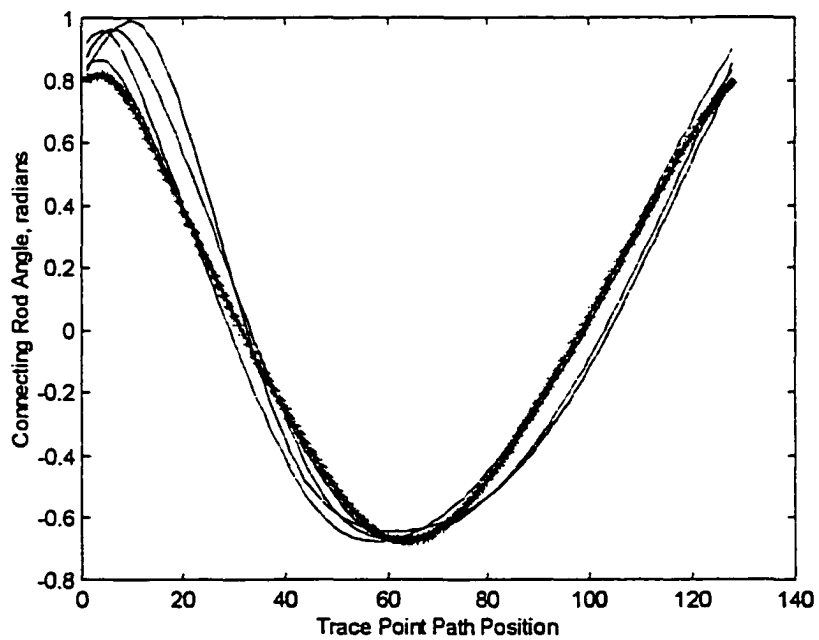


Figure B.6: Graph of the top 5 connecting rod angles identified by absolute difference (motion generation), $p=0.5$, $q=0.5$

Table B.3: Absolute difference measure, path and angle difference contributions. $p = 0.0$, $q = 1.0$

Desired Curve - Database Curve #3

Database Curve Number	Absolute Difference	Path Difference	Angle Difference
3.0000	0	0	0
11.0000	5.0621	14.6241	5.0621
40.0000	9.1930	2.7016	9.1930
124.0000	11.0976	9.1921	11.0976
86.0000	12.1521	8.8120	12.1521
2.0000	12.5890	1.9380	12.5890
115.0000	13.9866	6.4063	13.9866
39.0000	14.2272	6.6065	14.2272
77.0000	14.7138	6.3275	14.7138
48.0000	17.4352	8.4646	17.4352
123.0000	18.2644	4.1691	18.2644
85.0000	19.6676	3.8841	19.6676
1.0000	22.0110	7.0387	22.0110
47.0000	22.2719	3.6223	22.2719
10.0000	25.4248	8.2671	25.4248

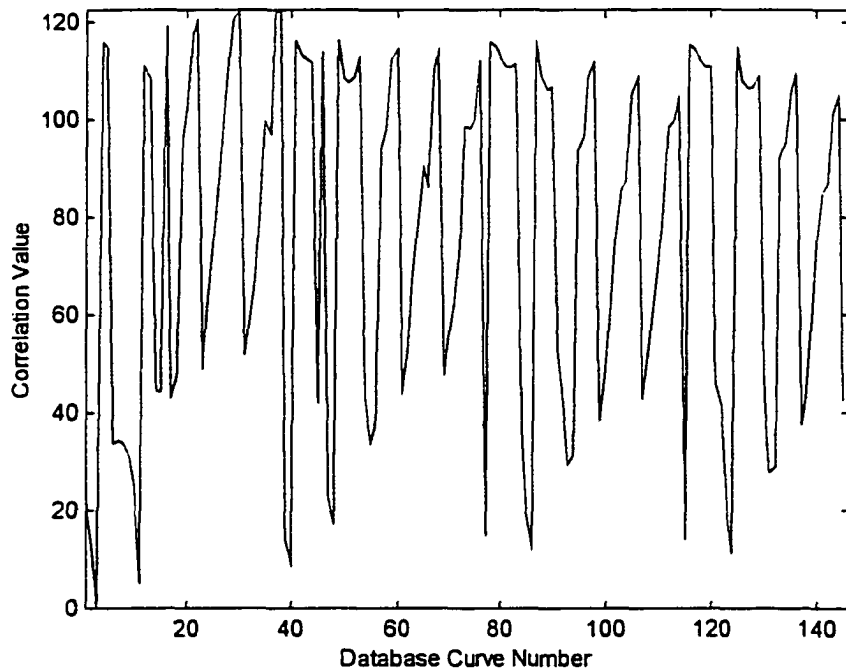


Figure B.7: Graph of absolute difference of desired motion with 145 candidate solutions, $p=0.0$, $q=1.0$

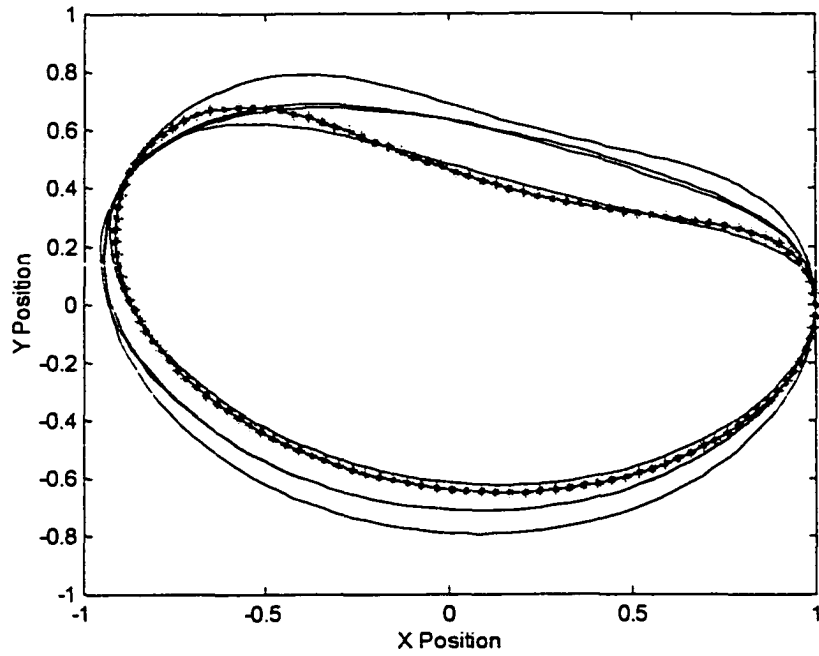


Figure B.8: Graph of the top 5 trace point paths identified by absolute difference (motion generation), $p=0.0$, $q=1.0$

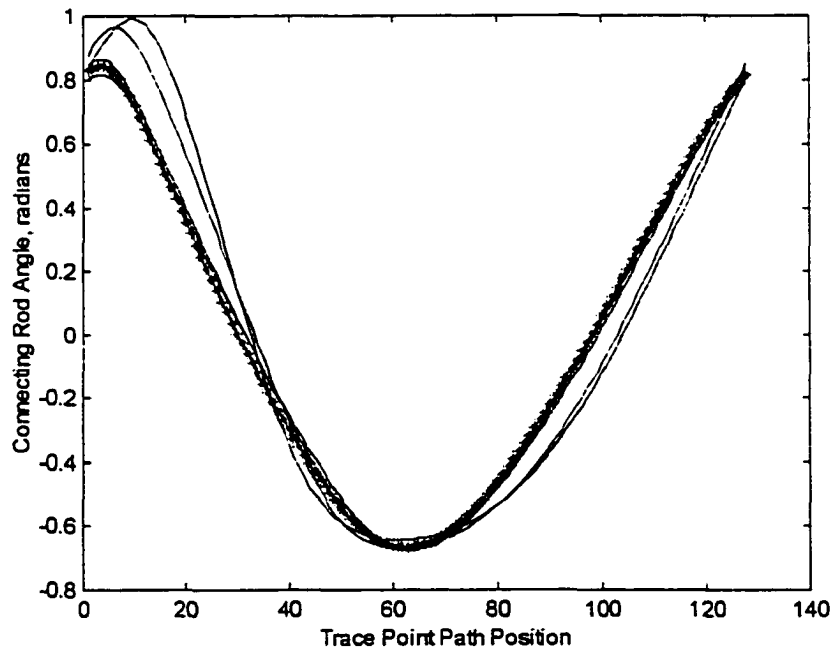


Figure B.9: Graph of the top 5 connecting rod angles identified by absolute difference (motion generation), $p=0.0$, $q=1.0$

Table B.4: Absolute difference measure, path and angle difference contributions. $p = 0.7$, $q = 0.3$

Desired Curve - Database Curve #3

Database Curve Number	Absolute Difference	Path Difference	Angle Difference
3.0000	0.0000	0.0000	0.0000
40.0000	4.6490	2.7016	9.1930
2.0000	5.1333	1.9380	12.5990
123.0000	8.3977	4.1691	18.2644
85.0000	8.6192	3.8841	19.6676
115.0000	8.6804	6.4063	13.9866
77.0000	8.8434	6.3275	14.7138
39.0000	8.8927	6.6065	14.2272
47.0000	9.2172	3.6223	22.2719
124.0000	9.7638	9.1921	11.0976
86.0000	9.8140	8.8120	12.1521
48.0000	11.1558	8.4646	17.4352
1.0000	11.5304	7.0387	22.0110
11.0000	11.7555	14.6241	5.0621

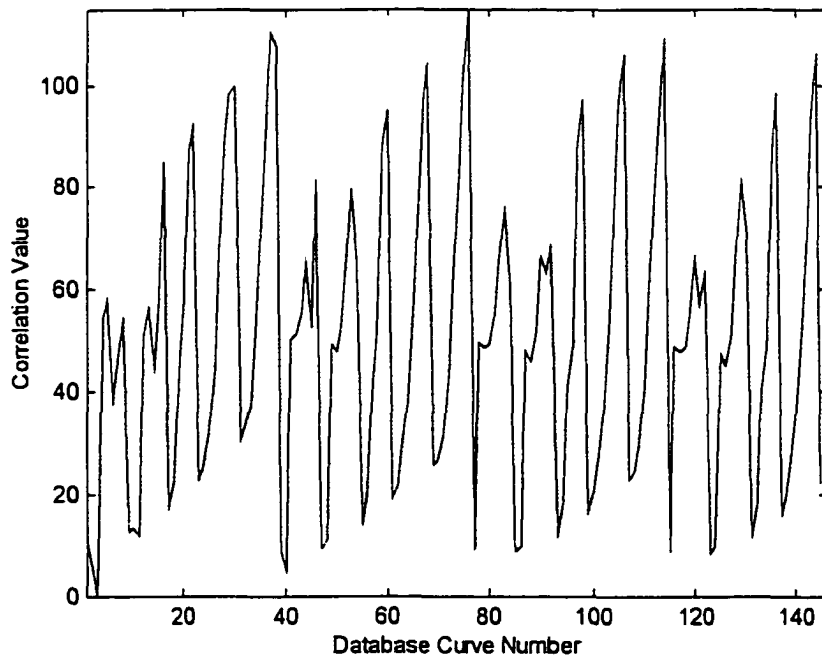


Figure B.10: Graph of absolute difference of desired motion with 145 candidate solutions, $p=0.7$, $q=0.3$

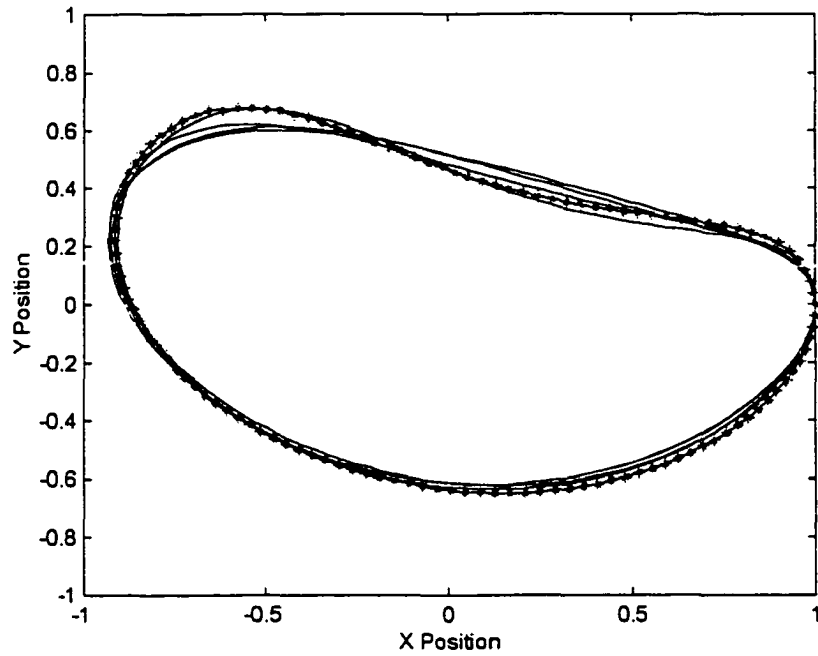


Figure B.11: Graph of the top 5 trace point paths identified by absolute difference (motion generation), $p=0.7$, $q=0.3$

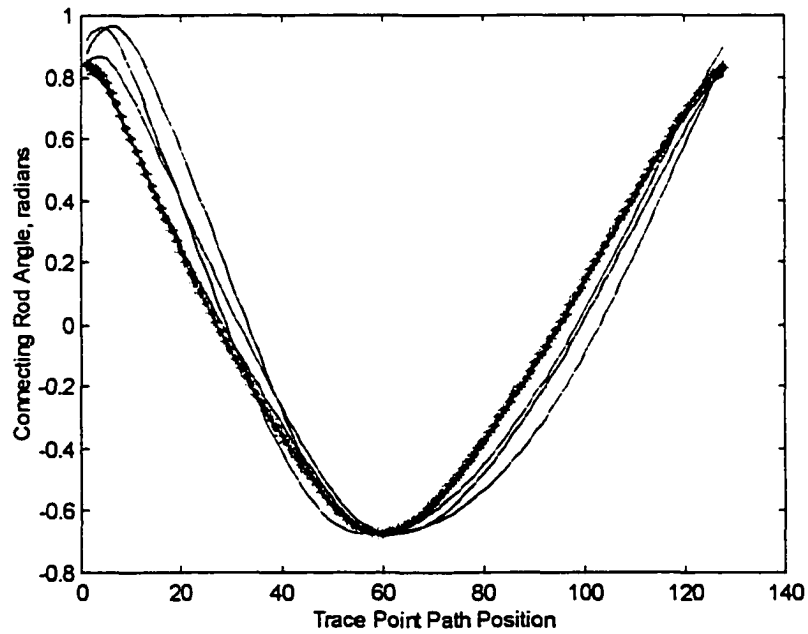


Figure B.12: Graph of the top 5 connecting rod angles identified by absolute difference (motion generation), $p=0.7$, $q=0.3$

When using the amplitude and phase difference of Fourier descriptors the overall measure is evaluated by the equation 8.4:

$$AP_t = p_{AP} * AP_p + q_{AP} * AP_a$$

Where:

AP_t = Total amplitude and phase difference measure

AP_p = Amplitude and Phase difference measure of trace point path

AP_a = Amplitude and Phase difference measure of connecting rod angle

p_{AP}, q_{AP} = Weighting factor where $p_{AP} + q_{AP} = 1.0$

As with the absolute difference weighting values, the values are used to address the difference in the contribution that the trace point path difference and the connecting rod angle differences have to the total difference measure. The weighting applied to the trace point path difference, p_{AP} , was varied from 0.0 to 1.0.

With a weighting value assignment of $p_{AP} = 1.0$ and $q_{AP} = 0.0$, the absolute difference measure in searching the database with a desired motion defined by database curve #3. The top 15 database candidate solutions are found in Table B.5 with the total absolute difference measure and the contributions of the path difference and the angle difference. The connecting rod average difference was 2.5 times as great as compared with the trace point path difference when $p_{AP} = 1.0$ and $q_{AP} = 0.0$. Figures B.13, B.14 and B.15 contain the graph of the absolute difference measure for the

145 database candidate solutions, the top 5 candidate solution trace point paths, and the top 5 candidate solution connecting rod angles respectively.

With a weighting value assignment of $p_{AP} = 0.5$ and $q_{AP} = 0.5$, the absolute difference measure in searching the database with a desired motion defined by database curve #3. The top 15 database candidate solutions are found in Table B.6 with the total absolute difference measure and the contributions of the path difference and the angle difference. The connecting rod average difference was 1.8 times as great as compared with the trace point path difference when $p_{AP} = 0.5$ and $q_{AP} = 0.5$. Figures B.16, B.17 and B.18 contain the graph of the absolute difference measure for the 145 database candidate solutions, the top 5 candidate solution trace point paths, and the top 5 candidate solution connecting rod angles respectively.

With a weighting value assignment of $p_{AP} = 0.0$ and $q_{AP} = 1.0$, the absolute difference measure in searching the database with a desired motion defined by database curve #3. The top 15 database candidate solutions are found in Table B.7 with the total absolute difference measure and the contributions of the path difference and the angle difference. The connecting rod average difference was 1.6 times as great as compared with the trace point path difference when $p_{AP} = 0.0$ and $q_{AP} = 1.0$. Figures B.19, B.20 and B.21 contain the graph of the absolute difference measure for the 145 database candidate solutions, the top 5 candidate solution trace point paths, and the top 5 candidate solution connecting rod angles respectively.

With a weighting value assignment of $p_{AP} = 0.7$ and $q_{AP} = 0.3$, the absolute difference measure in searching the database with a desired motion defined by database curve #3. The top 15 database candidate solutions are found in Table B.8 with the total absolute difference measure and the contributions of the path difference and the angle difference. The connecting rod average difference was 2.0 times as great as compared with the trace point path difference when $p_{AP} = 0.6$ and $q_{AP} = 0.4$. Figures B.22, B.23 and B.24 contain the graph of the absolute difference measure for the 145 database candidate solutions, the top 5 candidate solution trace point paths, and the top 5 candidate solution connecting rod angles respectively. A weighting value of $p_{AP} = 0.6$ and $q_{AP} = 0.4$ provides for a similar the contribution of the path difference and the angle difference to the total absolute difference measure.

Table B.5: Amplitude and Phase difference measure, path and angle difference contributions. $p = 1.0$, $q = 0.0$

Desired Curve - Database Curve #3

Database Curve Number	Absolute Difference	Path Difference	Angle Difference
3.0000	0.0000	0.0000	0.0000
2.0000	0.0486	0.0486	0.1382
40.0000	0.0909	0.0909	0.2386
47.0000	0.1128	0.1128	0.3396
9.0000	0.1247	0.1247	0.3204
85.0000	0.1292	0.1292	0.3675
39.0000	0.1386	0.1386	0.3033
123.0000	0.1391	0.1391	0.3829
55.0000	0.1508	0.1508	0.4292
77.0000	0.1540	0.1540	0.3539
93.0000	0.1588	0.1588	0.4252
131.0000	0.1644	0.1644	0.4337
1.0000	0.1653	0.1653	0.2531
115.0000	0.1708	0.1708	0.3677
17.0000	0.1782	0.1782	0.4559

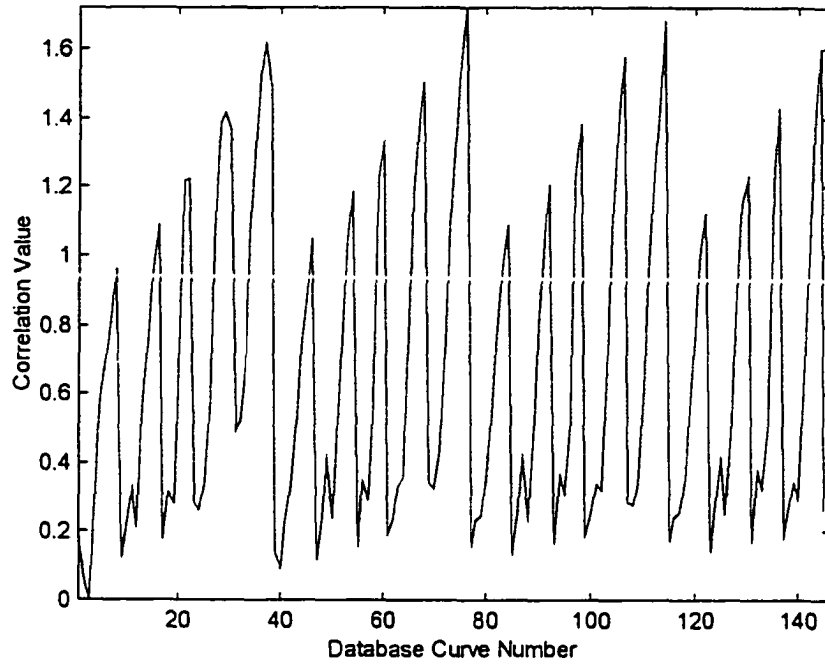


Figure B.13: Graph of amplitude and phase difference of desired motion with 145 candidate solutions, $p=1.0$, $q=0.0$

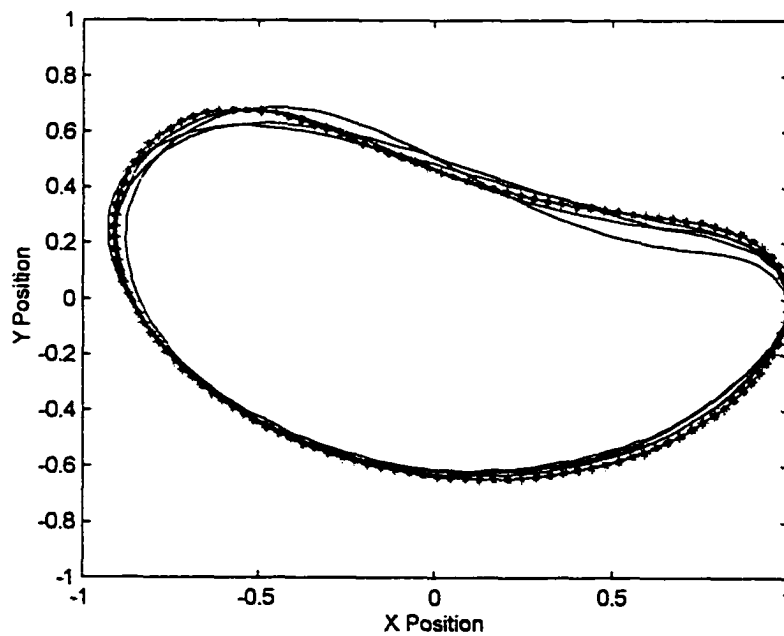


Figure B.14: Graph of the top 5 trace point paths identified by amplitude and phase difference (motion generation), $p=1.0$, $q=0.0$

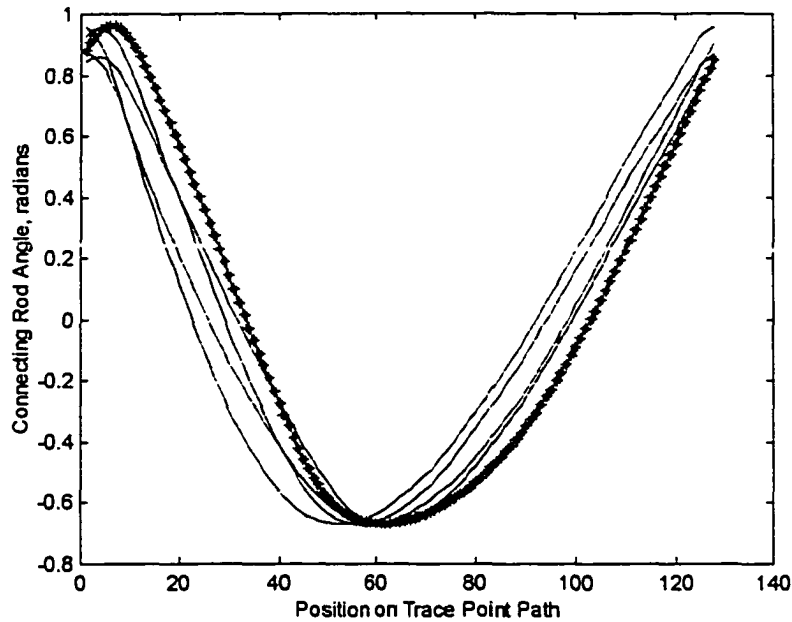


Figure B.15: Graph of the top 5 connecting rod angles identified by amplitude and phase difference (motion generation), $p=1.0$, $q=0.0$

Table B.6: Amplitude and phase difference measure, path and angle difference contributions. $p = 0.5$, $q = 0.5$

Desired Curve - Database Curve #3

Database Curve Number	Absolute Difference	Path Difference	Angle Difference
3.0000	0.0000	0.0000	0.0000
2.0000	0.0934	0.0486	0.1382
40.0000	0.1647	0.0909	0.2386
1.0000	0.2092	0.1653	0.2531
39.0000	0.2209	0.1386	0.3033
9.0000	0.2226	0.1247	0.3204
47.0000	0.2262	0.1128	0.3396
10.0000	0.2431	0.2119	0.2743
85.0000	0.2483	0.1292	0.3675
48.0000	0.2520	0.2363	0.2676
77.0000	0.2539	0.1540	0.3539
123.0000	0.2610	0.1391	0.3829
11.0000	0.2640	0.3237	0.2043
86.0000	0.2659	0.2562	0.2756
115.0000	0.2693	0.1708	0.3677

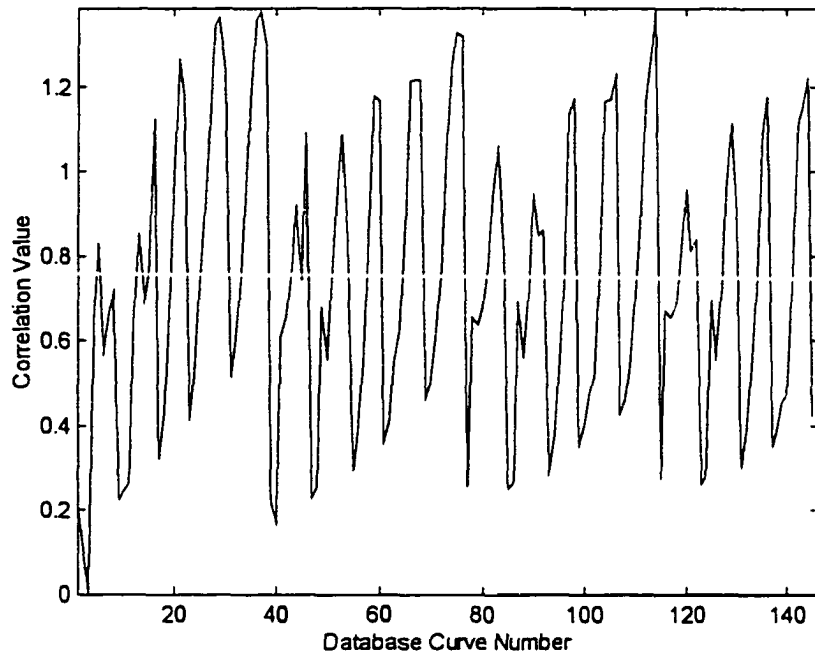


Figure B.16: Graph of amplitude and phase difference of desired motion with 145 candidate solutions, $p=0.5$, $q=0.5$

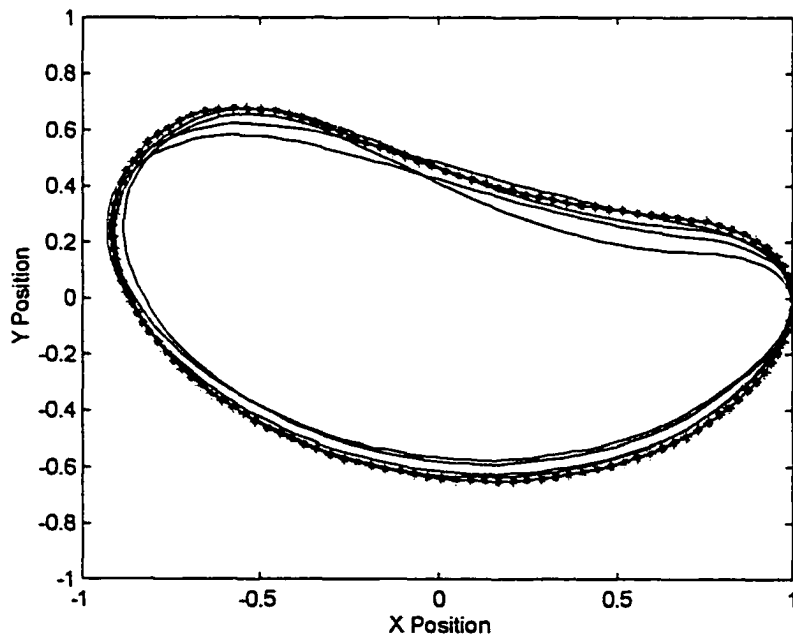


Figure B.17: Graph of the top 5 trace point paths identified by amplitude and phase difference (motion generation), $p=0.5$, $q=0.5$

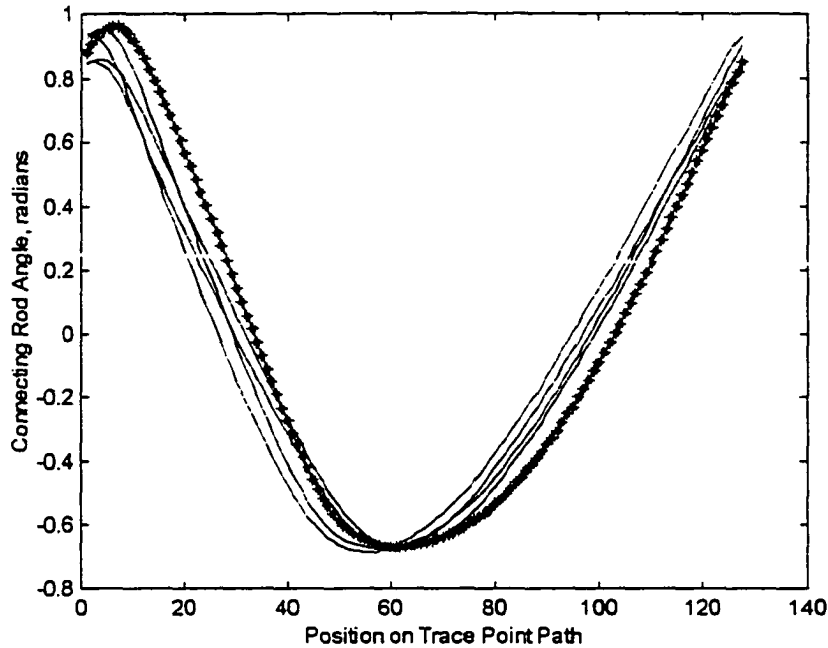


Figure B.18: Graph of the top 5 connecting rod angles identified by amplitude and phase difference (motion generation), $p=0.5$, $q=0.5$

Table B.7: Amplitude and phase difference measure, path and angle difference contributions. $p = 0.0$, $q = 1.0$

Desired Curve - Database Curve #3

Database Curve Number	Absolute Difference	Path Difference	Angle Difference
3.0000	0.0000	0.0000	0.0000
2.0000	0.1382	0.0486	0.1382
11.0000	0.2043	0.3237	0.2043
40.0000	0.2386	0.0909	0.2386
1.0000	0.2531	0.1653	0.2531
48.0000	0.2676	0.2363	0.2676
10.0000	0.2743	0.2119	0.2743
86.0000	0.2756	0.2562	0.2756
124.0000	0.2930	0.2712	0.2930
39.0000	0.3033	0.1386	0.3033
9.0000	0.3204	0.1247	0.3204
47.0000	0.3396	0.1128	0.3396
77.0000	0.3539	0.1540	0.3539
85.0000	0.3675	0.1292	0.3675
115.0000	0.3677	0.1708	0.3677

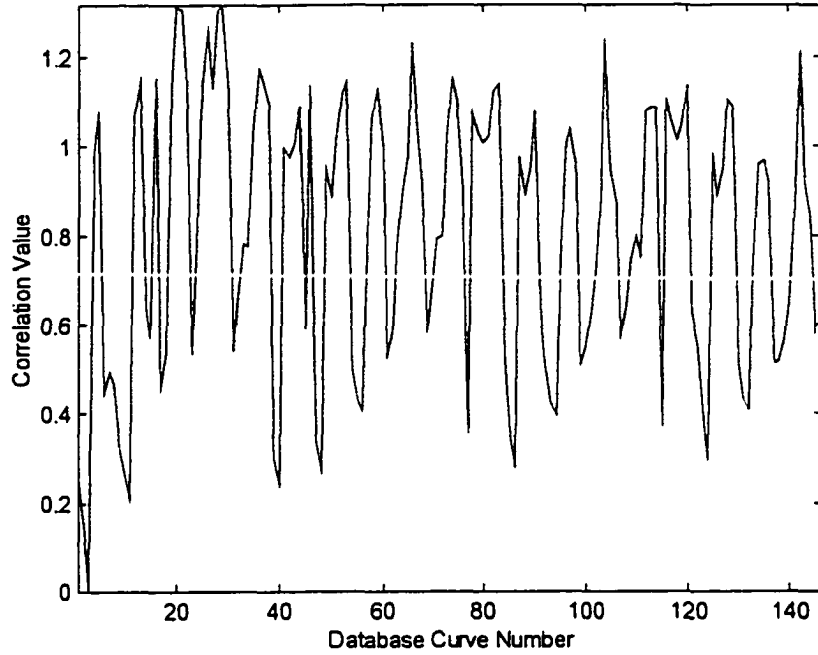


Figure B.19: Graph of amplitude and phase difference of desired motion with 145 candidate solutions, $p=0.0$, $q=1.0$

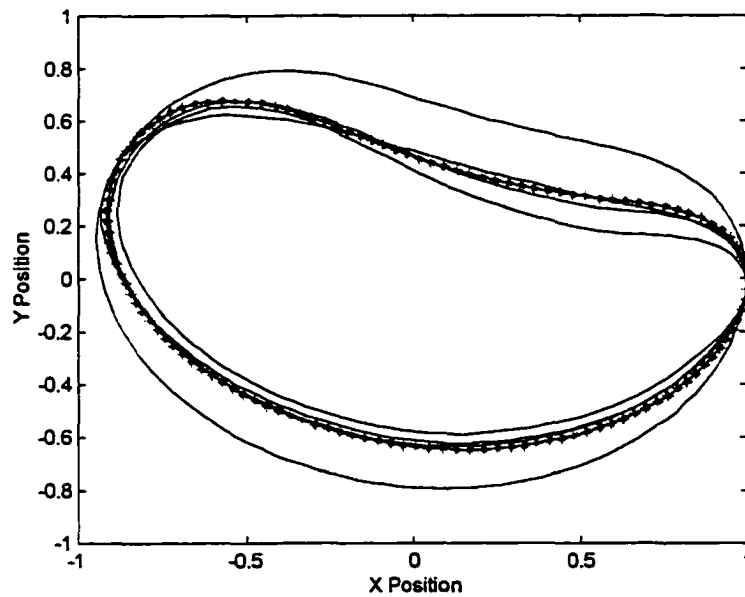


Figure B.20: Graph of the top 5 trace point paths identified by amplitude and phase difference (motion generation), $p=0.0$, $q=1.0$

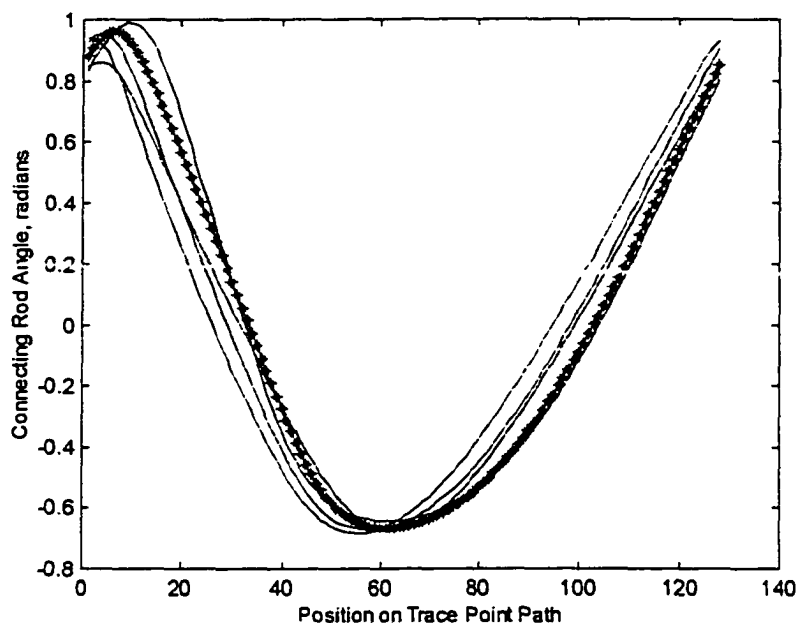


Figure B.21: Graph of the top 5 connecting rod angles identified by amplitude and phase difference (motion generation), $p=0.0$, $q=1.0$

Table B.8: Amplitude and phase difference measure, path and angle difference contributions. $p = 0.6$, $q = 0.4$

Desired Curve - Database Curve #3

Database Curve Number	Absolute Difference	Path Difference	Angle Difference
3.0000	0.0000	0.0000	0.0000
2.0000	0.0845	0.0486	0.1382
40.0000	0.1500	0.0909	0.2386
1.0000	0.2004	0.1653	0.2531
9.0000	0.2030	0.1247	0.3204
47.0000	0.2035	0.1128	0.3396
39.0000	0.2045	0.1386	0.3033
85.0000	0.2245	0.1292	0.3675
77.0000	0.2339	0.1540	0.3539
123.0000	0.2366	0.1391	0.3829
10.0000	0.2369	0.2119	0.2743
48.0000	0.2489	0.2363	0.2676
115.0000	0.2496	0.1708	0.3677
55.0000	0.2621	0.1508	0.4292
86.0000	0.2640	0.2562	0.2756

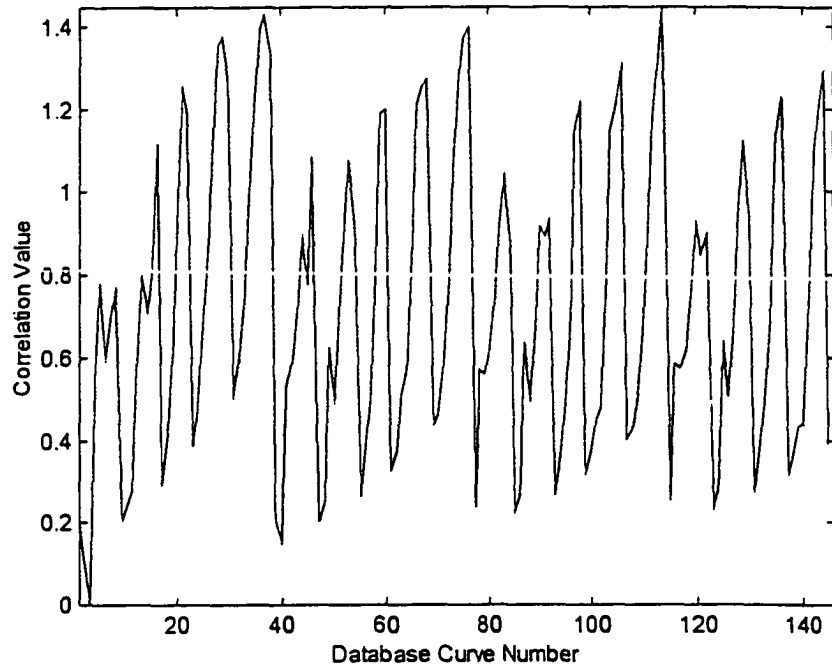


Figure B.22: Graph of amplitude and phase difference of desired motion with 145 candidate solutions, $p=0.6$, $q=0.4$

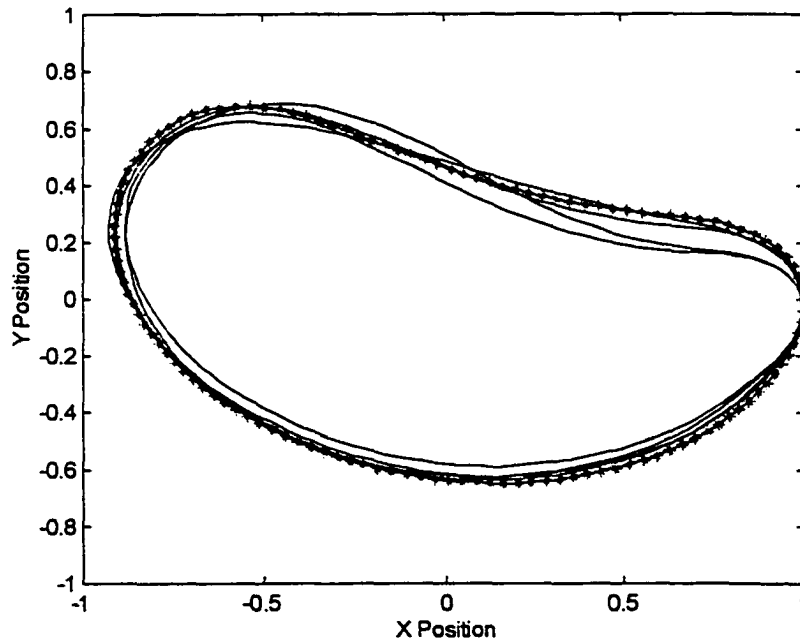


Figure B.23: Graph of the top 5 trace point paths identified by amplitude and phase difference (motion generation), $p=0.6$, $q=0.4$

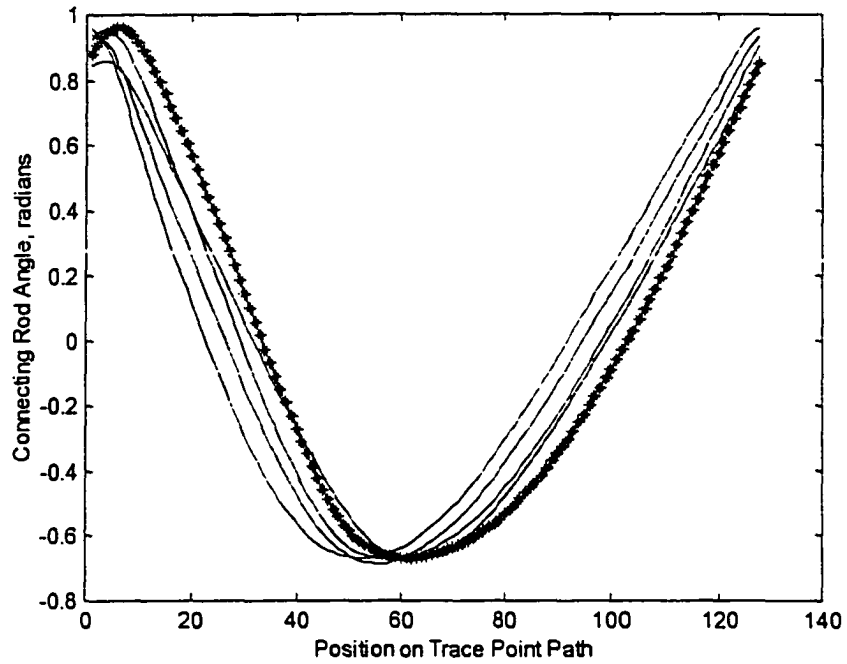


Figure B.24: Graph of the top 5 connecting rod angles identified by amplitude and phase difference (motion generation), $p=1.0$, $q=0.0$

APPENDIX C. SOLUTION GENERATION: MECHANISMS AND PATHS

Figures C.1, C.3, C.5, C.7, C.9, C.11, C.13, C.15, C.17 and C.19 are graphs of the desired trace point path and each of the ten candidate trace point paths synthesized by the random search and refinement process in Chapter 10. Figures C.2, C.4, C.6, C.8, C.10, C.12, C.14, C.16, C.18, and C.20 are the synthesized four-bar mechanism that generates the trace point path. A summary of the four-bar mechanism configuration is found in Table C.1.

Table C.1: Summary of candidate trace point paths generated through the random search and refinement process - closed curves

Curve	DC	CR	FC	GPD	TPD	TPA	A&P Diff.
1	1.0000	2.1741	2.4344	1.5998	2.4160	0.4827	0.0319
2	1.0000	3.5891	3.4255	1.6354	4.0794	0.3554	0.0308
3	1.0000	2.2816	2.5814	1.7054	2.7172	0.4808	0.0377
4	1.0000	1.9038	2.0929	1.6251	2.4368	0.4962	0.0359
5	1.0000	1.8380	1.6752	1.5498	2.4936	0.4923	0.0325
6	1.0000	2.3015	1.6801	1.8183	2.5273	0.5605	0.0428
7	1.0000	3.1259	2.9017	1.6391	3.3870	0.4192	0.0372
8	1.0000	1.5118	1.8548	1.6616	1.9443	0.5345	0.0271
9	1.0000	1.7446	2.3512	1.9543	2.4541	0.4590	0.0707
10	1.0000	2.9716	2.6252	1.6856	3.2038	0.4497	0.0386

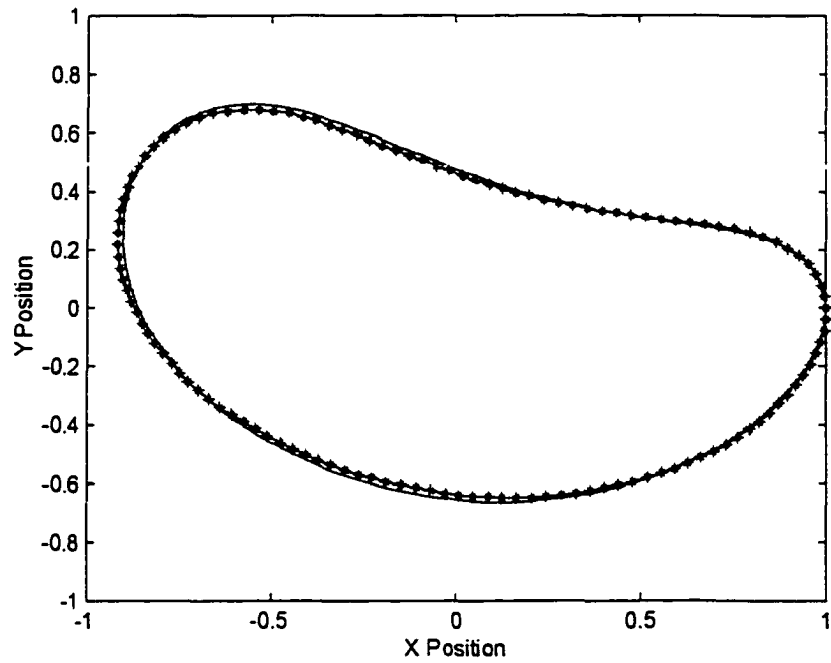


Figure C.1: Synthesized trace point path #1 and desired path

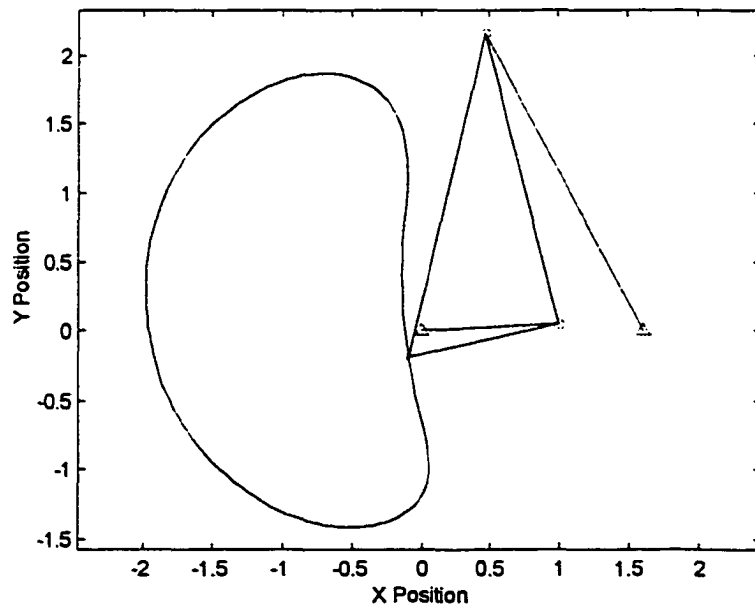


Figure C.2: Synthesized four-bar mechanism #1

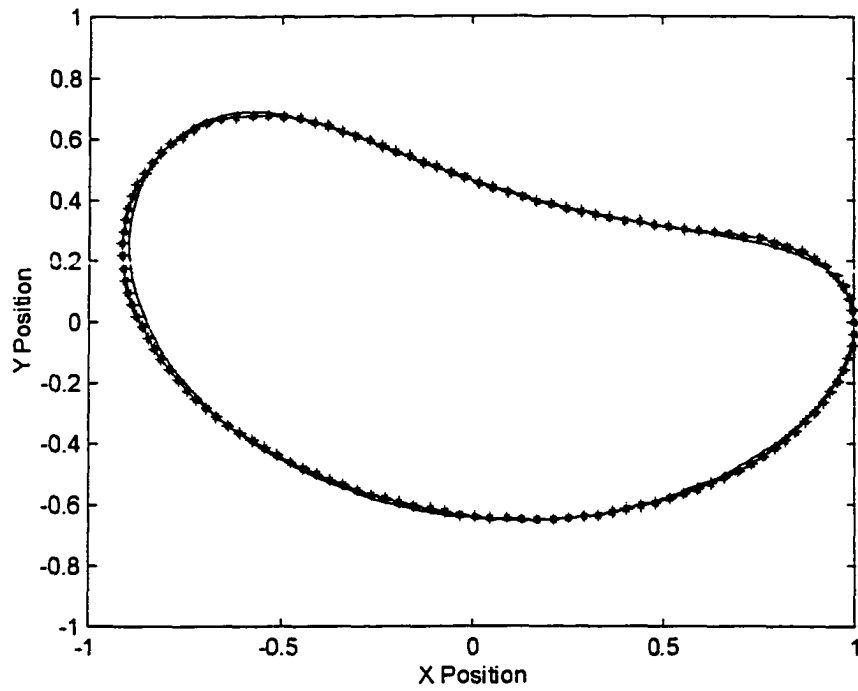


Figure C.3: Synthesized trace point path #2 and desired path

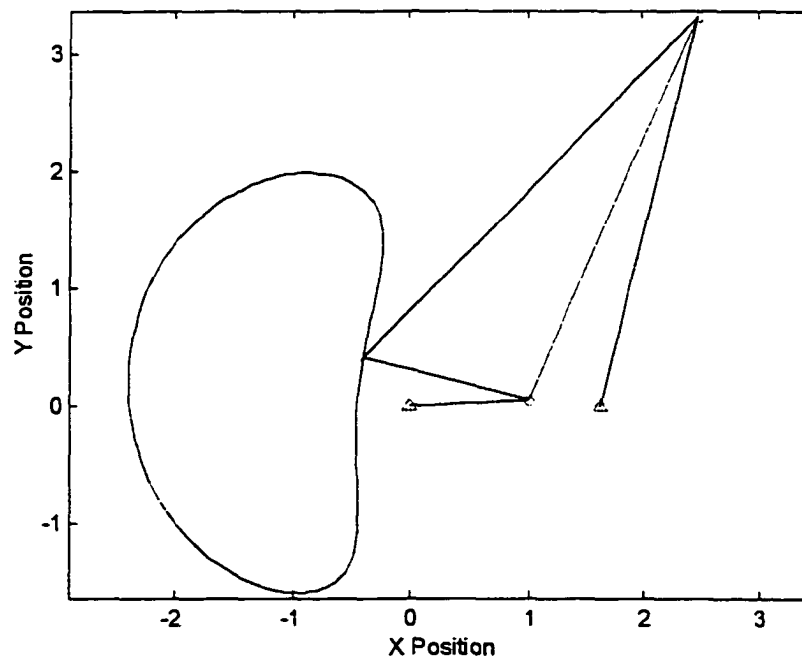


Figure C.4: Synthesized four-bar mechanism #2

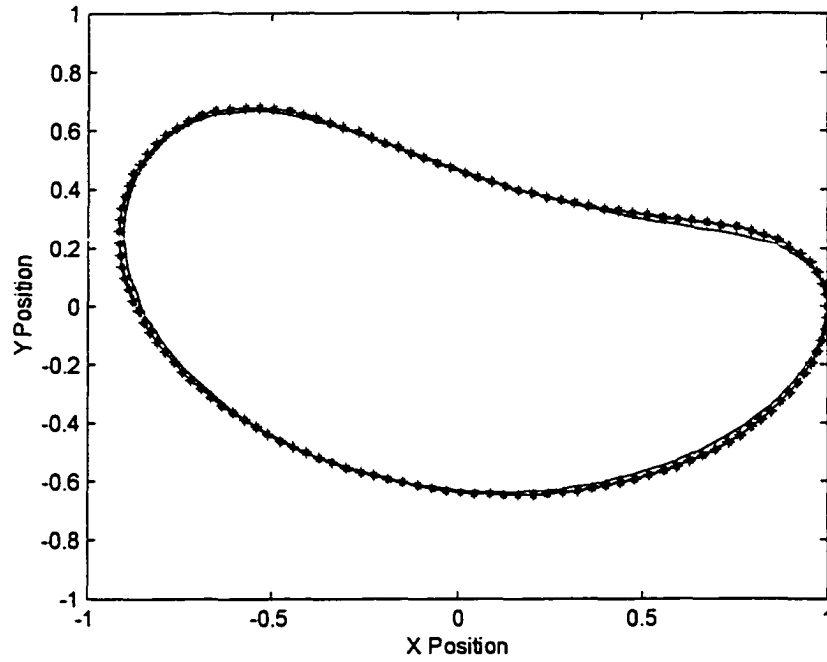


Figure C.5: Synthesized trace point path #3 and Desired path

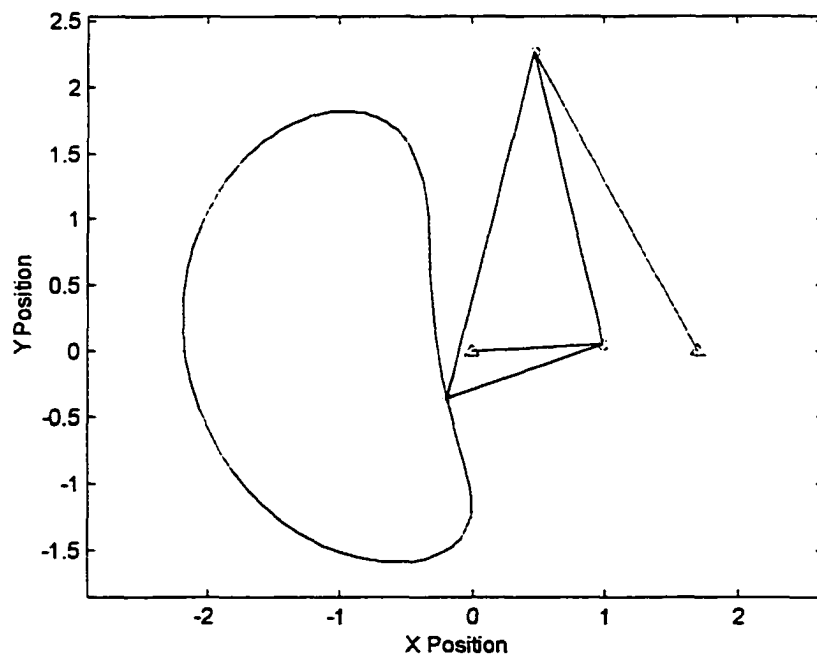


Figure C.6: Synthesized four-bar mechanism #3

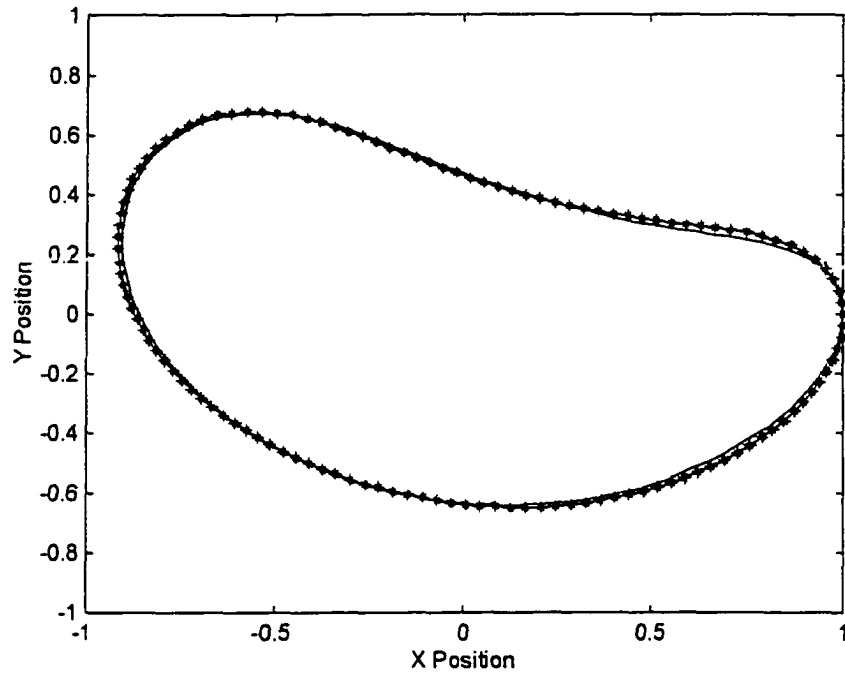


Figure C.7: Synthesized trace point path #4 and desired path

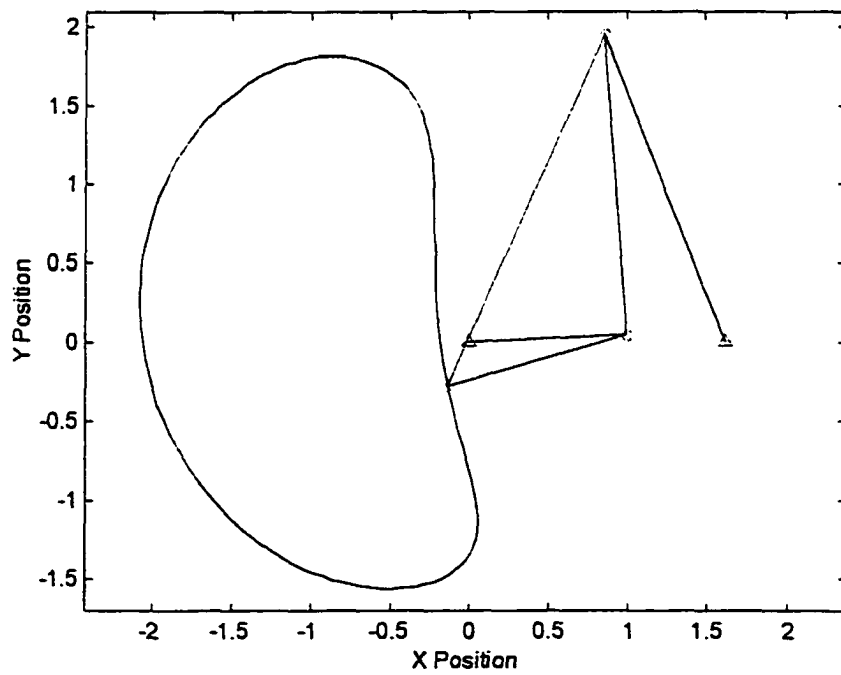


Figure C.8: Synthesized four-bar mechanism #4

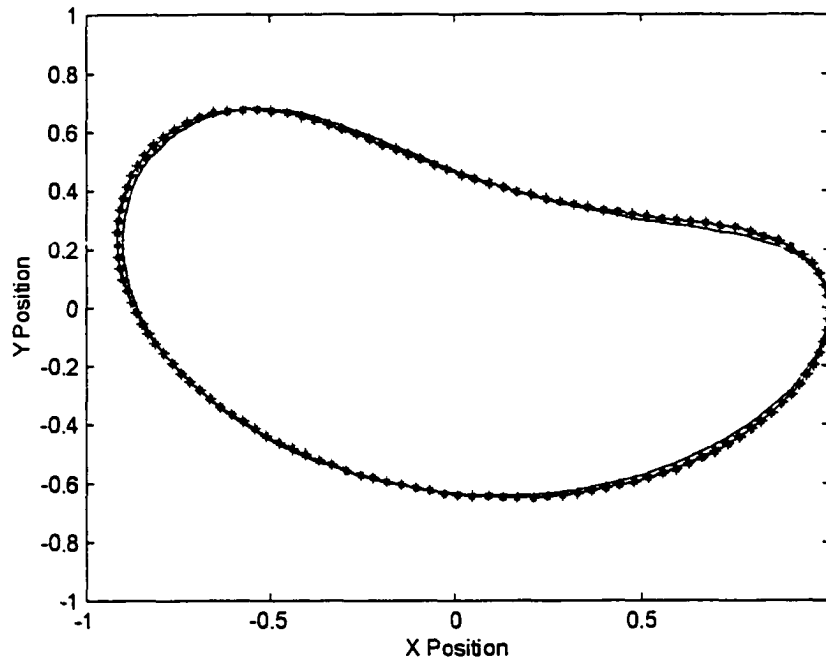


Figure C.9: Synthesized trace point path #5 and desired path

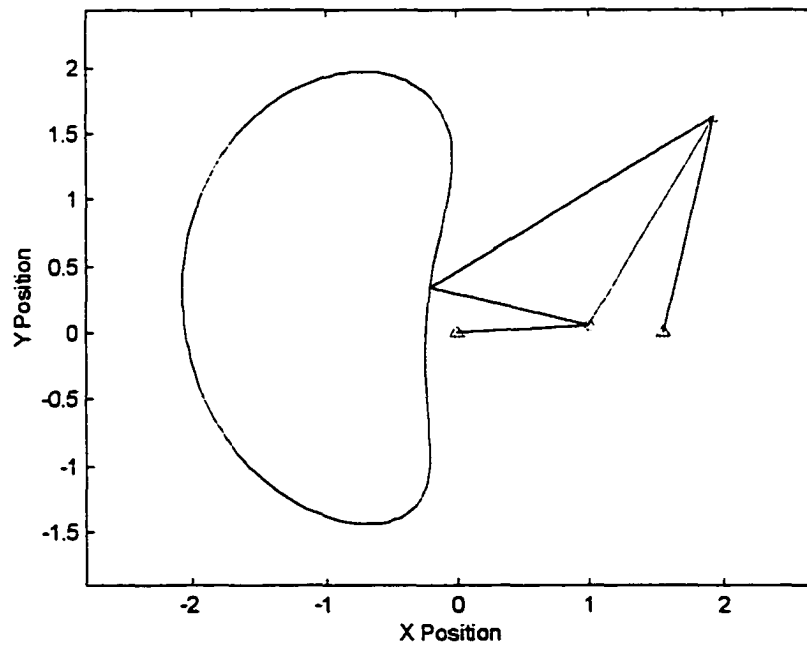


Figure C.10: Synthesized four-bar mechanism #5

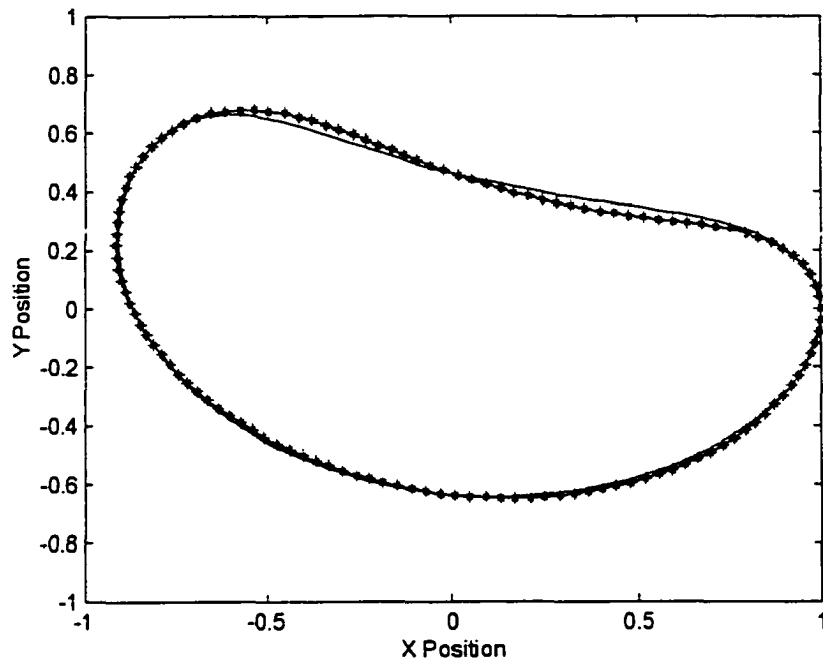


Figure C.11: Synthesized trace point path #6 and desired path

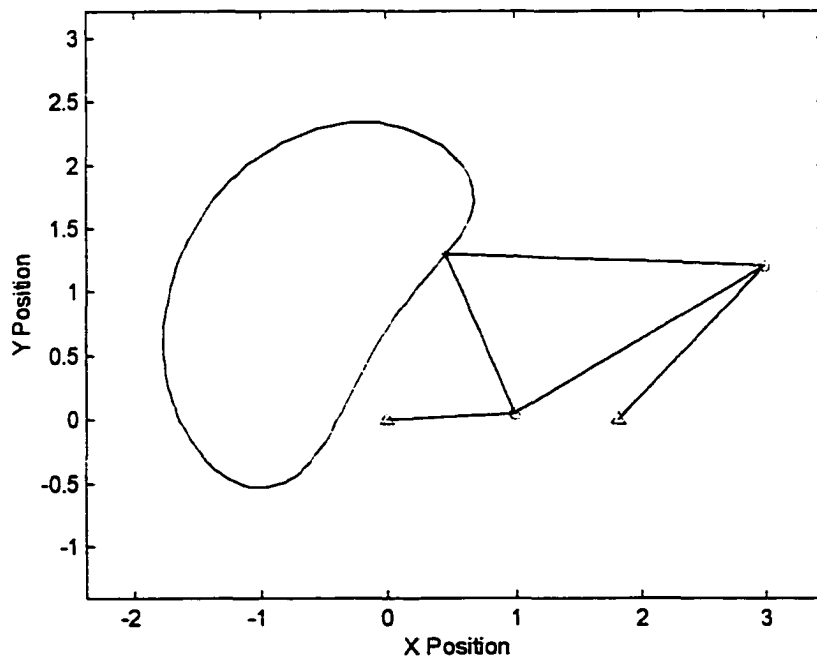


Figure C.12: Synthesized four-bar mechanism #6

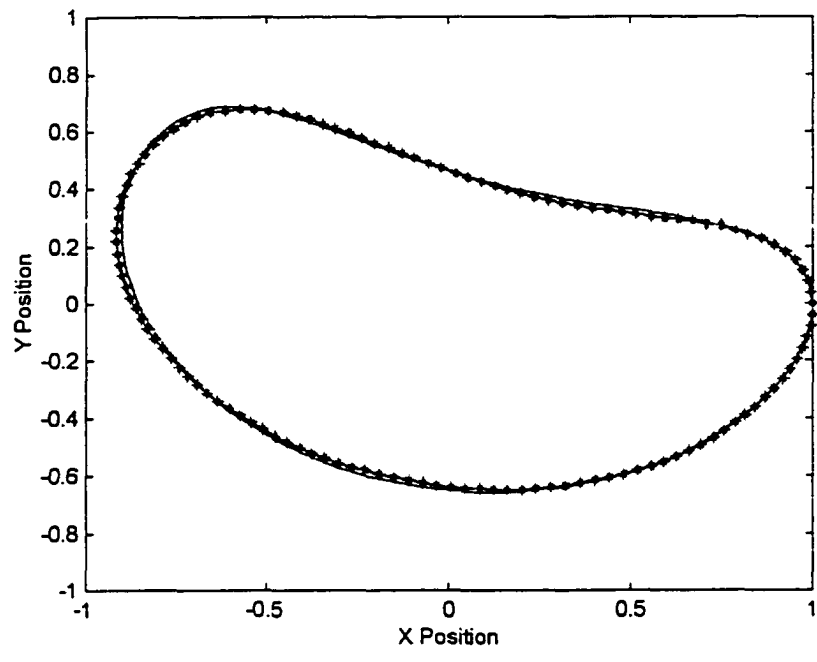


Figure C.13: Synthesized trace point path #7 and desired path

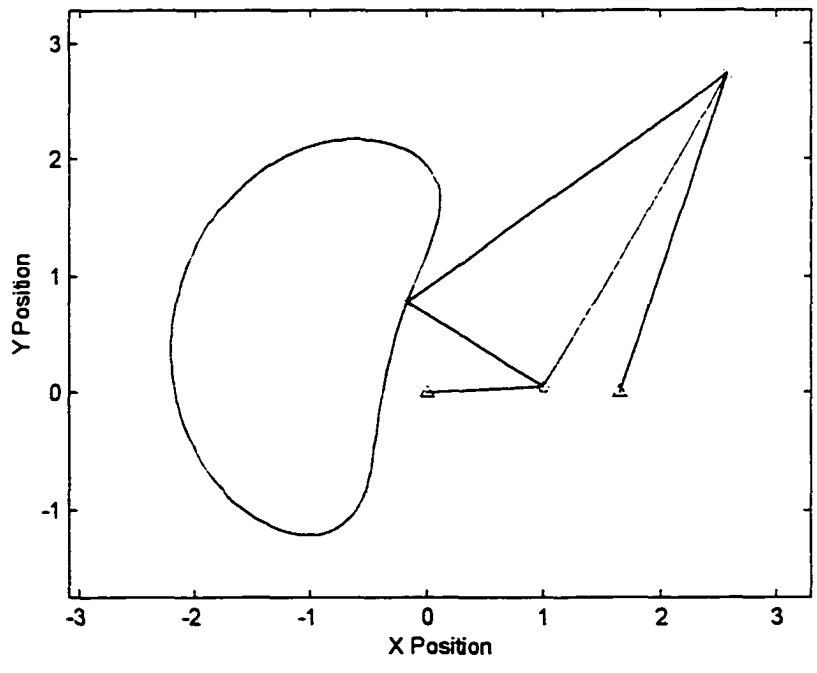


Figure C.14: Synthesized four-bar mechanism #7

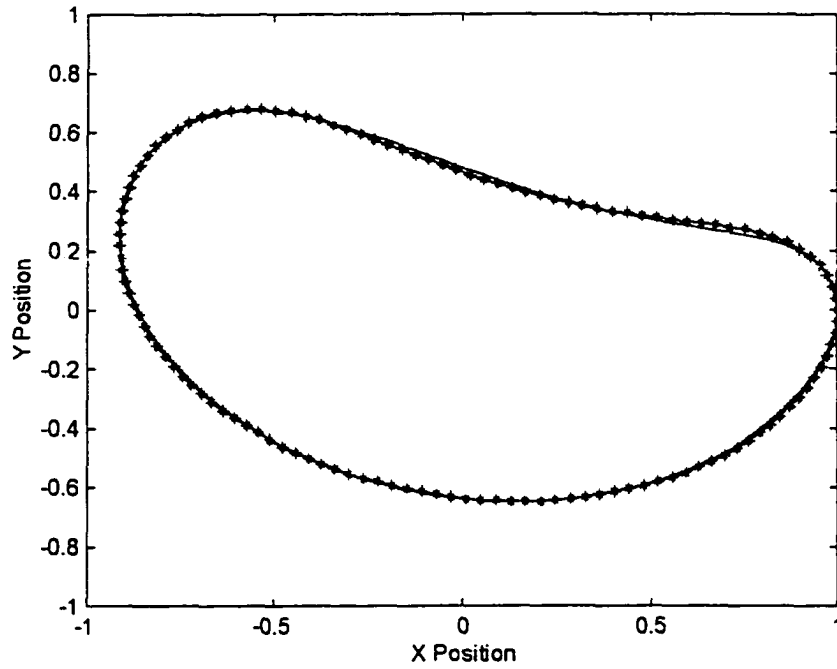


Figure C.15: Synthesized trace point path #8 and desired path

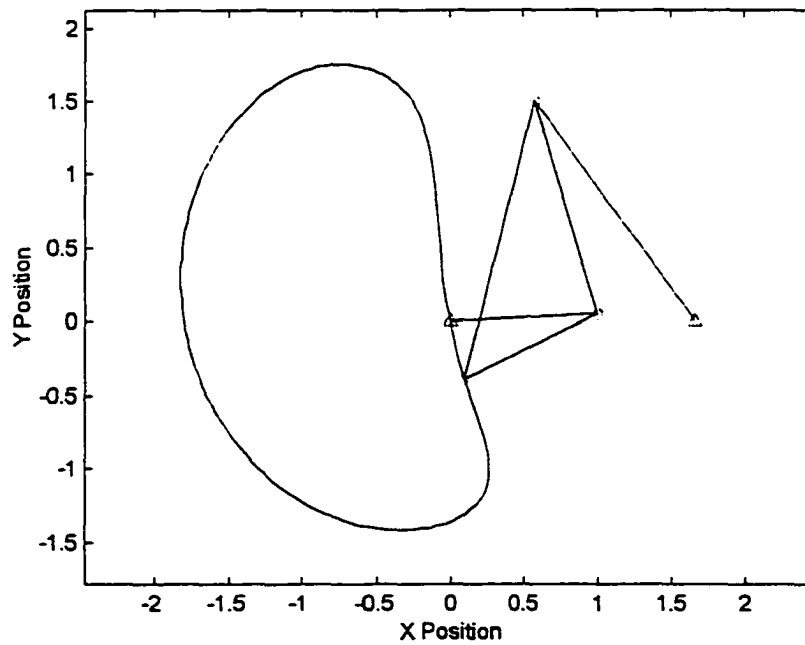


Figure C.16: Synthesized four-bar mechanism #8

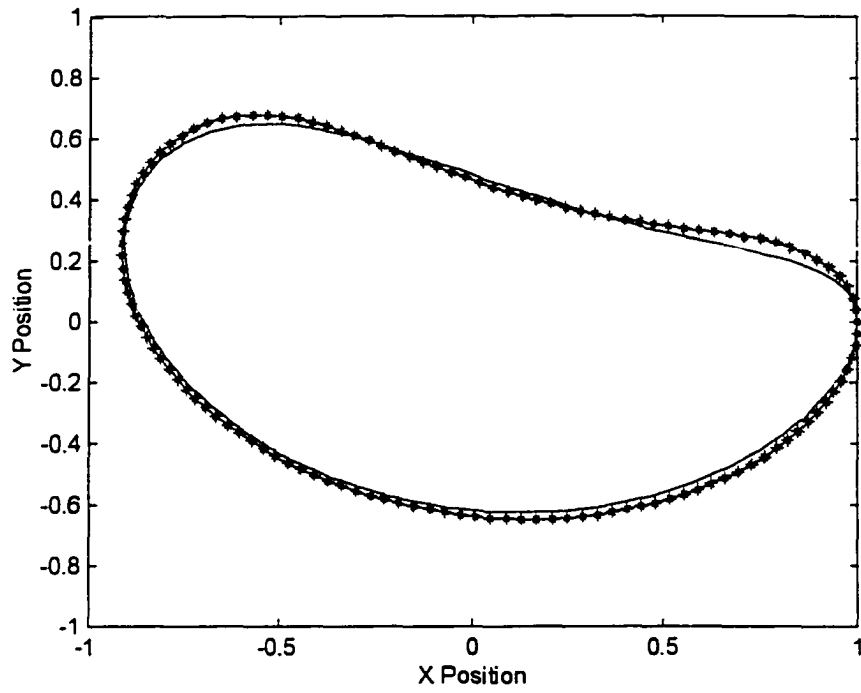


Figure C.17: Synthesized trace point path #9 and desired path

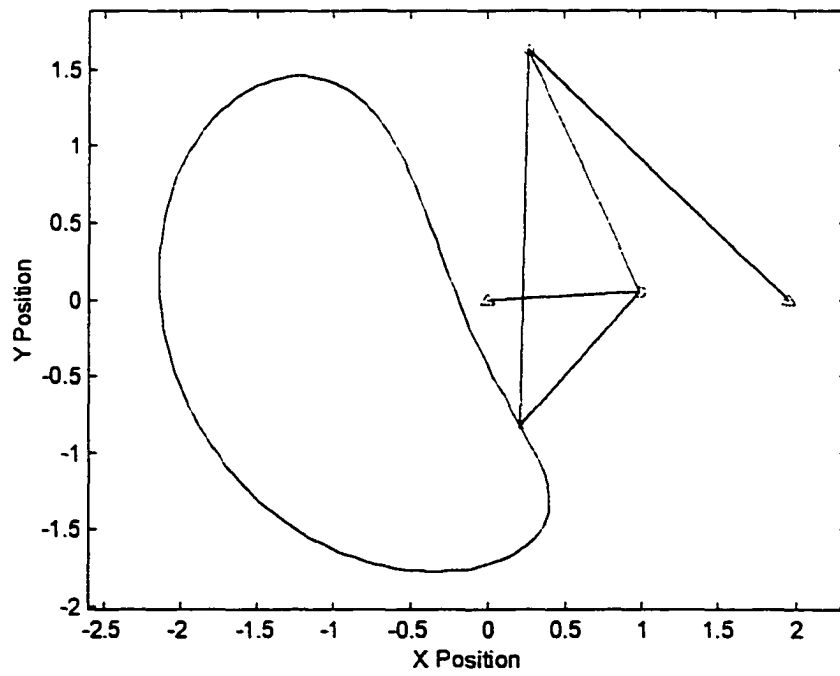


Figure C.18: Synthesized four-bar mechanism #9

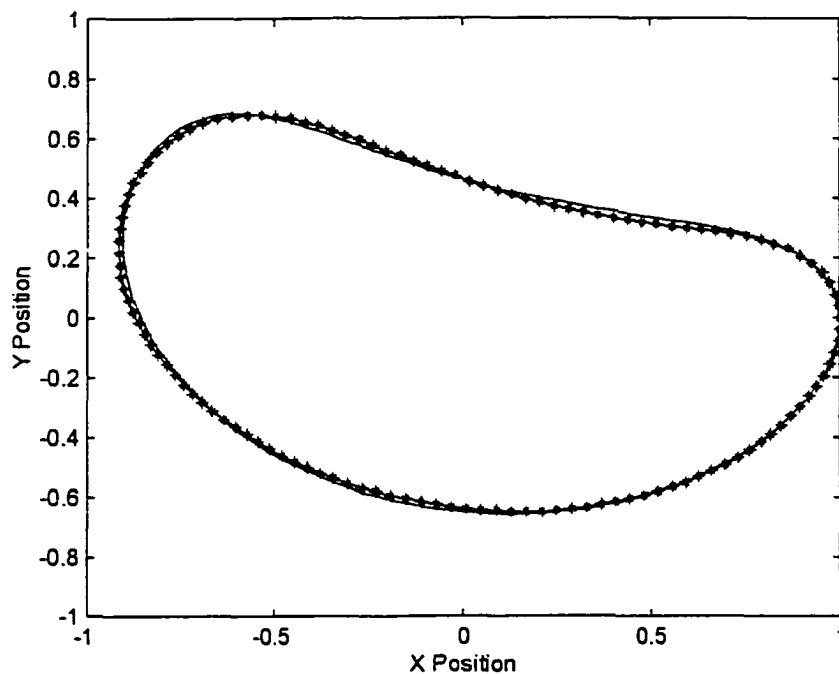


Figure C.19: Synthesized trace point path #10 and desired path

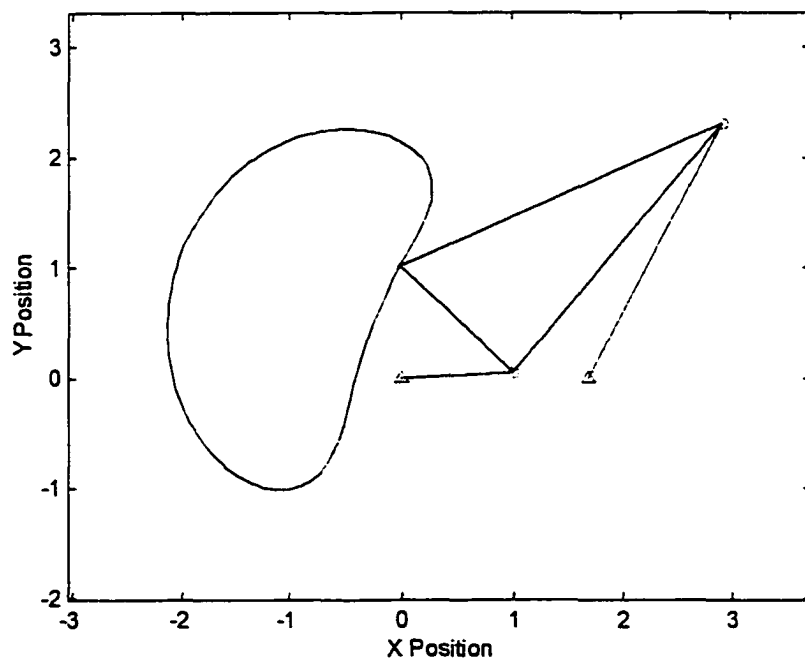


Figure C.20: Synthesized four-bar mechanism #10

Figures C.21, C.23, C.25, C.27, C.29, C.31, C.33, C.35, C.37 and C.39 are graphs of the desired partial trace point path and each of the ten candidate trace point paths synthesized by the random search and refinement process in Chapter 10. Figures C.22, C.24, C.26, C.28, C.30, C.32, C.34, C.36, C.38, and C.40 are the synthesized four-bar mechanism that generates the partial trace point path. A summary of the four-bar mechanism configuration is found in Table C.2.

Table C.2: Summary of candidate partial trace point paths generated through the random search process - partial curves

Curve	CR	FC	GPD	TPD	TPA	AStprt	AStp	A&P Diff.
11	3.0768	3.6118	1.8865	2.9217	0.5282	18	101	0.0404
12	3.2818	2.8000	2.5018	1.6665	0.6599	8	54	0.0725
13	3.3738	2.7892	2.7472	1.3096	0.1991	188	259	0.1325
14	2.7002	3.3017	2.2239	3.4412	-0.3120	8	185	0.0438
15	1.5847	3.6657	3.0871	1.0736	0.0440	12	99	0.0489
16	2.5390	3.3317	3.3517	1.3837	-0.3551	1	55	0.0678
17	1.8043	3.7563	3.0864	1.2497	-0.1399	7	85	0.0491
18	2.0111	4.0014	3.3027	1.4625	0.9476	50	114	0.0854
19	3.3465	2.4488	2.1415	3.1445	-1.0256	1	72	0.0260
20	2.8575	3.6647	2.0471	3.8274	-0.4980	4	115	0.0307

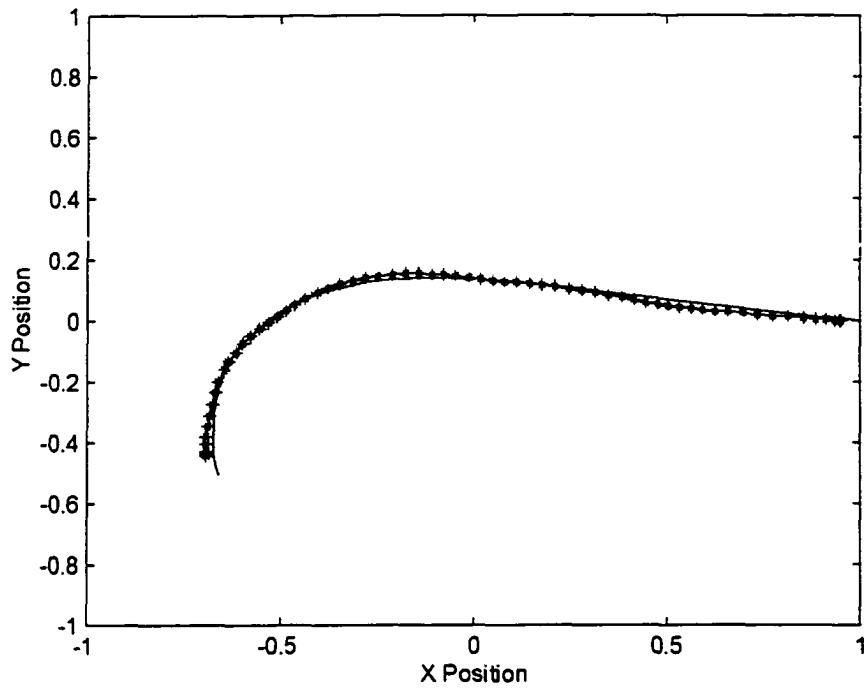


Figure C.21: Synthesized partial path #11 and desired path

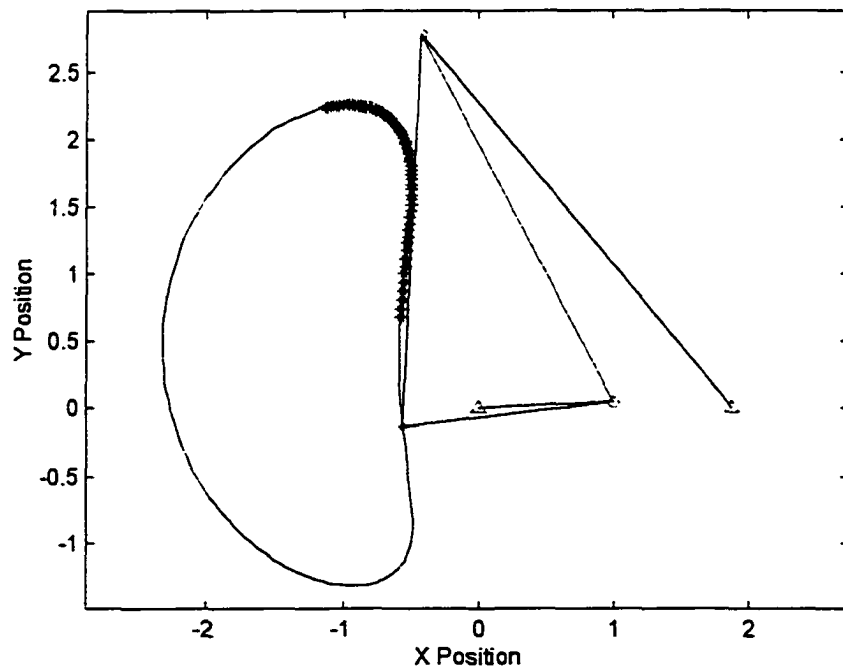


Figure C.22: Synthesized four-bar mechanism #11

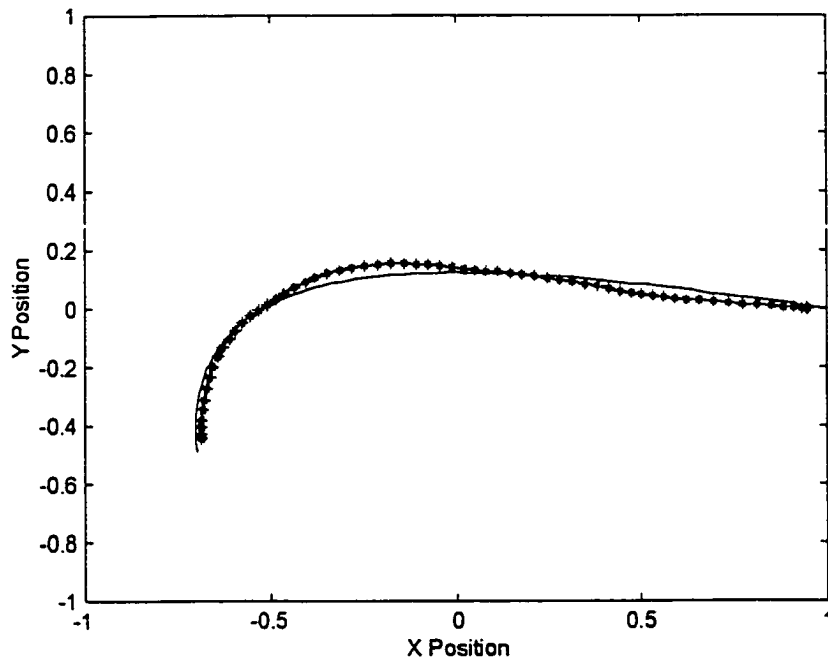


Figure C.23: Synthesized partial path #12 and desired path

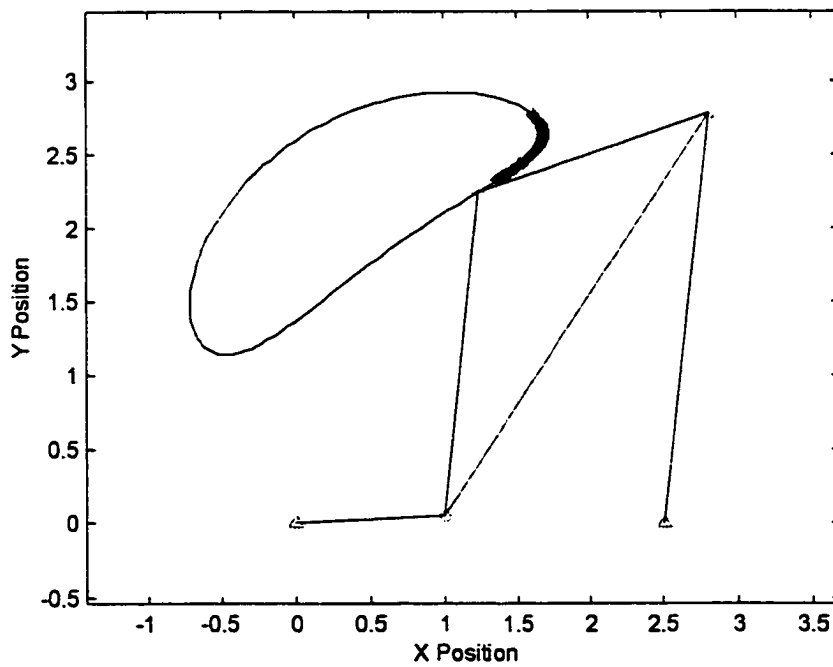


Figure C.24: Synthesized four-bar mechanism #12

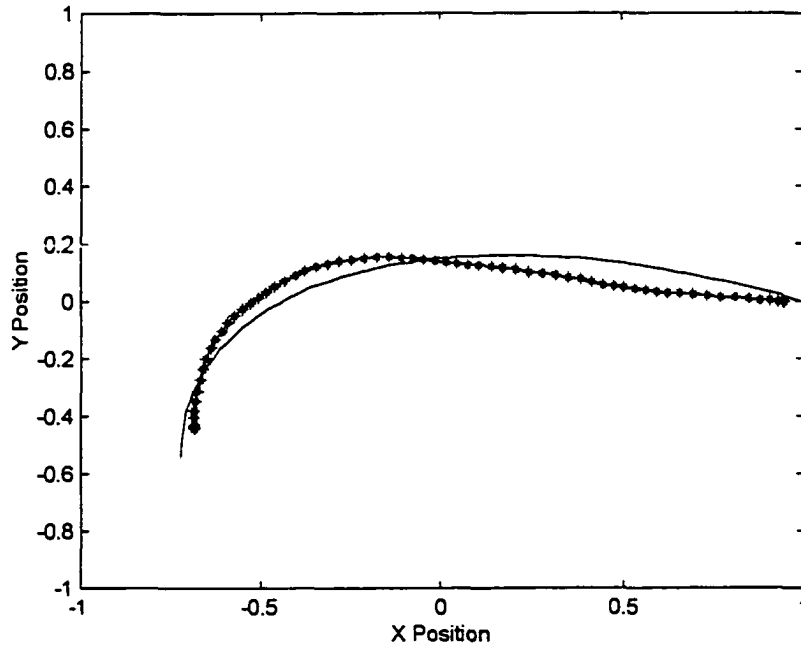


Figure C.25: Synthesized partial path #13 and desired path

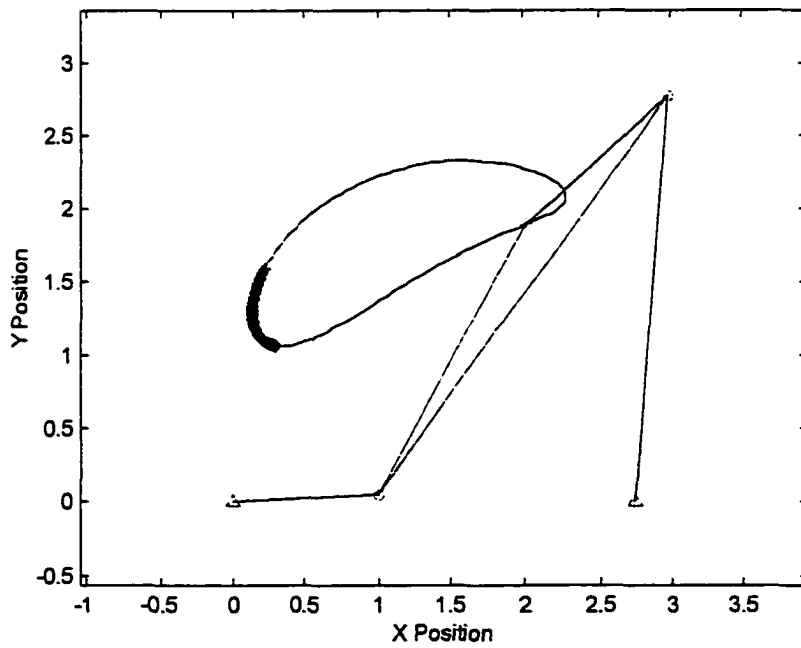


Figure C.26: Synthesized four-bar mechanism #13

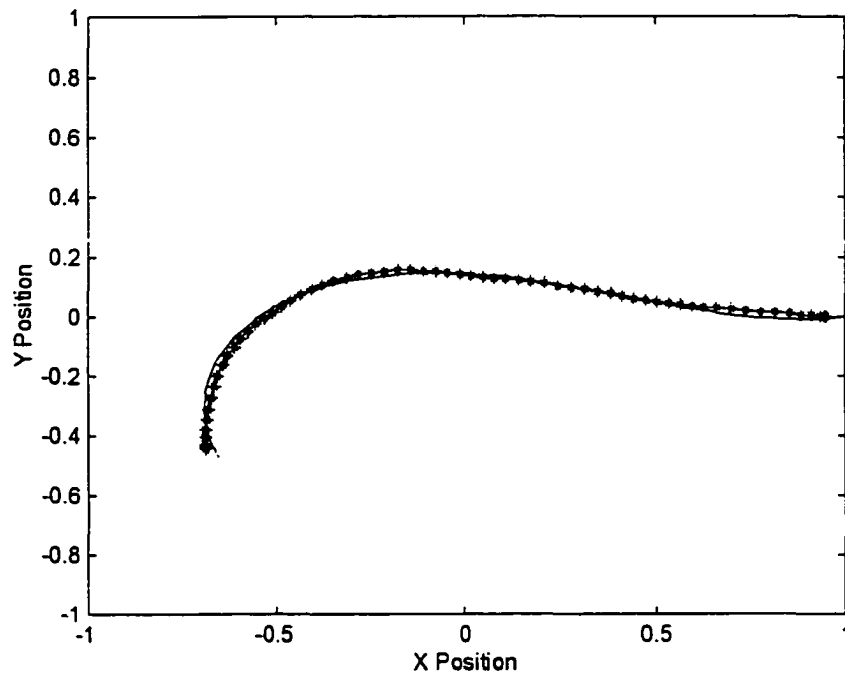


Figure C.27: Synthesized partial path #14 and desired path

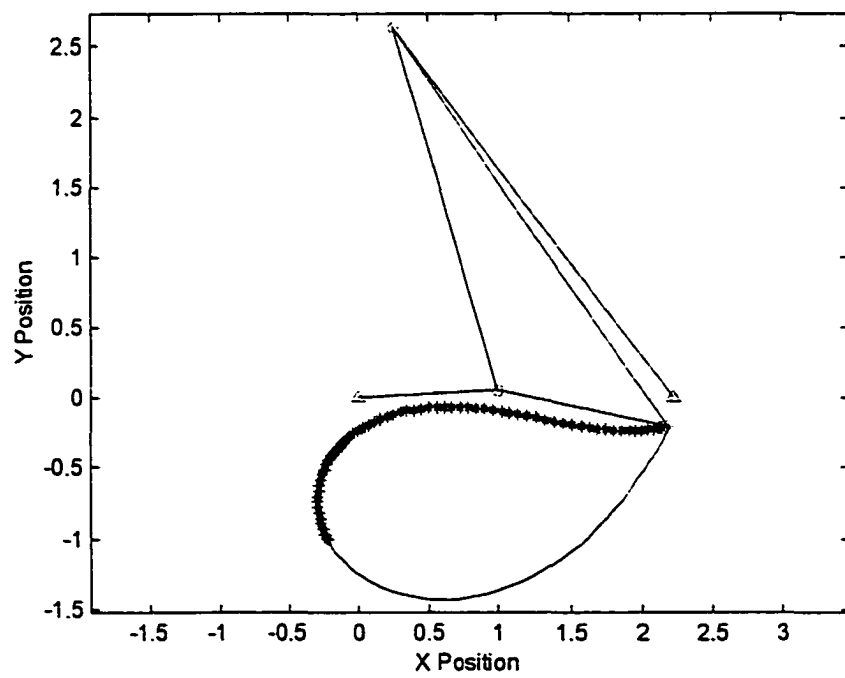


Figure C.28: Synthesized four-bar mechanism #14

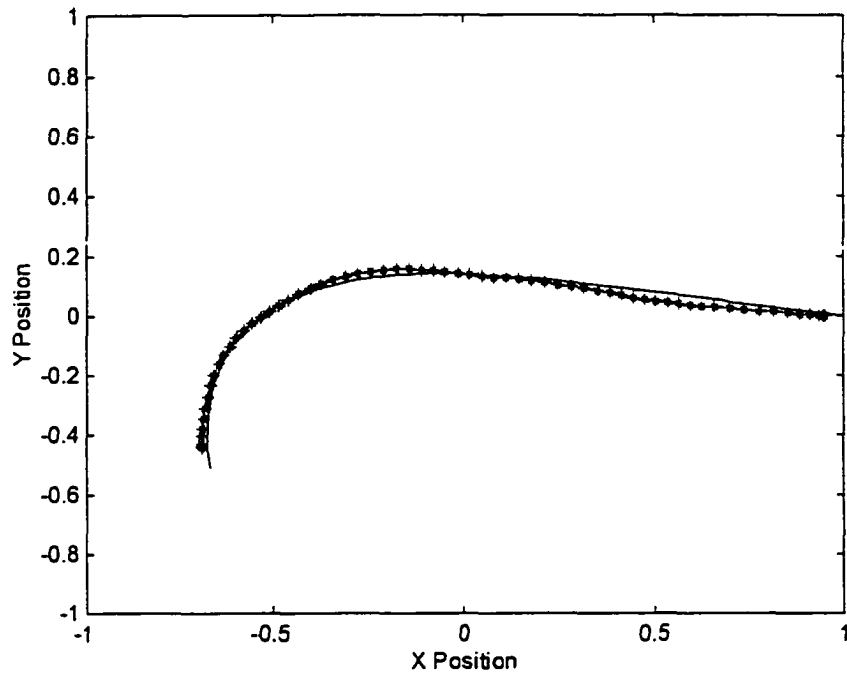


Figure C.29: Synthesized partial path #15 and Desired path

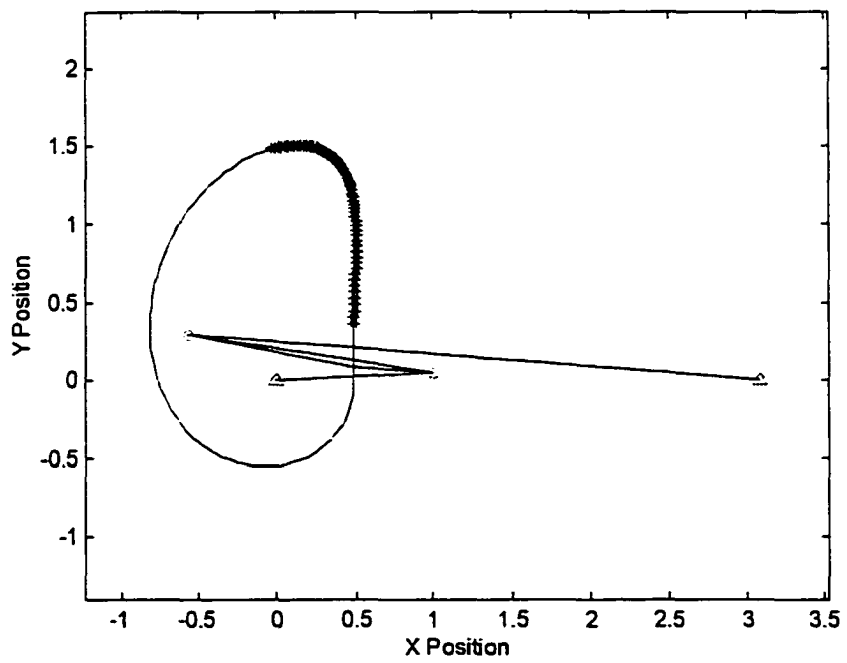


Figure C.30: Synthesized four-bar mechanism #15

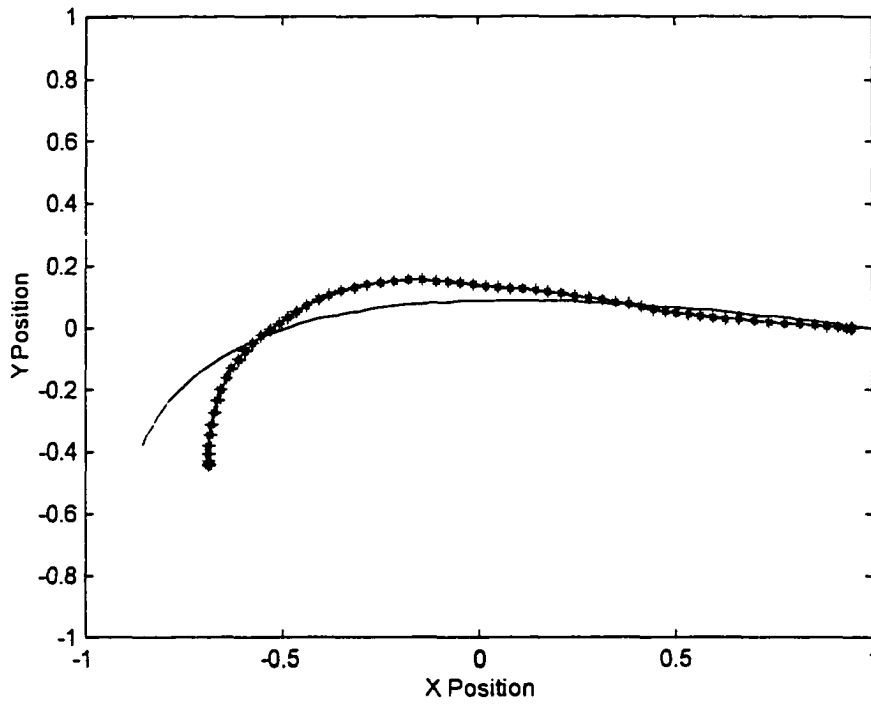


Figure C.31: Synthesized partial path #16 and desired path

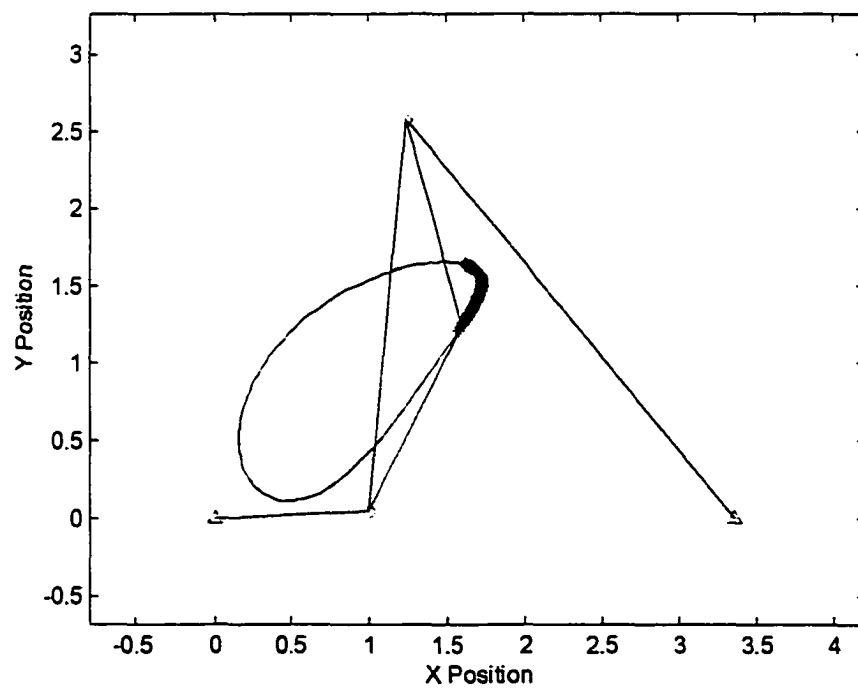


Figure C.32: Synthesized four-bar mechanism #16

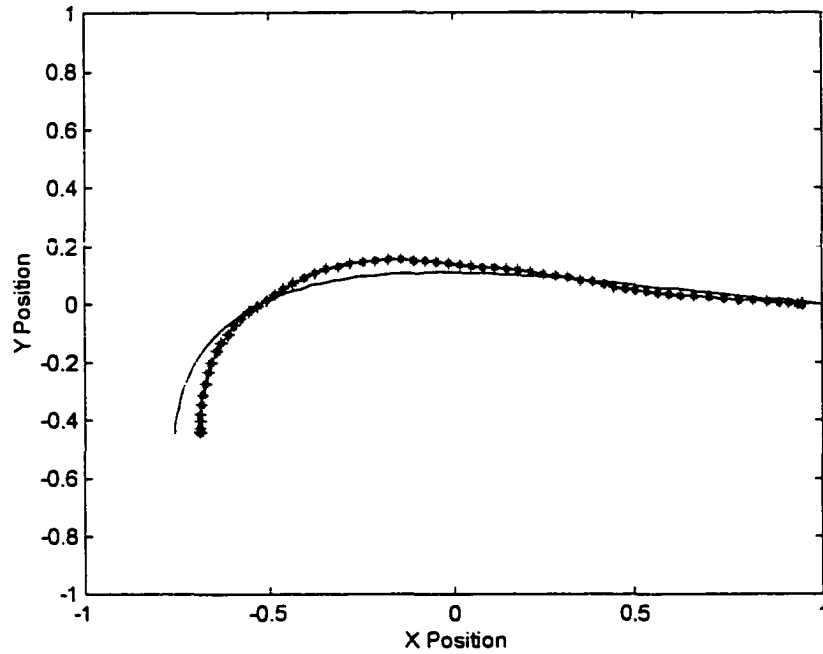


Figure C.33: Synthesized partial path #17 and desired path

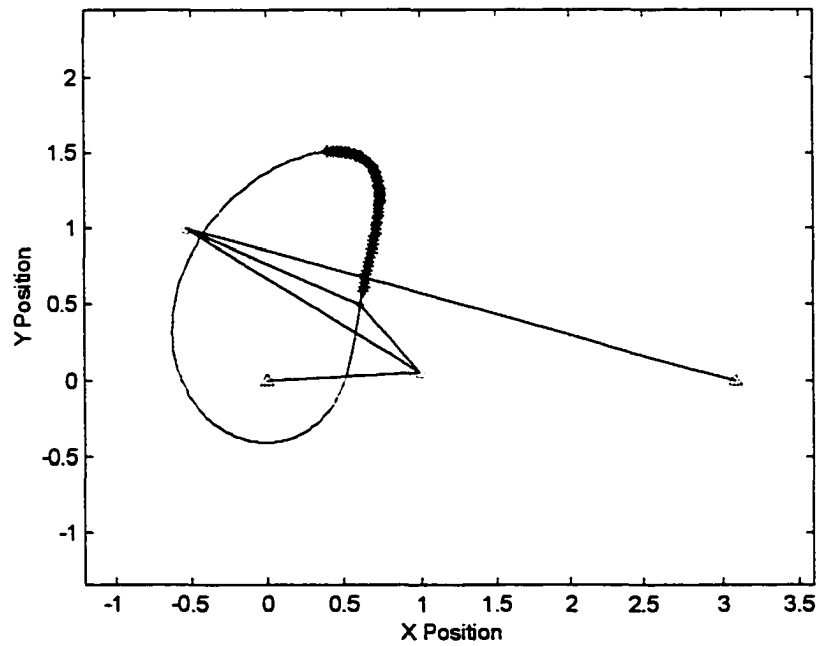


Figure C.34: Synthesized four-bar mechanism #17

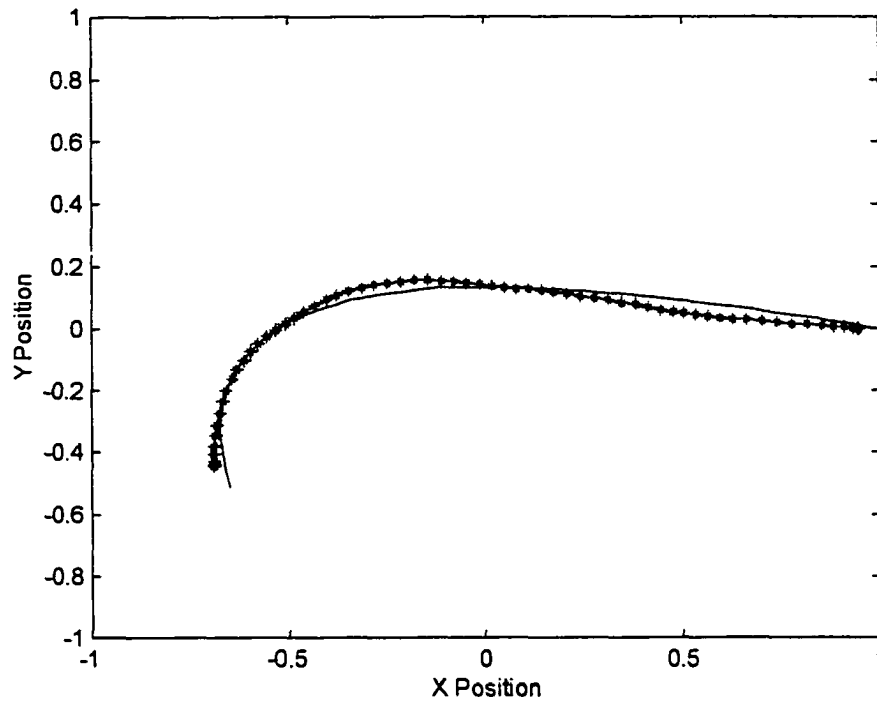


Figure C.35: Synthesized partial path #18 and desired path

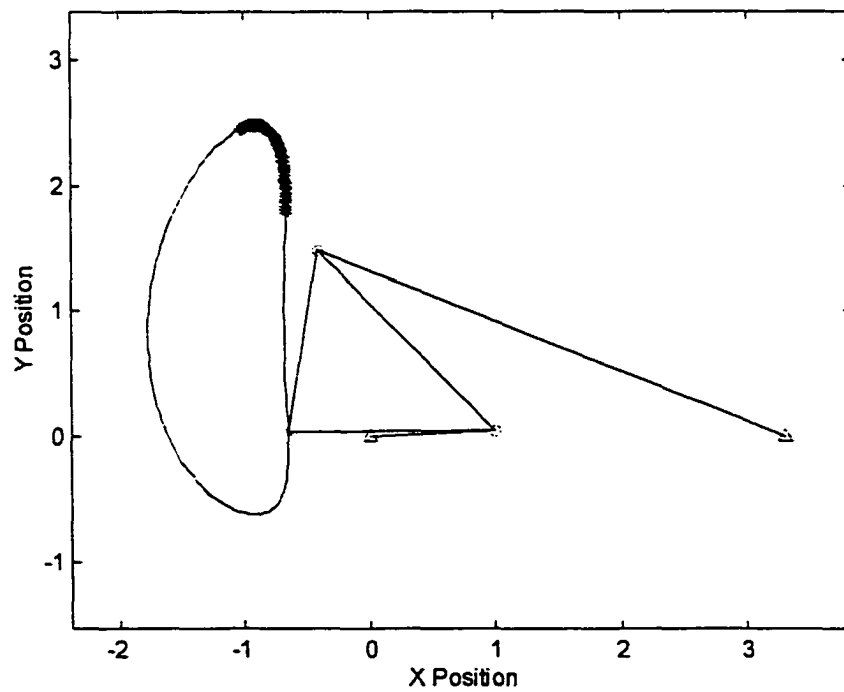


Figure C.36: Synthesized four-bar mechanism #18

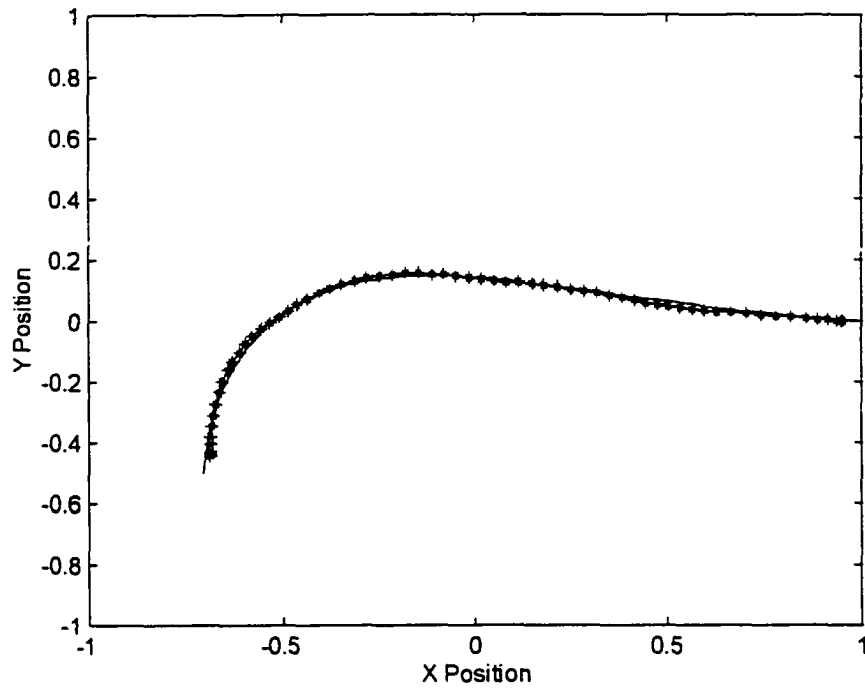


Figure C.37: Synthesized partial path #19 and desired path

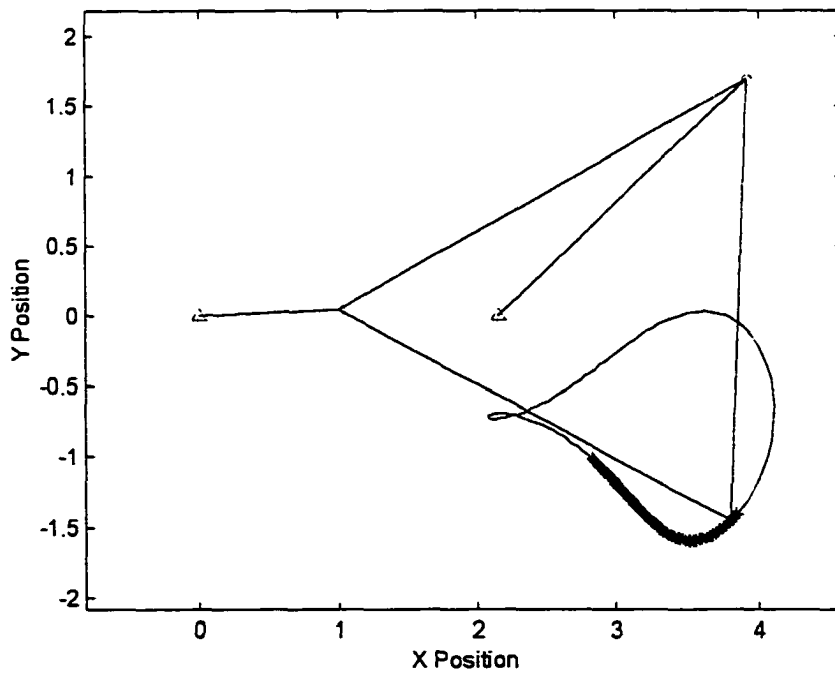


Figure C.38: Synthesized four-bar mechanism #19

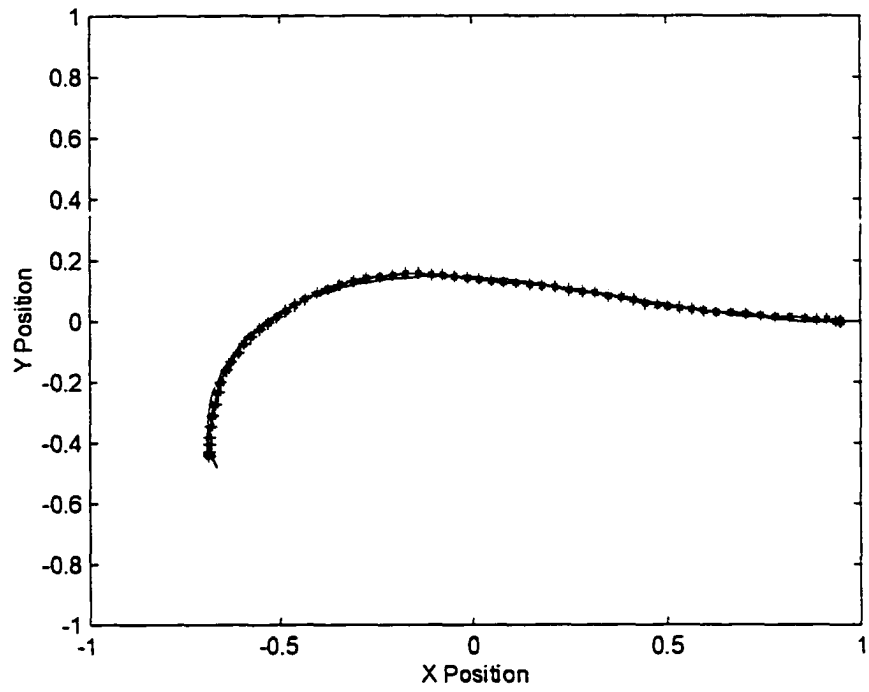


Figure C.39: Synthesized partial path #20 and Desired path

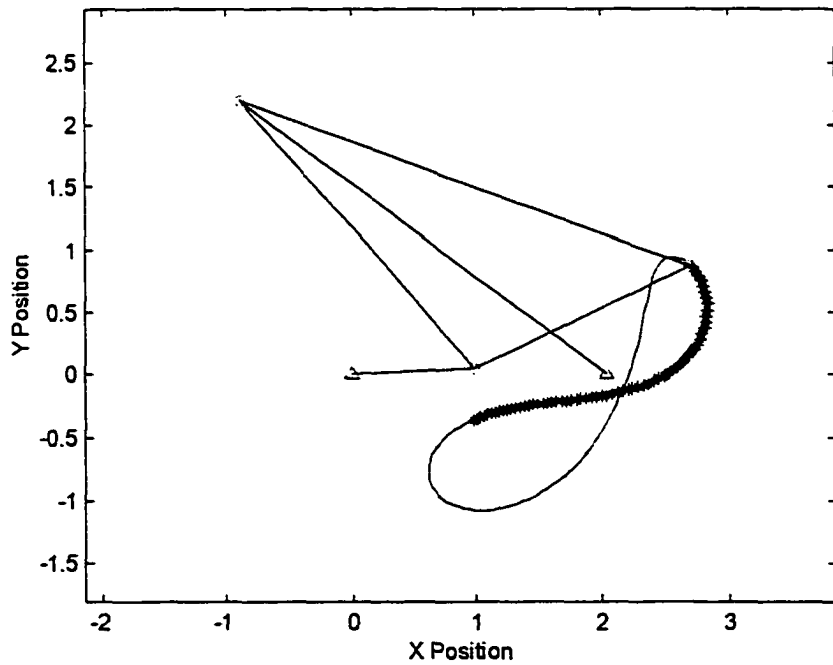


Figure C.40: Synthesized four-bar mechanism #20

REFERENCES

- H. Alt, Der Uebertragungswinkel und seine Bedeutung fuer das Konstruieren Periodischer Getriebe, *Werkstattstechnik*, vol. 26, no. 4, p. 61, 1932
- Anand, V.B., *Computer Graphics and Geometric Modeling for Engineers*, John Wiley & Sons, Inc., New York, New York, 1993.
- Bracewell, R.N., *The Fourier Transform and Its Applications*, McGraw-Hill Book Company, New York, New York, 1978.
- Bracewell, R.N., *Two-Dimensional Imaging*, Prentice-Hall, Englewood Cliffs, New Jersey, 1995.
- Chen, Q., Defrise, M. and Deconick, F., Symmetric phase-only matched filtering of Fourier-Mellin transforms for image registration and recognition, *IEEE Transactions on Pattern Analysis and Machine Intelligence*, Volume 16, July 1994.
- Chebyshev, P.L., "Theorie des mecanismes connus sous le nome de parallellograms (1953)," in *Oeuvres de P.L. Tchebychef*, Vol. 1. St. Petersburg: Markoff et Sonin, 1899; *Modern Mathematical Classics: Analysis*, S370. Ed. Richard Bellom. New York: Dover Publications, Inc., 1961
- Dudani, S.A., Breeding, K.J. and McGhee, R.B., Aircraft Identification by Moment Invariants, *IEEE Transactions on Computers*, C-26:39-26, 1977
- Erdman, A.G. and Sandor G.N., *Mechanism Design - Analysis and Synthesis*, Prentice Hall, Englewood Cliffs, New Jersey, 1991
- Flugrad, D.R., Jr. and Subbian, T., Four-Bar Path Generation Synthesis by a Continuation Method, *Journal of Mechanical Design*, March, 1991.
- Freudenstein, F. and Roth, B., Synthesis of Path-Generating Mechanisms by Numerical Methods. *Journal of Engineering for Industry* 85B, no. 3:298-306, 1963
- Freudenstein, F., Approximate Synthesis of Four-bar Linkages, *Transactions of the ASME*, vol. 77, no. 6, 1955

- Gonzalez, R.C., *Digital Image Processing*, Addison-Wesley Publishing Company, Reading, Massachusetts, 1977
- Gonzalez, R.C. and Wintz, P., *Digital Image Processing*, Addison-Wesley Publishing Company, Reading, Massachusetts, 1987.
- Hall, E.L., Wong, R.Y., Chen, C.C., Sadjadi, F. And Frei, W., *Invariant Features for Quantitative Scene Analysis*, Final Report, Image Processing Institute, Department of electrical Engineering, University of Southern California, July 1976.
- Hain, K., *Applied Kinematics*, 2nd ed. McGraw-Hill Book Company, New York, New York, 1967
- Hirschhorn, J., *Kinematics and Dynamics of Plane Mechanisms*, McGraw-Hill Book Company, San Francisco, California, 1962
- Hogben, L., *Elementary Linear Algebra*, West Publishing Company, St. Paul, Minnesota, 1987
- Hrones, J.A. and Nelson, G.L., *Analysis of the Four-Bar Linkage - Its Application to the Synthesis of Mechanisms*, The Technology Press of the Massachusetts Institute of Technology and John Wiley & Sons, New York, New York, 1951
- Hu, M., Visual Pattern Recognition by Moment Invariants, *IRE Transactions on Information Theory*, Volume IT-8, pp. 179-187, 1962
- Hussain, Z., *Digital Image Processing - Practical Applications of Parallel Processing Techniques*, Ellis Horwood Limited, West Sussex, England, 1991
- Jovanovic, V. and Kazerounian, Optimal Design Using Chaotic Decent Method, ASME Engineering Technical Conference, September, 1998.
- Kota, S. and Ullah, I., Optimal Synthesis of Mechanisms for Path Generation Using Fourier Descriptors and Global Search Methods, *Transactions of the ASME*, December, 1997.
- Lindholdm, J.C., "A Survey of the Graphical Techniques in Designing for Specific Input-Output Relationships of a Four-Bar Mechanism," *Proceedings of the First Applied Mechanisms Conference*, Stillwater, Oklahoma (Oklahoma State University), 1969
- Parker, S.P., *Dictionary of Scientific and Technical Terms*, McGraw-Hill, 1984

- Reints, D., *Development of an Algorithm for Mechanism Synthesis*, Mechanical Engineering Department, Iowa State University, Ames, Iowa, 1994.
- Reiss, T.H., *Recognizing Planar Objects Using Invariant Image Features*, *Lecture Notes in Computer Science*, Springer-Verlag Berlin Heidelberg, Germany, 1993
- Sandor, G.N., "On Computer-Aided Graphical Kinematic Synthesis," Technical Seminar Series, Princeton University, 1962.
- Subbian, T., 1990, *Use of Continuation Methods for Kinematic Synthesis and Analysis*, Phd Dissertation, Iowa State University, 1990.
- Titus, J., Erdman A.G. and Riley, D., "The Role of Type Synthesis in the Design of Machines," *Proceedings of the 1989 NSF Engineering Design Research Conference*, June 11-14, 1989), Amherst, Mass,: University of Massachusetts
- Wampler, C.W., Morgan, A.P. and Sommese, A.J., *Numerical Continuation Methods for Solving Polynomial Systems Arising in Kinematics*, General Motors Research Laboratories, Warren, Michigan, 1988
- Wong, R. Y. and Hall, E. L., *Scene Matching with Invariant Moments*, *Computer Graphics and Image Processing*, 8:16-24, 1978.
- Zahn, C.T. and Roskies, R.Z., "Fourier Descriptors for Plane Closed Curves," *IEEE Transactions on Pattern Analysis and Machine Intelligence*, vol. C-21, No. 3, pp 269-281, 1972